



Statistical analysis of traffic loads and traffic load effects on bridges

Xiao Yi Zhou

► To cite this version:

Xiao Yi Zhou. Statistical analysis of traffic loads and traffic load effects on bridges. Structural mechanics [physics.class-ph]. UNIVERSITE PARIS-EST, 2013. English. NNT : . tel-00949929

HAL Id: tel-00949929

<https://theses.hal.science/tel-00949929>

Submitted on 20 Feb 2014

HAL is a multi-disciplinary open access archive for the deposit and dissemination of scientific research documents, whether they are published or not. The documents may come from teaching and research institutions in France or abroad, or from public or private research centers.

L'archive ouverte pluridisciplinaire **HAL**, est destinée au dépôt et à la diffusion de documents scientifiques de niveau recherche, publiés ou non, émanant des établissements d'enseignement et de recherche français ou étrangers, des laboratoires publics ou privés.

STATISTICAL ANALYSIS OF TRAFFIC LOADS AND TRAFFIC LOAD EFFECTS ON BRIDGES

Using Weigh-in-Motion data collected in France

by

Xiao Yi ZHOU

A Thesis Submitted to

the École Doctorale Sciences Ingénierie et Environnement of
the Université Paris-Est in Partial Fulfillment of the Requirements for
the Degree of Doctor of Philosophy

Reviewers:	Prof.	E. Brühwiler	EPFL, Switzerland
	Prof.	A. C. W. M. Vrouwenvelder	TU Delft, Netherlands
Examinators:	Prof.	P. Croce	University of Pisa, Italy
	Prof.	B. Jourdain	CERMICS, ENPC
Supervisor	HDR	F. Toutlemonde	IFSTTAR
Advisors		B. Jacob	IFSTTAR
	Dr.	F. Schmidt	IFSTTAR

Paris, France

May 15, 2013

Abstract

Most of the bridges are less than 50 m (85%) in France. For this type of bridges, the traffic load may govern the design and assessment. Road freight transportation has increased by 36.2% between 1995 and 2010 in Europe, and the volume of freight transport is projected to increase by 1.7% per year between 2005 and 2030. It is thus vital important to insure European highway structures to cater for this increasing demand in transport capacity. Traffic load model in standard or specification for bridge design should guarantee all newly designed bridges to have sufficient security margin for future traffic. For existing bridges, the task is to assess their safety under actual and future traffic, and a prioritization of the measures necessary to ensure their structural integrity and safety. In addition, to address this growth without compromising the competitiveness of Europe, some countries are contemplating the introduction of longer and heavier trucks for reducing the number of heavier vehicles for a given volume or mass of freight, reducing labour, fuel and other costs.

Many different methods have been used to model extreme traffic load effects on bridges for predicting characteristic value for short or long return period. They include the fitting a Normal or Gumbel distribution to upper tail, the use of Rice formula for average level crossing rate, the block maxima method and the peaks over threshold method. A review of the fundament and the use of these methods for modelling maximum distribution of bridge is presented. In addition, a quantitative comparison work is carried out to investigate the differences between methods. The work involves two studies, one is based on numerical sample, and the other is based on traffic load effects. The accuracy of the methods is evaluated through the typical statistics of bias and root mean squared error on characteristic value and probability of failure. In general, the methods are less accurate on inferring the failure probability than on characteristic values, perhaps not surprising given such a small failure probability was being considered (10^{-6} in a year). Although none of methods provides predictand as accurately as expected with 1000 days of data, the tail fitting methods, especially the peaks over threshold method, are better than the others.

A study on peaks over threshold method is thus carried out in this thesis. In the POT method, the distribution of exceedances over a high enough threshold will be a member of generalized Pareto distribution (GPD) family. The peaks over threshold method is extensively used in the domains such as hydrology and finance, while seldom application can be found in bridge load-ing problem. There are numerous factors, which affect the application of peaks over threshold on modelling extreme value, such as the length and accuracy of data available, the criteria used to identify independent peaks, parameter estimation and the choice of threshold. In order

to provide some guidance on selecting parameter estimation when applying POT to bridge traffic loading, we focus on the effect that method used to estimate the parameters of the GPD has on the accuracy of the estimated characteristic values. Many parameter estimators have been proposed in the statistical literature, and the performance of various estimators can vary greatly in terms of their bias, variance and sensitivity to threshold choice and consequently affect the accuracy of the estimated characteristic values. The conditions, assumptions, merits and demerits of each parameter estimation method are introduced; especially their applicability for traffic loading is discussed. Through this qualitative discussion on the methods, several available methods for traffic loading are selected. It includes the method of moments (MM), the probability weighted moments (PWM), the maximum likelihood (ML), the penalized maximum likelihood (PML), the minimum density power divergence (MDPD), the empirical percentile method (EPM), the maximum goodness-of-fit statistic and the likelihood moment (LM). To illustrate the behaviour and accuracy of these parameter estimators, three studies are conducted. Numerical simulation data, Monte Carlo simulation traffic load effects and in-field traffic load effect measurements are analyzed and presented. The comparative studies investigate the accuracy of the estimates in terms of bias and RMSE of parameters and quantile. As expected, the estimators have different performance, and the same method has different performance in these three sets of data. From the numerical simulation study, the MM and PWM methods are recommended for negative shape parameter case, especially for small size sample (less than 200), while the ML is recommended for positive shape parameter case. From the simulated traffic load effect study, the ML and PML provide more accuracy estimates of 1000-year return level when the number of exceedances over 100, while the MM and PWM are better than others when sample size is less than 100. Moreover, application on monitored traffic load effects indicates that the outliers have significant influence on the parameter estimators as all investigated methods encounter feasibility problem.

As been stated in statistical literature, a frequent cause of outlier is a mixture of two distributions, which may be two distinct sub-populations. In the case of bridge loading, this can be a potential reason to result in the feasible problem of parameter estimator. Literature points out that the traffic load effect is induced by loading event that involves different number of vehicles, and the distribution of the load effects from different loading events are not identically distributed, which violates the assumption of classic extreme value theory that the underlying distribution should be identically independent distributed. With respect to non-identical distribution in bridge traffic load effects, non-identical distribution needs to be addressed in extreme modelling to account for the impacts in inference. Methods using mixture distribution (exponential or generalized extreme value) has been proposed in the literature to model the extreme traffic load effect by loading event. However, it should be noticed that the generalized extreme value distribution is fitted to block maxima, which implies the possibility of losing some extremes, and the use of exponential distribution is objective. We intend to explicitly model the non-identically distributed behaviour of extremes for a stationary extreme time series within a mixture peaks over threshold (MPOT) model to avoid the loss of information and predetermination of distribution type.

For bridges with length greater than 50 m, the governing traffic scenario is congested traffic,

which is out of the scope of this study. Moreover, the traffic loading may not govern the design for long span bridge. However, the traffic loading may be also importance if the bridge encounter traffic induced fatigue problem, components like orthotropic steel deck is governed by traffic induced fatigue load effects. We intend to explore the influence of traffic load on the fatigue behaviour of orthotropic steel deck, especially the influence of the loading position in terms of transverse location of vehicle. Measurements of transverse location of vehicle collected from by weigh-in-motion (WIM) systems in 2010 and 2011 four French highways showed a completely different distribution model of transverse location of vehicle to that recommended in EC1. Stress spectrum analysis and fatigue damage calculation was performed on the stresses induced traffic on orthotropic steel deck of Millau cable-stayed bridge. By comparing the stresses and damages induced by different traffic patterns (through distributions of transverse location of vehicle), it was found that the histogram of stress spectrum and cumulative fatigue damage were significantly affected by the distribution of transverse location of vehicle. Therefore, numerical analysis that integrates finite element modelling and traffic data with distributions of transverse location of vehicles can help to make an accurate predetermination of which welded connections should be sampled to represent the health of the deck.

Résumé

Une grande majorité (85%) des ponts français a une portée inférieure à 50m. Pour ce type d'ouvrage d'art, la charge de trafic peut être déterminante pour la conception et le recalcul. Or, en Europe, le fret routier a augmenté de 36.2% entre 1995 et 2010, et la croissance annuelle du volume transporté par la route a été évaluée à 1.7% par an entre 2005 et 2030. Il est donc essentiel de s'assurer que les infrastructures européennes sont en mesure de répondre à cette demande croissante en capacité structurelle des ouvrages. Pour les ouvrages neufs, les modèles de trafic dans les normes ou les législations pour la conception des ponts incluent une marge de sécurité suffisante pour que la croissance du trafic soit prise en compte sans dommage par ces ouvrages. Mais pour les ouvrages existants, la résistance structurelle aux trafics actuels et futur est à vérifier et une priorisation des mesures doit être faite pour assurer leur intégrité structurelle et leur sécurité. De plus, afin de préserver leur infrastructure tout en ne menaçant pas leur compétitivité nationale, certains pays réfléchissent à l'introduction de poids lourds plus longs, plus lourds, ce qui permet de réduire le nombre de véhicules pour un volume ou un tonnage donné, ainsi que d'autres coûts (d'essence, de travail, ...), ce qui justifie encore plus les calculs effectués.

Pour répondre à ce genre de problématique, différentes méthodes d'extrapolation ont déjà été utilisées pour modéliser les effets extrêmes du trafic, afin de déterminer les effets caractéristiques pour de grandes périodes de retour. Parmi celles-ci nous pouvons citer l'adaptation d'une gaussienne ou d'une loi de Gumbel sur la queue de distribution empirique, la formule de Rice appliquée à l'histogramme des dépassements de niveaux, la méthode des maxima par blocs ou celle des dépassements de seuils élevés. Les fondements et les utilisations faites de ces méthodes pour modéliser les effets extrêmes du trafic sur les ouvrages sont donnés dans un premier chapitre. De plus, une comparaison quantitative entre ces méthodes est réalisée. Deux études sont présentées, l'une basée sur un échantillon numérique et l'autre sur un échantillon réaliste d'effets du trafic. L'erreur induite par ces méthodes est évaluée à l'aide d'indicateurs statistiques simples, comme l'écart-type et les moindres carrés, évalués sur les valeurs caractéristiques et les probabilités de rupture. Nos conclusions sont, qu'en général, les méthodes sont moins précises lorsqu'il s'agit de déterminer des probabilités de rupture que lorsqu'elles cherchent des valeurs caractéristiques. Mais la raison peut en être les faibles probabilités recherchées (10^{-6} par an). De plus, bien qu'aucune méthode n'ait réalisée des extrapolations de manière correcte, les meilleures sont celles qui s'intéressent aux queues de probabilités, et en particulier des dépassements au-dessus d'un seuil élevé.

Ainsi une étude de cette dernière méthode est réalisée : en effet, cette méthode, nommé «

dépassements d'un seuil élevé », considère que les valeurs au-dessus d'un seuil correctement choisi, assez élevé, suit une distribution de Pareto généralisée (GPD). Cette méthode est utilisée de manière intensive dans les domaines de l'hydrologie et la finance, mais non encore appliquée dans le domaine des effets du trafic sur les ouvrages. Beaucoup de facteurs influencent le résultat lorsqu'on applique cette méthode, comme la quantité et la qualité des données à notre disposition, les critères utilisés pour déterminer les pics indépendants, l'estimation des paramètres et le choix du seuil. C'est pour cette raison qu'une étude et une comparaison des différentes méthodes d'estimation des paramètres de la distribution GPD sont effectuées : les conditions, hypothèses, avantages et inconvénients des différentes méthodes sont listés. Différentes méthodes sont ainsi étudiées, telles la méthode des moments (MM), la méthode des moments à poids (PWM), le maximum de vraisemblance (ML), le maximum de vraisemblance pénalisé (PML), le minimum de la densité de la divergence (MDPD), la méthode des fractiles empiriques (EPM), la statistique du maximum d'adaptation et la vraisemblance des moments (LM). Pour comparer ces méthodes, des échantillons numériques, des effets de trafic simulés par Monte Carlo et des effets mesurés sur un ouvrage réel sont utilisés. Comme prévu, les méthodes ont des performances différentes selon l'échantillon considéré. Néanmoins, pour des échantillons purement numériques, MM et PWM sont recommandées pour des distributions à paramètre de forme négatif et des échantillons de petite taille (moins de 200 valeurs). ML est conseillé pour des distributions à paramètre de forme positif. Pour des effets du trafic simulés, ML et PML donne des valeurs de retour plus correctes lorsque le nombre de valeurs au-dessus du seuil est supérieur à 100 ; dans le cas contraire, MM et PWM sont conseillés. De plus, comme c'est prouvé dans l'étude de valeurs réelles mesurées, les valeurs a priori aberrantes («outliers») ont une influence notable sur le résultat et toutes les méthodes sont moins performantes.

Comme cela a été montré dans la littérature, ces «outliers» proviennent souvent du mélange de deux distributions, qui peuvent être deux sous-populations. Dans le cas de l'effet du trafic sur les ouvrages, cela peut être la raison d'une estimation des paramètres non correcte. Les articles existant sur le sujet soulignent le fait que les effets du trafic sont dus à des chargements indépendants, qui correspondant au nombre de véhicules impliqués. Ils ne suivent pas la même distribution, ce qui contredit l'hypothèse classique en théorie des valeurs extrêmes que les événements doivent être indépendants et identiquement distribués. Des méthodes permettant de prendre en compte ce point et utilisant des distributions mélangées (exponentielles ou valeurs extrêmes généralisées) ont été proposées dans la littérature pour modéliser les effets du trafic. Nous proposons une méthode similaire, que nous appelons dépassement de seuils mélangés, afin de tenir des différentes distributions sous-jacentes dans l'échantillon tout en appliquant à chacune d'entre elles la méthode des dépassements de seuil.

Pour des ponts ayant des portées supérieures à 50m, le scénario déterminant est celui de la congestion, qui n'est pas ce qui est étudié ici. De plus, le trafic n'est pas la composante déterminante pour la conception des ponts de longue portée. Mais des problèmes de fatigue peuvent apparaître dans certains ponts, tels les ponts métalliques à dalle orthotrope, où l'étude du trafic peut devenir nécessaire. Ainsi nous avons fait une étude de l'influence de la position des véhicules sur le phénomène de fatigue. Pour cela, quatre fichiers de trafic réels,

mesurés en 2010 et 2011 par quatre stations de pesage différentes, ont été utilisés. Ils ont mis à jour des comportements latéraux différents d'une station à l'autre. Si nous les appliquons au viaduc de Millau, qui est un pont métallique à haubans et à dalle orthotrope, nous voyons que l'histogramme des effets et l'effet de fatigue cumulé est beaucoup affecté par le comportement latéral des véhicules. Ainsi, des études approfondies utilisant les éléments finis pour modéliser les ouvrages et des enregistrements de trafic réel, peuvent être utilisées pour pré-déterminer quels éléments, donc quelles soudures, doivent être examinés dans le pont afin d'estimer leur santé structurelle.

Résumé Long

Une grande majorité (85%) des ponts français a une portée inférieure à 50m. Pour ce type d'ouvrage d'art, la charge de trafic peut être déterminante pour la conception et le recalcul. Or, en Europe, le fret routier a augmenté de 36.2% entre 1995 et 2010, et la croissance annuelle du volume transporté par la route a été évaluée à 1.7% entre 2005 et 2030. Il est donc essentiel de s'assurer que les infrastructures européennes sont en mesure de répondre à cette demande croissante en capacité structurelle des ouvrages. Pour les ouvrages neufs, les modèles de trafic dans les normes ou les législations pour la conception des ponts incluent une marge de sécurité suffisante pour que la croissance du trafic soit prise en compte sans dommage par ces ouvrages. Mais pour les ouvrages existants, la résistance structurelle aux trafics actuels et futur est à vérifier et une priorisation des mesures doit être faite pour assurer leur intégrité structurelle et leur sécurité. De plus, afin de préserver leur infrastructure tout en ne menaçant pas leur compétitivité nationale, certains pays réfléchissent à l'introduction de poids lourds plus longs, plus lourds, ce qui permet de réduire le nombre de véhicules pour un volume ou un tonnage donné, ainsi que d'autres coûts (d'essence, de travail, ..), ce qui justifie encore plus les calculs effectués.

Le traitement de la problématique de l'accroissement du trafic dépend de notre degré de précision dans la connaissance des charges de trafic et de leurs effets sur les ouvrages. En effet, dans le cadre du recalcul d'ouvrages existants, on considèrera dans le cas déterministe qu'un ouvrage est en sécurité quand sa capacité de résistance est supérieure aux actions qu'il doit supporter. Par contre, dans le cadre de calculs statistiques, il suffira que la résistance soit supérieure avec une probabilité donnée. Ceci signifie, que quel que soit le mode d'étude choisi (déterministe ou probabiliste), la capacité de résistance structurelle et les actions appliquées à la structure doivent être connues le plus exactement possible. Ces dernières années, la compréhension des capacités de résistance a largement évolué, avec la mise au point de divers modèles pour les modéliser ainsi que les incertitudes inhérentes à leur définition. A contrario, l'étude des actions, appliquées aux ouvrages d'art, dues au trafic n'a pas reçu énormément d'attention jusqu'à ces dernières années. Pourtant, connaître et évaluer l'effet extrême rencontré par l'ouvrage au cours de sa durée de vie est crucial pour l'évaluer. Ceci peut être réalisé de diverses manières, comme des mesures empiriques de longue durée, des simulations Monte Carlo, des analyses statistiques. Des limites existent : même si les données relevées sur le terrain sont de plus en plus précises suite aux avancées dans le domaine du pesage en marche, des enregistrements de longue durée, sans interruption sont pratiquement impossibles à avoir, suite à la mise en place récente de ces stations sur routes. De même,

les simulations Monte Carlo peuvent augmenter considérablement la taille des données disponibles, mais des paramètres d'entrée erronés entraîneront des résultats faux.

Une solution pourrait être l'utilisation de la simulation pour augmenter la taille des données disponibles afin qu'elles puissent être utilisées dans des applications pratiques, et en particulier suffisamment importantes pour estimer les extrêmes rencontrés dans un futur lointain. Grâce à des développements théoriques, même un enregistrement de relative courte durée peut modéliser correctement l'évolution du trafic. Donc des méthodes pour modéliser le trafic sont connues depuis un certain temps, mais les méthodes d'extrapolation n'ont été introduites que récemment. Pourtant, la théorie des valeurs extrêmes a été utilisée dans beaucoup de domaines depuis les 50 dernières années, pour la détermination de crues fluviales extrêmes, l'estimation des variations extrêmes des valeurs boursières, le calcul de la résistance de rupture de matériaux. En effet, l'objectif de la théorie des valeurs extrêmes est de modéliser des processus stochastiques qui n'ont qu'une très faible probabilité de se produire, et même ceux qui ne seront probablement jamais observés physiquement. Ainsi modéliser les queues de distributions et les chargements extrêmes est important pour la conception de ponts et les calculs fiabilistes d'ouvrages. Ces modèles issus de la théorie des valeurs extrêmes donnent une approximation des queues de distribution tout en restant flexible sur les formes de queues de distribution potentiellement observées. De plus, l'attrait de cette théorie des valeurs extrêmes est qu'elle donne un socle mathématique et statistique suffisamment concret pour justifier l'utilisation de modèles paramétriques, ce qui est relativement simple et permet d'obtenir des extrapolations à long terme à moindres frais. La théorie des valeurs extrêmes est ainsi perçue comme un outil très utile permettant d'évaluer rapidement et simplement des extrêmes de charges ou d'effets de charges, comme par exemple le niveau de période de retour de 1000 ans. Pourtant appliquer cette théorie n'est pas toujours direct, et il reste des doutes à lever quant à son application. Un problème typique est la dépendance des événements extrêmes, qui pourtant empêcherait l'utilisation de la méthode. Un autre problème est le caractère peu usuel et donc rare des événements extrêmes, ce qui entraîne potentiellement des problèmes d'identification du modèle et de ses paramètres, en particulier pour une structure complexe. Pourtant, les effets du trafic sont un phénomène complexe qui est donc difficile à analyser avec des flux journaliers de 5000 poids lourds un jour (vendredi) et 3000 poids lourds le lendemain (samedi). D'autres problèmes existent également, tel l'échantillonnage des extrêmes ou le choix des seuils. Ainsi, appliquer la théorie des valeurs extrêmes peut être moins simple que prévu et des modifications pourraient être nécessaires pour permettre cette application. Ce doctorat se propose de répondre à certaines de ces questions.

Pour répondre à ce genre de problématique, différentes méthodes d'extrapolation ont déjà été utilisées pour modéliser les effets extrêmes du trafic, afin de déterminer les effets caractéristiques pour de grandes périodes de retour. Parmi celles-ci nous pouvons citer l'adaptation d'une gaussienne ou d'une loi de Gumbel sur la queue de distribution empirique, la formule de Rice appliquée à l'histogramme des dépassements de niveaux, la méthode des maxima par blocs ou celle des dépassements de seuils élevés. Chaque méthode a ses avantages et ses inconvénients. Par exemple, la méthode d'adaptation d'une loi normale ou de Gumbell aux données est simple à comprendre, mais le choix du début de la queue de distribution

relève d'une connaissance empirique des phénomènes. De même, un tel jugement n'est pas requis pour la méthode des maxima de blocs, mais il est nécessaire de choisir la taille des blocs. Une revue de ces méthodes et leurs requis est faite dans le chapitre 1. Dans le chapitre 2, une étude quantitative est alors réalisée pour investiguer les différences entre les méthodes : deux calculs sont réalisés, l'un basé sur un échantillon numérique alors que l'autre utilise des enregistrements d'effets du trafic mesurés. La précision des méthodes investiguées est évaluée à l'aide de statistiques bien connues, telles la déviation ou la norme 2 de l'erreur, pour les valeurs caractéristiques et la probabilité de défaillance. En général, les méthodes ont de moins bons résultats quand elles sont appliquées aux probabilités de défaillance qu'aux valeurs caractéristiques, mais ceci n'est peut-être qu'une conséquence des faibles probabilités recherchées (10^{-6} par an). Même si aucune des méthodes ne donne des résultats vraiment corrects en utilisant 1000 jours de données, les méthodes utilisant la queue de distribution, et en particulier celle des dépassements de seuil, donnent les meilleurs résultats. Plus de détails sur les résultats obtenus peuvent être trouvés dans le chapitre 2.

Sachant que les chapitres 1 et 2 ont montrés que la méthode des dépassements de seuils semblent donner des résultats meilleurs à ceux des autres, nous nous sommes intéressés à cette solution dans le chapitre 3 : en effet, le chapitre 1 nous a permis de découvrir que les méthodes statistiques utilisées dans le domaine des effets du trafic sur les ouvrages sont peu évoluées par rapport à celles que l'on peut trouver dans d'autres domaines, tels l'hydrologie avec la hauteur de crues ou la climatologie. En utilisant ces autres méthodes dans le chapitre 2, nous avons remarqué que la méthode des dépassements de seuil semble donner de meilleurs résultats. Cette méthode n'a été que très peu utilisée dans le domaine des effets du trafic sur les ouvrages. La théorie mathématique nous apprend que ces dépassements au-dessus d'un seuil, correctement choisis, peuvent être assimilés à une distribution statistique qui appartient à la famille de la distribution de Pareto généralisée. Pourtant des facteurs impactent l'utilisation de cette méthode, tels le choix du seuil, la taille et la précision des données disponibles, les critères pour identifier les pics indépendants. Ainsi dans le chapitre 3, nous étudions l'impact du choix des paramètres pour l'application de cette méthode et la précision des résultats obtenus. En effet, dans la bibliographie, un nombre impressionnant de méthodes d'estimation des paramètres a pu être déterminé, et leurs performances respectives sont différentes, selon le choix du seuil par exemple. Les méthodes les plus connues sont celles du maximum de vraisemblance la méthode des moments et la méthode des moments à poids, qui ont chacune leurs avantages et inconvénients. Par exemple, la méthode des moments est facile à utiliser mais se limite à des distributions dont le paramètre de forme est inférieur à 0.5. Ainsi dans le chapitre 3, nous présentons les conditions, les hypothèses, les avantages et les inconvénients de chacune de ces méthodes. En particulier, nous discutons de leur applicabilité au phénomène des effets du trafic dans les ouvrages. Les méthodes étudiées sont : la méthode des moments, la méthode des moments à poids, le maximum de vraisemblance, Le maximum de vraisemblance pénalisé, le minimum de divergence de la densité, la méthode du fractile empirique, le maximum d'adaptation, le moment de vraisemblance. Pour illustrer le comportement et la précision de ces méthodes, trois études ont été conduites : des données issues de simulations numériques, des effets du trafic simulés par Monte Carlo et des effets du

trafic mesurés sur un ouvrage réel sont présentés et analysés. Des comparaisons sont alors réalisées pour investiguer la précision et les divergences entre les résultats donnés par les différentes méthodes. Conformément à notre attente, les estimateurs ont des performances différentes. De plus, les performances d'un même estimateur diffèrent selon l'étude considérée. La conclusion générale que nous pouvons faire est qu'aucune méthode n'est meilleure que toutes les autres dans tous les cas. Mais des recommandations peuvent être faites : pour une étude avec des données numériques, la méthode des moments et celle des moments à poids sont conseillées pour des distributions avec des paramètres de forme négatifs, en particulier si la taille de l'échantillon est faible (<200), alors que la méthode du maximum de vraisemblance est recommandée pour des paramètres de forme positifs. Pour les effets du trafic simulés, le maximum de vraisemblance et le maximum de vraisemblance pénalisé donnent de meilleures estimations de la valeur de retour de 1000 ans quand le nombre de dépassements du seuil est supérieur à 100, alors que la méthode des moments et celle des moments à poids sont meilleures quand les données à considérer sont inférieures à 100 en nombre. Finalement, l'application effectuée sur des données de trafic mesurées montre que les données aberrantes ont un impact plus que significatif sur les estimations de paramètres, puisque toutes les méthodes ne peuvent être appliquées sans problème. Les détails sur ces calculs, les résultats, les commentaires sont présentés dans le chapitre 3.

Ainsi, une conclusion du chapitre 3 est que les données aberrantes ont un impact négatif non négligeable sur les résultats. Or une raison très fréquente d'existence de celles-ci est qu'elles sont souvent issues de deux sous-populations distinctes. Or les sous-populations correspondent, dans le cas des effets du trafic dans les ouvrages, aux phénomènes de croisement ou dépassement de nombres différents de véhicules. De plus, les distributions de ces sous-populations sont différentes, ce qui est en contradiction avec l'hypothèse d'événements identiquement distribués qui est sous-jacente dans les méthodes issues de la théorie des valeurs extrêmes. Des méthodes proposant l'utilisation de distributions mixtes (gaussiennes ou valeurs extrêmes généralisées) ont déjà été proposées dans la littérature, pour modéliser les effets extrêmes du trafic. Comme nous avons expliqué précédemment la supériorité de la méthode des dépassements de seuils par rapport aux autres, nous proposons dans ce chapitre 4 une généralisation de cette méthode des dépassements de seuils vers un dépassement des seuils mixtes. Cette méthode, nouvelle d'après nos recherches bibliographiques, permet non seulement de modéliser correctement la queue de distribution mais également de tenir compte des différentes sous-populations. Une évaluation de cette méthode est réalisée à l'aide de données issues de simulations numériques. Une étude de robustesse de la méthode vis-à-vis à des données erronées est également réalisée. Les résultats indiquent que la méthode des dépassements de seuils mixtes est plus flexible que la méthode conventionnelle. De plus, en utilisant des effets du trafic simulés sur divers ouvrages de différentes portées, il semblerait que la divergence entre ces deux méthodes augmente quand la portée augmente. Ceci est logique car les phénomènes observés sont plus compliqués lorsque la portée augmente, puisque le nombre de véhicules impliqués peut changer plus facilement. Il semblerait donc que cette nouvelle méthode modélise correctement la queue de distribution des effets du trafic sur les ouvrages.

Pour des ouvrages de portées supérieures à 50m, le scénario conditionnant pour le calcul d'ouvrage est la congestion qui ne nous intéresse pas ici. Pourtant, les ponts de grande portée peuvent également souffrir de l'effet du trafic, en particulier par le phénomène de fatigue. C'est ainsi que dans le chapitre 5, nous nous intéressons sur l'effet du chargement de trafic sur les ouvrages de longue portée ayant des effets locaux. Ce qui nous intéresse particulièrement est l'effet de la position latérale des véhicules. Des enregistrements de trafic de 2010 ont été utilisés et ont montrés que la " vraie " distribution du trafic n'est pas celle recommandée par l'Eurocode 1. Ainsi pour analyser l'effet de cette différence, des éléments finis ont été utilisés pour modéliser un pont à dalle orthotrope (le viaduc de Millau). En analysant les histogrammes d'effets du trafic et le dommage induit, il a été montré que la localisation transversale des véhicules affecte de manière significative les effets induits dans les ponts. De même, connaître correctement les localisations transversales des véhicules permet de déterminer plus précisément les soudures qui seront fragilisées en premier, et donc les besoins d'inspection d'ouvrages nécessaires prioritairement.

Les méthodes d'extrapolation issues en particulier de la théorie des valeurs extrêmes ont donc été explicitées ici et analysées. Une méthode innovante, permettant de mixer les sous-populations existant dans les phénomènes enregistrés a été développée et présentée ici. Les méthodes d'estimation de paramètres ont été revues. Une conclusion générale est qu'aucune méthode n'est supérieure aux autres dans tous les cas. Il semblerait pourtant que la méthode des dépassements de seuils est la plus intéressante. Pourtant une nécessité est la banalisation de données du trafic, précises et de longueur suffisante. Ces données peuvent être obtenues par les stations de pesage en marche, dont tout un réseau est actuellement installé en France. Une évaluation correcte de l'état actuel des ouvrages existants est alors possible.

Contents

Abstract (English/Français)	iii
Résumé Long	xi
Introduction	1
Background and Motivation	1
Thesis Objective	3
Structure of Thesis	4
1 Extreme Value Modeling - A Review in Bridge Traffic Load Effects Analysis	7
1.1 Introduction	7
1.2 Extreme value Modeling	8
1.2.1 Asymptotic Models of Extremes and Block Maxima Method	8
1.2.2 Generalized Pareto Distribution (GPD) and Peaks over Threshold (POT) Method	11
1.2.3 Level Crossings and Rice's Formula	13
1.3 Collecting and using weigh-in-motion data in bridge design and assessment . .	15
1.3.1 Develop load model for bridge design or evaluation	15
1.3.2 Calibrate load model	16
1.3.3 Evaluate bridge safety	17
1.4 Extreme Values in Bridge Traffic Load Effects	18
1.4.1 Tail of Parent Distribution Method	18
1.4.2 Block Maxima Method	21
1.4.3 Peaks over Threshold Method	28
1.4.4 Level Crossing Method	30
1.5 Summary	33
2 Performances of Some Prediction Methods for Bridge Traffic Load Effects	35
2.1 Introduction	35
2.2 Simple Extreme Value Problem	35
2.3 Traffic Load Effect Problem	38
2.3.1 Effect of Prediction Methods	40
2.3.2 Effects of Timeframe	42
2.4 Conclusion	45

3	A Comparative Evaluation for the Estimators of the GPD	49
3.1	Introduction	49
3.2	Methods for estimating GPD parameters	50
3.2.1	Method of moments	50
3.2.2	Method of probability weighted moments	52
3.2.3	Maximum likelihood	55
3.2.4	Likelihood moment estimator	56
3.2.5	Maximum goodness-of-fit statistic	57
3.2.6	Elemental percentile method	58
3.2.7	Minimum density power divergence estimator (MDPDE)	60
3.2.8	Other estimation methods	62
3.3	Evaluating the performance of estimators	63
3.3.1	Numerical simulation	64
3.3.2	Monte Carlo method simulated traffic load effect data	66
3.3.3	Field measurement of traffic load effects	76
3.4	Conclusion	81
4	Mixture POT Approach to Model Extreme Bridge Traffic Load Effect	87
4.1	Introduction	87
4.2	Methodology	88
4.3	Theoretical Examples	90
4.3.1	Sample Problems and Examples	90
4.3.2	Study 1: GPD distributed sample	91
4.3.3	Study 2: GEV Distributed Sample	95
4.3.4	Study 3: Normal Distributed Sample	98
4.4	Discussion	103
4.4.1	Effect of Sample Size	103
4.4.2	Composition	104
4.5	Simulated Traffic Load Effects	106
4.5.1	Introduction	106
4.5.2	Composition of Loading Event	109
4.5.3	Distribution	110
4.5.4	Results of Simulation	122
4.6	Conclusion	123
5	Effects of Transverse Location Distribution of Vehicles on Bridge Local Effects from WIM Measurements	129
5.1	Introduction	129
5.2	Related Research	130
5.3	Measurements, Finite Element Models	131
5.3.1	Vehicle Lateral Position Collection Device	131
5.3.2	Measurements of Transverse Location of Vehicles	132
5.4	Finite Element Model	137

5.4.1	Reinforced Concrete Bridge Deck Slab	137
5.4.2	Orthotropic Bridge Deck	139
5.5	Results from Orthotropic Deck Study	142
5.5.1	Results for Transverse Bending Moment	142
5.5.2	Discussion	146
5.5.3	Fatigue Damage	148
5.5.4	Inspection Strategy	150
5.6	Conclusion	152
Conclusions		155
	Conclusion of Thesis	155
	Discussion of Future Research	157
Bibliography		170
Appendix A Weigh-in-Motion Data and its Statistical Analysis		171
A.1	WIM data	171
A.2	Cleaning Unreliable WIM Data	172
A.3	Statistical Description of WIM Data	173
A.3.1	Traffic composition	173
A.3.2	Flow Rate	176
A.3.3	Gross vehicle weight	176
A.3.4	Axle Loads	178
A.3.5	Axle Spacing	179
A.3.6	Headway Distribution	180
Appendix B Bridge Traffic Load Effect Calculation and Simulation Program		183
B.1	Introduction	183
B.2	Program Description	183
B.2.1	Algorithm for Traffic Load Effect Calculation	183
B.2.2	Flowchart	184
B.3	Traffic Files	188
B.3.1	Traffic Composition and Flow	188
B.3.2	Axle Spacing	188
B.3.3	Axle Weight	189
B.3.4	Gross Vehicle Weight	189
B.3.5	Headway	190
B.4	Output	191
B.4.1	Time History File	191
B.4.2	Histograms of Value, Level Crossing, Rainflow Cycle Counting	192
B.4.3	Block Maximum Vehicle Files	195
B.4.4	Peaks over Threshold	198
Appendix C Mixture Peaks over Threshold Method		201

Definitions

List of Terminology

Term	Definition
Probability of exceedance	probability that a given value is exceeded
Return period	an average time interval between two occurrences of a given value
Return level or Characteristic value	a value that is expected to be exceeded once in a given return period
Heavy-vehicle	vehicle having a total weight greater than 3.5 t

List of Special Symbols

Symbol	Definition
F	cumulative distribution function (CDF), other symbols like G are used also;
f	probability density function (PDF), density of CDF F ;
F^m	m^{th} power of distribution function F
F^{-1}	quantile function (qf) pertaining to the CDF F ;
$F^{[u]}$	exceedance distribution function at u (left truncation at F of u);
Φ	standard normal (Gaussian) distribution function;
$x_{i:n}$	i^{th} ordered value of data x_1, \dots, x_n (in ascending order);
\hat{F}_n	empirical distribution function;
\hat{F}_n^{-1}	empirical quantile function;
$E(X)$	mean value or expectation of a random variable X ;
$V(X)$	variance of a random variable X ;
ν	intensity of level crossing;
x_p	p^{th} quantile;
X^*	bootstrap data set generated from the data set X ;
θ	parameter or parameter vector;
$\hat{\theta}$	estimate of parameter or parameter vector;
$T(F)$	parameter as function of distribution function F ;
I_A	indicator function of the set A ;

Definitions

List of Abbreviations

Term	Definitions
df	distribution function
iid	independent and identically distributed
rv	random variable
AASHTO	American Association of State Highway and Transportation Officials
AD	Anderson-Darling test
BM	block maximum (method)
EC	Eurocode
CDF	cumulative distribution function
CDS	composite distribution statistics
CM	Camera von-Mises test
CLT	central limit theorem
EDF	empirical distribution function
EPM	elemental percentile method
EVD	extreme value distribution
EVT	extreme value theory
GEV	generalized extreme value
GMM	generalized method of moments
GP(D)	generalized Pareto (distribution)
GPWM	generalized probability weighted moments
GVW	gross vehicle weight
KS	Kolmogorov Smirnov test
LE	load effect
LM	likelihood moment
LLN	law of large number
LSM	least squares method
MC	Monte Carlo simulation method
MDPD	minimum density power divergence
MGF	maximum goodness-of-fit
ML(E)	maximum likelihood
MM	method of moments
MPOT	mixture peaks over threshold method
PDF	probability density function
PML	penalized maximum likelihood
POT	peaks over threshold (method)
PWM	probability weighted moments
OSD	orthotropic steel deck
RMSE	root-mean-square error
WIM	Weigh-in-Motion

Introduction

Background and Motivation

Road transportation is growing worldwide: in Europe, road freight transportation has increased by 36.2% between 1995 and 2010 [European Commission, 2012]. Moreover the volume of freight transport is projected to increase by 1.7% per year between 2005 and 2030 [European Commission, 2008]. In addition, road transport is the most important mode of freight transport in Europe as it transports 45.8% of goods. It is thus of vital importance to ensure highway structures availability to cater for this increasing demand in transport capacity, especially as they are aging and deteriorating due to environment aggression (corrosion, loss of resistance).

For the design of new bridges, the codified load model should guarantee all newly designed bridge to have at least a minimum safety under future traffic. Therefore, the load model should be periodically calibrated using modern collected traffic data [Fu and van de Lindt, 2006; Ghosn et al., 2012; Kwon et al., 2011a; O'Connor et al., 2001; Pelphrey et al., 2008; van de Lindt et al., 2005].

For existing bridges, the task is to assess their safety under actual and future traffic, and a prioritization of the measures necessary to ensure their structural integrity and safety. In 2002, the economic cost of bridge repair, rehabilitation and maintenance in the Europe of 27 was estimated to be in the value of 2-3 billion€annually [COST 345, 2002b]. However, the budgets used for bridge management are usually limited, for example, the total rehabilitation expenditure was evaluated in 2006 to be 635 million€whereas the annual budget of maintenance was 45 million€for national bridges in France [Cremona, 2011]. It is thus crucial to allocate the available budgets reasonably. The use of design standards for assessment is too conservative and can lead to considerable unnecessary expenditure. Indeed bridges can often be shown to be safe for the individual site-specific traffic loading to which they are subject, even if they do not have the capacity to resist the notional assessment load for the network or road class [Getachew and O'Brien, 2007; O'Connor and Eichinger, 2007; O'Connor and Enevoldsen, 2008]. Hence, a site-specific assessment is a solution to quantify the safety of an existing bridge structure. Many works have been conducted to improve the assessment on highway bridges, and the procedures for the assessments of highway structures in Europe have been proposed under the European research COST 345 [COST 345, 2002a; O'Brien et al., 2005].

In addition, to address this growth without compromising the competitiveness of European, some countries are contemplating the introduction of longer and heavier trucks, with up to 8 axles and gross weights of up to 60 t. This has the advantage of reducing the number of vehicles for a given volume or mass of freight, reducing labour, fuel and other costs. This thesis originated in the need to assess the impacts of changes in truck weight regulations on bridges safety [Ghosn and Moses, 2000; O'Brien et al., 2008; Sivakumar and Ghosn, 2009], costs [Hewitt et al., 1999] and policy [Fekpe, 1997].

Clearly, issues caused by the increasing of traffic depend on the accurate knowledge of traffic loads and traffic load effects on bridges. For assessment of existing bridges, in deterministic definition, a bridge can be considered safe when its resistance exceeds the possible experienced load effect, while a bridge is safe when the resistance is exceeded with an considerably and legally defined low probability in probabilistic definition. Whatever choice is made to conduct a deterministic or probabilistic site-specific assessment, the loading capacity and the possible loads need to be established as accurately as possible. Understanding of load carrying capacity has greatly improved in recent decades, a number of work has been carried out on methods to model the load capacity of bridges and the associated uncertainties. However, an important component of applied load effects on bridges from traffic loading has not received enough attention until recent years. To know and establish the maximum in lifetime distribution of traffic load effects is crucial to carry out the assessment of bridge structures. This can be done by using huge number of measurements [Eymard and Jacob, 1989], Monte Carlo simulation [Enright and O'Brien, 2012], and statistical analysis. Although WIM techniques have been advanced in recent years, the relative recent adoption of WIM makes it not available to obtain long term measurements. It is thus impossible to model lifetime distribution. Monte Carlo simulation can extend the size of measured data, however, it depends on the statistical model used, and thus the simulated data has the same statistical feature as the measurements.

A suitable way is to use simulation to extend the data to a certain size, then use statistics of extremes to project them to remote future. Due to the theoretical and application development in WIM techniques [Jacob, 2000; Jacob et al., 2000], even a relative short term measurement can model the statistics of traffic well. Methods have been introduced to model traffic load effects on bridges [Cremona, 2001; Nowak et al., 1993], extreme value modeling methods have just been used in recent years [Bailey and Bez, 1999; Messervey et al., 2010; Siegert et al., 2008]. Extreme value modeling techniques have become widely used in the last 50 years in many disciplines, such as extreme levels of a river in hydrology, the largest claim in actuarial analysis, the failure load of material [Cebrian et al., 2003; Holmes and Moriarty, 1999; Huang et al., 2012]. The objective of extreme value modeling is to quantify the stochastic process of observations with small probability and the extreme events outside the scope of being observed. Modeling the tails of distributions is important in bridge engineering and the study of extreme loading events in reliability analysis. Extreme value models provide an asymptotic approximation for the tail distributions, which are very flexible in terms of the allowable tail shape behaviour. The attraction of the extreme value theory based methods is that they can provide mathematically and statistically justifiable parametric models for the tail distributions, which can give reliable

extrapolations beyond the range of the observed data.

Extreme value theory has been shown to be a very useful tool in estimating and predicting the extremal behavior of traffic loads or load effects, such as predicting the 1000-year return level, Caprani et al. [2008]. However, applying extreme value models is not always straightforward and there are common issues in applications. The typical problem is the dependence of extreme data, which will lead to the feasibility problem of the model. The inherent sparsity of extremal data is another common issue, which can result in the model identification and parameter estimation problem, particularly with a complex structure. Traffic load effects are actually of this type [Caprani et al., 2008], the load effects may be induced by traffic flow with traffic volume of 5000 trucks today and 3000 trucks tomorrow. Additionally, other issues such as sampling the extremes and the choice of threshold can also be problematic. Therefore, applying extreme value models is not always straightforward and the modification of traditional extreme value models needs to be considered to minimize the impact of these issues.

Thesis Objective

The rapid increase of global economics has induced growth in transportation demand. Safety assessment appears more and more important for both investors and regulators. In this thesis, we have applied the extreme value modeling to bridge traffic load effects with application in bridge engineering and focus on solving extreme value modeling issues such as complex model structure and parameter estimation.

The available traffic data is always limited in studying traffic load effects. The live load model of AASHTO was developed based on 9250 trucks representing 2-week heavy trucks [Nowak and Hong, 1991]. The traffic load model of EC was developed based on 2 weeks traffic collected from A6 highway in France [Sedlacek et al., 2006]. Sivakumar et al. [2011] suggest to collect one year's continuous data for load modeling. However, obtaining such long term measurements is time consuming and expensive. A suitable statistical tool needs to be introduced in order to acquire reliable extreme value modeling with short term measurements. Using Monte Carlo simulation to extend the data is a recently popular way in bridge traffic load effect analysis [Enright and O'Brien, 2012], however, it should be borne in mind the limitation of the Monte Carlo simulation that the generated data have the same statistical features as the measurements. In addition, the generalized Pareto distribution based extreme value modeling method is more suitable to small size sample of extremes than the generalized extreme value distribution based block maxima method as it uses all extremes over a certain high threshold. Usually, it will use the data more efficiently. In this thesis, we try to use the generalized Pareto distribution based Peaks over threshold (POT) method to establish the extreme value model of traffic load effect. The common issues of threshold choice, especially parameter estimation, have been discussed in this thesis to propose a suitable parameter estimation method in applying POT method to traffic load effects.

Caprani et al. [2008]; Harman and Davenport [1979] point out that the traffic load effect is

not identically distributed, which violates the assumption of classic extreme value theory that the underlying distribution should be identically independently distributed [Leadbetter et al., 1983]. With respect to non-identical distribution in bridge traffic load effects, non-identical distribution needs to be addressed in extreme modeling to account for the impacts in inference. Harman and Davenport [1979] propose a mixture exponential distribution to model the extreme value, Caprani et al. [2008] propose a mixture generalized extreme value distribution. Stimulated by their works, we have aimed to explicitly model the non-identically distributed behavior of extremes for a stationary extreme time series within a mixture peaks over threshold model to avoid the loss of information. This constitutes one of the main original developments of this thesis.

In many situations, the governing traffic load effect is the possible extreme value in service period, but components like orthotropic steel decks are governed by traffic induced fatigue load effects. In this thesis, we have attempted to explore the influence of traffic load on the fatigue behavior of orthotropic steel decks, especially the influence of the loading position in terms of transverse location of vehicle.

Structure of Thesis

The thesis focuses on applying statistical techniques in extreme value modeling on safety assessment in bridge engineering studies. The research presented in the thesis involves a variety of statistical methods, including extreme value theory. The relevant background, extreme value theory, and related applications in bridge traffic load effect are reviewed in Chapter 2. At the start of each chapter, a detailed literature review of relevance to only the corresponding chapter is given.

Chapter 2 reviews the relevant background to this work. Particular attention is given to the extreme value theory and the applications of extreme value modeling in bridge traffic load effects.

Many difference extreme value extrapolation methods have been used for traffic load effects as summarized in Chapter 2. A quantitative investigation of these methods is carried out in Chapter 3 through two extreme value samples. One is a numerical simulation sample, and another is Monte Carlo simulated traffic load effect sample. The performance of the methods are therefore evaluated and some suggestions are given to improve their applicability.

The qualitative and quantitative evaluation in Chapter 2 and 3 indicate that the seldom used peaks over threshold (POT) method has well performance in modeling extreme traffic load effect. A further exploration is carried out on this method. The use of POT method is limited by threshold choice and parameter estimation. We decided to pay our attention on parameter estimation methods. There are a number of parameter estimation methods available in the literature. Each method has its advantages and disadvantages, these are shown in Chapter 4. The performance of the parameter estimation is also evaluated by applying them to numerical

simulation data, simulated traffic load effect and monitored load effects.

A new method is proposed in Chapter 5 to simultaneously model both tails using GPD and to account for the non-identically distribution feature of traffic load effects. More specifically, we define a mixture generalized Pareto distribution with certain components corresponding to different types of loading events. The proposed method is firstly examined by using numerical simulation sample. Its performance is reported and comparison with standard POT is presented in this chapter. Furthermore, the proposed method is applied to traffic load effects data. The load effects and corresponding information of loading event are obtained by passing the WIM data or synthetic traffic data over influence lines.

Bridge structural components like orthotropic steel deck encounter fatigue problems rather than ultimate limit state problems, therefore traffic induced fatigue load effects are concerned. In Chapter 6, the influence of distribution of transverse location of vehicles on load effects on bridge decks like orthotropic steel decks and reinforced concrete bridge decks are evaluated through statistical analysis of load effects and fatigue damage analysis.

The conclusions drawn from this work are presented in Chapter 7 along with areas in which further research may be directed.

1 Extreme Value Modeling - A Review in Bridge Traffic Load Effects Analysis

1.1 Introduction

The objective of extreme value modeling is to quantify the outcome of a stochastic process for events which have a small probability of occurring and even to extrapolate outside the scope of observations. The issue belongs to extreme value statistics, which has been an important and extensively developed branch of the statistics in the last 60 years. Since they have been developed, extreme value techniques have been extensively used in many disciplines such as the hydrology [Deidda, 2010], insurance [Cebrian et al., 2003], and structural engineering [Pisarenko and Sornette, 2003]. Of course, they have been used in civil engineering, for instance traffic load effect [Messervey et al., 2010], wind loading [Holmes and Moriarty, 1999]. In the definition of live load for design or the evaluation of bridge safety, a critical step is to estimate maximum traffic load or load effects for long return period that represent the events possible occur in future during the expected life span or operational period of structures. The extrapolation for the tail behavior is performed by the asymptotic extreme value theory (EVT) which supplies the asymptotic justified distribution for extrapolating the underlying data generating process for these extremes providing a flexible and simple parametric model for capturing tail-related behaviors.

The study of extreme traffic load or load effects on bridges is important for bridge design and assessment. The increase of traffic demand, evolution of truck configuration and degradation of structural loading capacity have stimulated the interest in accurate modeling. In this thesis, extreme value modeling in the traffic loads or load effects on bridge is of interest, especially we are interested in estimating characteristic values for long return period. In this chapter, we review the extreme value theory and modeling with focus on traffic load effect applications with the discussion of issues in applying extreme value modeling in bridge traffic load effect.

The rest of this chapter is organized as follows: Section 1.2 reviews the EVT based distributions and Rice formula. Section 1.3 reviews the use of WIM data in bridge engineering. A review on modeling extreme bridge traffic loads is given in Section 1.4. Section 1.5 summarizes the chapter.

1.2 Extreme value Modeling

1.2.1 Asymptotic Models of Extremes and Block Maxima Method

Let X_1, \dots, X_n be a sequence of independent random variables having a common distribution function F , and let M_n be the maximum value of this sequence:

$$M_n = \max\{X_1, \dots, X_n\}. \quad (1.1)$$

In theory, there is no difficulty in writing down the distribution function of M_n exactly for all values of n :

$$\begin{aligned} Pr\{M_n \leq x\} &= Pr\{X_1 \leq x, \dots, X_n \leq x\} \\ &= Pr\{X_1 \leq x\} \times \dots \times Pr\{X_n \leq x\} \\ &= \{F(x)\}^n. \end{aligned} \quad (1.2)$$

From Eq. (1.2), it is straightforward to obtain the maximum value distribution by raising the parent distribution to a certain power. However, the distribution function F is always unknown in practice, it is thus needed to estimate F from observed data, and then to obtain the maximum distribution by substituting this estimate into Eq. (1.2). Due to the need to raise the parent distribution function to a certain power, it may lead to an unaccurate estimation of F^n if the estimate \hat{F} is unsufficiently accurate, and only the upper tail governs the behavior of extreme value, see Figure 1.1. For example, to estimate the daily maximum distribution of traffic load effects induced by traffic from a site of 5000 average daily traffic (ADTT), it is needed to raise the parent distribution to a power of 5000. It is clear that majority of F^n will suddenly lead to 0. The F needs to be close to 1 or larger than 0.999539 for F^n to be greater than 0.1, and more accuracy of F is required to well approximate the upper tail of F^n .

Fortunately, the advance in the discipline of *statistics of extreme* makes it possible to estimate the distribution of M_n . In fact, one does not have to know the df, F precisely to obtain the distribution of M_n as it can be obtained through asymptotic theory. If the distribution belongs to maximum attraction domain (Table 1.1 gives the commonly used maximum attraction domain.), the F^n , for any distribution function, F , converges to three types of extreme value distributions, Gumbel, Frechet and Weibull distributions (see Figure 1.2) as follows:

$$\text{Type I: Gumbel} \quad G(x) = \exp \left\{ -\exp \left[-\left(\frac{x-\mu}{\sigma} \right) \right] \right\} \quad \text{for } -\infty < x < \infty. \quad (1.3)$$

$$\text{Type II: Frechet} \quad G(x) = -\exp \left[-\left(\frac{x-\mu}{\sigma} \right)^{-\alpha} \right] \quad \text{for } x > \mu. \quad (1.4)$$

$$\text{Type III: Weibull} \quad G(x) = -\exp \left[-\left(\frac{x-\mu}{\sigma} \right)^{\alpha} \right] \quad \text{for } x < \mu. \quad (1.5)$$

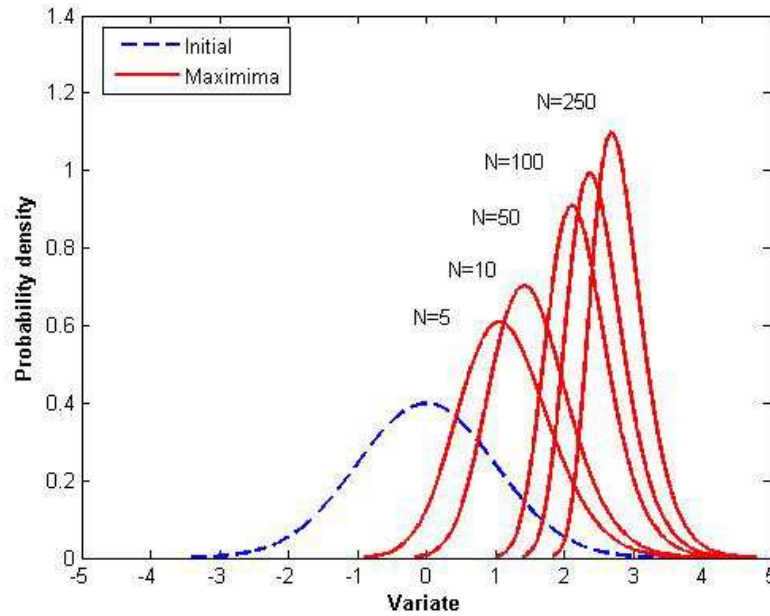


Figure 1.1: Raising distribution to a power

for parameters $\sigma > 0$, μ and in case of types II and III, $\xi \neq 0$.

Table 1.1: Domains of Attraction of the Most Common Distributions

Distribution	Domain Attraction	
	Maximum	Minimum
Exponential	Gumbel	Weibull
Lognormal	Gumbel	Gumbel
Gamma	Gumbel	Weibull
Gumbel	Gumbel	Gumbel
Uniform	Weibull	Weibull
$Weibull_M$	Weibull	Gumbel
$Frechet_M$	Frechet	Gumbel
M=maxima m=minima		

In early applications of extreme value theory, it was usual to adopt one of the three types, and then to estimate the relevant parameters of that distribution. But there are two weaknesses: first, a technique is required to choose which of the three families is most appropriate for the data at hand; second, once such a decision is made, subsequent inferences presume this choice to be correct, and do not allow for the uncertainty such a selection involves, even though this uncertainty may be substantial. These three families were combined into a single distribution by von Mises [1936] (see Jenkinson [1955] for an explanation in English), now

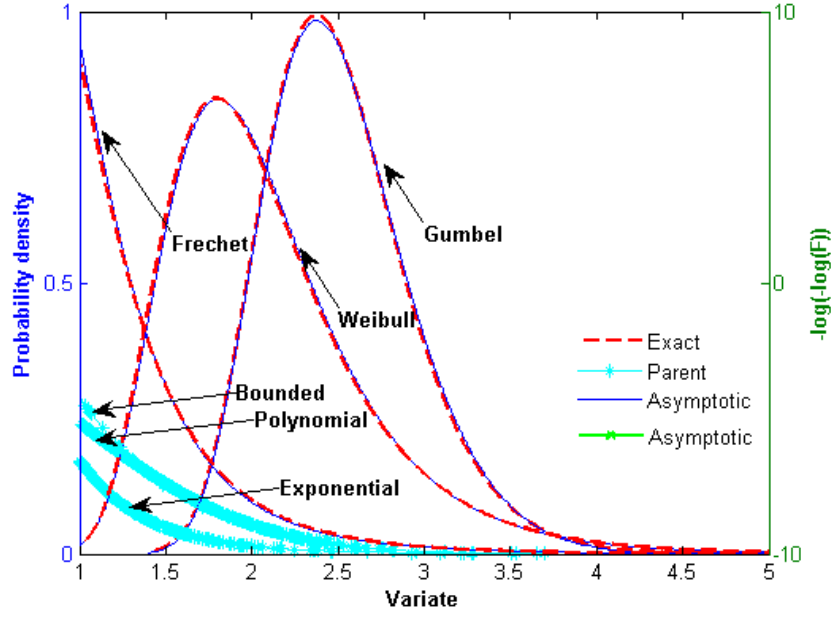


Figure 1.2: GEV distribution

universally known as the generalized extreme value (GEV) distribution:

$$G(x; \xi, \sigma, \mu) = \exp \left\{ - \left(\frac{x - \mu}{\sigma} \right)^{-1/\xi} \right\}, \quad (1.6)$$

defined on the set $\{z : 1 + \xi(z - \mu)/\sigma > 0\}$, where the parameter satisfy $-\infty < \mu < \infty$, $\sigma > 0$ and $-\infty < \xi < \infty$. It has three parameters: a shape parameter, ξ ; a location parameter, μ ; a scale parameter, σ . The type II and type III classes of extreme value distribution correspond respectively to the cases $\xi > 0$ and $\xi < 0$ in this parameterization. The subset of the GEV family with $\xi = 0$ is interpreted as the limit of Eq. (1.6) as $\xi \rightarrow 0$, leading to the Gumbel family as Eq. (1.3).

As the GEV is an approximation for maximum, M_n , of n observations, it thus suggests the use of GEV family for modeling the distribution of long sequences. Let x_1, x_2, \dots be a series of independent observations. Data are blocked into sequences of observations of length n generating a series of block maxima, $M_{n,1}, \dots, M_{n,m}$ as

$$M_{n,i} = \max \{x_{i,1}, \dots, x_{i,n}\}. \quad (1.7)$$

These block maxima M_n s can fit to GEV distribution, this method is called block maxima method (BM). In practice, the BM is often used to model extremes of natural phenomena such as river heights, sea levels, stream flows, rainfall and air pollutants, in order to obtain the distribution of daily or annual maxima.

The inverse of the distribution function of GEV for the maxima, $G^{-1}(1 - p)$ represents the quantile of $1 - p$, here p is the small probability as $P(x > x_p) = p$, which can be calculated as:

$$x_p = \begin{cases} \mu - \sigma \log[-\log(1 - p)], & \text{for } \xi = 0, \\ \mu - \frac{\sigma}{\xi} \left\{ 1 - [-\log(1 - p)]^{-\xi} \right\}, & \text{for } \xi \neq 0. \end{cases} \quad (1.8)$$

x_p is also known as return level with the return period of $1/p$. For example, if the GEV represents yearly maximum distribution, then x_p is the $\frac{1}{p}$ -year return level. It can be interpreted as it will appear an extreme value greater than the return level x_p once every $1/p$ period (e.g., years) on average, or as the mean time interval between specific extremal events. In traffic load effect on bridges, x_p is known as the characteristic value to denote the maximum possible load or load effect within a certain period $1/p$. For example, an allowed maximum load effect for a period of 50 years should not be greater than R_p , which is assumed to have a probability of exceedance of 5% in the 50 years. This implies that a return level of R_p with a return period 1000 years ($p = 0.001$) as solved for $P(LE(R_p) \leq 50) = 1 - (1 - p)^{50} = 0.05$, and $LE(R_p)$ denotes the time of first exceedance which assumed a Bernoulli distribution.

1.2.2 Generalized Pareto Distribution (GPD) and Peaks over Threshold (POT) Method

It should be noticed that the BM method does not use information efficiently and correctly. Only the maximum were kept in each block or epodic. Even if there are second, third largest values larger than the selected maxima in some blocks, these second, third largest values will not be considered to model maximum value distribution. See Figure 1.3 for example, more extremes are used by POT than BM method. If the block where the maximum is taken has a large sample size, m , then an extreme value distribution function can be accurately fitted to the actual df F^m of the maximum. Yet, one must cope with the disadvantage that the number of maxima, k , is small. Therefore there is a risk that some important data are discarded: if two unrelated extreme loading events occur in the same block of time, only one of the resulting load effect is retained. In such a case, the POT approach would retain both as valid data.

As been noted, POT approach is to use, instead of block maxima, all exceedances over a high threshold, u . This threshold method has been developed by hydrologists over the last 40 years. Early versions of the method assumed a non-homogeneous Poisson process to model the times of exceedances over the high thresholds in conjunction with independent exponentially distributed excesses. The first systematic developments are in Todorovic and Zelenhasic [1970]. This approach was generalized in Davison and Smith [1990] where excesses, $X - u$, are modeled as independent generalized Pareto random variables. The cumulative distribution function of the GPD with shape and scale location parameters ξ and σ , respectively, is defined

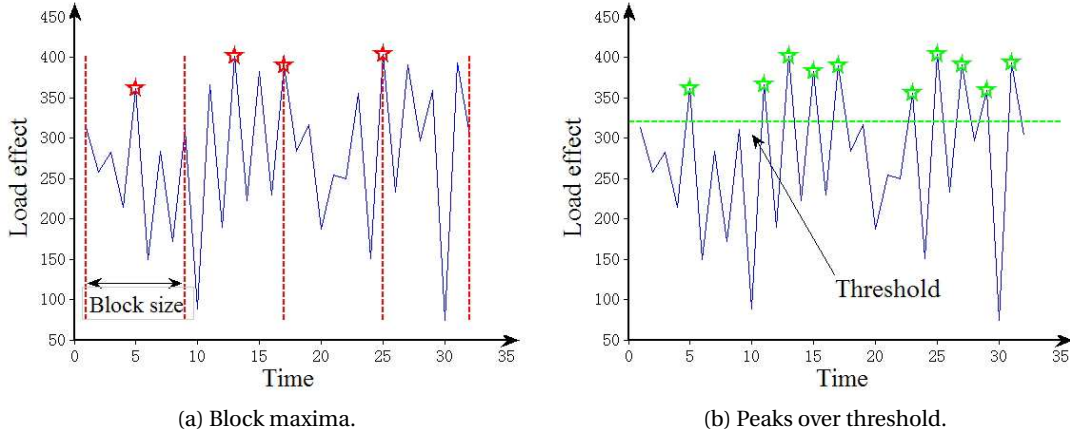


Figure 1.3: Extreme value modeling methods: block maxima and peaks over threshold

as

$$F(x|\xi, \sigma, u) = \begin{cases} 1 - \left[1 + \frac{\xi(x-u)}{\sigma} \right]^{-1/\xi}, & \text{for } \xi \neq 0, \\ 1 - \exp\left(-\frac{x-u}{\sigma}\right), & \text{for } \xi = 0. \end{cases} \quad (1.9)$$

and its probability density function (pdf) is

$$f(x|\xi, \sigma, u) = \begin{cases} \frac{1}{\sigma} \left[1 + \frac{\xi(x-u)}{\sigma} \right]^{-1/\xi}, & \text{for } \xi \neq 0, \\ \frac{1}{\sigma} \exp\left(-\frac{x-u}{\sigma}\right), & \text{for } \xi = 0. \end{cases} \quad (1.10)$$

For $\xi \leq 0$, the distribution function is defined in the range of $[u, \infty]$, while for $\xi < 0$, the range is $[u, u - \frac{\sigma}{\xi}]$. Similarly to GEV distribution, there are three types of tail distributions associated with GPD depending on the shape parameter value. When $\xi \rightarrow 0$, the GPD converges to exponential distribution. If $\xi > 0$, the excesses above the threshold have a slowly decaying tail and no upper bound. In contrast, the distribution of excesses has an upper bound of the distribution if $\xi < 0$. Therefore, the shape parameter of GPD is dominant in determining the qualitative behavior of the tail.

Similar to the GEV, the inverse of distribution function of GPD for the upper tail, $H^{-1}(1-p)$ represents the quantile of $1-p$ for the excess over threshold, here p is the small probability of exceedance as $P(x > x_p) = p$. Given that $x > u$, the conditional quantile or return level of x_p can be calculated as:

$$x_p = \begin{cases} u - \frac{\sigma}{\xi} (1 - p^{-\xi}), & \text{for } \xi \neq 0, \\ u - \sigma \log(p), & \text{for } \xi = 0. \end{cases} \quad (1.11)$$

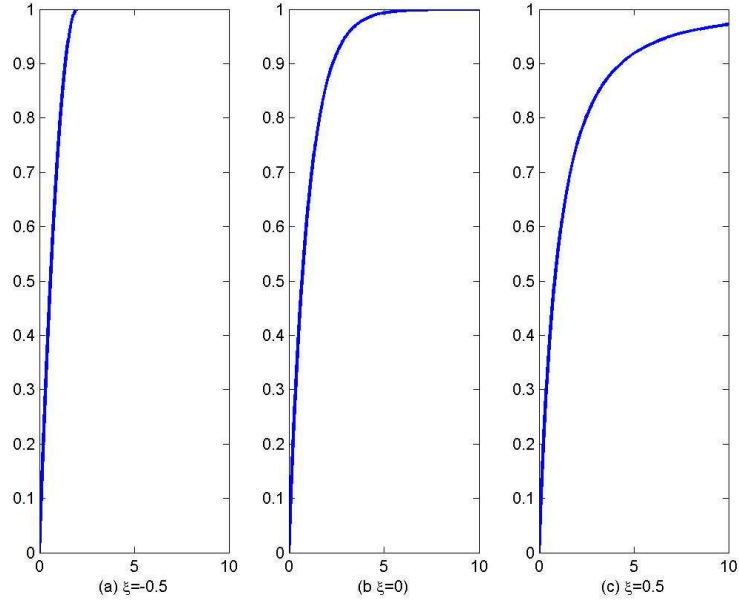


Figure 1.4: Cumulative distribution function for generalized Pareto distribution

According to

$$\begin{aligned}
 Pr\{X > u + y | X > u\} &= \frac{Pr\{X > u + y\}}{Pr\{X > u\}} \\
 &= \frac{1 - F(u + y)}{1 - F(u)} \\
 &\approx 1 - H(y; \xi, \sigma, u),
 \end{aligned} \tag{1.12}$$

assuming $Pr(X > u) = \zeta_u$, the unconditional return level of x_m is given by:

$$x_m = \begin{cases} u - \frac{\sigma}{\xi} [1 - (p/\zeta_u)^{-\xi}], & \text{for } \xi \neq 0, \\ u - \sigma \log(p/\zeta_u), & \text{for } \xi = 0. \end{cases} \tag{1.13}$$

For bridge traffic load effect, the quantile x_m refers to the maximum load effect within $1/p$ period.

1.2.3 Level Crossings and Rice's Formula

In the previous section we have answered the question of the distribution of the maxima of n iid random variables. We will now consider extremal properties of stochastic processes $X(t, t \in R)$ whose index set are the positive real numbers. The theory of stochastic processes

provides a useful tool for analyzing civil engineering structures subjected to random loadings, such as the static response of highway bridges under random truck loading.

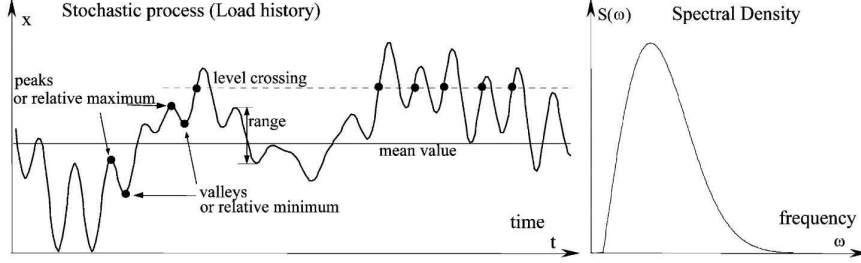


Figure 1.5: Principal parameters of a stochastic proces

In practice, level crossing counting is often used to describe the extremal behavior of a continuous stochastic processes. Since it is often easier to find the statistical properties of the number of level crossings than to find the maximum distribution, level crossing methods are of practical importance. For sample functions of a continuous process $\{X(t), t \in R\}$ we say that $X(t)$ has an upcrossing of the level u at t_0 if, for some $\epsilon > 0$, $X(t) \leq u$ for all $t \in (t_0 - \epsilon, t_0]$ and $X(t) \geq u$ for all $t \in (t_0, t_0 + \epsilon]$. For any interval $I = [a, b]$, write $N_I^+(x, u)$ for the number of upcrossings of level u by $x(t)$ in I ,

$$N_I^+ = N_I^+(x, u) = \text{the number of } u\text{-upcrossings by } x(t), t \in I.$$

By the *intensity of upcrossings* we mean any function $\nu_t^+(t)$ such that

$$\int_{t \in I} \nu_t^+(u) dt = E[N_I^+(x, u)].$$

For a stationary process, $\nu_t^+(u) = \nu^+(u)$ is independent of t . In general, the intensity is the mean number of events per time unit.

In reliability applications of stochastic processes one may want to calculate the distribution of the maximum of a continuous process $X(t)$ in an interval $I = [0, T]$. The following approximation is then often useful, and also sufficiently accurate for short intervals,

$$\begin{aligned} P(\max_{0 \leq t \leq T} X(t) > u) &= P(\{X(0) \leq u\} \cap \{N_I^+(x, u) \geq 1\}) + P(x(0) > u) \\ &\leq P(N_I^+ \geq 1) + P(x(0) > u) \\ &\leq E(N_I^+(x, u)) + P(x(0) > u) \\ &= T \cdot \nu^+(u) + P(x(0) > u). \end{aligned} \tag{1.14}$$

Studies on level-crossings in stationary Gaussian processes began about sixty years ago. Different approaches have been proposed. The intensity function of upcrossings, $\nu^+(u)$, were

1.3. Collecting and using weigh-in-motion data in bridge design and assessment

obtained by Rice [1944, 1945] for Gaussian processes, and the function is named in the literature Rice's formula as expressed:

$$v^+(u) = \frac{1}{2\pi} \frac{\sigma_{\dot{X}}}{\sigma_X} \exp\left(-\frac{(u - \mu_X)^2}{2\sigma_X^2}\right) = \frac{1}{2\pi} \left[\frac{-R_X''(0)}{R_X(0) - \mu_X^2} \right]^{0.5} \exp\frac{-(u - \mu_X)^2}{2[R_X(0) - \mu_X^2]}. \quad (1.15)$$

where t =time; $X = X(t)$, a continuous stationary normal process; u =a fixed threshold level; v^+ =instaneous up-crossing rate of X over u , a constant due to the stationarity of X ; $\dot{X} = \dot{X}(t)$, the derivative process of X ; μ_X =the mean of X ; R_X =the autocorrelation function of X ; R_X'' =the second-order derivative function of R_X ; σ_X =the standard deviation of X ; and $\sigma_{\dot{X}}$ =the standard deviation of \dot{X} . See more details of the derivation of the formula in Rice [1944, 1945]. Note that down crossings and up crossings are studied in the same way.

For the stationary stochastic process, the mean number of upcrossings over a period, R_t , is, $R_t \cdot v^+(u)$. According to the definition of return period, R_t , which is the mean period between two occurrences of the value x , the return level can be obtained using the concept of level crossing:

$$R_t \cdot v^+(u) = R_t \frac{1}{2\pi} \frac{\sigma_{\dot{X}}}{\sigma_X} \exp\left(-\frac{(u - \mu_X)^2}{2\sigma_X^2}\right) = 1, \quad (1.16)$$

thus, the return level for the return period R_t is:

$$u = \mu_X \pm \sigma_X \sqrt{-2 \log \left[\frac{2\pi \sigma_X}{R_t \sigma_{\dot{X}}} \right]} \quad (1.17)$$

1.3 Collecting and using weigh-in-motion data in bridge design and assessment

Weigh-in-Motion of road vehicles is essential for the management of freight traffic, road infrastructure design and maintenance and the monitoring of vehicle and axle loads. Literature for the collection, analysis and application of bridge-related WIM data concern all topics for example bridge health monitoring, validation of legislation and regulation. According to the cope of this thesis, this literature review concentrated on the following WIM data research topics concerning the use of WIM to: (a) develop load model for bridge design or evaluation; (b) calibrate current used load model; (c) evaluate safety of bridge; (d) study the evolution of traffic like the growth in truck weights.

1.3.1 Develop load model for bridge design or evaluation

Nowak and Hong [1991] use truck measurements to develop a probability based live load model for bridge design. The traffic database consists of 9250 heavily trucks representing 2

weeks traffic that was collected in 1975 at Ontario. Followed Nowak's method, Kozikowski [2009] develop a live load model for highway bridges based on newly collected WIM data. Three types of live load models were developed: heavy, medium, and light. The basis for the preparation of the traffic loads model in EN 1991-Part 2 has been developed in parallel at various locations in Europe with studies performed at SETRA, LCPC, University of Pisa, University of Liege, RWTH Aachen, TU Darmstadt, Flin & Neil, London. In order to determine the target values, researchers from these institutions independently studied the effect values that should reproduce the future European load system by considering various traffic scenarios based on traffic measurements at Liege, Paris, Pisa and Aachen [Sedlacek et al., 2006]. [Miao and Chan, 2002] use 10 years Hong Kong WIM data collected by WIM station located at Tolo Highway, Tun Mun Road, Lung Cheung Road, Island Eastern Corridor, and Kwai Chung Road to derive highway bridge live load models for short span (less than 40 m) bridges.

1.3.2 Calibrate load model

Fu and van de Lindt [2006]; Kwon et al. [2011a,b]; Pelphrey and Higgins [2006]; Pelphrey et al. [2008]; van de Lindt et al. [2005] use WIM data to calibrate live load factors for use on state-specific bridges. Pelphrey and Higgins [2006]; Pelphrey et al. [2008] use WIM data that collected at four WIM sites in Oregon state, including state and interstate routes, considering possible seasonal variation, and different WIM data collection windows. Kwon et al. [2011a,b] use WIM data that collected at WIM sites in Missouri to calibrate live load factor for Strength I Limit State in the AASHTO-LRFD Bridge Design Specifications. 105 of representative bridges are selected considering number of spans, maximum span length, and number of lanes. Approximately 41 million WIM data were collected from 24 WIM stations in Missouri. Based on the evaluated distribution of 75-year maximum live load, dead load, and minimum required resistance, reliability analyses were carried out and live load calibration factors proposed as a function ADTT (average daily truck traffic). Results of first stage reliability analysis show that most reliability indexes for positive moments and shear forces are higher than the target reliability index of 3.5. van de Lindt et al. [2005, 2002] present the process and results to examine the adequacy of current vehicle loads used to design bridges in the State of Michigan. Reliability indices were calculated for twenty different bridges selected randomly from the Michigan inventory of new bridges including types of steel girder, prestressed I-beam, prestressed adjacent box-girder, and prestressed spread box girder. WIM data procured from nine different bridge site belonging to five different functional classes in the Detroit area was processed to statistically characterize the truck load effect. To cover the variation of truck traffic volume, two values of truck traffic were used in the reliability analysis. The reliability indices were calculated for two cases of traffic: entire state of Michigan and Metro Region. The reliability indices were found to vary from bridge type to bridge type. Finally, the authors recommend that a new design load level be considered for bridge beam design in the Metro Region. A continuous research project [Fu and van de Lindt, 2006] was conducted to determine what scaling of the HL93 bridge design load configuration will provide Michigan's truckline bridges designed using the LRFD bridge design code a consistent reliability index of 3.5. 20 typical

1.3. Collecting and using weigh-in-motion data in bridge design and assessment

bridges as same as the pervious study [van de Lindt et al., 2005, 2002] were used again. Five years of truck data were procured from MDOT's Bureau of Transportation Planning, Asset Management Division. The data was organized again into 5 functional classifications of roadway. The total number of trucks was approximately 101 million. Critical load effects were calculated by using these recorded WIM data. The target reliability index used in AASHTO LRFD code was utilized in the study as the criterion for evaluating the adequacy. Reliability indices were calculated for the twenty selected bridges. The calibration results show that for the Metro Region, bridge design requires an additional live load factor of 1.2 to provide a reliability index consistent with the rest of the state. For the recommened live load increase for the Metro Region, a cost impact of 4.5% was estimated in order to achieve the higher bridge capacity.

1.3.3 Evaluate bridge safety

Fu and You [2009] evaluated the bridge capacity using WIM data gathered from stations on highways in three provinces of China. The WIM data were collected continuously over 1-16 months in 2006 and 2007. But the time stamp is 1 second, which is impossible to estimate simultaneous presence of trucks on a bridge span of short- or medium-length. A set of WIM consisting of data from five New York stations were used to investigate the behaviour of simultaneous truck presence. The data were processed and projected to model the live-load spectrum over 3-year and 100-year periods, respectively. The former is the required bridge inspection interval and the latter the bridge design lifetime, according to current Chinese maintenance and design specifications. The calculated traffic load effects were projected to obtain corresponding maximum distribution functions for using to reliability assessment. Four most representative highway bridges in China, reinforced concrete beams (RC), prestressed concrete T beams (PCT), prestressed concrete box beam (PCB), and steel I beam (SI), were selected. Guo et al. [2011] present a probabilistic procedure for the assessment of the time-dependent reliability of existing prestressed concrete box-girder bridges. These bridges are subject to increased traffic loads and an aggressive enviroment, which result in structural deterioration such as cracking and corrosion. To obtain maximal vehicle loads during the remaining life of bridges, a renew load model established based on measured traffic data from WIM systems. Time-dependent corrosion models were adopted to account for pitting corrosion because of chloride attack as well as uniform corrosion because of concrete carbonation. A degenerated shell element was used for accurate and efficient modeling of the PSC box-girder. The time-dependent reliabilities were calculated by an adaptive importance sampling method.

1.4 Extreme Values in Bridge Traffic Load Effects

1.4.1 Tail of Parent Distribution Method

It is straightforward to get the maximum distribution through Eq. (1.2) if the underlying parent distribution function, F , is known. Perhaps inspired by this, the extreme value distribution is realized by finding the parent distribution in the early stage of extreme traffic load effect modeling [Jacob, 1991; Nowak and Hong, 1991]. Normal (or Gaussian) distribution [Nowak and Hong, 1991] is commonly assumed, but Gumbel distribution [Jacob, 1991] can also be adopted.

As a comparison method to predict extreme traffic loads or load effects in the background study of the development of current used Eurocode 1 traffic load model in early 1990's, the normal distributions of traffic loads or load effects were found by fitting the distribution to the upper tail of histogram using the least square method.

During the development of live load model for AASHTO LRFD code, [Nowak, 1993; Nowak and Hong, 1991; Nowak et al., 1993] have used the tail distribution method to predict the mean 75-year maximum load effects. The truck data used to predict these mean 75-year maximum level were collected over a period of approximately 2 weeks consisting of 9250 trucks [Nowak and Hong, 1991]. Due to limitation of sample size, Nowak et al. [1993] point out that the traditional histogram method can not provide a sufficient accuracy in fitting the particular important upper tails, thus the parameter estimates may not be accurate. They propose to use an alternative method, which is based on plotting the empirical CDF on normal probability paper, to fit the upper tail. Each vehicle from truck survey was run over the influence lines to determine the calculated maximum bending moment, shear force and negative moment at the interior support of two span bridges. The calculations were carried out for span length from 10 ft through 200 ft to simple span and two-span continuous bridges. The resulting cumulative distribution functions were plotted on the normal probability paper as shown in Figure 1.6. The upper tails were assumed to have normal distribution as straight lines are superimposed on them. Therefore, the effects corresponding to the probability of occurrence can be read directly from the plots. For a design lifetime of 75 years, the total number of trucks will be 15 million [Nowak and Hong, 1991] or 20 million [Nowak, 1993], and the corresponding exceedance probability are therefore $1/15000000 = 7e-8$ and $1/20000000 = 5e-8$, respectively. The return levels for various return periods from 1 day to 75 year were graphically shown in the plots.

To improve accuracy of Monte Carlo simulation of traffic loading on bridges, [O'Brien et al., 2010] have proposed to model gross vehicle weight (GVW) with a semi-parametric method, which uses the measured histogram where there are sufficient data and parametric fitting to a Normal distribution in the tail region where there are less data. The parameters of the normal distribution is estimated by the maximum likelihood method with a constraint equation:

$$|\hat{F}(x_0) - \tilde{F}(x_0)| \leq \epsilon. \quad (1.18)$$

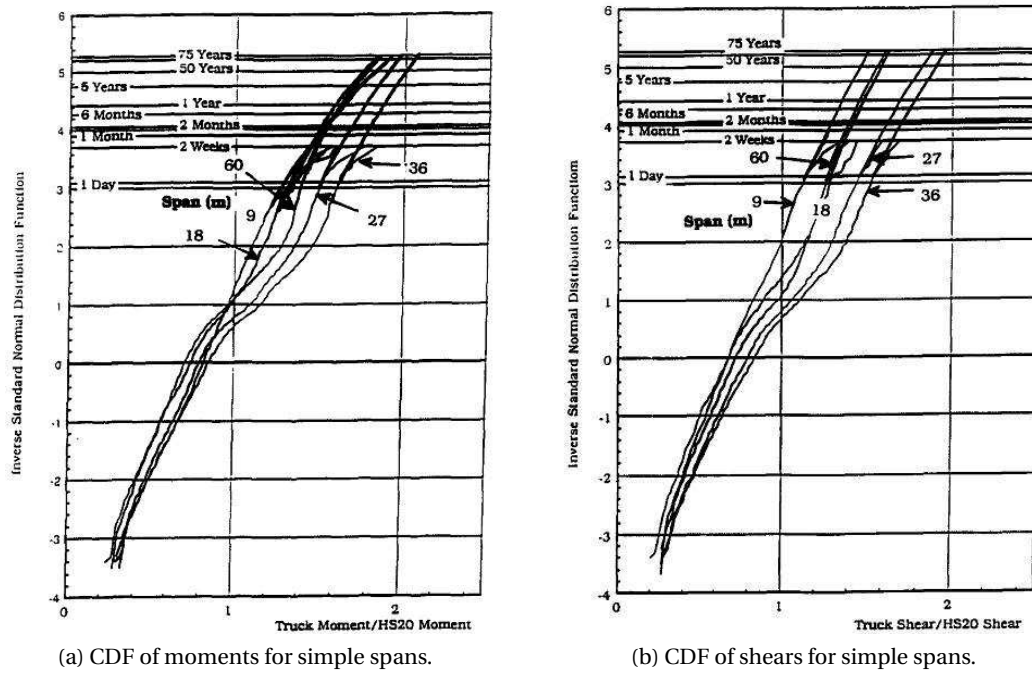


Figure 1.6: CDF of moment and shear effect on normal probability paper. Reproduced from [Nowak and Hong, 1991]

where $\hat{F}(x_0)$ is the fitted normal distribution function, ϵ is a tolerance value of a small positive number (e.g., 1×10^{-8}) and $\tilde{F}(x_0)$ is the empirical distribution function. The maximum likelihood method based fitting is compared with others like least square method and Chi-square statistic method as shown in Figure 1.7. The authors have stated that the fitting of tail of GWV has significant influence on bridge assessment.

The previous methods that extend the upper tail of CDF with a normal distribution involves a considerable dose of engineering judgement. Indeed, the load effects do not follow a normal distribution as the curves on normal probability paper do not appear as straight lines, and also for the tails (see Figure 1.8). To avoid this subjective aspect, Kozikowski [2009] proposes to use a nonparametric approach of Kernel density estimation to fit the data. The best fit to the whole data was found by using kernel function as normal and selecting certain bandwidth for the distribution of live load. However, for the important tail, trend of the end of the fit tail depended on the distance of the last point of the data set from the other points. Then the characteristic value for long return period was interpolated according to its probability of occurrence. Sivakumar et al. [2011] evaluated the performance of the normal fit of the tail method on estimating maximum load effects for long return periods (see Figure 1.9). The verification results show that the method can obtain good estimates for short return period like less than 1 month, but is not accurate enough to obtain the maximum load effect for longer return period. Therefore, an alternative more analytic and better founded method is proposed in [Sivakumar et al., 2011]. The fitted normal distribution is raised to a power to

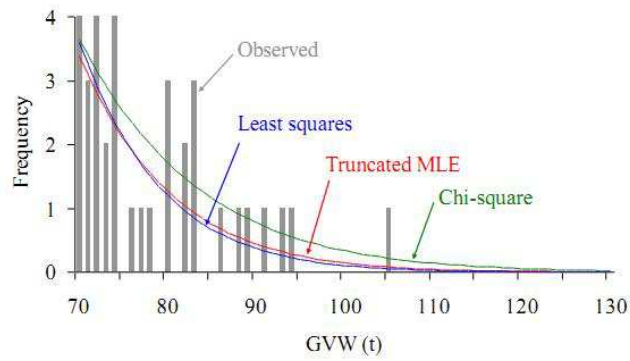


Figure 1.7: Fitting normal distribution to upper tail of GVW histogram. Reproduced from [O'Brien et al., 2010]

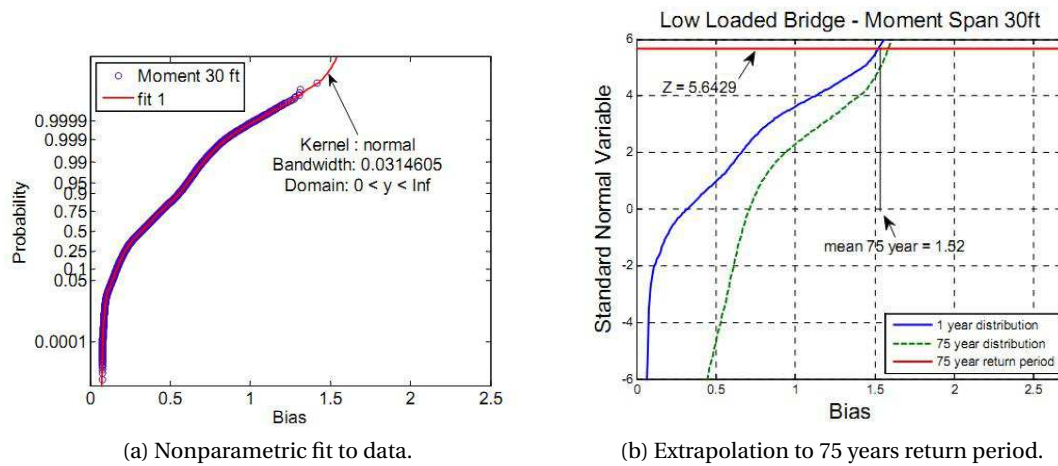


Figure 1.8: Extrapolation with nonparametric fit. Reproduced from [Kozikowski, 2009]

obtain the maximum distribution, which is the Extreme Value Type I (Gumbel) distribution according to the attraction domain. The parent distribution of the initial variable is a general normal distribution with mean, μ , and standard deviation, σ , then the maximum value after N repetitions approaches asymptotically an Extreme Value Type I (Gumbel) distribution. Its mean μ_{max} and standard deviation, σ_{max} , are derived analytically as follows related to the mean and standard deviation of parent distribution:

$$\mu_{max} = \mu + \frac{\ln N}{\pi} \sqrt{6} \sigma, \quad (1.19)$$

$$\sigma_{max} = \sigma. \quad (1.20)$$

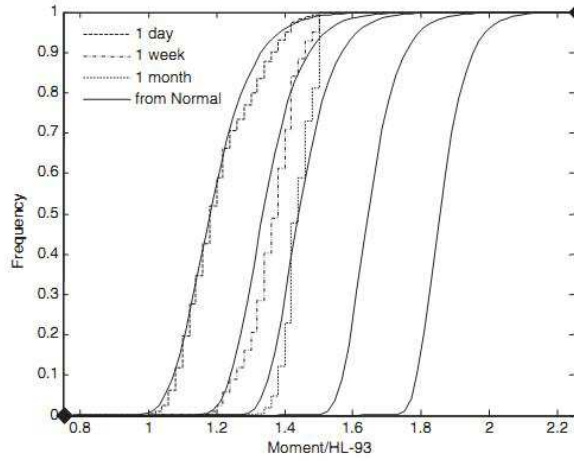


Figure 1.9: Cumulative distribution maximum load effect of single lane events for different return periods. Reproduced from [Sivakumar et al., 2011]

In Cooper [1997], histograms of 2-week traffic load effects are established from WIM data. The histograms were then converted into cumulative distribution functions (CDFs), which are then raised to a power equal to the number of daily trucks, to obtain the distribution of daily maxima. The points of the CDF of daily maxima are then plotted on Gumbel paper and a straight line is fitted. Although this approach is straightforward, it has the risk of obtaining unreasonable estimation as the CDF needs to be raised to a high power such as average daily truck traffic. 2-week WIM data is short compared with the required daily maxima distribution. However, this method can have better performance when a large amount of WIM data is available.

1.4.2 Block Maxima Method

The extreme value theory used for extrapolating data to the required/considered return period is well established. It has been widely applied to model traffic load effects on bridges in recent

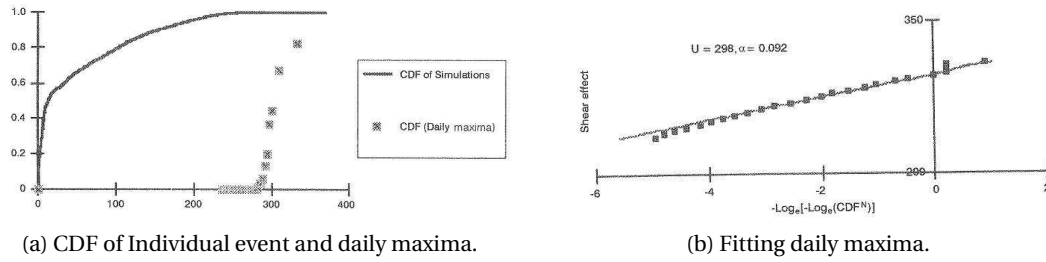


Figure 1.10: Daily maxima CDF fitted to Gumbel distribution (Reproduced from [Cooper, 1997])

years. Many authors approach the problem by identifying the maximum load effect recorded during a loading event or in a reference period such as a day or a week, and then fit these maxima to an extreme value distribution. In all cases, the fitted distributions are extrapolated to obtain an estimate of the lifetime maximum load effect. This approach is based on the assumption that individual loading events are independent and identically distributed (iid).

Standard Block Maxima Method

In the early application of BM method, it was usual to fit one of the three extreme value distributions to data of traffic loads or load effects from measurements or Monte Carlo Simulation. Due to the tail behavior, the Gumbel and Weibull distributions were the most adopted. Cooper [1997]; Grave et al. [2000]; O'Brien et al. [2003, 1995] have fitted Gumbel distribution to their data, and Bailey [1996] has used Weibull distribution to approximate his data. Both Gumbel and Weibull distributions have been investigated in Enright [2010]; Grave et al. [2000], and it seems that both methods can be used to model extreme traffic load effects. However, these two types of distribution have distinct shapes of behavior, corresponding to the different forms of tail for the underlying parent distribution function. Weibull has a finite upper bound with value of $\frac{\mu}{\sigma}$, while the tail of Gumbel distribution is infinite, see Figure 1.2. Actually, many of the governing factors like GVWs follow normal distribution or have normal distribution type tail [O'Brien et al., 2010], thus it is reasonable that the maximum distributions of load effect follow a Gumbel law. In addition, due to the length of effective influence lines or the size of influence areas, the total number of heavy-vehicles on bridges and their total weight have a finite limit, thus the induced load effects should converge to an extreme value distribution with upper bound.

However, it is hard to say which type of extreme value distribution the extreme traffic load effect belongs to. Therefore, once unsuitable type distribution is chosen, doubtful inferences are gained. A better choice is to use the unified form of extreme value distribution of GEV distribution. Through parameter estimation, the data itself determines the most appropriate type of tail behavior, and it is unnecessary to make subjective a priori judgement about which individual extreme value family to adopt. In the recent publications, GEV distribution has

been widely adopted to model traffic loads and load effects [Caprani, 2005; Gindy, 2004; James, 2003; Siegert et al., 2008].

The use of extreme value distribution to model maximum traffic loads or load effects is more rational than directly model them by some distributions like normal, but the data should be independent and identically distributed. In the literature, the block maxima of traffic loads or load effects are drawn from very different sizes of block, hourly maxima [Caprani et al., 2002; O'Brien et al., 2003], daily maxima [Caprani, 2005], weekly maxima [Siegert et al., 2008], yearly maxima [Enright, 2010]. There seems to be no criteria for determining how large or how long the interval should be to draw the maximum. The condition that block maxima can well converge to an asymptotic extreme value distribution is that the maximum should be taken out of a sample with sufficient large block size to ensure the data is independent.

Many researchers have noticed that their data do not really follow asymptotic extreme value distribution, and then the extreme value distributions are used to fit only the upper tails of their data. For instance, O'Brien et al. [2003] assume that the upper $2\sqrt{n}$ points follow Gumbel distribution.

When block maxima are well prepared, the problem to obtain well modeled distribution of load effect is decided by the estimates of the parameters of the distribution. Maximum likelihood estimation, method of moments and probability weighted moments are preferred by statisticians. However, the graphic method, which is used to check the quality of the modeling, is used widely in the papers on bridge traffic loads related topics. To determine the characteristic deflection of the Foyle Bridge, which has a total length of 866 m, O'Brien et al. [1995] used 8 minute periods of measurements taken during each 4 hour rush hour period of a day. Each day of measurement is then represented by a 48 minute sample. 155 daily samples were recorded. The authors then consider the daily maximum deflection, from which the effect induced by wind and temperature is removed, as an extreme value population. The data is plotted on a Gumbel probability paper, and the parameters of the distribution are determined directly from the plot by linear regression as shown in Figure 1.11.

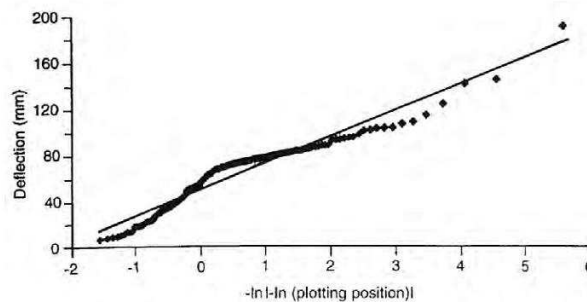


Figure 1.11: Gumbel extrapolation for the Foyle bridge, Reproduced from [O'Brien et al., 1995]

In [O'Brien et al., 2003], hourly maximum strain values are plotted on Gumbel probability paper. Through least-squares method, straight line is used to the upper $2\sqrt{n}$ data points as

shown in Figure 1.12.

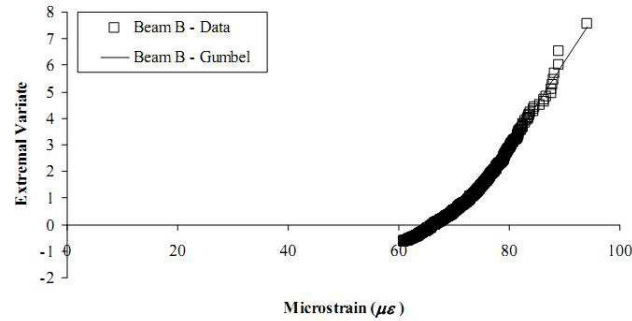


Figure 1.12: Gumbel extrapolation for the strain, Reproduced from [Grave et al., 2000]

To predict extreme load effects, Caprani et al. [2002] use a sample of two-week simulated traffic. The authors assume maxima hourly load effect induced by the traffic conform to an extreme value distribution. Hence, 240 maxima for each type of load effect are generated. Gumbel probability paper is used to determine the parameters of presumed Gumbel distribution of hourly maxima. The author then carries out a least squares fit to the upper $2\sqrt{n}$ point as suggest by Castillo. In the simulations carried out as part of his work, O'Connor [2001] has

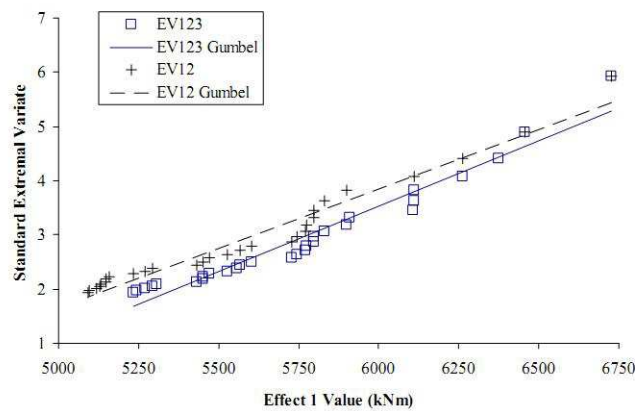


Figure 1.13: Gumbel plot of load effect, Reproduced from [Caprani et al., 2002]

fitted Gumbel and Weibull distribution to a population of 'extreme' load effects. Maximum likelihood fitting is carried out on a censored population. O'Connor [2001] has censored for the upper \sqrt{n} , $2\sqrt{n}$ and $3\sqrt{n}$ data points, and noted that different estimates of lifetime load effect result from different censoring.

Siegert et al. [2008] fit Gumbel distribution to daily or weekly maximum measurements of deformation at mid-span of a prestressed concrete bridge, which is located on a heavy trafficked highway in Northern France. The deformations at mid-span were measured during a 256 days period in 2004 and 2005. The return values for long return periods in the range from 50 years

to 1000 years are estimated by using both maximum likelihood and least squares methods. The parameter estimates are similar from both methods.

Two Steps Block Maxima Method

The reliability of extrapolation obtained by block maxima method depends on the way to use the data. In practice, the number of available data is always limited. To use the block maxima method, if the block size is large, then an EV df can be accurately fitted to the actual df F^m of the maximum. However, the smaller the number of maxima with increasing block size, the larger bias and variance are introduced to estimates for distribution parameters or quantile. More truck load data have been made in recent years due to the wide use of WIM system. As an example Gindy and Nassif [2006] have collected 11-year WIM data from sites at the State of New Jersey. It is possible to obtain more accurate parent distribution. However, the data are insufficient to ensure to obtain accurate maximum distribution when the estimated distribution has to be raised to a large power. Fu and You [2010] state that reduction of the power N can significantly lower the requirements on fitting quality for the parent distribution. To obtain the N -event maximum distribution, the authors propose to group the N measurements into n subset with sample size of M and to take out the maximum of each group, then fitting GEV distribution to the n -maxima of M -event maximum, therefore the M -event maximum distribution can be obtained and the N -event maximum is easier to obtain by raising the M -event maximum distribution to power N/M . The principle of the method is to reduce the raised power to improve the fitting accuracy. The method is applied to traffic load effects induced by traffic load collected from different sites, the difference between the proposed method and the method directly raising a large power is shown in Figure 1.14. It has been found that the difference of the estimated PDFs from the proposed method and the NCHRP 12-76 method is significant. The method proposed by Fu and You [2010] has better performance on estimating the maximum distribution. As the authors stated, the possible reason is the proposed method reduce the power needed to raise the parent distribution to obtain the maximum distribution.

Composite Distribution Statistics

Harman and Davenport [1979] state that traffic load effects are not identically distributed as the load effects are induced by different loading events, which are identified by the number of involved trucks. The histograms for load effects caused by five different types of loading event are shown in Figure 1.15. It can be seen that they are considerably different in the histograms either from the measured traffic configuration (in full line) or from simulated traffic (in dash line). Harman and Davenport [1979] have noted that each mechanism may be represented by a negative exponential function. Hence, the authors use a mixture distribution to model the upper tail of the load effect distribution, and then the maximum distribution is obtained by raising the mixture model to a given power. Caprani et al. [2002, 2008] confirm this statement

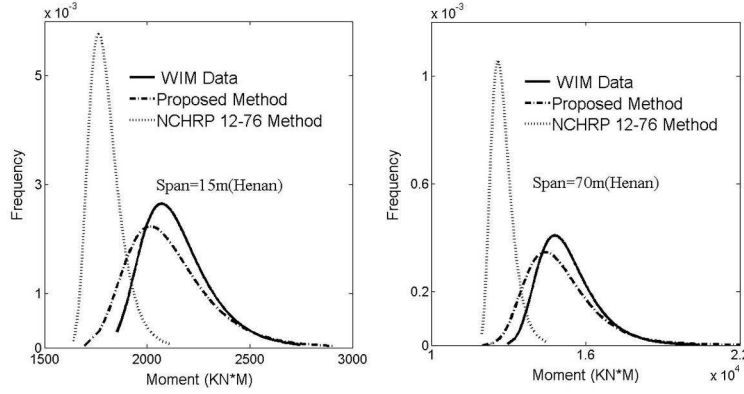


Figure 1.14: A comparison of extrapolated PDF by NCHRP 12-76 method and the two steps block maxima method for load effect, Reproduced from [Fu and You, 2010]

(see Figure 1.16), but suggest to characterize the extreme traffic load effects with a mixture models that is a linear combination of GEV distribution. The distribution of each component is obtained by fitting GEV to the daily maxima of the load effect induced by the corresponding loading events. The proposed method is applied to model traffic load effects and compared with the conventional method. Their results show that the proposed method provides much more reasonable prediction especially when the mixed distributions are quite different. As shown in Figure 1.16-b, the fitting to a single GEV is governed by mixed maxima in the range between 1600 and 1650, which are mainly from 2-truck and 3-truck event. However, the load effects from 4-truck loading events actually govern the upper tail. The difference between the conventional method and mixture distribution on characteristic value prediction are shown in Figure 1.16-c.

Other work

The relatively new theory of predictive likelihood can be used to estimate the variability of the predicted value, or predictand. Fisher [1973] is the first clear reference to the use of likelihood as a basis for prediction in a frequentist setting. A value of the predictand z is postulated and the maximized joint likelihood of the observed data y and the predictand is determined, based on a probability distribution with given parameters. The graph of the likelihoods thus obtained for a range of values of the predictand, yields a predictive distribution. Such a predictive likelihood is known as the profile predictive likelihood. Denoting a normed likelihood by $\bar{L}(\theta; x)$, this is given by:

$$L_p(z|y) = \sup_{\theta} \bar{L}_y(\theta; y) \bar{L}_z(\theta; z) \quad (1.21)$$

This formulation states that the likelihood of the predictand, z , given the data, y , is proportional to the likelihood of both the data (L_y) and the predictand (L_z) for a maximized parameter vector [Caprani and O'Brien, 2010].

1.4. Extreme Values in Bridge Traffic Load Effects

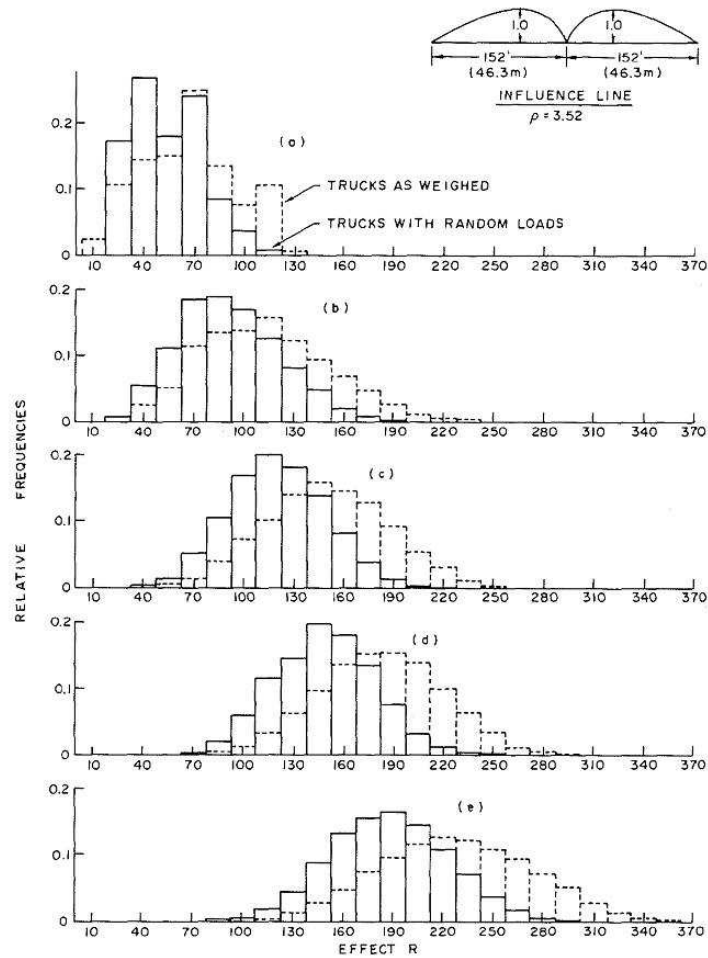


Figure 1.15: Histograms of load effect for different loading events, (a)-(e) represent 1- to 5-truck events, Reproduced from [Harman and Davenport, 1979]

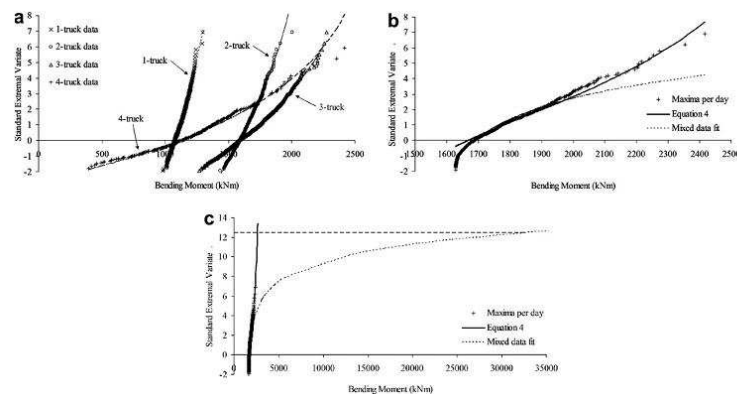


Figure 1.16: Mixture model of loading events, Reproduced from [Caprani et al., 2008]

Caprani and O'Brien [2010] use the Predictive Likelihood method proposed by Butler [1986], based on that of Fisher [1973] and Mathiasen [1979]. This Predictive Likelihood is the Fisherian approach, modified so that the variability of the parameter vector resulting from each maximisation is taken into account.

As been stated in Eq. (1.21), the main advantage of this method is that it involves the predictand like 1000-year return level into the process of parameter estimation. Therefore the estimated parameters are more suitable to estimate the maximum distribution function. However, it should be noticed, this method is very time consuming as it needs to test a number of possible predictand to find the optimal one.

1.4.3 Peaks over Threshold Method

To the best of our knowledge, GPD for the extreme traffic load effect was not addressed until the article by Crespo-Minguillon and Casas [1997]. The authors point out that: (i) the method of raising parent distribution to a power needs a large size of sample to obtain accurate parent data, (ii) the way of using information of the block maxima method is rather uneconomical, (iii) the method of fitting an extreme type I distribution to upper endpoints of maxima lacks of theoretical supporting bases and also lacks of objectiveness when setting the threshold value from where the fitting starts. The POT method is applied to weekly maxima of internal force induced by simulated traffic load. Gindy [2004] use POT method to predict maximum live load and load effect. James [2003] use POT method to analyse traffic load effects on railway bridges.

Threshold selection is an important step in the use of POT method. [Gindy, 2004] uses two typical graphical methods of mean residual life plot and stability plot of estimates of parameter. Crespo-Minguillon and Casas [1997] use a graphical method that is based on both function, $L(x_i|u, \xi, \sigma)$ and $L_i (i = 1, n)$, for different threshold, u_j , with $F_x(u_j) > 0.90$. The optimal threshold value is selected by approximating both curves. An example of fitting of a GPD to a load effect of bending moment is presented in Figure 1.17. [James, 2003] states that using only the graphical method cannot make a good decision on threshold selection. Therefore, the author proposes a hybrid method that combines graphical methods with computational methods. The mean exceedance plot was used for the first criterion, attempting to locate signs of linearity, while a plot of the estimated shape parameter versus the threshold level was used in assessing the second criterion. Figure 1.18a shows the mean exceedance plot for the 20 m span case. As one can see from this plot, linearity occurs at approximately $u = 0.42$. A plot of the estimated against the threshold level can be seen in Figure 1.18b. From this figure it can be seen that $\hat{\xi}$ remains relatively constant over a range of threshold level from approximately $0.42 - 0.49$. Also for varying values of threshold, goodness-of-fit statistics were also evaluated and used in the decision process. Figure 1.18c shows these plots for the 20 m span. The uppermost sub-figure shows the R^2 value versus threshold. A value of $R^2 = 1$ represents a perfect fit, likewise the KS test indicates a good fit as the significance level Q_{KS} approaches 1. For the Anderson-Darling test, at the 5% significance level, the value of 2.492 is suggested in literature, i.e. the test value should fall below this level if there is no significant difference at

this probability level. In the third sub-figure the Anderson-Darling test value falls below this value for all the threshold values $u > 0.41$. In the case of the χ^2 goodness-of-fit test the test value, shown continuous in the sub-figure, should fall below the χ^2 distribution value, for the correct degree of freedom, at the required significance level. This value is shown dashed in the sub-figure. The test value falls below the χ^2 value shortly after 0.38. Another measure of the goodness-of-fit used in this process was the mean square error (MSE). This is a measure of the variation of the data from that predicted by the fitted theoretical model, and small values of MSE indicate a good fit. Figure 1.18d shows the MSE versus the threshold level and as can be seen from this figure a threshold of between 0.40 and 0.47 may be justified. Finally, the author states that a value of anywhere in the range of $0.42 < u < 0.46$ would therefore seem a reasonable choice, and the final choice was $u = 0.458$ which was quite long into the tail, thus hopefully avoiding bias, but still had a large number of data points (695) on which to make the parameter estimates. The procedure was applied to other cases of load effects in the thesis.

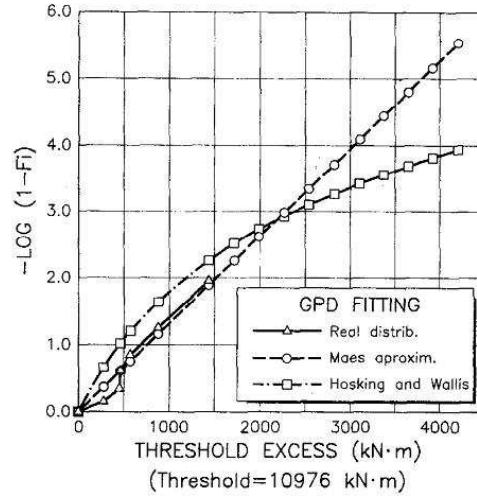


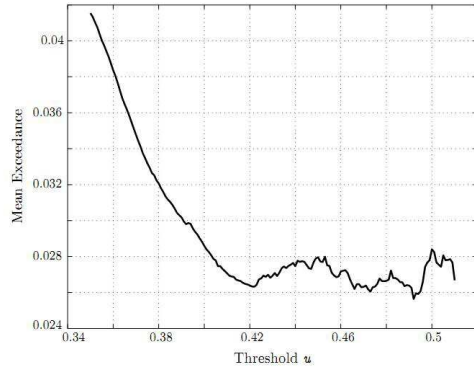
Figure 1.17: Example of fitting a generalized Pareto distribution, Reproduced from [Crespo-Minguillon and Casas, 1997]

After determining the threshold, the next step is to estimate the parameters for the GPD. A number of methods are available in the literature, maximum likelihood, probability weighted moments and method of moment are the most frequently used amongst. There does not exist a method that is available for all, therefore the choice of the parameter estimation method is also important to utilize POT method. Maximum likelihood estimation is used in [Gindy, 2004]. The three typical methods are used to estimate the parameters in [James, 2003]. Crespo-Minguillon and Casas [1997] adopt an estimator proposed by Maes [Maes, 1995] that is based on the minimization of the weighted sum of square errors:

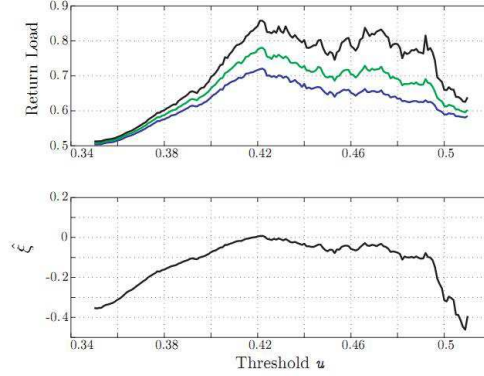
$$SWSE = \sum_{i \in T} w_i [L_i - L(x_i | u, \xi, \sigma)]^2 \quad (1.22)$$

where the function $L(x_i | u, \xi, \sigma)$ refers to the value of the minus logarithm of the probability of

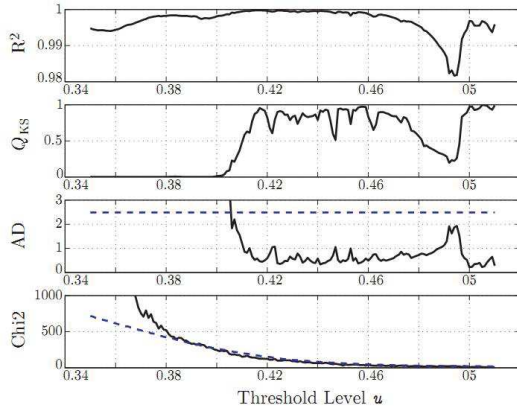
exceedance of x_i , given a chosen threshold, u , and the parameters of the GPD, ξ and σ .



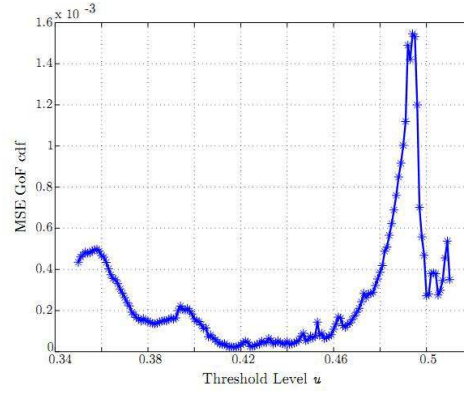
(a) Mean excesses plot.



(b) Return level and shape parameter stability plot.



(c) Threshold selection.



(d) Mean Square Error.

Figure 1.18: Application of POT to load effect for a 20 m span, Reproduced from [James, 2003].

1.4.4 Level Crossing Method

Although the classic extreme value theory based methods are the natural choice to model maximum distribution of traffic load effect, level crossing method has also got some attention by researchers. The level crossing method deals with the full time history of load effect or load process, more information are involved in the analysis. However, this method is more popular with analyzing simulation data than with measured data as the full time history is always impossible to obtain in practice. In developing the theoretical model to traffic load effect, Ghosn and Moses [1985] have used Rice formula to approximate the maximum distribution of load effect. Using Rice's formula to approximate the level crossing rates is one of the five methods adopted to develop load model for Eurocode during the background study, its performance is presented in [Jacob, 1991] on extrapolating traffic load effects. O'Connor et al. [1998, 2001] use the method in the study of re-calibration of the normal load model with

modern traffic. The method is introduced to evaluate the safety of bridge structures under site-specific traffic [Cremona, 1995; Cremona and Carracilli, 1998]. Getachew [2003] use it to extrapolate characteristic value with long return period.

The condition to use Rice's formula to approximate the level crossing rates is well known. It consists in assuming that the effect should be a stationary Gaussian process Bulinskaya [1961]; Ito [1963]; Ivanov [1960]; Ylvisaker [1965]. Ditlevsen [1994] state that if the influence function for the considered load effect is slowly varying along the lane over steps not containing a discontinuity and of length as the mean distance between consecutive vehicles and the contributing lane length is large compared to this mean vehicle distance, the load effect can be modeled to be Gaussian.

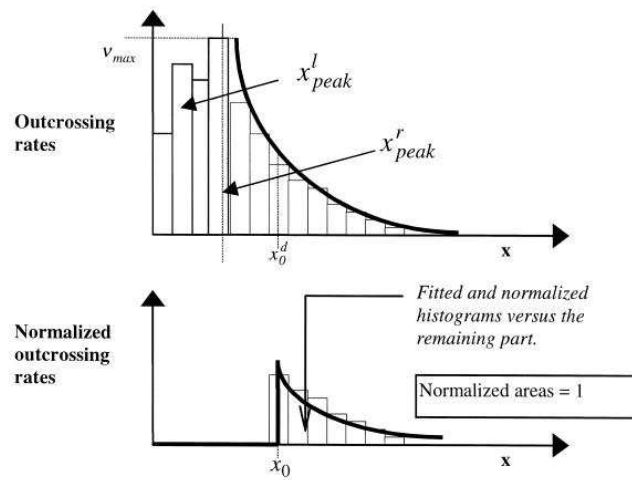


Figure 1.19: Principles of optimal fitting. Reproduced from [Cremona, 2001]

As the stochastic processes of traffic load effects satisfy the condition of stationary Gaussian processes, therefore Rice's formula can be used to estimate the upcrossing rate. However, it is hard to obtain the \dot{X} , $\sigma_{\dot{X}}$, and R_X'' , and therefore the implementation of Rice formula is still difficult. Cremona [2001] proposes to use the level crossing histogram to estimate the parameters of the Rice formula. The author simplifies the Rice formula into a second order polynomial function by taking the logarithm of Rice's formula, and thus the problem becomes to fit a curve to the level crossing histogram. The determination of the polynomial coefficients can easily be carried out by the least squares method. The goal of extrapolation is to estimate as accurately as possible the high quantile, thus only the upper tail should be concerned. However, the selection of tail fraction is problematic. Cremona [2001] points out that the crucial point for the use of Rice's formula is the selection of proportion of upper tail to be approximated by Rice's formula. The choice of the starting point should be a trade off variation and bias. If the starting point is chosen very close to the tail end, the fitting is expected to be a good approximation of the very far tail, but it introduces large variation as few points involved. In contrast, if the starting point is far from the end of tail, the fitting can be expected to be more representative for extrapolating load effects, but would increase the bias

of approximation. In the preparatory studies of Eurocodes, the choice of the optimal starting point was performed by successive tests [Jacob, 1991], it is very time-consuming when many datasets need to be dealt with. An automatic selection method is presented in [Cremona, 2001], the principle of this automatic optimal starting point selection (see Figure 1.19) is to use KS test to select automatically the optimal starting based on the KS statistic $D(x)$, which represents the supremum of the set of distance, $S(x) - F(x)$, provided by the fitted and empirical level crossing rates. As a result, each selected starting point has a corresponding P-value of KS (see Figure 1.20), the point can be selected by relative optimal fitting or absolute optimal fitting. The absolute optimal fitting is to select the smallest start point corresponding to the highest P-value; while the relative optimal fitting is to select the smallest starting point with P-value over a given reference value.

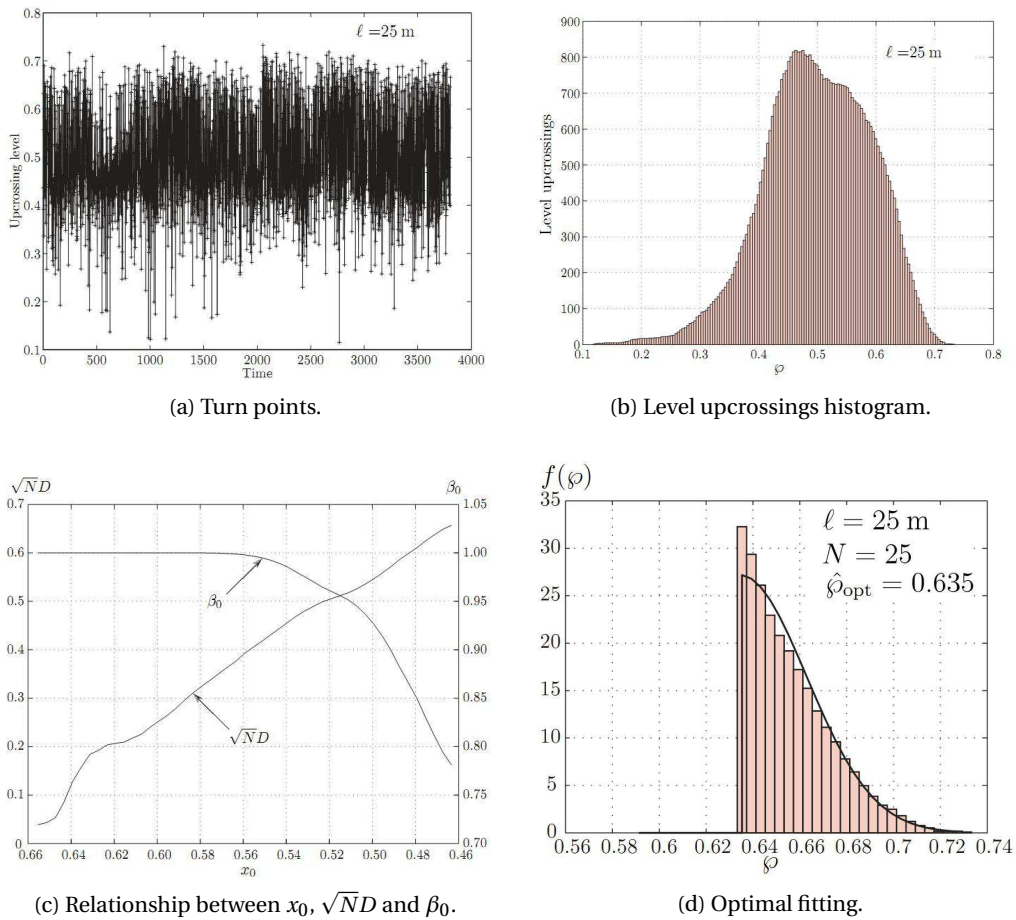


Figure 1.20: Application of fitting Rice's formula to level crossing histogram. For queue length of 25 meters. Each value is a yearly maximum value, therefore the figure shows values that represent 3805 years' signal with one year interval. Reproduced from [Getachew, 2003]

After obtaining the optimal starting point, the parameters of Rice's formula can be calculated simply. When the optimal fitting is obtained, the extrapolation of maximal and minimal effects, for any return period, R , can be assessed according to the definition of the return period that

is the mean period between two occurrences of a value x . The value, x , therefore can directly be calculated from $R \cdot \nu(x) = 1$. In O'Connor and O'Brien [2005], the extremes predicted by level crossing method (or Rice's formula) are compared with those calculated using extreme value distributions of Gumbel and Weibull, some extent differences have been found. The author does not state which method gives more precise prediction. Indeed, the extrapolated extremes from Rice's formula follow Gumbel distribution as been demonstrated in [Cremona, 2001] with an effective variable of $\frac{1}{2} \left(\frac{x-m}{\sigma} \right)^2 - \lg(\nu_0 T_{ref})$.

1.5 Summary

Many different methods have been used in modeling the extreme traffic loads or load effects. All of them focus on the tail behavior. However, the early stage used fitting tail distribution approach needs to pre-select the type of distribution and choose the suitable fraction to be fitted, thus subjective judgements are involved in the modeling. Level crossing method needs full time history of stochastic process, and the available method to model the level crossing histogram requires the stochastic process to be stationary and Gaussian. These methods are restricted to use in specific situations. However, extreme value modeling makes it possible to concentrate on the tail behavior suited towards tail-related inference. For measurements from bridge structures, such as traffic loads and load effects, extreme value based models are advantageous in reliable extrapolation to rare events as they turn out flexible of the tail behaviours. The GEV distribution is feasible to any shape of tail behavior, therefore the extreme value can be easily modelled if enough information for the tail is obtained. However, the typical problems in tail related inferences is the inherent lack of extreme informations. The period of available data is always very short compared to the expected lifetime of the structure. Therefore, attentions should be put on using short term measurement to model the extreme value as accurately as possible. The literature review on extreme bridge traffic load effect modeling reveals that it is possible to achieve the objectivity. The extensively used extreme value modeling method is block maximum method, which deals with the extreme data in a very waste manner. We will focus on introducing POT method to model extreme bridge traffic load effects. In applying this method, difficulties like applicability of parameter estimation method, optimal threshold choice and mixture behavior of traffic load effects needs to be sloved. We will focus on these issues in the following chapters with application to problems in bridge traffic load effects.

2 Performances of Some Prediction Methods for Bridge Traffic Load Effects

2.1 Introduction

The objective of extreme value modeling is to quantify the outcome of a stochastic process which have a small probability of occurring and even to extrapolate outside the scope of observations. The issue belongs to extreme value statistics, which has been an important and extensively developed branch of the statistics in the last 60 years. Since it was developed, extreme value techniques are extensively used in many disciplines such as the hydrology, wind engineering, insurance, and structural engineering. Of course, it was used in civil engineering. The methods in the literature for modeling maximum traffic load effects have been reviewed in the previous chapter. In this section, we will evaluate the performance of some reviewed prediction methods by using numerical simulation sample and traffic load effect data.

In practice, a limited quantity of data is generally used to infer a probability of failure and a characteristic maximum to evaluate the safety of a bridge with deterministic and probabilistic assessment approach, respectively. Probability of failure is clearly the most definitive measure of bridge safety. However, it is strongly influenced by resistance which varies greatly from one example to the next. In order to retain the focus on load effect, the resistance distribution is here assumed to be a mirrored version of the exact LE distribution, shifted sufficiently to the right to give an annual probability of failure of 10^{-6} - see Figure 2.1.

2.2 Simple Extreme Value Problem

A simple example is used here to compare the alternative methods of extrapolation. A Normally distributed random variable (such as gross vehicle weight in tonnes), $N(40, 5)$, is considered. Three thousand values of Z are considered in a given block, say per day, with maximum $X_j = \max\{Z_{j,1}, \dots, Z_{j,3000}\}$. Typically, a finite number of days of data is available and extreme value distributions are inferred from a dataset of daily maximum values. Hence, a finite number of daily maxima (X values) may be used to infer, for example, annual maximum distributions. In all cases, the days are considered to be working days and a year is taken to

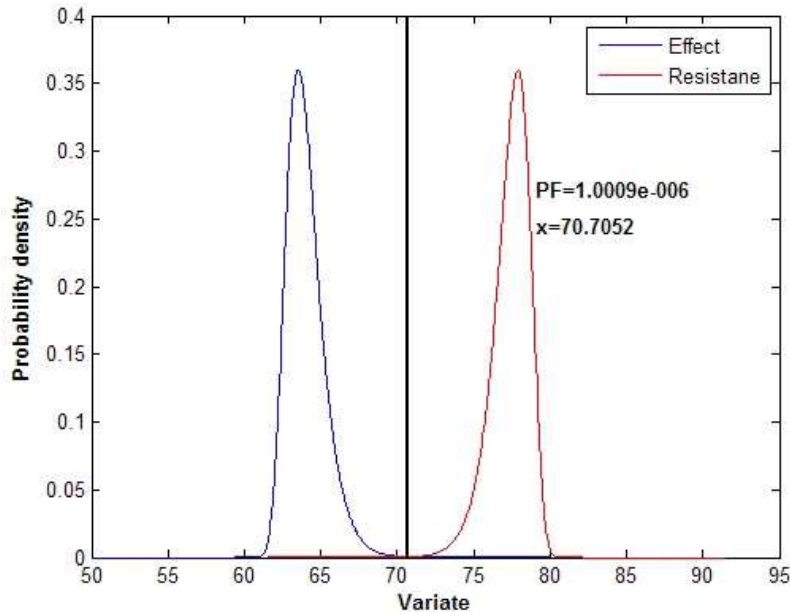


Figure 2.1: Load Effect and Mirror Resistance

consist of 250 such days. The exact solution to this problem is readily calculated through $F = F^n$.

For the first two tail fitting methods - Normal and Rice - the parameters of the daily maximum distributions are inferred from the best fits to the upper tail of the daily maximum data. The choice of fraction of upper tail is determined by using KS goodness-of-fit test statistic. Allowing for public holidays and weekends, 250 days are assumed per year. The annual maximum distribution can then be found by raising the CDF for daily maximum to the power of 250.

Characteristic values are calculated for a 75-year return period. The process is repeated for three different quantities of daily maximum data: 200, 500 and 1000 days. For each of the three quantities, the characteristic values are calculated 20 times so that a measure of the variability in the results can be found. Errorbar plot in Figure 2.2 shows the mean of the 20 runs in each case, \pm one standard deviation.

For 1000 days of data, the results are moderately accurate in most cases, most falling in the 64 to 73 range. For POT, GEV and Box-Cox, the exact value falls within the error bars and the mean error is less than 1 from that value. Errors in individual results are less good, being as high as 6.1 in one case for GEV. There is no significant difference between these three methods. The Rice formula is relatively good.

Results from tail fitting to a Normal distribution do not include the exact value in the error bars. However, the mean error is only 0.94 from the exact value and all the results are reasonably close. Predictive Likelihood is good - the mean is very close to the exact value and the error bars

are small. For Bayesian Updating, the error bars are very small - results are highly repeatable - but it is consistently a little conservative for these 20 examples.

Not surprisingly, results are considerably less accurate when fewer days of data are available for inference. With 500 days of data, Normal includes the exact result within its error bars. Bayesian Updating looks better than before with the error bars coming close to the exact solution for both 500 and 200 days of data. Rice is again better than POT, GEV and Box-Cox with a mean very close to the exact and reasonably small error bars. For 200 days of data, PL looks less good than before, with the error bars becoming greater than Normal and Rice.

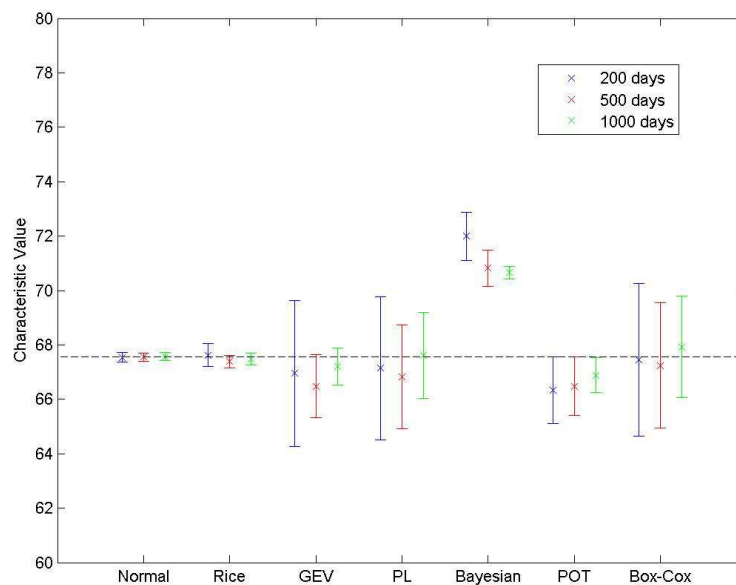


Figure 2.2: Errorbar Plot for Inferred 75-year Characteristic Values

In order to compare inferred probabilities of failure, the exact annual maximum probability density function is mirrored to give a resistance distribution that implies a failure probability of 10^{-6} . This resistance distribution is then used with each of the inferred distributions to determine the apparent probability of LE exceeding resistance. The calculated probabilities are illustrated in Figure 2.3.

Even when plotted on a Normal distribution scale, the probabilities for this example are quite inaccurate - this could be viewed as an extrapolation from 200 - 1000 days of data, to 1 million years. While the variability in the results is hardly surprising, it has significant implications for any Reliability Theory calculation. The Rice formula approach is also a tail fitting method but, in this case, the CDF for annual maximum is found directly from Rice formula. Bayesian Updating and Predictive Likelihood both infer the annual maximum distribution directly as described above.

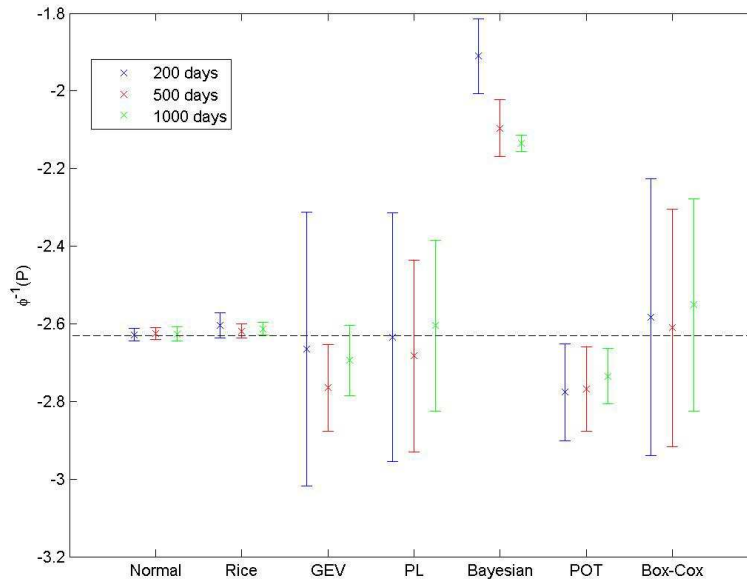


Figure 2.3: Errorbar Plot for Inferred Probabilities of Failure

As before, for inference using POT, GEV and Box-Cox, the exact value falls within the error bars. On an inverse Normal scale, the mean error from 1000 days of data is less than about 0.5 from the exact value. Errors in individual results are considerably worse, being as high as 2.1 in the case of one outlier for GEV. The Rice formula is again relatively good, perhaps benefiting from not having an inferred daily maximum distribution raised to the power of 250.

Predictive Likelihood is relatively good and, while results from the Normal distribution do not include the exact value in the error bars, all results are reasonably close to the exact. Bayesian Updating is similar to the results for characteristic value. The error bars are again small and the mean is not near the exact value.

2.3 Traffic Load Effect Problem

In this section, we evaluate the performance of previous examined predictions on traffic load effect. The load effects are generated by using Enright's Monte Carlo simulation program to reproduce traffic from a WIM station in Slovakia. Measurements were collected at this site for 750000 trucks over 19 months in 2005 and 2006. A detailed description of the methodology adopted is given by Enright and O'Brien [2012], and is summarised here. For Monte Carlo simulation, it is necessary to use a set of statistical distributions based on observed data for each of the random variables being modelled. For gross vehicle weight and vehicle class (defined here simply by the number of axles), a semi-parametric approach is used as described by O'Brien et al. [2010]. This involves using a bivariate empirical frequency distribution in the

regions where there are sufficient data points. Above a certain GVW threshold value, the tail of a bivariate Normal distribution is fitted to the observed frequencies which allows vehicles to be simulated that may be heavier than, and have more axles than, any measured vehicle. Results for lifetime maximum loading vary to some degree based on decisions made about extrapolation of GVW, and about axle configurations for these extremely heavy vehicles, and these decisions are, of necessity, based on relatively sparse observed data.

Bridge load effects for the spans considered here (Table 2.1) are very sensitive to wheelbase and axle layout. Within each vehicle class, empirical distributions are used for the maximum axle spacing for each GVW range. Axle spacings other than the maximum are less critical and trimodal Normal distributions are used to select representative values. The proportion of the GVW carried by each individual axle is also simulated in this work using bimodal Normal distributions fitted to the observed data for each axle in each vehicle class. The correlation matrix is calculated for the proportions of the load carried by adjacent and non-adjacent axles for each vehicle class, and this matrix is used in the simulation using the technique described by Iman and Conover [1982].

Traffic flows measured at the site are reproduced in the simulation by fitting Weibull distributions to the daily truck traffic volumes in each direction, and by using hourly flow variations based on the average weekday traffic patterns in each direction. A year's traffic is assumed to consist of 250 weekdays, with the very much lighter weekend and holiday traffic being ignored. This is similar to the approach used by Caprani et al. [2008] and Cooper (1995). For same-lane multi-truck bridge loading events, it is important to accurately model the gaps between trucks, and the method used here is based on that presented by O'Brien and Caprani [2005]. The observed gap distributions up to 4 seconds are modelled using quadratic curves for different flow rates, and a negative exponential distribution is used for larger gaps.

The modelled traffic is bidirectional, with one lane in each direction, and independent streams of traffic are generated for each direction. In simulation, many millions of loading events are analysed, and for efficiency of computation, it is necessary to use a reasonably simple model for transverse load distribution on two-lane bridges. For bending moment the maximum LE is assumed to occur at the centre of the bridge, with equal contribution laterally from each lane. In the case of shear force at the supports of a simply supported bridge, the maximum occurs when each truck is close to the support, and the lateral distribution is very much less than for mid-span bending moment. In this case a reduction factor of 0.45 is applied to the axle weights in the second lane. This factor is based on finite element analyses performed for different types of bridge [O'Brien and Enright, 2013]. The load effects and bridge lengths examined in the simulation runs are summarized in Table 2.1.

Two series of simulation runs are performed - one to represent possible measurements over 1000 days, repeated 20 times, and another to represent the benchmark ('exact') results, consisting of 5000 years of traffic. For the benchmark run, the outputs consist of annual maximum LE's, and these can be used to calculate the characteristic values and annual maximum distri-

Chapter 2. Performances of Some Prediction Methods for Bridge Traffic Load Effects

Table 2.1: Load Effects and Bridge Lengths

Load Effect	Description	Bridge Length (m)
LE1	Mid-span bending moment, simply supported bridge	15, 35
LE2	Shear force at left support of a simply supported bridge and two-span continuous bridge	15, 35
LE3	Central support hogging moment, two-span continuous bridge	35

butions to a high degree of accuracy.

Sample results are plotted on Gumbel probability paper in left panel on Figure 2.4 for the 20 times 1000-day simulation runs and right panel for 5000-year simulation run. Two features can be found from the figures of 1000-day simulations that (i) the variability in the upper tail is evident, and (ii) for some load effects and spans, the distribution of the data is multi-modal, i.e. the curves change direction around 400 kN in the case of shear force at left support for 15 m simply supported bridge. Due to the randomness inherent in the process, there is some variability in the results of long term simulation also, particularly in the upper tail region (top 1% of data approximately). This long-run simulation process is considered to be highly accurate, subject to the assumptions inherent in the model and is used as the benchmark against which the accuracy of all other methods is measured.

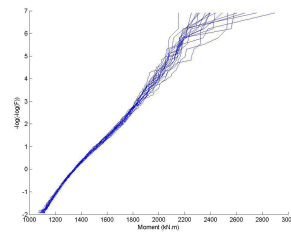
2.3.1 Effect of Prediction Methods

For the tail fitting method of normal distribution, the distribution is fit to the upper tail. The fraction of upper tail is selected by using KS test statistic based method. For POT method, the optimal threshold is chosen also by using KS test statistic based criteria. For Rice formula, the histogram of level crossing is generated firstly, then the Rice formula is fitted to the upper tail of the histogram, and the optimal starting point is chosen by using the method proposed by Cremona that is based on the KS statistic also. For the BM method, GEV is fitted to the daily maxima, and the parameters of GEV distribution are estimated by MLE and PL methods.

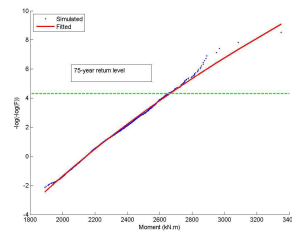
The 75-year characteristic maximum LE's are inferred from the assumed measurements consisting of 1000 daily maxima. This process is carried out for the 5 load effects and repeated 20 times to determine the variability in results. The results are illustrated in Figure 2.5. These figures show, in each case (i) the median value, (ii) the 25% to 75% range (boxed), (iii) the 0.7% to 99.3% range (median ± 2.7 standard for normally distributed data) (dashed lines) and (iv) individual outliers beyond that range.

Figure 2.5 shows that the three tail fitting methods (normal distribution, Rice formula, POT) are reasonably good, with modest range and median value close to the benchmark result from the 5000 year run. As for the simple example, fitting to a Normal distribution gives a lesser range of results which, in this case, are all reasonably close to the benchmark. The Rice method is generally better than all the others.

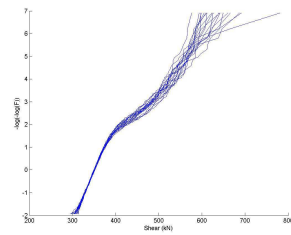
2.3. Traffic Load Effect Problem



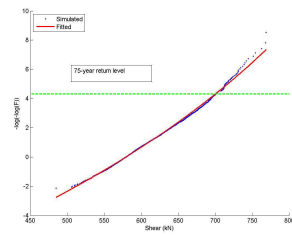
(a) LE1-Mid-span Moment, 15 m Span.



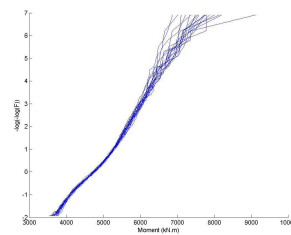
(b) LE1-Mid-span Moment, 15 m Span.



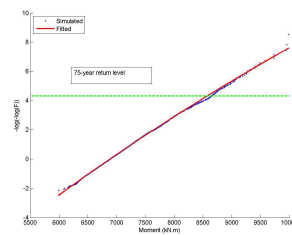
(c) LE2-Left Support Shear, 15 m Span.



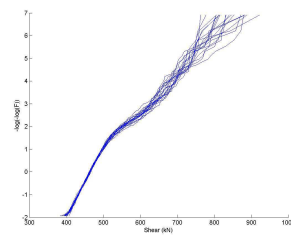
(d) LE2-Left Support Shear, 15 m Span.



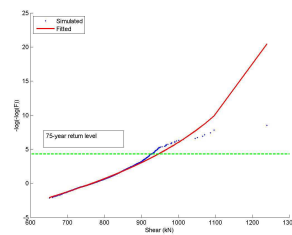
(e) LE1-Mid-span Moment, 35 m Span.



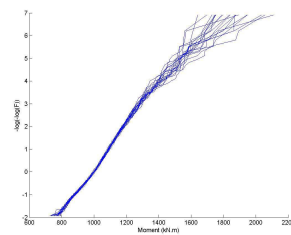
(f) LE1-Mid-span Moment, 35 m Span.



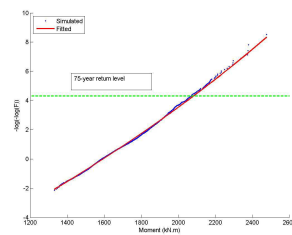
(g) LE2-Left Support Shear, 35 m Span.



(h) LE2-Left Support Shear, 35 m Span.



(i) LE3-Mid-span Moment, 35 m Span.



(j) LE3-Mid-span Moment, 35 m Span.

Figure 2.4: Daily maximum vs. Yearly maximum.

The two BM methods that estimate the distribution parameters by maximum likelihood and predictive Likelihood gives poor results for these traffic loading problems. Characteristic values are sometimes under-estimated and other times over-estimated, with no clear trend.

Annual probabilities of failure are also inferred for five the load effects/spans. As before, the probability of failure for the benchmark example is set at 10^{-6} in each case and the resistance distribution is taken to be a mirrored version of the benchmark LE distribution.

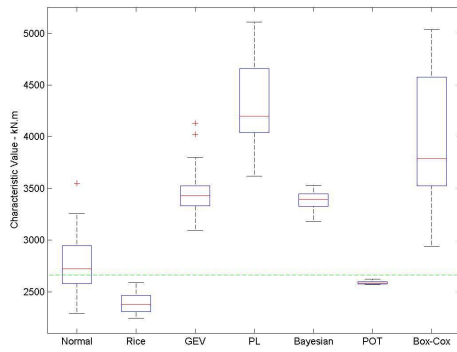
The results are illustrated in Figure 2.6. As for the simple example, the errors in the probabilities, even when plotted on an inverse Normal scale, are much higher than for characteristic values. Most of the tail fitting methods - POT, GEV, Box-Cox and Rice formula - give relatively good results, with the Rice formula generally beating the others. As before, when fitting to a Normal distribution, the benchmark result is sometimes outside the 25% – 75% range, but not by a great deal. As for the characteristic values, Bayesian Updating and Predictive Likelihood are less accurate than the other methods.

2.3.2 Effects of Timeframe

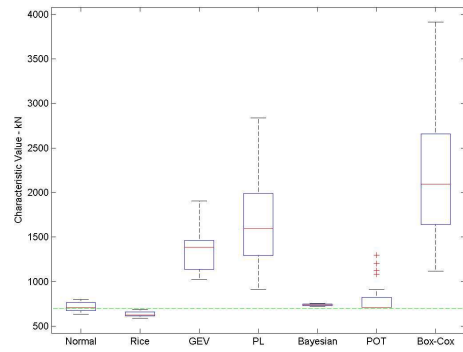
The previous results show that the tail fitting methods have better performance than the methods fitting distribution to the whole data. The possible reason can be read from the figure 2.4. Some types of load effect, i.e shear force at left support for a simply supported bridge, is multimodal distribution as the plotted curves on Gumbel probability paper change direction - around 400 kN. However, it should be noted that the curves on Gumbel probability paper for yearly maxima seems have a single distribution. The change in slope is possibly caused change in daily traffic, side-by-side truck occurrence, and the effects of vehicle speeds. For example, daily truck volume may be 300 trucks today and 500 trucks tomorrow, thus the daily maxima may not identically distributed. In the literature, the extreme value distribution or the generalized extreme value distribution is proposed to fit on the upper tail. Enright [2010] proposed to fit distribution to the top 30% after comparing with the empirical fraction of $2\sqrt{n}$ recommended by Castillo et al. [2004]. Although this method can facilitate and improve the application of GEV distribution on traffic load effect, it is lack of theory background.

The principle of BM method is the maxima drawn out of a sample should be identically and independently distributed (iid). Therefore, when the condition is violated then the fitting extreme value distribution to data is inaccurate. As mentioned, the variation of daily traffic volume may lead to non-identically distributed daily maximum. The comparison of daily maxima and yearly maxima in figure 2.4 indicates that a longer observation timeframe can avoid the violation of iid condition. In practice, the observation is always limited. Although a longer observation timeframe is generally more desirable, it must be balanced against the fact that it reduces the number of maximum values available to determine the parameter using the same amount of data. In the following, we firstly illustrate how timeframe influence the fitting of GEV or EV distributions to data.

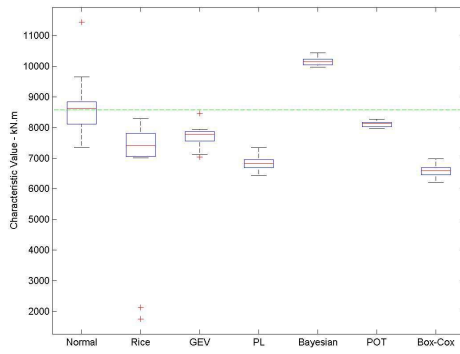
2.3. Traffic Load Effect Problem



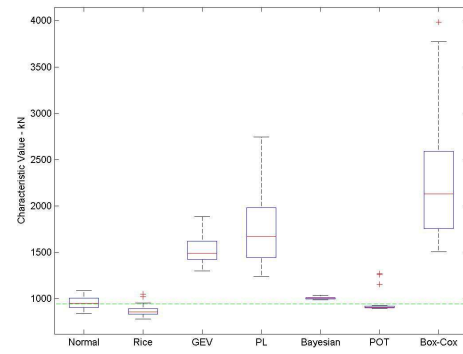
(a) LE1-Mid-span Moment, 15 m Span.



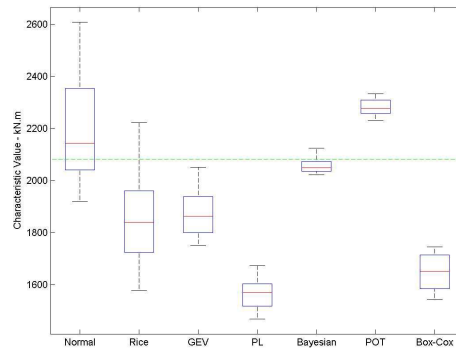
(b) LE2-Left Support Shear, 15 m Span.



(c) LE1-Mid-span Moment, 35 m Span.



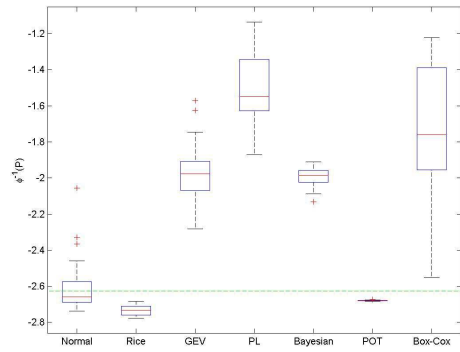
(d) LE2-Left Support Shear, 35 m Span.



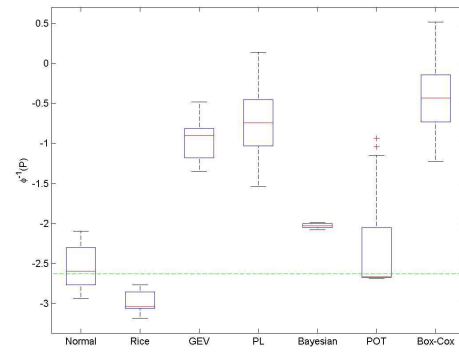
(e) LE3-Mid-support Moment, 35 m Span.

Figure 2.5: Range of Inferred 75-year Return Level from 1000 Days of Data.

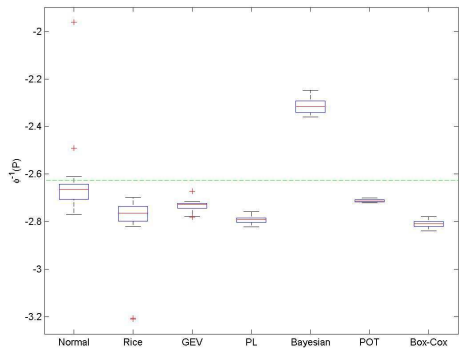
Chapter 2. Performances of Some Prediction Methods for Bridge Traffic Load Effects



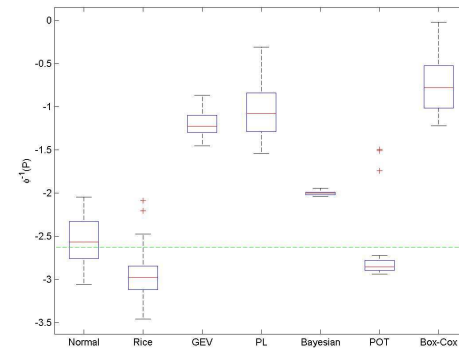
(a) LE1-Mid-span Moment, 15 m Span.



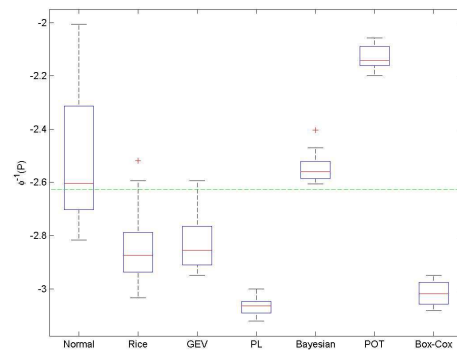
(b) LE2-Left Support Shear, 15 m Span.



(c) LE1-Mid-span Moment, 35 m Span.



(d) LE2-Left Support Shear, 35 m Span.



(e) LE3-Mid-support Moment, 35 m Span.

Figure 2.6: Range of Inferred Probabilities of Failure from 1000 Days of Data.

Table 2.2: Characteristic values for 75-year return period for various timeframes

Type	LE1-15	LE2-15	LE1-35	LE2-35	LE3-35
Max-per-year	2651	701	8646	928	2070
Max-per-day	3341 (26.05)	1498 (113.82)	7791 (-9.89)	1372 (47.85)	1713 (-17.24)
Max-per-5 days	2445 (-7.76)	866 (23.60)	7935 (-8.22)	1389 (49.68)	2320 (12.11)
Max-per-10 days	2607 (-1.65)	714 (1.93)	7927 (-8.31)	851 (-8.27)	2126 (2.73)
Max-per-25 days	2638 (-0.47)	669 (-4.48)	8037 (-7.04)	855 (-7.86)	2428 (17.29)
Max-per-50 days	2785 (5.06)	711 (-4.48)	8753 (1.24)	904 (-2.57)	2093 (1.14)

For this purpose, maxima are selected from the same data sets by picking the maximum value from timeframes of increasing length (e.g. every five days and so on) creating a new vector of maximum values for each timeframe. Once each vector is established, the GEV distribution is fitted to them to define the respective EVDs. The results from these calculations are shown in Figure 2.7 for all the five types of load effects investigated.

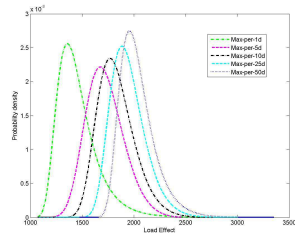
As expected, each successive distribution shifts slightly to the right on the abscissa as maxima are taken out of longer observation timeframes. The impact of the choice of timeframe is illustrated in Figure 2.7, which shows the transformation of 1 day, 5 day, 10 day, 25 day and 50 day EVDs to an annual EVD. It is seen that a selection of daily observation timeframe for this data would result in a significantly greater mean value and standard deviation for the annual EVD. The true annual EVDs obtained from the 5000-year long term simulation run are given in the figures, it indicates that the annual EVDs transformed from 10-day maxima are very close to the true distribution. Further investigating the various timeframes, Table 2.2 provides the 75-year return levels estimated from the BM method. The percentage differences between estimated return level from various timeframes and exact value given from long term simulation indicates that longer timeframe can improve the prediction accuracy. For example, the return level provided by max-per-day data is 113% larger than exact value for effect of LE2-15, while the difference significantly reduce to around 2% when the distribution is fitted to max-per-10 days' data.

The previous results show that extending timeframe to 10-day can reasonably improve the extrapolation. For the 20 sets of 1000 daily maxima, three types of timeframe of 1 day, 5 day and 10 day are used to drawn maxima, and the GEV distributions are fitted to the data. The results are given in Figure 2.8 in term of boxplot again. From these results, the 10 day distribution is selected as the optimal timeframe from which to select the maximum values because it provides reasonable estimates of return level and maximises the number of available maxima.

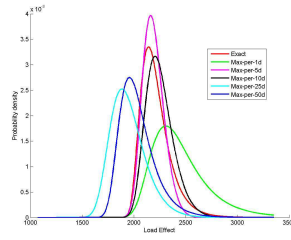
2.4 Conclusion

In this chapter, seven methods of statistical inference have been quantitatively evaluated. Each method has been checked using two examples. The first example is derived from a Normal

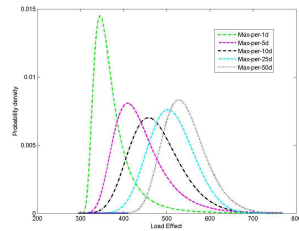
Chapter 2. Performances of Some Prediction Methods for Bridge Traffic Load Effects



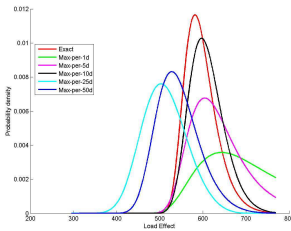
(a) LE1-Mid-span Moment, 15 m Span.



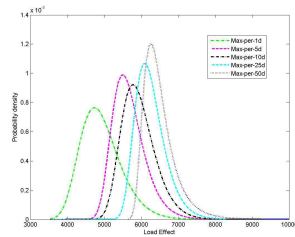
(b) LE1-Mid-span Moment, 15 m Span.



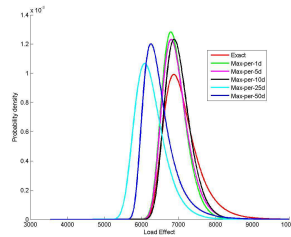
(c) LE2-Left Support Shear, 15 m Span.



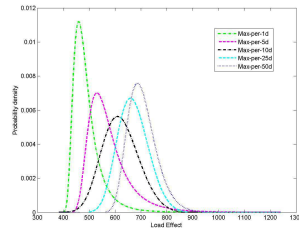
(d) LE2-Left Support Shear, 15 m Span.



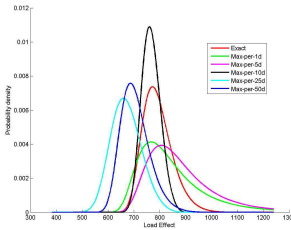
(e) LE1-Mid-span Moment, 35 m Span.



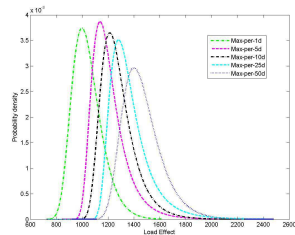
(f) LE1-Mid-span Moment, 35 m Span.



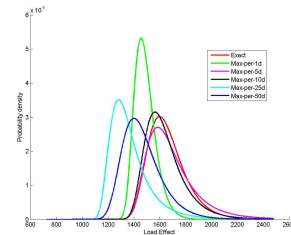
(g) LE2-Left Support Shear, 35 m Span.



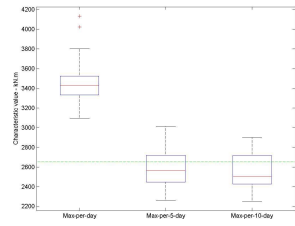
(h) LE2-Left Support Shear, 35 m Span.



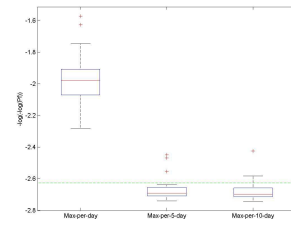
(i) LE3-Mid-span Moment, 35 m Span.



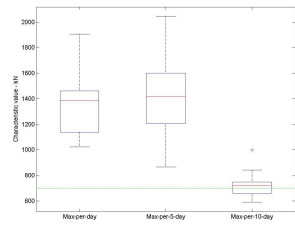
(j) LE3-Mid-span Moment, 35 m Span.



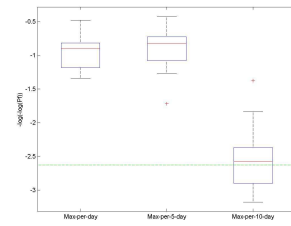
(a) LE1-Mid-span Moment, 15 m Span.



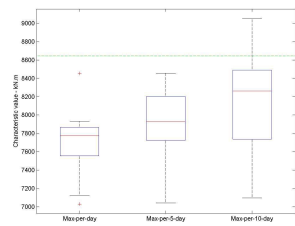
(b) LE1-Mid-span Moment, 15 m Span.



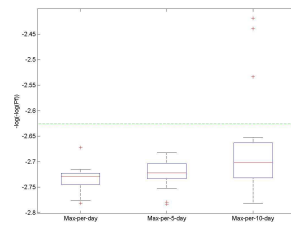
(c) LE2-Left Support Shear, 15 m Span.



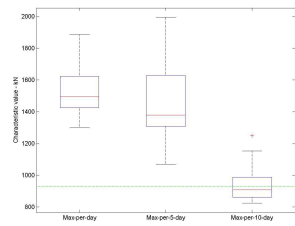
(d) LE2-Left Support Shear, 15 m Span.



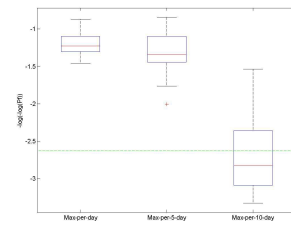
(e) LE1-Mid-span Moment, 35 m Span.



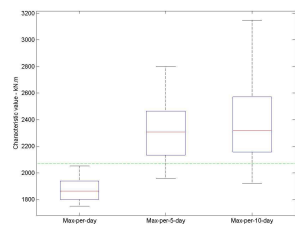
(f) LE1-Mid-span Moment, 35 m Span.



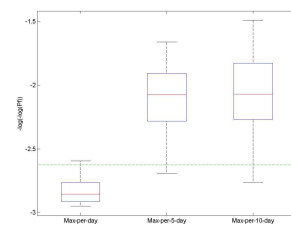
(g) LE2-Left Support Shear, 35 m Span.



(h) LE2-Left Support Shear, 35 m Span.



(i) LE3-Mid-span Moment, 35 m Span.



(j) LE3-Mid-span Moment, 35 m Span.

Figure 2.8: Effect of length of timeframe (left) characteristic value and (right) probability of failure.

Chapter 2. Performances of Some Prediction Methods for Bridge Traffic Load Effects

distribution and the exact solution is known. A total of 3000 normally distributed values (e.g., vehicle weights) are considered per day and the daily maxima are used to infer the characteristic maximum for 75-year return period. In the second example, a Monte Carlo traffic loading simulation program is used to generate a traffic stream with vehicle weights and axle configurations consistent with measured Weigh-in-Motion data. Five different load effect/span combinations have been considered, and characteristic values have been calculated in each case. In the second example, the exact solutions are unknown but the simulation is run for 5000 years to determine benchmark references against which inferences based on 1000 days of data can be compared.

All methods are used to infer the annual probabilities of failure as well as the characteristic values. To avoid the need for any assumption on the distributions for resistance, the benchmark load effect distribution is mirrored and this mirrored version is used in the calculation of probability of failure. The inferred failure probabilities are considerably less accurate than the inferred characteristic values, perhaps not surprising given that such a small failure probability was being considered (10^{-6} in a year). As for characteristic values, the tail fitting methods especially POT method are better than the others but none of the methods gives an accurate inference with 1000 days of data.

Suggestions are given to improve the performance of BM. Directly fitting GEV distribution to commonly obtained daily maxima may not capture the distribution well as the daily maxima of traffic load effect usually do not follow a single distribution. Although a GEV distribution is fitted to the upper tail of daily maximum data in practice, it is lack of theoretical background. Through a sensitive analysis, maximum taken out of a 10-day time frame can well capture the maximum distribution.

3 A Comparative Evaluation for the Estimators of the GPD

3.1 Introduction

The qualitative and quantitative evaluation results in Chapter 2 and 3 point out that generalized Pareto distribution (GPD) based POT method is deemed to approximate the CDF of excesses well. There are numerous factors, which affect the accuracy of estimates of the expected return values, such as the length and accuracy of data available, the criteria used to identify independent traffic load effects, the choice of threshold. For the choice of threshold, there is still no one that can be suitable for all situations, thus even the graphic diagnosis approaches are still used. Hence it is still an open topic in statistic of extremes [Scarrott and MacDonald, 2012]. Even though we assume that a sample follows generalized Pareto distribution, the estimated parameters can be very different as numerous parameter estimation methods exist in the literature.

In this chapter, we focus on the influence that the method used to estimate the parameters of the GPD has on the accuracy of the estimated return values. Each parameter estimation methods has its advantages and disadvantages. Traditional methods such as maximum likelihood and method of moments are undefined in some regions of the parameter space. Alternative approaches exist but they lack robustness (e.g., PWM) or efficiency (e.g., method of medians), or present significant numerical problems (e.g., minimum divergence procedures). In the domains of the applications of GPD, there are some preferred parameter estimators according to the statistical properties. For instance, the probability weighted moment (PWM) is extensively used in hydrological applications [Moharram et al., 1993], the ML is a common choice for engineering, wheather, insurance, etc. Since the application of GPD on traffic load effects is still not very active, it is necessary to provide some guidance in the choice of the most suitable estimators for its application. The performance of various estimation methods for parameter and quantile estimators will be investigated in terms of their bias, variance, and their sensitivity to threshold choice and consequently affect the accuracy of the estimated return values. In addition, the specific goodness-of-fit tests for the GPD have been established by Choulakian and Stephens [2001] for the shape parameter space that either

maximum likelihood (ML) or method of moments (MM) estimates exists, and Villasenor-Alva and Gonzalez-Estrada [2009] proposed a method that is valid for a wider shape parameter space. It makes the possibility to evaluate the performance of the estimation method through goodness-of-fit test.

The rest text of this chapter is organized as follows: an overview of parameter estimation methods is presented in Section 2. In section 3, the performance of the estimators is compared using the Monte Carlo simulation. The results are discussed in Section 4 and an example is presented to illustrate the difference in practical situations. Finally, conclusions are presented in Section 5.

3.2 Methods for estimating GPD parameters

Numerous methods have been proposed for estimating the parameters of the GPD from data, statistics of an observed process, since Pickands III [1975] introduced it to model exceedances over thresholds. The methods can be grouped into those for three-parameter GPD and those for two-parameter GPD. The difference is that the former has to estimate the shape, the scale and the location parameters, while the latter assumes that the location parameter is known. Several estimators have been proposed for the threshold, u , at which GPD can be considered a valid model for the data Singh and Ahmad [2004]. The parameter estimators for two-parameter GPD were extensively developed in the literature. For instance, Hosking and Wallis [1987] investigated the method of moments (MM) and the method of probability weighted moments (PWM). Rasmussen [2001] proposed the use of the generalized probability weighted moments (GPWM) to estimate the shape and scale parameters of the GPD as he notes that the standard PWM method may not be suitable to some shape space like $\xi < 0$. Dupuis and Tsao [1998] introduced hybrid-MM and PWM estimators. Dupuis [1996] observed that the MM and PWM fitting methods may produce estimates of the GPD upper bound that are inconsistent with the observed data. A review of the various methods existing in the literature for that type of GPD has been presented by de Zea Bermudez and Kotz [2010], the mathematical advantages and disadvantages of each method were listed in the article. However, it may not be easy to identify which estimation method is better for modeling GPD to bridge traffic load effects due to their properties. In this section, we qualitatively and quantitatively review the estimation methods that may be the most suitable for estimating characteristic values of extreme bridge traffic load effects. Moreover, the newly proposed methods, like Luceno [2006]; Zhang [2007], which were not considered by de Zea Bermudez and Kotz [2010], are considered in addition and compared all of them.

3.2.1 Method of moments

The method of moments is a method to estimate population parameters such as mean, variance, etc., by equating sample moments with underlying theoretical moments and then solving these equations for the quantities to be estimated. The principle is very clear that the

3.2. Methods for estimating GPD parameters

theoretical moments can be equated to the sample moments, and thus the parameters can be obtained through these equation. The moments of the GPD are given by

$$E \left[\left(1 + \xi \frac{X}{\sigma} \right)^r \right] = \frac{1}{1 + r\xi} \quad \text{for } 1 + \xi r > 0 \quad (3.1)$$

and the r th moments around zero is given as

$$E(X^r) = r! \frac{\sigma^r}{(-\xi)^{r+1}} \frac{\Gamma\left(-\frac{1}{\xi} - r\right)}{1 - \frac{1}{\xi}} \quad \text{for } 1 + \xi r > 0 \quad (3.2)$$

where $\Gamma(\cdot)$ stands for the Gamma function. From Eq. (3.1) or Eq. (3.2), we can easily obtain some commonly used characteristics of the GPD. The mean, variance, skewness and kurtosis have the following expressions:

$$E(x) = \frac{\sigma}{1 - \xi}, \quad \xi < 1, \quad (3.3)$$

$$Var(X) = \frac{\sigma^2}{(1 - \xi)^2(1 - 2\xi)}, \quad \xi < \frac{1}{2}, \quad (3.4)$$

$$Skew(X) = \frac{2(1 + \xi)(1 - 2\xi)^{1/2}}{1 - 3\xi}, \quad \xi < \frac{1}{3}, \quad (3.5)$$

$$Kurt(X) = \frac{3(1 - 2\xi)(3 + \xi + 2\xi^2)}{(1 - 3\xi)(1 - 4\xi)} - 3, \quad \xi < \frac{1}{4}, \quad (3.6)$$

The MM estimates of parameters ξ and σ can be easily obtained by utilizing these moments, for instance, the shape parameter, ξ , can directly be obtain from Eq. (3.5), and the scale parameter σ can be obtained if ξ is known. The classical MM estimator uses the first two moments of mean and variance since the other two moments are restricted to a narrower shape parameter space. The corresponding estimates for ξ and σ are, therefore,

$$\hat{\xi} = \frac{1}{2} \left(1 - \frac{\bar{x}^2}{s^2} \right), \quad (3.7)$$

$$\hat{\sigma} = \frac{1}{2} \bar{x} \left(1 + \frac{\bar{x}^2}{s^2} \right), \quad (3.8)$$

where \bar{x} and s^2 are the sample mean and variance, respectively.

Ashkar and Ouarda [1996] point out that the order of the moments that the classic MM uses

to estimate the parameters of a given distribution is somewhat arbitrary. The use of the first two moments may not be the best option for some distributions, while other combination of moments can be more efficient. The authors propose to address this issue of estimating the parameters of GPD by using generalized method of moments (GMM). Actually, this method is originally proposed to other types of distributions (e.g., Gamma distribution). The performance of the GMM has been assessed by means of simulation studies. Based on the results from the simulation studies, the authors conclude that using the traditional MM estimators is optimal for GPDs with $\xi < 0$ but has less performance than the GMM with pair $(r = 0, r = -1)$ of the moments combination for GPDs with $\xi > 0$.

Although the MM estimator is very simple and easy to implement, it is strictly restricted in the shape parameter space of $\xi < 1/2$ since the variance is undefined for $\xi \geq 1/2$. This limitation may have no influence on the application for traffic load effects since it is commonly accepted that the asymptotic distributions of extreme traffic load effects belongs to upper-bound type extreme value distribution (see e.g., Bailey [1996]). Nevertheless, another drawback of the MM estimators should be noted for bridge traffic load effect applications. Outliers in the sample may cause considerable distortion of the results, because the MM estimators involve squaring the sample observations. Three types of abnormal observations may exist in sample of traffic loads or load effects. The first type is that some trucks may load much more than others. For example, [O'Brien et al., 2010] report that majority truck weighed less than 70 t in the Netherlands, while 892 vehicles weighted over 70 t, with a maximum recorded weight of 165 t. The second type may be arisen from different traffic conditions. Load effects induced by free flowing traffic are quite different from those induced by congested traffic for certain types of load effects; the traffic in weekdays differ from those in weekends or holidays, even the night traffic is different from the daily one. The third type may be caused by the mixture of loading events as the load effects induced by different loading events are generally different, such the effects caused by single truck events are lesser than those from multiple trucks events [Caprani et al., 2008; Ghosn and Moses, 1985; Harman and Davenport, 1979].

According to the conditions and assumptions of MM estimator, it needs to take following considerations when applying to estimate parameters of GPD for traffic loads or load effects. The data should have light tails or medium as the MM estimator is stricted to $\xi < 0.5$. The abnormal observations may have significant influence on the estimates, for example special permission vehicle like low crane with GVW much higher than weight limit should be excluded from the WIM if it is recorded. This do not mean to eliminate the extreme highly loaded truck, but these observation should be treat in other manner.

3.2.2 Method of probability weighted moments

Probability weighted moments (PWM) were first introduced for estimating parameters of the GPD by Hosking and Wallis [1987] when the GPD was applied to hydrological data. Before it was applied on GPD, the PWM was already extensively used in hydrological applications. The

PWM was introduced by Greenwood et al. [1979] as a tool for estimating the parameters of probability distributions, especially for those distributions which are easier to be expressed in the inverse form as $x = x(F)$ than the conventional, while these types of distribution are commonly used in hydrology like the generalized lambda distribution. In such situations, it is easier to express the parameters of a distribution as function of the PWM, rather than through the ordinary moments. Although the GPD is not a distribution that can be expressed only in its inverse distribution function, the parameter estimators are convenient to compute through its PWMs [Hosking and Wallis, 1987]. The PWM of a continuous variable X with cdf F is defined as

$$M_{p,r,s} = E \left[X^p (F(X))^r (1 - F(X))^s \right], \quad (3.9)$$

where p, r, s are real numbers. For the generalized Pareto distribution, it is convenient to work with the PWM given as follows

$$\alpha_s = E \left[X (1 - F(X))^s \right] = \frac{\sigma}{(s+1)(s+1-\xi)}, \quad \xi < 1, s = 0, 1, 2, \dots, \quad (3.10)$$

and the parameters can be obtained

$$\hat{\xi} = 2 - \frac{\alpha_0}{\alpha_0 - 2\alpha_1}, \quad (3.11)$$

$$\hat{\sigma} = \frac{2\alpha_0\alpha_1}{\alpha_0 - 2\alpha_1}. \quad (3.12)$$

The quantities α_0 and α_1 are then replaced by appropriate sample estimates denoted by α_s :

$$\alpha_s = \frac{1}{n} \sum_{i=1}^n x_{i:n} (1 - p_{i:n})^s \quad (3.13)$$

with $s = 0$ and $s = 1$. The plotting positions, $p_{i:n}$, imply that $1 - p_{i:n}$ estimates $1 - F$, the tail of the distribution. Various expressions for $p_{i:n}$ are available in the literature, for example Hosking and Wallis [1987] recommend to use

$$p_{i:n} = \frac{i + \gamma}{n + \delta} \quad (3.14)$$

with $\gamma = -3.5$, and $\delta = 0$. An estimate of the upper limit $-\sigma/\xi$ is then given by

$$-\frac{2\alpha_0\alpha_1}{4\alpha_1 - \alpha_0},$$

where α_0 and α_1 are presented in Eq. (3.13).

Actually, the method is similar in nature to the aforementioned method of moments but has advantage of avoiding the squaring of observations, which in case of bridge traffic load effects may give undue weight to large observations from abnormal loading or loading events.

Several transformations of the PWM were proposed for estimating the parameters of GPD. The first was actually a transformation of MM but has similar structure as the PWM, therefore we discussed it here. The estimator proposed by Hosking [1990] is based on linear combinations of the expectations of order statistic, and is named as L-moments. L-moments are more easily related to distribution shape and spread than PWMs. Refer to [Hosking, 1990] for more details and the exact expressions for the estimators of the GPD parameters, using the L-moments. Following a similar idea to the L-moments, high order linear combination of moments (LH-moments) were proposed by Wang [1997] to characterize generalized extreme value distribution, by using the upper part of the distributions. Meshgi and Khalili [2009] extend them to the GPD, and the estimators for the GPD parameters are provided. Actually, the objective of using these moments to parameter estimation is to be able to use them in the situations where observations have large size. Since the L-moments and LH-moments can actually be expressed as linear combinations of the PWMs, there is no reason to distinguish them from PWMs for the purpose of parameter estimation, and hence we will not consider them further.

As found by Rasmussen [2001], the moments used by Hosking and Wallis [1987] are actually a particular case based on the principle of analytical simplicity, but this may not be the best option. Rasmussen states that any pair M_{1,r_1,s_1} and M_{1,r_2,s_2} for $(r_1, s_1) \neq (r_2, s_2)$ can be used to estimate the parameters of the GPD. Therefore, a generalized probability weighted moments (GPWM) based estimator was proposed in [Rasmussen, 2001].

Although the available shape parameter space for the PWM is restricted to $\xi < 1$, which is wider than the one provided by the MM, simulation studies [Castillo and Hadi, 1997] have shown that the PWMs perform especially well when the sample size is not large and $0 < \xi < 0.5$, and the PWM is recommended for estimating parameters under these situations. For the shape parameter space of $\xi < 0$, the GPWM outperforms the traditional PWM as shown by the simulation presented by Rasmussen [2001].

Even though the existing estimators can cover a wide range of shape parameter, the PWM and MM methods have nonfeasibility problem that is the estimates of shape and scale parameters of the GPD are inconsistent with the observed data. To the best of our knowledge, the feasibility of estimation for the GPD was not addressed until the articles by Dupuis [1996] and Ashkar and Nwentsa Tatsambon [2007]. Dupuis points out that the nonfeasibility of PWM and MM when $\xi < 0$, Ashkar and Nwentsa Tatsambon [2007] study the other two extensively used estimators of ML and GPWM and find that the GPWM also provides estimates that are inconsistent with the observed data. Dupuis [1996] states that may be caused by the fact that one or more sample observations are greater than the estimated upper bound of X , which is $-\frac{\sigma}{\xi}$, and the finding is confirmed by Ashkar and Nwentsa Tatsambon [2007] via

simulation studies. It is a notable issue that may be encountered when applying these moment based methods to fit GPD to traffic load effects. As been stated before, some effects caused by abnormal loadings or loading events may be greater than the estimated upper bound which relies on the majority of the data. Moreover, Dupuis and Tsao [1998] state that the nonfeasibility problem cannot be avoided by collecting more samples.

3.2.3 Maximum likelihood

The maximum likelihood estimators (ML) of ξ and σ have been considered by many authors, including Chaouche and Bacro [2006]; Grimshaw [1993]; Husler et al. [2011]; Smith [1984], and this approach has become the most extensively used parameter estimation method in applications like rainfall, assurance.

For a sample of \mathbf{x} of size n form a GPD, the logarithm of the likelihood can be expressed as

$$l(\xi, \sigma) = \begin{cases} -n \ln \sigma - \left(1 + \frac{1}{\xi}\right) \sum_{i=1}^n \ln \left(1 + \frac{\xi x_i}{\sigma}\right), & \text{for } \xi \neq 0, \\ -n \ln \sigma - \frac{1}{\sigma} \sum_{i=1}^n x_i, & \text{for } \xi = 0. \end{cases} \quad (3.15)$$

The maximum likelihood estimators are considered to be the values $\hat{\xi}$ and $\hat{\sigma}$, which yield a local maximum of the log-likelihood of Eq. (3.15). However, no explicit nor exact solutions for Eq. (3.15) can be exhibited. In practice, graphical or numerical methods are used and approximate solutions are considered. In the most cited reference on fitting the GPD model, Hosking and Wallis [1987] use a procedure based on Newton-Raphson algorithm to find the local maximum of $\log L$. By comparing the other two estimators of the MM and the PWM, the ML is recommended for sample with large size that is suspected to have $\xi < -0.2$. This algorithm encounter convergence problems in other situations. Due to this reason, at the GPD application active domain of hydrology, the ML is almost ignored, and the PWM and its relevant estimators are extensively used.

The issue of the high rate of failure is due to the algorithm used to find the local maximum of loglikelihood. A handy method is the one proposed by Grimshaw [1993] which has the benefit of reducing a two-dimensional maximum search to an one dimensional, by applying an appropriate transformation. Ashkar and Nwentsa Tatsambon [2007] adopt the algorithm proposed by Smith [1984] to find estimates by ML, their study show that this algorithm has excellent performance as it never encounters convergence problem. Chaouche and Bacro [2006] also proposed a new algorithm to overcome the non-convergence issues during finding the local maximum of log-likelihood, but the authors point out that although their method seems to be theoretically sound and promising, several issues are still to be solved. Therefore, in our study, we will use the algorithm proposed by Smith [1984] to find estimates of the GPD parameters.

Except improvement of the algorithm to find local maximum of log-likelihood, another im-

provement of ML has been conducted by Coles and Dixon [1999]. Coles and Dixon have noted that superior performance of the MM and the PWM estimators to the ML estimator for small sample size is due to the assumption of a restricted parameter space, corresponding to finite population moments. To incorporate similar information into likelihood-based inference they suggest to use a likelihood function, which penalizes larger estimates of ξ (with an infinite penalty at $\xi = 1$), similar to assuming a prior distribution for ξ . The corresponding penalised likelihood function is given by

$$l_{pen}(\xi, \sigma) = l(\xi, \sigma)P(\xi) \quad (3.16)$$

where $P(\xi)$ is the penalty function. Estimators are found as the values of σ and ξ , which maximise Eq.(3.16). In the following we will refer to these estimators as the penalized maximum likelihood (PML) estimators. Coles and Dixon [1999] states the PML performs very well for $\xi > 0$, and the performance of the PML is the same as the regular ML for $\xi < 0$.

The tails of traffic loads or load effects are always around medium and light, which have shape parameter ξ around zero. Therefore the PML should at least have same performance as the ML and even better performance than ML if the data have shape parameter greater than zero. Additionally, the PML has better performance than ML for small size sample.

3.2.4 Likelihood moment estimator

Zhang [2007] has noted the defects of the traditional PWM, MM and ML methods, and an estimator has been proposed to replace the PWM and MM methods through combining likelihood with moments. The author uses the method proposed by Smith [1984] to reduce the two-dimensional optimization to find local maximum of log-likelihood, Eq. (3.15), to one-dimension, by introducing $b = \frac{\xi}{\sigma}$.

$$\frac{1}{n} \sum_{i=1}^n \frac{1}{1 + bx_i} - \left(1 + \frac{1}{n} \sum_{i=1}^n \log(1 + bx_i) \right)^{-1} = 0 \quad (3.17)$$

The author then introduce

$$\frac{1}{n} \sum_{i=1}^n (1 + bx_i)^p - \frac{1}{1 + r} = 0 \quad (3.18)$$

where

$$p = \frac{-rn}{\sum_{i=1}^n \log(1 - bx_i)}$$

and $r > -1$ is chosen before estimation. Having solved this equation and found the unknown b , the GPD parameter estimators are given by

$$\hat{\xi} = \frac{1}{n} \sum_{i=1}^n \log 1 - bx_i \quad (3.19)$$

$$\hat{\sigma} = -\frac{\xi}{b} \quad (3.20)$$

Zhang [2007] shows that the solution to Eq.(3.18) is simply obtained since it is a smooth monotonous function of b with a unique solution in $(-\infty, \frac{1}{x(n)})$, unless $r = 0$ or $x_1 = x_2 = \dots = x_n$. He notes that a Newton-Raphson method will usually converge within 4-6 iterations to a margin of relative errors less than 10^{-6} .

3.2.5 Maximum goodness-of-fit statistic

The nonfeasibility issue motivates several new estimators, like the previous presented Likelihood moments approach. Luceno [2006] has proposed to use statistics based on the empirical distribution function to estimate the parameters of probability distribution. The estimators were found by minimising the squared differences between empirical and model distribution functions, given in terms of various goodness-of-fit statistics. Luceno consider several goodness-of-fit statistics, including the three classical statistics of Kolmogorov distance, Cramer-von Mises (CM) and Anderson-Darling (AD), and the modified versions of AD (right-tail AD (ADR), left-tail AD (ADL), right-tail AD of second degree (AD2R), left-tail AD of second degree (AD2L), and AD of second degree (ADR)). The three classical EDF statistics and the five modified EDF statistics are given in Table 3.1 and 3.2, and the computational forms are listed in Table 3.3.

Table 3.1: Three classical EDF statistics

Statistic	Acronym	Fomula
Kolomogrov distance	KS	$D_n = \sup F(x) - S_n(x)$
Cramer-von Mises	CM	$W_n^2 = n \int_{-\infty}^{\infty} \{F(x) - S_n(x)\}^2 dF(x)$
Anderson-Darling	AD	$A_n^2 = n \int_{-\infty}^{\infty} \frac{\{F(x) - S_n(x)\}^2}{F(x)\{1 - F(x)\}} dF(x)$

Luceno [2006] demonstrated that the estimators can be used for any types of distribution, and even these estimators show better performance than the ML method in the types of distribution considered in the simulation study. As the author emphasized, unlike the aforementioned estimation methods that can just be used for single distribution, the MGF based estimators could be applied also in the case where the dataset results from a combination of several statistic processes. Therefore, in the simulation study, in addition to evaluating the performance of the maximum goodness-of-fit estimation methods on standard homogeneous population, the author also assesses their performance for the heterogeneous populations,

Table 3.2: Modified Anderson-Darling statistics

Statistic	Acronym	Fomula
Right-tail AD	ADR	$R_n^2 = n \int_{-\infty}^{\infty} \frac{\{F(x) - S_n(x)\}^2}{1 - F(x)} dF(x)$
Left-tail AD	ADL	$L_n^2 = n \int_{-\infty}^{\infty} \frac{\{F(x) - S_n(x)\}^2}{F(x)} dF(x)$
Right-tail AD of second degree	AD2R	$r_n^2 = n \int_{-\infty}^{\infty} \frac{\{F(x) - S_n(x)\}^2}{\{1 - F(x)\}^2} dF(x)$
Left-tail AD of second degree	AD2L	$l_n^2 = n \int_{-\infty}^{\infty} \frac{\{F(x) - S_n(x)\}^2}{\{F(x)\}^2} dF(x)$
AD of second degree	AD2	$a_n^2 = r_n^2 + l_n^2$

Table 3.3: Computational forms for the EDF statistics

Acronym	Formula
KS	$D_n = \frac{1}{2n} + \max_{1 \leq i \leq n} \left z_i - \frac{i-1/2}{n} \right $
CM	$W_n^2 = \frac{1}{12n} + \sum_{i=1}^n \left(z_i - \frac{i-1/2}{n} \right)^2$
AD	$A_n^2 = -n - \frac{1}{n} \sum_{i=1}^n (2i-1) \{ \ln z_i + \ln(1 - z_{n+1-i}) \}$
ADR	$R_n^2 = \frac{n}{2} - 2 \sum_{i=1}^n z_i - \frac{1}{n} \sum_{i=1}^n (2i-1) \ln(1 - z_{n+1-i})$
ADL	$L_n^2 = -\frac{3n}{2} + \sum_{i=1}^n z_i - \frac{1}{n} \sum_{i=1}^n (2i-1) \ln z_i$
AD2R	$r_n^2 = 2 \sum_{i=1}^n \ln(1 - z_i) + \frac{1}{n} \sum_{i=1}^n \frac{2i-1}{1 - z_{n+1-i}}$
AD2L	$l_n^2 = 2 \sum_{i=1}^n \ln z_i + \frac{1}{n} \sum_{i=1}^n \frac{2i-1}{z_i}$
AD2	$a_n^2 = 2 \sum_{i=1}^n \{ \ln z_i + \ln(1 - z_i) \} + \frac{1}{n} \sum_{i=1}^n \left(\frac{2i-1}{1 - z_{n+1-i}} + \frac{2i-1}{z_i} \right)$

which are generated by using generalized linear models based on the GPD. The performance of the MGF estimators are evaluated by RMSE and Bias with two samples. Simulation results show that the AD statistics has the better performance.

3.2.6 Elemental percentile method

The ML method encounters convergence problem for $\xi < -1$ as stated by Chaouche and Bacro [2006]; Smith [1984]. Both MM and PWM estimates do not exist when $\xi \geq 1/2$. Even when the MM and PWM estimates exist, a serious problem with the MM and PWM estimates is that they may not be consistent with the observed sample values; that is, some of the sample values may fall outside the range suggested by the estimated parameter values. To address these issues, Castillo and Hadi [1997] have proposed an estimator by equating percentiles of the empirical and evaluated distribution. It was named elemental percentile method (EPM). The EPM is developed from a reparameterized version of the GPD with $\mu = 0$ by substituting σ/ξ by δ . The cdf is then given by

$$F(x) = 1 - \left(1 + \frac{x}{\delta} \right)^{-1/\xi}, \xi \neq 0. \quad (3.21)$$

The procedure starts with equating the cdf in Eq. (3.21) to two percentile values

$$F(x_{i:n}) = p_{i:n}$$

and

$$F(x_{j:n}) = p_{j:n} \quad (3.22)$$

where $x_{i:n}$ and $x_{j:n}$ are the i th and j th order statistics in a sample of size n , respectively. The authors suggest using

$$p_{i:n} = \frac{i - \gamma}{n + \beta}$$

with $\gamma = 0$ and $\beta = 1$. Taking the logarithm, the last two expressions can be rewritten as

$$\ln\left(1 - \frac{x_{i:n}}{\delta}\right) = kC_i \quad (3.23)$$

and

$$\ln\left(1 - \frac{x_{j:n}}{\delta}\right) = kC_j, \quad (3.24)$$

where $i \neq j$ and the constants C_i and C_j are functions of $p_{i:n}$ and $p_{j:n}$, respectively, given by

$$C_i = \ln(1 - p_{i:n})$$

and

$$C_j = \ln(1 - p_{j:n}).$$

Solving Eqs. (3.23) and (3.24) for ξ and σ . We arrive at

$$C_j \ln\left(1 - \frac{x_{i:n}}{\delta}\right) = C_i \ln\left(1 - \frac{x_{j:n}}{\delta}\right) \quad (3.25)$$

and

$$x_{i:n} \left[1 - (1 - p_{j:n})^\xi\right] = x_{j:n} \left[1 - (1 - p_{i:n})^\xi\right] \quad (3.26)$$

The solutions of Eqs. (3.25) and (3.26), which can be obtained by using the bisection method, provide a procedure for obtaining estimates for ξ and σ corresponding to the two selected order statistics, $x_{i:n}$ and $x_{j:n}$. The estimate of ξ and σ will be of the following form:

$$\hat{\xi}(i, j) = -\frac{\ln\left(1 - \frac{x_{i:n}}{\hat{\delta}(i, j)}\right)}{C_i} \quad (3.27)$$

and

$$\hat{\sigma}(i, j) = \hat{\delta}(i, j)\hat{\xi}(i, j). \quad (3.28)$$

Castillo and Hadi [1997] proposed an algorithm for computing the estimates of ξ and σ described above. They recommend applying the algorithm for all possible pairs of order statistics $x_{i:n}$ and $x_{j:n}$ for all $i, j = 1, 2, \dots, n$. After computing $\hat{\delta}(i, j)$ and $\hat{\xi}(i, j)$ for all values i and j , the final EPM estimates for ξ and σ are given by the median of the $\hat{\delta}(i, j)$ and $\hat{\xi}(i, j)$, respectively. The number of pairs of order statistics involved in this algorithm could be quite large, especially for large n . To overcome this technical difficulty, the authors suggest various alternatives. Possibly the simplest one is to consider only the pairs $(x_{i:n}, x_{n:n})$, $i = 1, 2, \dots, n-1$, which would correspond to setting $j = n$.

3.2.7 Minimum density power divergence estimator (MDPDE)

Even though the non-robustness of maximum likelihood and probability weighted moments was pointed out in Davison and Smith [1990], only recently have robustness issues come into consideration for fitting the GPD. Robust estimation for the GPD was firstly addressed by Peng and Welsh [2001], who have proposed rather complicated estimators for the shape and scale parameters of the GPD that are obtained by using the method of the medians (MM). Basing on a simulation study by comparing with ML estimator and the optimal bias robust estimator (OBRE), the authors showed that the MM is superior to the ML estimation and to the OBRE in the intervals in which the ML is not regular. Juárez and Schucany [2004] showed that the minimum density power divergence estimator (MDPD) is more efficient than the ML for the contaminated data, while the ML has the highest efficiency under uncontaminated GPDs. It is interesting to consider such kind of robust estimator for practical use as the observations always have some extent of contamination.

Let X_1, X_2, \dots, X_n be a random sample of size n from a distribution G with probability density function (pdf) g and let

$$F = \{f(x|\theta), x \in \chi, \theta \in \Theta\}$$

be a parametric family of pdfs. This family is supposed to be identifiable in the sense that, for $\theta_1 \neq \theta_2$,

$$\{x \in \chi : f(x|\theta_1) \neq f(x|\theta_2)\}$$

has a positive Lebesgue measure.

The density power divergence (DPD) between two pdfs f and g is defined as:

$$d_\alpha(g, f) = \begin{cases} \int_X [f^{1+\alpha}(x) - (1 + \frac{1}{\alpha}) g(x) f^\alpha(x) + \frac{1}{\alpha} g^{1+\alpha}(x)] dx, & \text{for } \alpha > 0, \\ \int_X g(x) \log \left[\frac{g(x)}{f(x)} \right] dx, & \text{for } \alpha = 0. \end{cases} \quad (3.29)$$

The expression for $\alpha = 0$ is obtained as the $\lim_{\alpha \rightarrow 0} d_\alpha(g, f)$ and is known as Kullback-Leibler divergence. For $\alpha = 1$, the divergence is the well known mean square error,

$$d_1(g, f) = \int_X [f(x) - g(x)]^2 dx.$$

We search for a pdf f , amongst the parametric family of pdfs F defined above, which is as close as possible (in a certain sense) to the pdf g . Formally, for a given $\alpha > 0$, the aim is to search, within the parameter space Θ , for the minimum DPD functional T_α at G given as

$$d_\alpha(g, f(\cdot | T_\alpha(G))) = \inf_{\theta \in \Theta} d_\alpha(g, f(\cdot | \theta)).$$

The minimum DPD function, $\theta_0 = T_\alpha(G)$, is then the parameter of interest. [Basu et al., 1998] propose using $\hat{\theta}_{\alpha,n} = T_\alpha(G_n) \in \Theta$, where G_n is the empirical cdf. Consequently, $\hat{\theta}_{\alpha,n}$ is considered to be the value of θ associated with the pdf $f \in F$ which bears the greatest similarity with the empirical pdf g_n . The minimum density power divergence estimator (MDPDE) is then the value of θ which minimizes, over the space Θ ,

$$H_\alpha = \int_X f^{\alpha+1}(x|\theta) dx - \left(1 + \frac{1}{\alpha}\right) \frac{1}{n} \sum_{i=1}^n f^\alpha(X_i|\theta).$$

In the framework of the GPD parameter estimation, the parametric family F is the collection of the two-parameter GPD pdfs defined in Eq.(1.9). According to Juárez and Schucany [2004], and for $\xi \neq 0$, the estimator of the pair (ξ, σ) is obtained by minimizing the function

$$H_\alpha(\xi, \sigma) = \frac{1}{\sigma^\alpha(1 + \alpha + \alpha\xi)} - \left(1 + \frac{1}{\alpha}\right) \frac{1}{n} \sum_{i=1}^n \left(1 + \xi \frac{X_i}{\sigma}\right)^{(-1/\xi - 1)\alpha} \quad (3.30)$$

over

$$\{(\xi, \sigma) \in \Theta : \sigma > 0, \xi X_{n:n} < \sigma, (1 + \alpha)/\alpha < \xi < 0 \text{ and } \xi > 0\}.$$

For traffic load effects on bridges, the issue that of the data violates the condition of identically independent distribution was pointed in the literature. Caprani et al. [2008]; Harman and Davenport [1979] have pointed out that load effects can be treated as independently

distributed, but they are unsuitable to say that they are identically distributed. Caprani et al. [2008] proposed to use a composite extreme value distribution to characterize the load effects from a mixture loading events, their results show that the characteristic values from standard block maxima are drastically different from those obtained using the new proposed method. However, the parameters were fitted by ML estimators, therefore, this results in a robustness problem as been demonstrated in Dupuis and Field [1998]. As the load effects in Caprani et al. [2008] are calculated by Monte Carlo simulation, therefore it is possible to identify the loading events and group the load effects by loading events. However, it is always impossible from monitoring to identify what are the loading events which induce the considered effect, therefore it is impossible to apply the mixture GP distribution or composite GEV distribution to predict long term characteristic value. Using the classical single component POT method is a better choice, although it avoid the underlied rule of identical distribution.

In recent years, the statisticians have noticed that the data may come from mixture populations, and methods have been proposed to solve the problem. They have defined the data coming from a mixture populations as one data contaminated by the other. A single extreme that is not consistent with the bulk of extremes may jeopardize the inferences drawn, since the traditional estimators like maximum likelihood, method of moments, and probability weighted moment are not robust. Dupuis and Field [1998] has implemented Hampel's optimally-biased robust estimator (OBRE), the algorithm is based on the algorithm given by Victoria-Feser and Ronchetti [1994] in the context of estimating income distributions. Peng and Welsh [2001] derive an estimator named Medians from equating medians of sample and population score functions. This method was originally proposed by He and Fung [1999] in a survival analysis context. Juárez and Schucany [2004] use the concept of density power divergence, originally proposed by Basu et al. [1998], to derive a class of estimators (MDPDE). A numerical study has been performed to evaluate the performance of these three estimators in Juárez and Schucany [2004]. The Medians and the OBRE encounter convergence problem when $\xi < -1$. The author also reported that the MDPDE has better performance when the severe contaminated by the performance improves when the amount of contamination data increased from 10% to 20%. Finally, the author conclude: if the true GPD model is not very heavy-tailed and contaminated by a heavier-tailer distribution, the MDPDE or the OBRE should be used; and when the GPD model has a positive upper bound and is contaminated by another GPD with upper bound then the MDPDE is the recommended method [de Zea Bermudez and Kotz, 2010]. The bridge traffic load effects were recommended to be modeled by Weibull distribution that has a upper bound. Therefore, the MDPDE is the proper method for our study.

3.2.8 Other estimation methods

Bayesian techniques have seen increasing applications with the developement in computers' technology in the last decades. Several but not many parameter estimation approaches for the GPD parameters are developed in the Bayesian framework. A review on Bayesian methods for

estimating the parameters of the GPD was provided in de Zea Bermudez and Kotz [2010]. They state that the Bayesian approach can provide satisfactory estimates as it uses all available information, but they also clarify that the Bayesian methods can be very time-consuming to implement and, most of the times, they require the use of Markov chain Monte Carlo algorithm. In addition, the parameter space is also limited such as the one provided by Eugenia Castellanos and Cabras [2007] can only be used for $\xi > 0.5$. We will not consider Bayesian methods further more in the following study as the traffic load effect shows light tail behavior that has shape value less than zero or around zero. In additional, the current available algorithm on implementing Bayesian method is too time consuming. It should be noticed that it works in many situations better or at least as well as the traditional approaches and provides much lower variance [de Zea Bermudez and Turkman, 2003].

3.3 Evaluating the performance of estimators

A qualitative evaluation of the performance the estimators has been conducted in the previous section, and estimators of MM, PWM, ML, PML, LM, MGE, EPM and MDPD are expected to have good performance on fitting GPD to exceedance of bridge traffic load effects over threshold. Simulation studies are commonly used to assess the performance of estimators among others, for instance Ashkar and Nwentsa Tatsambon [2007]; Ashkar and Ouarda [1996]; Castillo and Hadi [1997]; Hosking and Wallis [1987]; Moharram et al. [1993]; Singh and Ahmad [2004]. However, these studies have either compared only a few estimators or compared more estimators but for a limited range of sample sizes or GPD shape parameters. Two recently published articles on parameter estimators comparison involve more estimators. Deidda and Puliga [2009] evaluate the performance of the MM, the ML, the PWM, the MDPD, the LM and the PML estimators for estimating parameters of the GPD for over rounded-off samples, the performance is evaluated by bias and RMSE for shape and scale parameters. Mackay et al. [2011] also assess the performance of several existing methods in literature, but the performance is evaluated through the bias and RMSE of quantiles at a non-exceedance probability of 0.999. Existing simulation results in the literature confirm that the performance of an estimator can vary considerably with both the sample size and the value of the GPD shape parameter. Moreover, Ashkar and Nwentsa Tatsambon [2007] show that the measure used to evaluate the performance of estimators is also very important. Ashkar and Nwentsa Tatsambon utilize bias and RMSE for quantiles with different return period to perform the comparison. They note that the considered four estimators of the MM, the PWM, the ML and the GPWM have litter differnce on estimating quantiles with a return period that is smaller than the sample size, while the difference between various methods of estimation arise when the required quantiles are for longer return period that is greater than the sample size.

In this section, we will conduct a quantitative evaluation of the performance through applying them to model GPDs to numerical simulation samples, Monte Carlo simulated bridge traffic load effects and measured realistic traffic load effects on bridges. The purpose of this comparison study is thus to evaluate the performance of the estimators by using bias and RMSE of

shape parameter, quantile with shorter and longer return period. The Bias and the root mean square error (RMSE) are:

$$Bias = E(\theta_{est} - \theta_{true}) \quad (3.31)$$

$$RMSE = \sqrt{E[(\theta_{est} - \theta_{true})^2]} \quad (3.32)$$

where $\theta_{est}, \theta_{true}$ are the estimated and the true values of the parameter respectively. In our case θ can be the ξ , the σ parameter and/or quantile of the GPD.

3.3.1 Numerical simulation

Using numerical simulation samples to evaluate the performance of proposed method and compare with the existings is a common approach (see e.g., Hosking and Wallis [1987]), and it is also used to evaluate the performance of methods adapted in applications (see e.g., Deidda and Puliga [2009]). In Hosking and Wallis [1987], simulations were performed for sample sizes $n = 25, 50, 100, 200, 500$. The scale parameter σ was set to 1. The range of shape parameter is always set in $[-0.5, 0.5]$ to ensure the existence of estimates for various methods, regardlessly, there are some exception such as Castillo and Hadi [1997] who considered the range of $-2 < \xi < 2$. In particular the values of ξ observed for significant traffic load effect are usually in the range of $-0.5 \leq \xi \leq 0.5$. In this section we also carry out a simulation study to compare the reviewed methods for the generalized Pareto distribution. We have restricted our interest to this range with $\xi = -0.5, -0.4, -0.25, 0, 0.25, 0.4, 0.5$. For each combination of values of n and ξ , 10000 random samples were generated from the generalized Pareto distribution. For each sample, comparisons were made on the parameters σ and ξ and the quantiles at non-exceedance probabilities of 0.9 and 0.999 estimated by methods described in Section 3.2.

Our simulation results are summarized in Tables 3.4-3.11 which present the bias and root mean squared error (RMSE) of estimates for the shape parameters ξ , the scale parameter σ and the upper-tail quantiles at non-exceedance probability of 0.9 and 0.999. Biases and RMSE's of quantile estimators have been scaled by the true value of the quantile being estimated. Some observations can be drawn from the results:

Parameter estimator

- Overall, the bias and RMSE become smaller with sample size increasing. Most of methods perform better for large size sample than small size sample. The bias and RMSE decrease as the size of sample increases, which is an indication that all the estimates are consistent.
- For the MM and the PWM, it seems that the PWM has better performance than the MM with lower bias.

- For the three commonly used methods of MM, PWM and ML, all of them have low bias the MM outperforms than the others when $\xi \leq 0.25$ for small size sample, and it has better performance than PWM when $\xi \leq 0$. The PWM estimator almost possesses the smallest RMSE when $\xi \geq 0.25$. The ML possesses the smallest RMSE when $\xi \leq -0.25$, and it outperforms than MM and PWM for samples with size of 500. These findings confirm the conclusion made by Hosking and Wallis [1987].
- For the four selected maximum goodness-of-fit statistics based methods of MGF-KS, MGF-CM, MGF-AD, MGF-ADR, the parameter estimators with the smallest RMSE are generally the MGF-ADR, but the MGF-CM estimators outperform the MGF-ADR when $\xi \geq 0.4$ for large size samples. The second best estimator appears to be the MGF-AD estimator, and the KS statistics based MGF-KS estimator always provides the worst estimator. As known, the KS method takes the same weight, while CM and AD give more weight to the tail. AD statistics give even more weight to the tails of the CDF than the CM statistics, while the ADR assigns more weight to the selected tail of the CDF. Overall, the ADR statistics outperform the others.
- The ML and MPLE estimators have almost the same performance among all the considered cases with similar RMSE's and biases. The two methods provide the best estimator for shape parameter in the case of large size samples.

Quantile estimator

- The estimators seem to have similar performance on the estimating quantile at lower non-exceedances probability, here is 0.9. The estimators show very consistent features that the bias and RMSE decrease with increasing of sample size.
- The MM and PWM estimators have low bias but has a larger RMSE than other methods in small samples.
- Amongst all estimators, the LM estimator consistently has the lowest RMSE and a small negative bias.
- The sample has a great influence on quantile estimates as smaller size samples generate larger RMSE than the larger size samples. For $\xi < 0$, the RMSE's are always greater than 0.20 (or 20%) when sample size is 25, and the RMSE's are less than 0.10 (or 10%) when sample size is 500. For $\xi > 0$, all estimators have a high RMSE.
- Once again, the present findings confirm the conclusions of Hosking and Wallis [1987] for the three commonly used estimators of MM, PWM and ML. Moment estimators of quantiles have large negative biases, however, the PWM estimators also have the smallest bias when $\xi \geq 0.25$.

- The well performed maximum goodness-of-fit statistics based estimators for shape parameters do not have the consistent performance in quantile estimation situation, the estimators place is below 6th on the rank table.

Above simulation results indicate that there is not a single estimator better than all the others in all the situations considered. Actually, it is not a surprising conclusion. First, the extensively stated disadvantages of the traditional methods indicate that they cannot cover all situation. Second, the revised form of the traditional methods were designed to address the unsatisfied factors of the traditional methods.

3.3.2 Monte Carlo method simulated traffic load effect data

In this section, we fit the GPD to traffic load effects data calculated by combining measured traffic data and influence lines of interest load effects. The dataset present here is the hourly maximum bending momentd at mid-span of a simply supported bridge with span of 30m and carrying 4 lanes of traffic.

Traffic data, taken from a piezo-ceramic weigh-in-motion system on the A9 motorway near Saint Jean de Vedas, in the South-East of France, is used to validate the proposed method on the estimation of characteristic bridge traffic load effects. This WIM station is very close to the famous station at which WIM data collected in 1986 was used to develop current traffic load model of Eurocode. It can have the same manner as a representative of current European traffic. Weight and dimensional data were collected for trucks travelling in the slow and fast lanes in one direction of the 6-lane motorway from January 2010 to May 2010. Unreliable data (e.g. interaxle spacing greater than 20 m) were eliminated from records under the recommended WIM data cleaning criteria [Enright and O'Brien, 2011; Sivakumar et al., 2011]. Measurements for days during which the WIM system may not be active for some hours were excluded also, as it is important to exclude these days to ensure having a series of homogenous traffic days and maximum determination. In the data, the truck traffic on weekends shows different pattern from those on weekdays, and this results in difference in extreme traffic load and load effects between weekdays and weekends traffic [Zhou et al., 2012]. Finally, 581011 trucks for 86 days were kept from the original 138 days' measurements excluding data of error, weekends and system inactive days. The more details of the statistics of the data are presented in Appendix A.

To obtain representative information on bridges, a large amount of data is required to figure out the actual situation on load carrying capacity, load subjected. Although traffic collections from WIM system have excellent quality, it is still very expensive to collect data in long term. The 86 days validated data is insufficient to estimate characteristic values or extreme value distributions of traffic load effect required to evaluate and design bridge structure, but it can help adjusting statistical models of traffic characteristics. Long term traffic can be obtained by using Monte Carlo method based on these mathematical models. Using Monte Carlo method to simulate traffic loads or load effects has been demonstrated as efficient and accurate by

Table 3.4: Bias of estimators of shape parameter for GPD

Shape	n	Estimator										
		MM	PWM	ML	PML	LM	MGF-KS	MGF-CM	MGF-AD	MGF-ADR	EPM	MDPD
-0.4	25	-0.06	-0.05	-0.17	-0.17	0.43	0.09	-0.08	0.01	-0.02	0.02	-0.15
	50	-0.02	-0.01	-0.08	-0.08	0.39	0.08	-0.03	0.03	0.01	0.02	-0.06
	100	-0.01	-0.01	-0.04	-0.04	0.38	0.06	-0.02	0.01	0.00	0.01	-0.03
	200	-0.01	-0.01	-0.02	-0.02	0.37	0.03	-0.01	0.01	0.00	0.01	-0.02
	500	0.00	0.00	-0.01	-0.01	0.37	0.01	0.00	0.01	0.00	0.01	-0.01
-0.25	25	-0.06	-0.05	-0.16	-0.16	0.18	0.07	-0.06	0.03	-0.01	0.05	-0.13
	50	-0.03	-0.02	-0.08	-0.08	0.09	0.06	-0.03	0.02	0.00	0.03	-0.06
	100	-0.02	-0.02	-0.04	-0.04	0.04	0.04	-0.02	0.00	0.00	0.02	-0.03
	200	0.00	0.00	-0.02	-0.02	0.01	0.04	0.00	0.01	0.01	0.02	-0.01
	500	0.00	0.00	-0.01	-0.01	0.00	0.02	0.00	0.00	0.00	0.01	-0.01
0	25	-0.08	-0.06	-0.13	-0.15	-0.03	-0.02	-0.06	0.03	0.00	0.28	-0.09
	50	-0.05	-0.03	-0.06	-0.07	-0.03	-0.01	-0.02	0.02	0.01	0.19	-0.04
	100	-0.02	-0.01	-0.03	-0.03	-0.01	-0.01	-0.01	0.01	0.01	0.13	-0.02
	200	-0.01	-0.01	-0.01	-0.02	-0.01	-0.01	0.00	0.01	0.00	0.10	-0.01
	500	-0.01	0.00	-0.01	-0.01	0.00	0.00	0.00	0.00	0.00	0.07	0.00
0.25	25	-0.16	-0.09	-0.12	-0.19	-0.08	-0.13	-0.07	0.02	-0.01	0.12	-0.08
	50	-0.11	-0.06	-0.06	-0.11	-0.05	-0.11	-0.04	0.01	0.00	0.09	-0.04
	100	-0.07	-0.02	-0.02	-0.05	-0.02	-0.07	0.00	0.01	0.01	0.07	-0.01
	200	-0.04	-0.01	-0.01	-0.02	-0.01	-0.05	-0.01	0.01	0.00	0.06	0.00
	500	-0.02	0.00	0.00	-0.01	0.00	-0.03	0.00	0.00	0.00	0.05	0.00
0.4	25	-0.23	-0.12	-0.11	-0.23	-0.09	-0.20	-0.06	0.03	0.00	0.16	-0.07
	50	-0.17	-0.08	-0.06	-0.14	-0.06	-0.17	-0.06	-0.01	-0.02	0.09	-0.04
	100	-0.13	-0.04	-0.02	-0.07	-0.02	-0.08	0.00	0.01	0.00	0.08	-0.01
	200	-0.10	-0.02	-0.01	-0.04	-0.01	-0.06	-0.01	-0.02	-0.02	0.07	-0.01
	500	-0.07	-0.01	0.00	-0.01	0.00	-0.03	0.00	-0.06	-0.06	0.05	0.00

Table 3.5: Bias of estimators of scale parameter for GPD

Shape	n	Estimator										
		MM	PWM	ML	PML	LM	MGF-KS	MGF-CM	MGF-AD	MGF-ADR	EPM	MDPD
-0.4	25	0.07	0.06	0.18	0.18	-0.28	0.00	0.08	0.03	0.04	0.01	0.15
	50	0.02	0.01	0.07	0.07	-0.27	-0.02	0.02	-0.01	0.00	0.00	0.06
	100	0.02	0.01	0.04	0.04	-0.26	-0.01	0.02	0.00	0.00	0.00	0.03
	200	0.01	0.01	0.02	0.02	-0.26	-0.01	0.01	0.00	0.00	0.00	0.02
	500	0.00	0.00	0.01	0.01	-0.27	0.00	0.00	0.00	0.00	0.00	0.01
-0.25	25	0.06	0.05	0.16	0.17	-0.13	0.01	0.07	0.02	0.04	0.00	0.13
	50	0.03	0.02	0.08	0.08	-0.07	0.00	0.03	0.01	0.01	0.00	0.06
	100	0.02	0.02	0.04	0.04	-0.03	0.00	0.02	0.01	0.01	0.00	0.03
	200	0.01	0.00	0.02	0.02	0.00	-0.01	0.00	0.00	0.00	0.00	0.01
	500	0.00	0.00	0.01	0.01	0.00	0.00	0.00	0.00	0.00	0.00	0.01
0	25	0.08	0.06	0.14	0.16	0.04	0.05	0.07	0.02	0.04	0.02	0.11
	50	0.04	0.02	0.06	0.07	0.03	0.02	0.03	0.00	0.01	-0.01	0.04
	100	0.02	0.01	0.02	0.03	0.01	0.01	0.01	0.00	0.00	-0.01	0.01
	200	0.01	0.01	0.02	0.02	0.01	0.01	0.01	0.00	0.00	-0.01	0.01
	500	0.01	0.00	0.01	0.01	0.00	0.00	0.00	0.00	0.00	-0.01	0.00
0.25	25	0.19	0.09	0.15	0.21	0.10	0.11	0.10	0.04	0.06	-0.02	0.11
	50	0.13	0.05	0.07	0.10	0.05	0.07	0.05	0.02	0.02	-0.02	0.05
	100	0.08	0.01	0.02	0.04	0.01	0.03	0.01	0.00	0.00	-0.03	0.01
	200	0.05	0.01	0.01	0.02	0.01	0.03	0.01	0.01	0.01	-0.02	0.01
	500	0.03	0.00	0.00	0.01	0.00	0.01	0.00	0.01	0.01	-0.02	0.00
0.4	25	0.32	0.11	0.13	0.23	0.09	0.14	0.08	0.03	0.05	-0.03	0.09
	50	0.24	0.07	0.06	0.12	0.06	0.11	0.06	0.03	0.03	-0.01	0.05
	100	0.19	0.03	0.03	0.06	0.02	0.05	0.01	0.04	0.03	-0.02	0.02
	200	0.15	0.02	0.01	0.03	0.01	0.03	0.01	0.06	0.06	-0.02	0.01
	500	0.11	0.01	0.01	0.01	0.01	0.02	0.00	0.13	0.12	-0.02	0.01

Table 3.6: Bias of estimators of quantile at non-exceedance probability of 0.9

Shape	n	Estimator										
		MM	PWM	ML	PML	LM	MGF-KS	MGF-CM	MGF-AD	MGF-ADR	EPM	MDPD
-0.4	25	-0.01	-0.01	-0.02	-0.02	0.15	0.09	0.00	0.02	0.01	0.02	-0.02
	50	-0.01	-0.0	-0.01	-0.01	0.11	0.06	-0.01	0.01	0.00	0.01	-0.01
	100	0.00	0.00	0.00	0.00	0.11	0.05	0.00	0.01	0.00	0.01	0.00
	200	0.00	0.00	0.00	0.00	0.09	0.02	0.00	0.00	0.00	0.00	0.00
	500	0.00	0.00	0.00	0.00	0.09	0.01	0.00	0.00	0.00	0.00	0.00
-0.25	25	-0.02	-0.02	-0.03	-0.03	0.05	0.08	0.00	0.03	0.01	0.04	-0.03
	50	-0.01	-0.01	-0.02	-0.02	0.02	0.05	0.00	0.01	0.00	0.02	-0.02
	100	-0.01	-0.01	-0.01	-0.01	0.01	0.04	0.00	0.01	0.00	0.01	-0.01
	200	0.00	0.00	0.00	0.00	0.00	0.03	0.00	0.01	0.00	0.01	0.00
	500	0.00	0.00	0.00	0.00	0.00	0.01	0.00	0.00	0.00	0.01	0.00
0	25	-0.02	-0.02	-0.02	-0.03	-0.01	0.02	0.02	0.06	0.03	0.09	-0.01
	50	-0.02	-0.02	-0.02	-0.02	-0.02	0.01	0.01	0.02	0.01	0.05	-0.01
	100	-0.01	-0.01	-0.01	-0.01	-0.01	0.00	0.00	0.01	0.00	0.03	-0.01
	200	0.00	0.00	0.00	0.00	0.00	0.00	0.01	0.01	0.01	0.03	0.00
	500	0.00	0.00	0.00	0.00	0.00	0.00	0.00	0.00	0.00	0.02	0.00
0.25	25	-0.01	-0.03	-0.01	-0.05	-0.01	-0.03	0.04	0.08	0.05	0.18	0.01
	50	-0.01	-0.0	-0.01	-0.04	-0.01	-0.05	0.02	0.04	0.02	0.12	0.00
	100	-0.01	-0.01	-0.01	-0.02	0.00	-0.04	0.01	0.02	0.01	0.08	0.00
	200	0.00	0.00	0.00	0.00	0.00	-0.04	0.01	0.01	0.01	0.06	0.00
	500	0.00	0.00	0.00	0.00	0.00	-0.02	0.00	0.01	0.00	0.04	0.00
0.4	25	0.00	-0.05	-0.01	-0.08	-0.01	-0.06	0.06	0.10	0.07	0.28	0.02
	50	0.00	-0.04	-0.02	-0.06	-0.02	-0.08	0.00	0.03	0.02	0.15	-0.01
	100	0.02	-0.01	0.00	-0.03	0.00	-0.04	0.03	0.04	0.03	0.11	0.01
	200	0.01	-0.01	0.00	-0.02	0.00	-0.04	0.00	0.02	0.02	0.08	0.00
	500	0.02	0.00	0.00	0.00	0.00	-0.02	0.01	0.02	0.02	0.07	0.00

Table 3.7: Bias of estimators of quantile at non-exceedance probability of 0.999

Shape	n	Estimator										
		MM	PWM	ML	PML	LM	MGF-KS	MGF-CM	MGF-AD	MGF-ADR	EPM	MDPD
-0.4	25	0.02	0.08	-0.10	-0.10	2.14	0.65	0.47	0.43	0.13	0.16	-0.07
	50	0.02	0.04	-0.06	-0.06	1.49	0.40	0.14	0.13	0.06	0.06	-0.04
	100	0.01	0.02	-0.04	-0.03	1.32	0.26	0.05	0.05	0.03	0.03	-0.03
	200	0.00	0.01	-0.02	-0.02	1.16	0.11	0.02	0.02	0.02	0.02	-0.02
	500	0.00	0.00	-0.01	-0.01	1.07	0.03	0.01	0.01	0.01	0.01	-0.01
-0.25	25	0.01	0.09	-0.10	-0.11	0.82	0.93	2.43	1.76	0.26	0.36	0.01
	50	0.00	0.04	-0.07	-0.08	0.33	0.39	0.26	0.20	0.09	0.13	-0.04
	100	-0.01	0.01	-0.04	-0.04	0.13	0.22	0.07	0.06	0.03	0.07	-0.03
	200	0.01	0.02	-0.02	-0.02	0.03	0.16	0.05	0.05	0.03	0.05	-0.01
	500	0.00	0.01	-0.01	-0.01	0.00	0.07	0.02	0.02	0.01	0.03	0.00
0	25	-0.06	0.07	-0.01	-0.15	0.15	0.89	3.49	633.16	0.68	1.08	1162.60
	50	-0.04	0.03	-0.03	-0.09	0.03	0.40	1.00	0.64	0.25	0.47	0.07
	100	-0.01	0.02	-0.01	-0.03	0.02	0.13	0.20	0.16	0.10	0.25	0.02
	200	-0.01	0.02	-0.01	-0.02	0.01	0.07	0.11	0.09	0.06	0.17	0.01
	500	-0.01	0.00	-0.01	-0.01	0.00	0.03	0.04	0.03	0.02	0.12	0.00
0.25	25	-0.24	0.05	0.38	-0.28	0.33	2.94	6.84	5.15	1.34	7.27	1.48
	50	-0.20	0.01	0.18	-0.17	0.16	0.62	2.31	1.42	0.65	1.88	0.55
	100	-0.12	0.03	0.06	-0.06	0.08	0.13	0.47	0.35	0.23	0.97	0.13
	200	-0.07	0.03	0.04	-0.02	0.05	0.00	0.19	0.15	0.11	0.55	0.07
	500	-0.04	0.01	0.01	-0.01	0.02	-0.04	0.07	0.05	0.03	0.35	0.03
0.4	25	-0.40	-0.01	0.82	-0.40	0.66	3.09	9.75	7.56	2.70	33.96	2.87
	50	-0.33	-0.01	0.29	-0.27	0.27	1.23	2.06	1.32	0.80	4.20	0.58
	100	-0.27	0.02	0.15	-0.13	0.15	0.28	0.77	0.52	0.35	1.98	0.27
	200	-0.22	0.01	0.05	-0.07	0.05	0.00	0.21	0.10	0.08	1.23	0.08
	500	-0.16	0.02	0.03	-0.02	0.03	-0.01	0.11	-0.04	-0.04	0.69	0.05

Table 3.8: RMSE of estimators of shape parameter for GPD

Shape	n	Estimator										
		MM	PWM	ML	PML	LM	MGF-KS	MGF-CM	MGF-AD	MGF-ADR	EPM	MDPD
-0.4	25	0.29	0.31	0.30	0.30	0.48	0.39	0.41	0.29	0.25	0.25	0.29
	50	0.18	0.20	0.17	0.17	0.43	0.28	0.26	0.18	0.16	0.15	0.16
	100	0.13	0.15	0.10	0.10	0.41	0.22	0.18	0.12	0.11	0.09	0.10
	200	0.08	0.10	0.06	0.06	0.40	0.15	0.12	0.08	0.07	0.06	0.06
	500	0.05	0.06	0.04	0.04	0.39	0.09	0.08	0.05	0.04	0.03	0.04
-0.25	25	0.25	0.28	0.30	0.31	0.27	0.33	0.42	0.31	0.26	0.25	0.30
	50	0.16	0.19	0.18	0.18	0.19	0.25	0.27	0.19	0.17	0.16	0.17
	100	0.11	0.13	0.10	0.10	0.12	0.19	0.18	0.12	0.11	0.10	0.10
	200	0.07	0.09	0.07	0.07	0.07	0.14	0.12	0.09	0.07	0.07	0.07
	500	0.05	0.06	0.04	0.04	0.04	0.09	0.08	0.05	0.05	0.04	0.04
0	25	0.22	0.24	0.30	0.28	0.21	0.30	0.43	0.31	0.26	0.28	0.31
	50	0.14	0.17	0.18	0.17	0.16	0.22	0.29	0.21	0.18	0.19	0.18
	100	0.10	0.12	0.11	0.11	0.11	0.16	0.19	0.14	0.12	0.13	0.11
	200	0.07	0.08	0.08	0.07	0.08	0.12	0.14	0.10	0.09	0.10	0.08
	500	0.04	0.05	0.05	0.04	0.05	0.07	0.08	0.06	0.05	0.07	0.05
0.25	25	0.25	0.25	0.33	0.31	0.27	0.37	0.46	0.34	0.30	0.37	0.33
	50	0.18	0.18	0.21	0.20	0.19	0.29	0.32	0.24	0.21	0.25	0.21
	100	0.12	0.12	0.13	0.13	0.13	0.20	0.20	0.16	0.14	0.20	0.14
	200	0.09	0.09	0.09	0.09	0.09	0.16	0.15	0.12	0.10	0.15	0.09
	500	0.06	0.05	0.05	0.05	0.06	0.10	0.09	0.08	0.07	0.11	0.06
0.4	25	0.29	0.27	0.34	0.33	0.30	0.46	0.46	0.35	0.32	0.44	0.35
	50	0.22	0.20	0.24	0.22	0.22	0.38	0.33	0.26	0.24	0.30	0.24
	100	0.16	0.13	0.15	0.14	0.14	0.26	0.22	0.18	0.16	0.23	0.16
	200	0.12	0.10	0.10	0.10	0.10	0.17	0.15	0.15	0.14	0.18	0.11
	500	0.09	0.07	0.06	0.06	0.06	0.11	0.09	0.17	0.16	0.15	0.07

Table 3.9: RMSE of estimators of scale parameter for GPD

Shape	n	Estimator										
		MM	PWM	ML	PML	LM	MGF-KS	MGF-CM	MGF-AD	MGF-ADR	EPM	MDPD
-0.4	25	0.33	0.35	0.38	0.38	0.32	0.34	0.36	0.30	0.29	0.30	0.37
	50	0.20	0.22	0.22	0.22	0.29	0.22	0.23	0.19	0.18	0.19	0.21
	100	0.15	0.16	0.14	0.14	0.28	0.18	0.17	0.14	0.13	0.13	0.13
	200	0.10	0.11	0.09	0.09	0.27	0.12	0.11	0.10	0.09	0.09	0.09
	500	0.06	0.07	0.06	0.06	0.27	0.08	0.07	0.06	0.06	0.05	0.06
-0.25	25	0.32	0.34	0.39	0.39	0.26	0.34	0.37	0.32	0.31	0.29	0.38
	50	0.22	0.23	0.24	0.24	0.19	0.24	0.25	0.22	0.21	0.20	0.23
	100	0.14	0.16	0.14	0.14	0.13	0.17	0.17	0.15	0.14	0.14	0.14
	200	0.10	0.11	0.10	0.10	0.10	0.12	0.11	0.10	0.10	0.10	0.10
	500	0.06	0.07	0.06	0.06	0.06	0.08	0.07	0.07	0.06	0.06	0.06
0	25	0.32	0.34	0.40	0.40	0.30	0.36	0.40	0.33	0.33	0.32	0.38
	50	0.20	0.22	0.23	0.23	0.21	0.23	0.25	0.22	0.21	0.21	0.23
	100	0.14	0.15	0.15	0.15	0.15	0.17	0.18	0.16	0.15	0.15	0.15
	200	0.10	0.11	0.10	0.10	0.10	0.12	0.13	0.11	0.11	0.11	0.10
	500	0.06	0.07	0.06	0.06	0.06	0.07	0.08	0.07	0.07	0.07	0.06
0.25	25	0.38	0.35	0.44	0.45	0.36	0.40	0.42	0.36	0.36	0.34	0.42
	50	0.25	0.24	0.25	0.26	0.24	0.28	0.28	0.25	0.24	0.23	0.25
	100	0.17	0.16	0.16	0.17	0.16	0.18	0.18	0.17	0.16	0.16	0.16
	200	0.12	0.11	0.11	0.11	0.11	0.13	0.13	0.12	0.12	0.12	0.11
	500	0.08	0.07	0.07	0.07	0.07	0.09	0.08	0.10	0.09	0.08	0.07
0.4	25	0.51	0.36	0.43	0.46	0.37	0.47	0.42	0.36	0.37	0.37	0.40
	50	0.37	0.26	0.29	0.30	0.27	0.37	0.30	0.27	0.27	0.26	0.28
	100	0.28	0.17	0.18	0.19	0.18	0.25	0.20	0.36	0.35	0.18	0.22
	200	0.19	0.12	0.12	0.13	0.12	0.15	0.14	0.30	0.30	0.13	0.15
	500	0.14	0.08	0.08	0.08	0.08	0.09	0.08	0.34	0.33	0.09	0.09

Table 3.10: RMSE of estimators of quantile at non-exceedance probability of 0.9

Shape	n	Estimator										
		MM	PWM	ML	PML	LM	MGF-KS	MGF-CM	MGF-AD	MGF-ADR	EPM	MDPD
-0.4	25	0.13	0.13	0.13	0.13	0.28	0.23	0.17	0.14	0.13	0.14	0.13
	50	0.09	0.09	0.09	0.09	0.19	0.16	0.12	0.09	0.09	0.09	0.08
	100	0.06	0.06	0.06	0.06	0.16	0.12	0.08	0.06	0.06	0.07	0.06
	200	0.05	0.05	0.04	0.04	0.13	0.08	0.06	0.05	0.05	0.05	0.04
	500	0.03	0.03	0.03	0.03	0.11	0.04	0.04	0.03	0.03	0.03	0.03
-0.25	25	0.15	0.15	0.15	0.15	0.20	0.24	0.23	0.18	0.16	0.17	0.15
	50	0.11	0.11	0.11	0.11	0.13	0.16	0.15	0.12	0.11	0.12	0.11
	100	0.07	0.08	0.07	0.07	0.08	0.12	0.10	0.08	0.08	0.08	0.07
	200	0.05	0.05	0.05	0.05	0.05	0.09	0.07	0.06	0.05	0.06	0.05
	500	0.03	0.03	0.03	0.03	0.03	0.05	0.04	0.03	0.03	0.04	0.03
0	25	0.20	0.20	0.21	0.20	0.21	0.26	0.30	0.37	0.23	0.27	0.36
	50	0.14	0.14	0.14	0.14	0.14	0.19	0.21	0.17	0.16	0.18	0.15
	100	0.10	0.10	0.10	0.10	0.10	0.13	0.13	0.11	0.11	0.13	0.10
	200	0.07	0.07	0.07	0.07	0.07	0.09	0.10	0.08	0.08	0.10	0.07
	500	0.04	0.04	0.04	0.04	0.04	0.06	0.06	0.05	0.05	0.07	0.04
0.25	25	0.27	0.25	0.26	0.24	0.26	0.38	0.42	0.37	0.31	0.48	0.29
	50	0.20	0.19	0.19	0.18	0.19	0.27	0.29	0.25	0.22	0.31	0.21
	100	0.14	0.13	0.14	0.13	0.14	0.18	0.19	0.16	0.15	0.22	0.14
	200	0.10	0.09	0.09	0.09	0.09	0.13	0.12	0.11	0.10	0.16	0.10
	500	0.06	0.06	0.06	0.06	0.06	0.09	0.08	0.07	0.07	0.12	0.06
0.4	25	0.39	0.30	0.34	0.29	0.33	0.44	0.51	0.45	0.40	0.73	0.38
	50	0.29	0.22	0.23	0.21	0.23	0.32	0.32	0.27	0.25	0.42	0.24
	100	0.22	0.16	0.16	0.15	0.16	0.22	0.21	0.24	0.23	0.30	0.17
	200	0.14	0.11	0.11	0.11	0.11	0.15	0.14	0.15	0.15	0.23	0.12
	500	0.09	0.07	0.07	0.07	0.07	0.10	0.09	0.10	0.10	0.17	0.07

Table 3.11: RMSE of estimators of quantile at non-exceedance probability of 0.999

Shape	n	Estimator										
		MM	PWM	ML	PML	LM	MGF-KS	MGF-CM	MGF-AD	MGF-ADR	EPM	MDPD
-0.4	25	0.28	0.39	0.22	0.21	3.11	1.24	3.43	2.81	0.61	0.40	0.26
	50	0.19	0.25	0.13	0.13	2.03	0.78	0.79	0.53	0.28	0.19	0.14
	100	0.13	0.17	0.08	0.08	1.69	0.55	0.31	0.20	0.13	0.10	0.09
	200	0.09	0.11	0.06	0.06	1.36	0.32	0.18	0.11	0.08	0.07	0.06
	500	0.06	0.07	0.03	0.03	1.18	0.16	0.10	0.06	0.05	0.04	0.03
-0.25	25	0.33	0.48	0.36	0.30	1.69	7.35	35.71	26.99	1.26	0.80	1.55
	50	0.22	0.31	0.21	0.20	0.77	0.89	1.28	1.01	0.42	0.34	0.24
	100	0.16	0.21	0.14	0.14	0.41	0.51	0.45	0.29	0.21	0.19	0.14
	200	0.11	0.15	0.09	0.09	0.15	0.37	0.27	0.18	0.13	0.13	0.10
	500	0.07	0.09	0.05	0.05	0.06	0.22	0.15	0.09	0.08	0.08	0.06
0	25	0.43	0.63	0.84	0.45	0.95	5.12	40.43	19907.05	3.58	2.79	36758.19
	50	0.33	0.44	0.49	0.36	0.51	2.25	8.35	4.40	1.01	1.12	0.87
	100	0.25	0.30	0.29	0.26	0.30	0.84	0.86	0.56	0.41	0.58	0.32
	200	0.18	0.22	0.19	0.18	0.21	0.42	0.52	0.35	0.28	0.41	0.21
	500	0.12	0.13	0.12	0.11	0.12	0.23	0.25	0.18	0.15	0.28	0.12
0.25	25	0.57	1.00	3.37	0.58	2.34	31.20	52.40	35.12	5.54	40.17	14.26
	50	0.47	0.72	2.75	0.53	1.77	4.07	25.32	11.21	5.53	5.72	7.81
	100	0.37	0.47	0.56	0.40	0.55	1.39	1.77	1.19	0.81	2.50	0.70
	200	0.30	0.34	0.37	0.32	0.37	0.73	0.82	0.60	0.48	1.33	0.42
	500	0.22	0.21	0.21	0.20	0.21	0.38	0.40	0.30	0.26	0.84	0.23
0.4	25	0.64	1.12	4.33	0.62	3.22	22.95	90.00	64.75	11.52	241.08	25.53
	50	0.56	0.94	1.69	0.55	1.57	11.05	11.88	5.81	3.81	19.53	2.87
	100	0.47	0.72	0.86	0.45	0.83	1.97	3.17	2.01	1.22	7.93	1.21
	200	0.37	0.50	0.49	0.37	0.49	0.87	0.96	0.67	0.59	6.48	0.54
	500	0.29	0.35	0.29	0.26	0.29	0.50	0.51	0.45	0.40	1.95	0.32

many authors in recent years [Caprani, 2005; Enright and O'Brien, 2012; O'Connor and O'Brien, 2005]. The description of the method is provided in Appendix B, but a simple summary of the models used is presented. The vehicles are classified by their silhouettes, and to each vehicle type we attached statistical models for gross vehicle weight, percentage of GVW taken by axle load and inter-axle spacing. The best fit is selected among the normal, bi- and tri-modal normal distribution. For the circulation characteristics, a refined hourly truck flow rate depended headway model proposed by O'Brien and Caprani [2005] is adopted. The observed gap distributions up to 4 seconds are modelled using quadratic curves for different flow rates, and a negative exponential distribution is used for larger gaps. Results for load effects from the simulation show reasonable agreement with those calculated from measured data as displayed in Figure 3.1. However, the tails do not match very well, the possible reasons is that the number of simulation days is too short, here 86 days data were simulated in order to have the same number of data with measured periods. Therefore, 1500 days traffic were simulated for the following analysis.

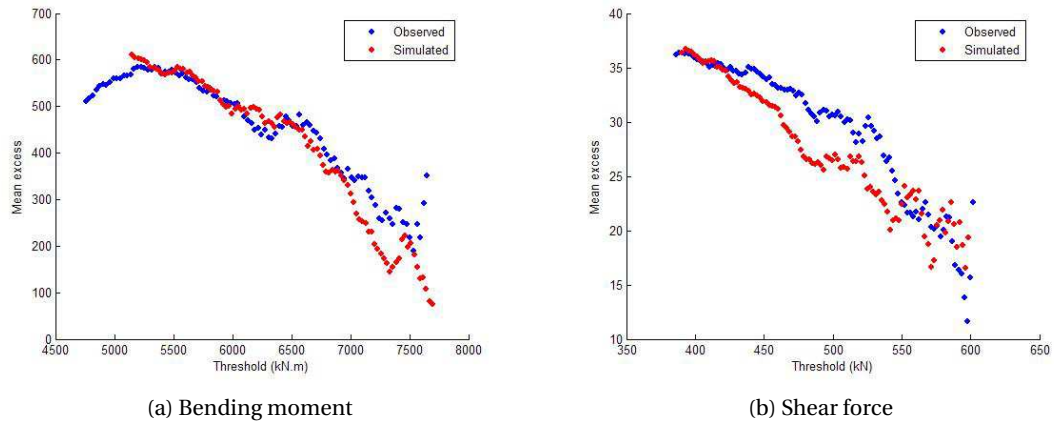


Figure 3.1: Comparison of simulated and observed load effects on ME plot

We adopt the forecast accuracy measure proposed by Hyndman and Koehler [2006], which is called mean absolute scaled error (MASE) that measures the forecast accuracy by scaling the error based on the mean absolute error (MAE) from the benchmark forecast method, to judge the performance of estimation methods. The commonly used RMSE is useful when comparing different methods applied to the same set of data, but is sensitive to outliers. A scaled error is defined as

$$q_t = \frac{Y_t - F_t}{\frac{1}{n-1} \sum_{i=2}^n |Y_i - Y_{i-1}|}, \quad (3.33)$$

which is independent of the scale of the data. A scaled error is less than one if it arises from a better forecast than the benchmark method. Conversely, it is greater than one if the forecast is worse than the benchmark. In this study, linear interpolated empirical quantiles are used as the benchmarks.

The MASEs, $mean(|q_t|)$, are given in Table 3.12 for several threshold values u and corresponding number of exceedance m , and some remarks can be drawn from the results:

- For all estimators, the MASEs decrease as the value of threshold increases, it is an indication that the GPD fits well the high tail.
- The ML and MPLE almost provide the smallest MASE for the samples with size greater than 100. Thus the two estimators perform better than the others for larger size samples. It confirms the conclusion from numerical simulations that MPLE has excellent performance for quantile estimation.
- In contrast, the PWM appears to provide the smallest MASE for the samples with size smaller than 100, and the MM, MGF-AD, and MDPD estimators have similar performance. Note that the bad performing MDPD method in the numerical case has well performance here.

3.3.3 Field measurement of traffic load effects

To evaluate the performance of visited estimators for realistic observations, we consider the measured maximum deformations analyzed by Siegert et al. [2008] using block maxima method. The measurements were from a highway prestressed concrete bridge, which consists of five simply supported concrete girders connected by an overall concrete deck and five cross beams as shown in figure. The instrumented span is 33 m long and carries three one way lanes. The bridge is located on a heavy trafficked motorway in the North of Paris.



Figure 3.2: View of the tested girder bridge

Table 3.12: Mean absolute scaled error for the competition of estimators traffic load effect data

Threshold	Num	MM	PWM	ML	MPLE	MDPD	MGF-KS	MGF-CM	MGF-AD	MGF-ADR	EPM
4737	619	17.36	28.28	13.11	13.11	25.26	47.34	55.00	44.73	28.36	31.09
4804	528	9.75	15.01	7.16	7.16	18.15	48.14	50.74	27.14	28.52	28.75
4872	462	7.49	11.93	7.99	8.00	16.25	47.10	49.46	26.75	28.40	26.99
4940	398	3.08	4.30	3.19	5.22	12.48	53.20	48.01	24.61	24.43	24.59
5007	351	3.66	3.51	5.30	5.28	10.85	47.91	44.71	21.43	14.64	22.71
5075	316	3.92	5.65	5.05	5.34	10.70	36.19	42.03	7.27	21.87	21.70
5143	283	4.93	8.04	3.81	3.82	10.29	37.34	40.78	22.82	22.18	21.03
5210	244	4.06	6.20	3.94	3.94	9.29	39.23	39.17	23.11	19.97	19.13
5278	207	3.33	3.34	2.90	2.90	7.30	41.09	35.25	17.14	14.45	16.51
5346	182	3.50	3.93	2.92	2.92	6.24	30.84	33.90	13.84	11.83	14.82
5414	156	5.48	6.91	2.84	2.79	5.02	48.62	30.03	3.74	3.45	11.54
5481	139	5.93	7.51	2.96	2.81	4.66	51.09	23.71	4.91	9.13	10.06
5549	126	4.64	6.48	2.97	2.98	3.95	46.44	22.84	8.25	6.92	9.90
5617	113	3.81	5.69	2.92	2.93	3.65	35.40	16.67	6.19	5.42	9.22
5684	102	2.24	4.33	2.32	3.35	3.27	23.83	9.14	2.89	4.16	8.43
5752	91	2.10	1.61	2.65	2.65	3.03	9.57	6.80	1.65	3.51	8.22
5820	79	2.52	2.41	2.66	2.66	2.85	5.55	5.27	3.54	3.55	7.82
5887	62	2.34	1.96	2.55	2.55	2.70	7.58	4.98	1.82	3.34	6.42
5955	51	2.07	1.53	2.04	2.12	2.16	5.01	2.85	2.70	2.74	5.73
6023	42	2.57	2.63	2.43	2.43	2.51	2.07	2.16	2.77	2.70	6.62

Figure 3.3 shows a scheme of the instrumented span with three resistive strain gauges J1, J2 and J3, which were on the mid-span of girder P1 under the slow lane. Bending deformations were measured, and the measurements were processed to filtrate the thermal effects and electrical drift. The monitoring system has a sampling frequency of 75 Hz, but only the maximum and minimum values of 120s duration signals were recorded for the purpose to study extreme traffic load effects. Considering the length and type of instrumented bridge, the 2-minute maxima load effects can be treated as independently distributed population. 256 days' measurements were collected during two periods, one was conducted from February, 2004 to June, 2004, and the other was from January, 2005 to June 2005. Due to traffic patterns, the load effects collected on weekends and holidays differ from those from weekdays, these days' measurement were excluded and 178 days were kept finally. The histogram for these filtrated measurements is given in Figure 3.4.

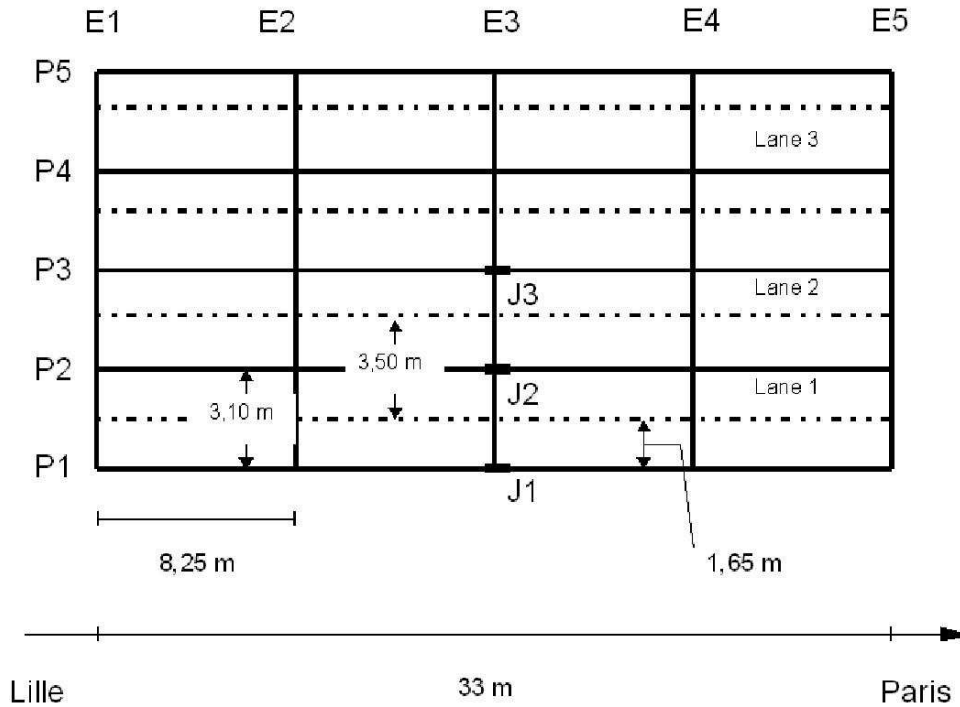


Figure 3.3: Instrumented span, after Siegert et al. [2008]

We use the GPD model to fit the exceedances over high threshold. To study the sensitivity of the estimates to the specification of the threshold, we repeat the calculations for several thresholds and monitor the effect of changing the threshold on the obtained results. The estimated parameters and their standard errors for three estimation methods are given in table for several thresholds u . The standard errors are computed based on 1000 bootstrap samples. The estimated parameters and their standard errors for various estimation methods are given in Tables 3.14 to 3.16. The selected estimation methods include the MM, the PWM, the ML, the PML, the ML, the MDPD, the MGF-AD and the MGF-ADR. The MGF-KS and MGF-CM

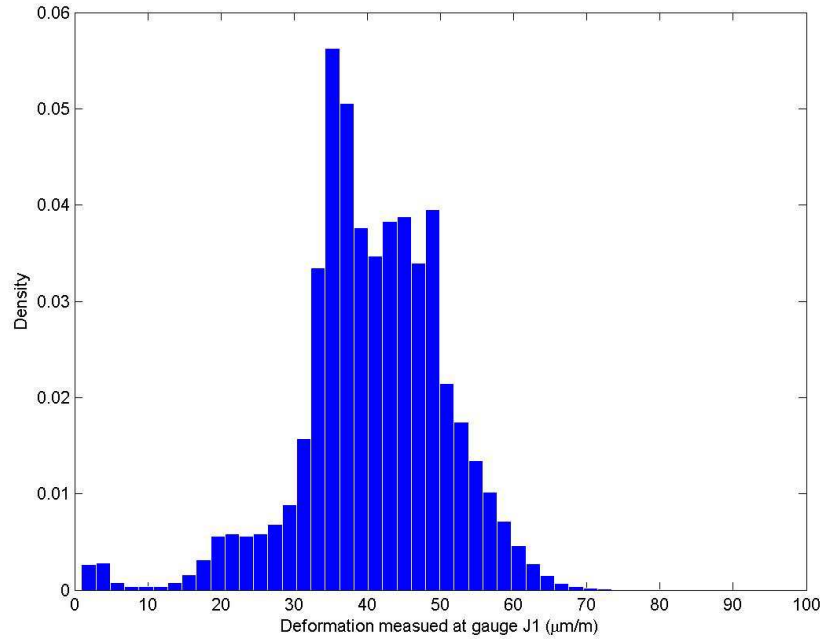


Figure 3.4: Histogram of the measured bending deformations

were abandoned as they do not work well in previous preliminary studies as compared to the others, and the EPM also has similar performance as the MGF-KS estimator.

Two observations, which are $95.2 \mu/m$ and $99.4 \mu/m$, measured in June 2004 were close to $100 \mu/m$ and were much larger than the others less than 70. Siegert et al. [2008] kept them in the extreme value extrapolation by using block maxima method, but their influence on the extrapolation was not reported. As noted, the outliers have great influence on estimation methods like MM in application of POT method. Therefore, our first objective will be to test how they influence the parameter estimates through consistency analysis. The inconsistency issue refers to the upper bound defined by $-\frac{\sigma}{\mu}$ is less than the data considered.

Table 3.13 shows, for each threshold, the percentage of times that each method of estimation produced an estimate of the GPD upper bound that is inconsistent with the data. The values in parentheses are those for data when the two outliers are removed. It is apparent that the two outliers have severe influence on the consistency issue, the rates of inconsistency for basis data including the two outliers are larger than those for data excluding the two outliers. Especially, only the ML and PML encounter feasibility problems for data without the two outliers when threshold is higher than 61, while all methods report the feasibility problem for data with two outliers. Moreover, for all methods considered, it can be seen that the inconsistency rate increases with decreasing threshold level or increasing sample size. Although it is counterintuitive, similar observations were reported in [Ashkar and Nwentsa Tatsambon, 2007; Dupuis, 1996]. Therefore, the outliers should be dealt with very carefully, it is better

Table 3.13: Inconsistency rate for method of estimation

Threshold	MM	PWM	Hybrid	ML	PML	MDPD	LM	MGF-AD	MGF-ADR
56	100 (99.5)	100 (100)	67.3 (56.6)	13.4 (0)	13.4 (0)	37.5 (2.3)	37.5 (13.7)	37.5 (14)	37.5 (14)
57	97.9 (39.2)	100 (100)	68.9 (58.3)	14.5 (0)	14.5 (0)	37.3 (0)	39 (4.9)	39.1 (12.5)	39.1 (11.1)
58	67.1 (1.2)	100 (99.4)	65.6 (54)	8.4 (0)	8.4 (0)	24.4 (0)	33.7 (0)	35.8 (10.9)	35.8 (1.7)
59	11.7 (0)	99.3 (34.2)	67.5 (20.6)	2.6 (0)	2.6 (0)	6.9 (0)	15.2 (0.2)	34.9 (1.8)	28.9 (0)
60	0.79 (0)	60.8 (1)	42.4 (0.4)	0.1 (0)	0.13 (0)	0.6 (0)	2.7 (0.3)	22.7 (0)	6.9 (0)
61	0 (0)	4.3 (0)	3.4 (0)	0 (0)	0 (0)	0 (0)	0 (0)	1.3 (0)	0.2 (0)
62	0 (0)	0.3 (0)	0.3 (0)	0 (0)	0 (0)	0 (0)	0 (0)	0 (0)	0.4 (0)
63	0 (0)	0.8 (0)	0.8 (0)	0 (0)	0 (0)	0 (0)	0 (0)	0 (0)	0 (0)
64	0 (0)	0 (0)	0 (0)	0 (0)	0 (0)	0 (0)	0 (0)	0 (0)	0 (0)
65	0 (0)	0 (0)	0 (0)	0 (0)	0 (0)	0 (0)	0 (0)	0 (0)	0 (0)
66	0 (0)	0 (0)	0 (0)	0 (0)	0 (0)	0 (0)	0 (0)	0 (0)	0 (0)
67	7.7 (0)	8.9 (0)	8.9 (0)	9.3 (0)	8.6 (0)	7.8 (0)	11.1 (0)	9.1 (0)	4.5 (0)
68	0 (0)	0 (0)	0 (0)	0 (0)	0 (0)	0 (0)	0 (0)	0 (0)	0 (0)
69	5.9 (0)	25 (0)	25 (0)	5.6 (0)	4.3 (0)	14.3 (0)	14.3 (0)	0 (0)	6.5 (0)
70	5.6 (0)	0 (0)	0 (0)	9.1 (0.7)	8.3 (0.7)	18.2 (0)	0 (0)	0 (0)	17.3 (0)

to keep them to capture information on extreme if they do not induce feasibility problem in parameter estimation. The same consideration should be made in threshold selection, since lower threshold may induce feasibility problem.

Following the consistency analysis, the two outliers were removed in the analysis. Further, the thresholds were set between 61 and 69 to avoid nonfeasibility modeling. The results in terms of the mean and standard deviation of shape and scale parameter, and three return periods' characteristic values from the 1000 bootstrap samples were listed in Tables 3.14, 3.15 and 3.16. Some remarks can be made:

- For different threshold levels, the mean value and standard deviation of the shape parameter increase with increasing threshold values; the scale parameter has similar feature but the mean value decreases with increasing thresholds. It seems that a threshold over 67 leads to unreasonable modeling of GPD to the exceedances, the mean value shape parameters are greater than 0.1 that violates the conclusions that the type of extreme value distribution of traffic load effect should be upper bounded (see e.g., Bailey [1996]). In contrast, the shape parameter estimates for exceedances with thresholds less than 67 are negative or close to zero.
- For parameter estimates, it turns out that all methods have similar performance except the standard Anderson-Darling test statistic based MGF estimator, which gives a larger mean value for shape parameter but a smaller mean value for the scale parameter for all threshold levels considered.
- For return level, values for three different return periods, which are 10 years, 100 years and 1000 years, and represent short term and remote term, have been considered. It can be seen that the extrapolated values for 10-year and 100-year return period are stable with thresholds and estimation methods, but the predictands for 1000-year return periods are sensitive to the thresholds and also the estimation methods. Hence, one must cope with the disadvantage that the number of available measurements is relatively small when extrapolating return level for a long period compared with the measured period. Again, the MGF-AD has worse performance than the others, thus it should not be considered as an estimator for GPD in the traffic load effect applications. In addition, it is seen that the moments based estimation methods provide smaller estimates for return level.
- The MDPD does not perform as well as expected, even if it provides unreasonable return level for 1000-year return period.

3.4 Conclusion

One of the main problems in using POT to model extreme events is the need to obtain optimal parameters for generalized Pareto distribution. The parameters are important to describe the

Table 3.14: The Bridge of Roberval Measurements: shape and scale parameters

Parameter	Threshold	Mean									Standard error								
		61	62	63	64	65	66	67	68	69	61	62	63	64	65	66	67	68	69
Shape	No.	2334	1719	1243	904	654	462	320	243	175	2334	1719	1243	904	654	462	320	243	175
	MM	-0.02	0.00	0.01	0.03	0.05	0.03	0.00	0.05	0.05	0.02	0.02	0.02	0.03	0.03	0.04	0.05	0.05	0.05
	PWM	-0.06	-0.01	0.01	0.06	0.11	0.09	0.04	0.13	0.15	0.02	0.03	0.03	0.03	0.04	0.05	0.06	0.07	0.08
	Hybrid	-0.06	-0.01	0.01	0.06	0.11	0.09	0.04	0.13	0.15	0.02	0.03	0.03	0.03	0.04	0.05	0.06	0.07	0.08
	ML	-0.02	0.00	0.02	0.04	0.08	0.05	0.01	0.09	0.11	0.02	0.02	0.03	0.03	0.05	0.06	0.06	0.08	0.11
	PML	-0.02	0.00	0.01	0.04	0.08	0.05	0.01	0.08	0.09	0.02	0.02	0.03	0.03	0.05	0.05	0.06	0.08	0.10
	MDPD	-0.03	0.01	0.02	0.06	0.12	0.09	0.03	0.15	0.20	0.02	0.02	0.03	0.04	0.05	0.07	0.07	0.11	0.16
	LM	-0.03	0.01	0.03	0.06	0.12	0.09	0.04	0.14	0.16	0.02	0.02	0.03	0.04	0.05	0.06	0.06	0.09	0.11
	MGF-AD	-0.04	0.02	0.06	0.13	0.26	0.25	0.13	0.38	0.53	0.03	0.03	0.04	0.05	0.07	0.11	0.10	0.18	0.27
	MGF-ADR	-0.03	0.01	0.03	0.08	0.13	0.07	0.02	0.11	0.13	0.02	0.03	0.04	0.04	0.06	0.07	0.07	0.10	0.12
Scale	MM	3.06	2.90	2.82	2.70	2.58	2.69	2.81	2.51	2.47	0.08	0.09	0.11	0.12	0.15	0.18	0.22	0.22	0.28
	PWM	3.16	2.92	2.81	2.62	2.43	2.53	2.72	2.31	2.23	0.09	0.10	0.12	0.13	0.16	0.20	0.25	0.25	0.31
	Hybrid	3.16	2.92	2.81	2.62	2.43	2.53	2.72	2.31	2.23	0.09	0.10	0.12	0.13	0.16	0.20	0.25	0.25	0.31
	ML	3.05	2.89	2.81	2.67	2.52	2.64	2.81	2.43	2.35	0.08	0.10	0.12	0.14	0.18	0.22	0.25	0.29	0.37
	PML	3.05	2.90	2.81	2.67	2.53	2.65	2.81	2.45	2.38	0.08	0.10	0.12	0.14	0.17	0.21	0.24	0.28	0.36
	MDPD	3.06	2.88	2.79	2.62	2.43	2.56	2.75	2.31	2.19	0.08	0.10	0.12	0.14	0.18	0.23	0.25	0.31	0.41
	LM	3.08	2.88	2.78	2.61	2.43	2.54	2.73	2.31	2.22	0.08	0.10	0.12	0.13	0.17	0.22	0.25	0.28	0.35
	MGF-AD	3.10	2.86	2.74	2.51	2.23	2.30	2.59	1.99	1.79	0.09	0.11	0.13	0.15	0.18	0.25	0.29	0.34	0.44
	MGF-ADR	3.07	2.90	2.79	2.64	2.49	2.68	2.82	2.47	2.43	0.09	0.10	0.12	0.14	0.18	0.23	0.25	0.29	0.36

Table 3.15: The Bridge of Roberval Measurements: Return levels for various return periods - Mean

Method	Threshold	Mean								
		61	62	63	64	65	66	67	68	69
	No.	2334	1719	1243	904	654	462	320	243	175
MM	10	89	92	93	94	96	94	91	94	93
	100	95	99	100	103	106	103	99	103	103
	1000	100	106	108	113	119	113	106	115	115
PWM	10	86	91	93	98	104	100	95	102	103
	100	90	97	101	110	122	116	105	122	126
	1000	93	103	109	124	147	136	117	151	161
Hybrid	10	86	91	93	98	104	100	95	102	103
	100	90	97	101	110	122	116	105	122	126
	1000	93	103	109	124	147	136	117	151	161
ML	10	89	92	93	95	99	96	92	98	101
	100	95	99	101	106	114	107	100	114	123
	1000	100	106	109	117	132	120	109	137	166
PML	10	89	92	93	95	99	95	92	97	98
	100	95	99	101	105	113	106	99	111	116
	1000	100	106	109	117	130	119	108	131	145
MDPD	10	89	92	94	98	107	101	94	109	129
	100	94	100	103	111	128	118	104	144	269
	1000	100	107	112	126	159	142	116	213	1129
LM	10	89	92	94	99	105	101	95	105	108
	100	94	100	103	111	126	117	105	129	141
	1000	99	107	113	126	153	139	117	167	205
MGF-AD	10	88	95	99	114	154	155	111	269	839
	100	93	104	112	141	248	265	143	977	9825
	1000	97	114	127	181	441	534	197	5040	166872
MGF-ADR	10	89	93	96	102	110	100	95	104	106
	100	94	101	106	117	134	115	104	126	136
	1000	99	109	117	136	169	134	116	162	194

Chapter 3. A Comparative Evaluation for the Estimators of the GPD

Table 3.16: The Bridge of Roberval Measurements: Return levels for various return periods - Standard deviation

Method	Threshold	Standard deviation								
		61	62	63	64	65	66	67	68	69
	No.	2334	1719	1243	904	654	462	320	243	175
MM	10	2.34	2.67	2.93	3.11	3.51	3.57	3.57	3.84	3.83
	100	3.49	4.19	4.76	5.30	6.34	6.36	6.21	7.34	7.61
	1000	4.83	6.10	7.14	8.31	10.46	10.29	9.76	12.67	13.57
PWM	10	2.38	3.19	3.85	4.80	6.42	6.44	5.69	8.05	8.96
	100	3.38	4.95	6.32	8.65	13.04	13.01	10.76	18.55	22.51
	1000	4.48	7.13	9.56	14.33	24.22	23.88	18.44	38.75	51.20
Hybrid	10	2.38	3.19	3.85	4.80	6.42	6.44	5.69	8.05	8.96
	100	3.38	4.95	6.32	8.65	13.04	13.01	10.76	18.55	22.51
	1000	4.48	7.13	9.56	14.33	24.22	23.88	18.44	38.75	51.20
ML	10	2.25	2.88	3.42	4.37	6.66	6.21	4.91	10.06	17.15
	100	3.36	4.55	5.64	7.72	13.11	12.00	8.99	24.40	59.54
	1000	4.66	6.65	8.55	12.51	23.60	21.14	14.89	56.25	219.03
PML	10	2.24	2.84	3.36	4.28	6.44	5.90	4.64	8.77	11.93
	100	3.34	4.48	5.53	7.54	12.58	11.31	8.41	20.30	33.28
	1000	4.63	6.54	8.38	12.18	22.50	19.74	13.81	43.88	90.50
MDPD	10	2.33	3.20	4.01	5.70	10.55	10.44	6.69	25.02	134.35
	100	3.45	5.11	6.71	10.49	22.74	22.75	13.02	85.14	1314.78
	1000	4.77	7.54	10.36	17.76	45.35	46.08	23.08	302.34	13763.98
LM	10	2.38	3.21	3.94	5.29	8.39	8.19	6.14	12.71	18.50
	100	3.51	5.12	6.60	9.71	17.59	17.07	11.80	32.60	58.93
	1000	4.83	7.55	10.19	16.37	33.88	32.55	20.60	78.45	185.84
MGF-AD	10	2.94	5.07	6.97	13.49	39.14	61.64	22.51	322.36	2573.30
	100	4.30	8.38	12.40	28.86	116.45	222.56	60.68	2520.62	60698.45
	1000	5.86	12.84	20.44	57.56	331.45	797.54	160.98	20543.59	1564691.00
MGF-ADR	10	2.85	4.04	5.19	7.53	12.41	9.69	7.19	14.71	21.30
	100	4.23	6.48	8.84	14.29	27.35	20.05	13.73	37.89	66.44
	1000	5.85	9.62	13.91	25.06	56.16	38.53	24.03	95.11	205.36

model of extremes and to predict extreme quantiles. A number of estimation methods exist in the literature, some have extensive application, while some are just applied to numerical samples. The main objective of the study presented was to provide an evaluation of the relative performance of methods for estimating parameters and quantiles of the GPD through numerical samples and realistic traffic load effects, and it can provide a guidance to apply the POT method to traffic load effects. The forecast accuracy measures of RMSE, bias and MASE were introduced to perform the evaluation.

Although no method is uniformly best based on the simulation results and realistic applications, there are still some valuable findings. The MGF-KS, MGF-CM, MGF-AD and EPM do not seem to be the optimal for modeling GPD of traffic load effects among these considered in this study. Sample size has a great influence on the accuracy of parameter estimation, almost all estimators perform better for larger size sample than smaller, that is illustrated by the decreasing of bias and RMSE. However, the different methods have a various sensitivity to size of sample. The most influenced method is ML, which has extremely different performance between small size sample and large size sample. The PWM and MM have the best performance in small size sample, while the ML and MPLE are the optimal choice for large sample. Although the quantile is a function of parameters, the performance of estimators differs according to the considered parameter and quantile. The PWM and MM seem the better choice for parameter estimations than others, while MPLE shows excellent performance for quantile estimation. These findings based on simulations are confirmed by realistic applications. An interesting finding to be noted is the worst performing MDPD method in simulation study has a better performance in realistic application. The realistic data are always contaminated, while the better performance of the MDPD for contaminated data has been demonstrated by Juárez and Schucany [2004]. For modeling traffic load effects, the MDPD method is an optimal choice. However, the traditional methods can also be a option. The ML and MPLE are preferable methods for large size sample as the shape parameter is always in the range of $[-0.5, 0.5]$; the MM method is proposed to be used in the case of small size samples only.

4 Mixture POT Approach to Model Extreme Bridge Traffic Load Effect

4.1 Introduction

As concluded in Chapter 3, the outliers cause feasible problem on parameter estimator. As been stated in statistical literature, a frequent cause of outlier is a mixture of two distributions, which may be two distinct sub-populations. The aim of this chapter is to introduce a modification to the POT method to address the mixture feature of traffic load effects on short to medium span bridges. Caprani et al. [2008]; Harman and Davenport [1979] have pointed out that the traffic load effect is induced by loading event that involves different number of vehicles, and the distribution of the load effects from different loading events are not identically distributed. Hence, it violates the assumption of classic extreme value theory that the underlying distribution should be identically independent distributed. With respect to non-identical distribution in bridge traffic load effects, non-identical distribution needs to be addressed in extreme modelling to account for the impacts in inference. Harman and Davenport [1979] have proposed to model the traffic load effect with an exponential distribution. Caprani et al. [2008] have addressed the maximum distribution of mixing of non-identically distributed load effects by a composite generalized extreme value distribution.

However, it should be noticed that the generalized extreme value distribution is fitted to block maxima, which implies the possibility of losing some extremes, and the use of exponential distribution is objective. We has attempt to explicitly model the non-identically distributed behaviour of extremes for a stationary extreme time series with a mixture peaks over threshold (MPOT) model to avoid the loss of information and predetermination of distribution type in the present chapter. The new method is to simultaneously model both tails using GPD and to account for the non-identically distribution feature of traffic load effects. More specifically, we have defined a mixture generalized Pareto distribution with certain components corresponding to different types of loading events. To illustrate the behaviour and accuracy of the proposed method, numerical simulation data generated from three commonly used types of distributions (GPD, GEV and Normal) are used as it is possible to compare with the true value. Comparison has also been donducted to investigate the difference between the mixture peaks

over threshold method and the conventional peaks over threshold. Finally, the method has been applied to model the extreme traffic load effects on bridges.

4.2 Methodology

The bridge loading event (BLE) sample can be partitioned in j -truck loading events, where the probability that the maximum possible maximum load effect in the i^{th} event of BLEs in a given reference period such as a day, S_i , is less than or equal to some value, is then given by the law of total probability:

$$P(S_i \leq s) = F(s) = \sum_{j=1}^{n_t} F_j(s) \cdot \varphi_j \quad (4.1)$$

Where $F_j(\cdot)$ is the cumulative distribution function (CDF) for the local extremal load effect in a j -truck event and φ_j is the probability of occurrence of a j -truck event, where $j = 1, \dots, n_t$.

$$\bar{F}(x) = 1 - F(x) = \sum_{j=1}^{n_t} [1 - F_j(s)] \varphi_j \quad (4.2)$$

According to the classic extreme value theory, the CDF of the maximum load effect from a sample with distribution function F of size n is then given by:

$$G(x) = F^n(x) = \left[\sum_{j=1}^{n_t} F_j(s) \varphi_j \right]^n \quad (4.3)$$

Reiss and Thomas [2007] state that if the iid condition fails, then a df of the form F^n may still be an accurate approximation of the actual df of the maximum. For independent, yet heterogeneous random variables X_j with df F_j , the previous equation holds with F^n replaced by $\prod_{j=1}^{n_t} F_j$. Caprani et al. [2008] obtain similar functions from the GEV distribution, and the parameters are found by fitting GEV to block maxima of each BLE types. It is expressed:

$$P[S \leq s] = \left[\sum_{j=1}^{n_t} F_j(s) \varphi_j \right]^{n_d} = \prod_{j=1}^{n_t} G_j$$

$$G_j(s) = \exp \left\{ - \left[1 + \xi_j \left(\frac{s - \mu_j}{\sigma_j} \right) \right]^{-\frac{1}{\xi_j}} \right\}$$

Where μ_j is the location parameter; σ_j is the scale parameter; and ξ_j is the shape parameter - all for loading event type j .

The maximum distribution function can also be expressed as:

$$G(x) = F^n(x) = [1 - F(x)]^n \quad (4.4)$$

Where $\bar{F}(x) = 1 - F(x)$ is the survivor function given in Eq. (eq:SFun). The parameter, n , is the number of loading events for a reference period such as 1 day, which is a sufficiently large value. For large values of x , a Taylor expansion leads to:

$$G(x) \approx \exp[-n\bar{F}(x)] \quad (4.5)$$

For the case of mixture distribution, Harman and Davenport [1979] approximate it by a convolution of exponential distributions:

$$G(x) = \exp[-n\bar{F}(x)] = \prod_{j=1}^{n_t} \exp[-n\varphi_j \bar{F}_j(x)] \quad (4.6)$$

Therefore, the authors used negative exponential distribution to fit the upper tail of each effect induced by corresponding type of loading event, and the distribution parameters were estimated by a graphic method. Actually, the exponential distribution is a special case of the GPD and is obtained from CDF of GPD by taking the limit as $\xi \rightarrow 0$. The use of CDF of GPD to model excesses is a natural as GPD has an interpretation as a limit distribution similar to that which motivates the GEV distribution. See Pickands III [1975] and Davison and Smith [1990] for further developments and applications. However, from extreme value theory, the tail distribution has the following relationship with GPD:

$$Pr(X > u) = \frac{1 - F(x)}{1 - F(u)} = 1 - H(y) \quad (4.7)$$

Thus, the survivor function is

$$1 - F_j(x) = [1 - H_j(y)][1 - F_j(u_j)] \quad (4.8)$$

Then,

$$\bar{F}(x) = \sum_{j=1}^{n_t} [1 - H_j(x - u_j)][1 - F_j(u_j)]\varphi_j \quad (4.9)$$

Therefore,

$$F(x) = 1 - \bar{F}(x) = 1 - \sum_{j=1}^{n_t} [1 - H_j(x - u_j)][1 - F_j(u_j)]\varphi_j \quad (4.10)$$

Substitution into (Eq. 4.6) yields:

$$G(x) = \exp - \sum_{j=1}^{n_t} n\varphi_j [1 - F_j(u_j)] [1 + \xi_j (\frac{x - u_j}{\sigma_j})]^{-\frac{1}{\xi_j}} \quad (4.11)$$

There is no need to know the underlying parent distribution function of F , the parameters of the distribution are determined by fitting the upper tail of load effects induced by each type of loading event to GPD separately.

4.3 Theoretical Examples

The studies presented stipulate the parent distributions of load effect. Therefore, via Eq. (4.10) or Eq. (4.3), the exact distribution of load effect is known. Further, random values of local extremes from each component mechanism are simulated. Such data samples form the basis of the application of mixture peak-over-threshold (MPOT) and the conventional peak-over-threshold (CPOT) methods; the results from both methods are compared to the exact return level for a given return period, or the exact distribution. In this way, the studies mirror the real-life application of the proposed method and its behaviour in such problems can be assessed and compared.

4.3.1 Sample Problems and Examples

In what follows we show simulation results for quantiles corresponding to a 1000-year return period, from samples corresponding to generalized Pareto, generalized extreme value, and normal distributions. Three studies are performed to evaluate the performance of the MPOT approach and to compare the MPOT with conventional POT. The first is designed to explore the performance of MPOT on Monte Carlo samples drawn by GPDs with difference combination of parameters: specifically, we compare MPOT results with those of a standard fit with a single distribution. The second and the third studies are designed to reflect the true relationships between mechanisms that comprise the loading events, provide insight into the nature of the asymptotic theory of extreme order statistics, and cases in which careful consideration of its applicability is required. For CPOT method, the GPD is fit to the mixed data, and the parameters are estimated by five estimators described in following. For MPOT method, the data is separated by its type of event, and these coming from same event are fitted to a standard GPD.

The parameters of GPD are estimated by the method of moments (MM), the probability-weighted moment (PWM), the maximum likelihood (ML), the Right-tail Anderson-Darling (ADR), and the minimum density power divergence (MDPD). These estimators have shown their excellent performance in estimating parameters of GPD either for numerical sample or traffic load effects in Chapter 3, and also they are representative of the most commonly used estimators [de Zea Bermudez and Kotz, 2010]. The MM, PWM, and ML are the most common

and quite useful ones in practice. The MM and PWM methods use the first and second order moments to estimate the parameters, and they have good performance in the situations of small size samples. The ML is the most efficient method for estimating the parameters of the GPD for sample size larger than 500.

4.3.2 Study 1: GPD distributed sample

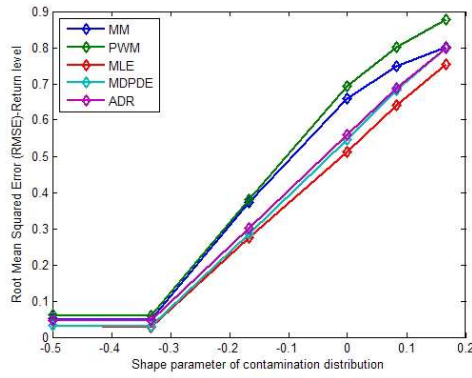
In this section we assess the performance of the conventional POT approach and the mixture POT approach on quantile estimation when the underlying generalized Pareto distribution is not identically distributed. Dupuis and Field [1998]; Juárez and Schucany [2004]; Peng and Welsh [2001] call that one distribution of $F_1(\xi_1, \sigma_1)$ is contaminated by another $F_2(\xi_2, \sigma_2)$, and the distribution $F_2(\xi_2, \sigma_2)$ is called contamination distribution. Both Peng and Welsh [2001] and Juárez and Schucany [2004] state that the slight change of scale parameter has small influence on shape parameter estimates, hence, only a change of shape parameter is considered in this study. We have generated five hundred samples of size $n = 2000$ from the 10% mixture distribution $0.90F_1(\xi_1, \sigma_1) + 0.1F_2(\xi_2, \sigma_2)$ and applied the estimators MM, PWM, ML, MDPD and ADR to estimate parameters for the cases $(\xi_1, \sigma_1, \epsilon, \xi_2, \sigma_2) = (-1/3, 1, 0.1, -1/2, 1), (-1/3, 1, 0.1, -1/3, 1), (-1/3, 1, 0.1, -1/6, 1), (-1/3, 1, 0.1, 0, 1), (-1/3, 1, 0.1, 1/12, 1)$, and $(-1/3, 1, 0.1, 1/6, 1)$, where ϵ is the probability weight of contamination distribution. The data generated by $F_1(\xi_1, \sigma_1)$ are denoted as event 1, and those generated by $F_2(\xi_2, \sigma_2)$ are denoted as event 2. Therefore, it is possible to identify the data through the denoted type of events. In order to avoid the influence of threshold estimation on modelling, the distributions are set to have the same threshold. In all cases, the contamination is chosen to be fairly mild as the objective is to reflect its influence on extreme value prediction and modelling. However, in practice like traffic load effects may comprise of several types of loading events with almost the same weight, another sensitivity study is given in Section 4.4.2 to discuss the influence of component composition on modelling.

Results are presented here in terms of the quantile estimates from CPOT and MPOT approaches, since most often we are interested in the accuracy of the predicted extreme values. Quantile estimators from CPOT approach are obtained by using Eq. (1.13), while quantile estimators from MPOT are obtained by using Eq. (4.10). Substituting the parameters of the six cases into Eq. (4.10) and equating to a probability of $1 - 1/(1000 \times 250 \times 2000/500)$ gives the 1000-year return levels, x_{1000} , of 2.9689, 5.1193, 11.5129, 19.3219, and 34.8775, respectively for the five contaminated cases, while the corresponding return level for uncontaminated case is 2.97. The return levels are reported in terms of the ratio of predicted values with respect to the corresponding accuracy values as $r = \hat{x}_{1000}/x_{1000}$. When the ratio is less than one, the predicted value is smaller than accuracy ones. We consider the root mean squared errors of the estimators in Table 4.1, the biases in Table 4.2, the means in Table 4.3 and their standard errors in Table 4.4 of parameter and quantile estimates. For a subset of the estimators results are presented graphically in Figure 4.1 - 4.4 for all cases considered.

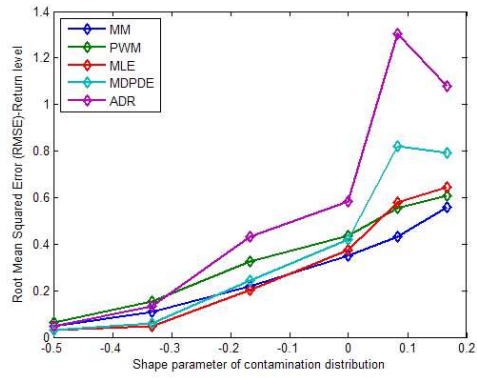
Chapter 4. Mixture POT Approach to Model Extreme Bridge Traffic Load Effect

Table 4.1: Simulation results for the estimation methods of MM, PWM, ML, MDPD and ADR. The results presented are the RMSEs over 500 replicates.

$(\xi_0, \sigma_0, \epsilon, \xi_1, \sigma_1)$	Parameter	MM	PWM	ML	MDPD	ADR
$(-1/3, 1, 0.1, -0.5, 1)$	CPOT	0.0517	0.0626	0.0330	0.0318	0.0454
	MPOT	0.0486	0.0614	0.0299	0.0318	0.0471
$(-1/3, 1, 0.1, -1/3, 1)$	CPOT	0.0476	0.0603	0.0280	0.0297	0.0461
	MPOT	0.1093	0.1538	0.0485	0.0577	0.1325
$(-1/3, 1, 0.1, -1/6, 1)$	CPOT	0.3719	0.3805	0.2746	0.2865	0.3019
	MPOT	0.2206	0.3242	0.2034	0.2449	0.4310
$(-1/3, 1, 0.1, 0, 1)$	CPOT	0.6589	0.6940	0.5118	0.5473	0.5584
	MPOT	0.3483	0.4359	0.3731	0.4211	0.5816
$(-1/3, 1, 0.1, 1/12, 1)$	CPOT	0.7487	0.8016	0.6401	0.6837	0.6883
	MPOT	0.4329	0.5561	0.5810	0.8206	1.3039
$(-1/3, 1, 0.1, 1/6, 1)$	CPOT	0.8012	0.8787	0.7537	0.7991	0.7991
	MPOT	0.5588	0.6063	0.6451	0.7931	1.0792

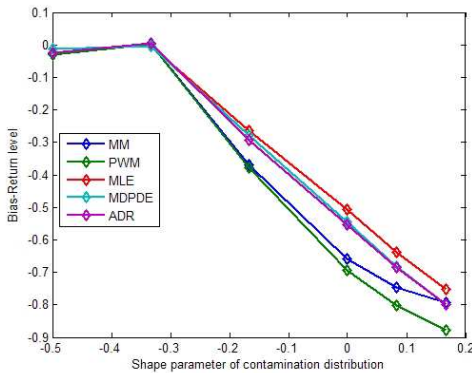


(a) Return level - CPOT.

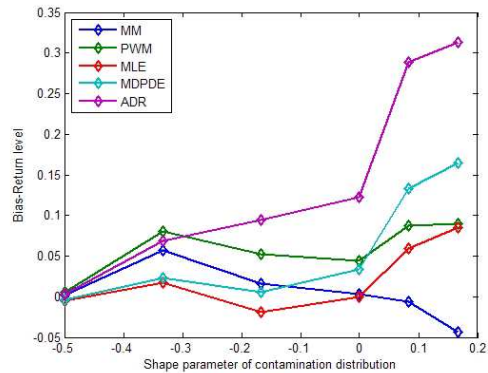


(b) Return level - MPOT.

Figure 4.1: RMSE of quantile estimators.



(a) Return level - CPOT.



(b) Return level - MPOT.

Figure 4.2: Bias of quantile estimators.

4.3. Theoretical Examples

Table 4.2: Simulation results for the estimation methods of MM, PWM, ML, MDPD and ADR. The results presented are the biases over 500 replicates.

$(\xi_0, \sigma_0, \epsilon, \xi_1, \sigma_1)$	Parameter	MM	PWM	ML	MDPD	ADR
$(-1/3, 1, 0.1, -0.5, 1)$	CPOT	-0.0267	-0.0303	-0.0131	-0.0124	-0.0231
	MPOT	0.0023	0.0050	-0.0047	-0.0043	0.0031
$(-1/3, 1, 0.1, -1/3, 1)$	CPOT	0.0023	0.0035	-0.0046	-0.0037	0.0037
	MPOT	0.0574	0.0802	0.0175	0.0233	0.0687
$(-1/3, 1, 0.1, -1/6, 1)$	CPOT	-0.3705	-0.3786	-0.2644	-0.2788	-0.2946
	MPOT	0.0163	0.0519	-0.0191	0.0061	0.0944
$(-1/3, 1, 0.1, 0, 1)$	CPOT	-0.6579	-0.6936	-0.5062	-0.5444	-0.5547
	MPOT	0.0038	0.0443	-0.0005	0.0342	0.1225
$(-1/3, 1, 0.1, 1/12, 1)$	CPOT	-0.7468	-0.8014	-0.6371	-0.6826	-0.6865
	MPOT	-0.0057	0.0871	0.0597	0.1335	0.2889
$(-1/3, 1, 0.1, 1/6, 1)$	CPOT	-0.7936	-0.8786	-0.7521	-0.7987	-0.7984
	MPOT	-0.0430	0.0895	0.0855	0.1642	0.3130

Table 4.3: Simulation results for the estimation methods of MM, PWM, ML, MDPD and ADR. The results presented are the means over 500 replicates.

$(\xi_0, \sigma_0, \epsilon, \xi_1, \sigma_1)$	Parameter	MM	PWM	ML	MDPD	ADR
$(-1/3, 1, 0.1, -0.5, 1)$	CPOT	0.9733	0.9697	0.9869	0.9876	0.9769
	MPOT	1.0023	1.0050	0.9953	0.9957	1.0031
$(-1/3, 1, 0.1, -1/3, 1)$	CPOT	1.0023	1.0035	0.9954	0.9963	1.0037
	MPOT	1.0574	1.0802	1.0175	1.0233	1.0687
$(-1/3, 1, 0.1, -1/6, 1)$	CPOT	0.6295	0.6214	0.7356	0.7212	0.7054
	MPOT	1.0163	1.0519	0.9809	1.0061	1.0944
$(-1/3, 1, 0.1, 0, 1)$	CPOT	0.3421	0.3064	0.4938	0.4556	0.4453
	MPOT	1.0038	1.0443	0.9995	1.0342	1.1225
$(-1/3, 1, 0.1, 1/12, 1)$	CPOT	0.2532	0.1986	0.3629	0.3174	0.3135
	MPOT	0.9943	1.0871	1.0597	1.1335	1.2889
$(-1/3, 1, 0.1, 1/6, 1)$	CPOT	0.2064	0.1214	0.2479	0.2013	0.2016
	MPOT	0.9570	1.0895	1.0855	1.1642	1.3130

Chapter 4. Mixture POT Approach to Model Extreme Bridge Traffic Load Effect

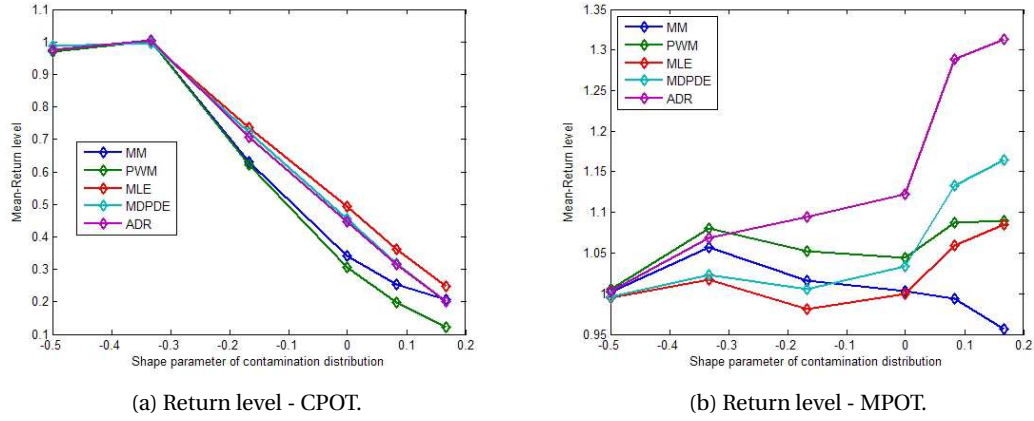


Figure 4.3: Mean of quantile estimators.

Table 4.4: Simulation results for the estimation methods of MM, PWM, ML, MDPD and ADR. The results presented are the standard deviations (STDs) over 500 replicates.

$(\xi_0, \sigma_0, \epsilon, \xi_1, \sigma_1)$	Parameter	MM	PWM	ML	MDPD	ADR
$(-1/3, 1, 0.1, -0.5, 1)$	CPOT	0.0444	0.0548	0.0303	0.0293	0.0391
	MPOT	0.0486	0.0613	0.0295	0.0315	0.0471
$(-1/3, 1, 0.1, -1/3, 1)$	CPOT	0.0476	0.0603	0.0277	0.0295	0.0460
	MPOT	0.0931	0.1313	0.0453	0.0528	0.1134
$(-1/3, 1, 0.1, -1/6, 1)$	CPOT	0.0325	0.0384	0.0740	0.0662	0.0658
	MPOT	0.2202	0.3203	0.2027	0.2451	0.4210
$(-1/3, 1, 0.1, 0, 1)$	CPOT	0.0372	0.0243	0.0758	0.0564	0.0643
	MPOT	0.3486	0.4341	0.3735	0.4202	0.5692
$(-1/3, 1, 0.1, 1/12, 1)$	CPOT	0.0535	0.0179	0.0618	0.0396	0.0500
	MPOT	0.4333	0.5497	0.5785	0.8105	1.2728
$(-1/3, 1, 0.1, 1/6, 1)$	CPOT	0.1105	0.0143	0.0490	0.0257	0.0345
	MPOT	0.5577	0.6002	0.6401	0.7767	1.0339

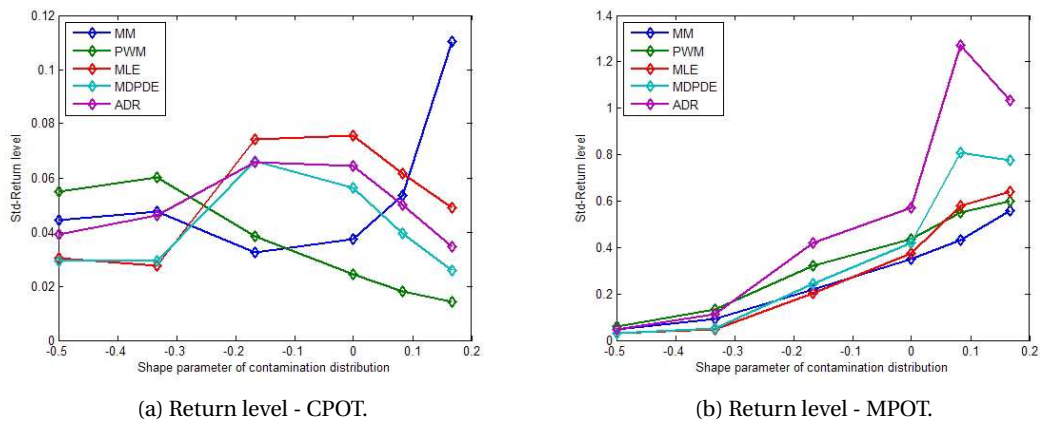


Figure 4.4: Standard deviation of quantile estimators.

An overall look at the tables clearly reveals how performances can drastically change depending on the shape parameter value of contaminated distributions. Consider first the case that core distribution with $\xi_0 = -1/3$ is contaminated by a distribution with only as slightly less shape parameter, $\xi_0 = -1/2$, it has little effect on the estimation of quantile. The statistics of RMSE, bias, mean and standard deviation are almost the same as the no contamination form. When the contaminated distribution has a larger shape parameter, the difference becomes apparent. The CPOT method is insensitive to the contamination, and hence the performance of the CPOT becomes worse as the shape parameter increases. Even though the proportion of contaminated distribution is only 10 percent, it dominates the tail distribution. The high quantile is rather close to the contaminated distribution than to the core distribution. From Table 4.4 and Figure 4.3 it is apparent that the MPOT method estimates the return level with good accuracy. The CPOT method does not estimate the return level accurately but has a lower coefficient of variation as shown in Figure 4.4. The mean for the CPOT method are less than the accuracy estimates. For parameter estimators, various estimators give consistent estimates of quantile for either conventional POT or mixture POT.

From these results, it is clear that the "contamination" distribution has severely distorted the quantile estimates. Thus there is no doubt about the advantage of applying the MPOT approach on samples with non-identical distributions. In light of these results we strongly suggest the use of the MPOT in the case when the main distribution is contaminated by distribution with larger shape parameter. While for the case that the main distribution is contaminated by distribution with smaller shape parameter, the conventional POT method can model the data with sufficient accuracy, similar conclusion is remarked in Dupuis and Field [1998]; Juárez and Schucany [2004]; Peng and Welsh [2001].

4.3.3 Study 2: GEV Distributed Sample

In this study, we used several of the parameter values from Caprani et al. [2008] to evaluate the performance of MPOT comparing with conventional POT method, and also comparing with approach proposed by Caprani et al. [2008], which model the mixture traffic load effects with a composite generalized extreme value distribution. Two examples are used to conduct this study. The first represents that the main distribution is contaminated by distributions with small shape parameters, while the second represents that the main distribution is slightly contaminated by a distribution from different loading event. The information about these two example are listed in Table 4.5. The first example represents load effects due to three loading event types. The probabilities of occurrence, f_j , of each event type, also given in the table, reduces from type 1 to 3. Type 1 events are more than twice as probable as type 2 events and type 3 events only occur 2% of the time. The total number of events per day of all types is specified as $n_d = 2800$. Similar, the second example represents load effects due to two types of loading event. The type 1 event contributes 95% to the total, while the type 2 takes the rest 5%. Monte Carlo simulation is used to sample the distributions for each event-type. This is repeated for a total of 1000 days to obtain a 1000-day sample. Additionally, the procedure is

Table 4.5: Parameters of mechanisms for study 2

Example	Event type number	Shape ξ	Scale σ	Location μ	Probability of occurrence f_j	Daily number of events n_d
First	Type 1	0.07	31	370	0.7	2800
	Type 2	-0.19	127	300	0.28	
	Type 3	-0.19	128	380	0.02	
Second	Type 1	-0.18	270	610	0.95	800
	Type 2	-0.21	310	840	0.05	

repeated 100 times to consider the variation.

For adopting standard block maximum method, GEV distribution is fitted to the maximum-per-day data regardless of the event types. On each sample we estimate the shape parameter, ξ , scale parameter, σ , and location parameter, μ , with maximum likelihood estimator. For applying Eq. (4.2), Maximum-per-day data for each of the event types are drawn, and these data are fit to GEV distributions. The parameters of the GEV distributions are used to calculate the 1000-year return level. In the case using POT method to model the data, the entire data of each simulation sample is used. For applying the CPOT approach, a series of thresholds is investigated and an optimal threshold is selected by using KS test. The parameters of the GPD are estimated by five previous utilized estimators. For applying the proposed MPOT approach, GPD is fitted to the exceedances over high threshold for data with respect to type of loading event. The threshold selection method is also based on the statistics of KS test. Then the estimated parameters are used to calculate 1000-year return level.

We firstly present the result for the first example. Substituting the parameters of Table 4.5 into Eq. (4.3) and equating to a probability of $1 - 1/(250 \times 1000)$ (assuming 250 working days per year excluding weekends and holidays) give the exact characteristic value for 1000-year return period, here is 1724. In Figure 4.5, the estimated 1000-year return levels are presented in terms of ratio with respect to the exact return level, and the performances of the prediction methods are assessed by this ratio. From Figure 4.5 it is apparent that either the conventional block maxima method or the conventional POT method does not estimate the return level accurately. The return levels estimated by the conventional methods are less than the exact solution. However, it should be noticed that the POT has better performance than the BM even in the standard use. Among the convention methods, the return level found from the BM method is about 30% less than the exact solution, while these found from the POT method are more close to the exact value with ratio ranging from 0.75 to 0.9. The POT with parameter estimator of method of moments is the best one which provides the return level only about 10% less than the exact value.

Although the POT method performs better than the BM method, the assumption of convergence to a single GPD or GEV distribution is not valid as the source data are mixed. The mean ratios from mixture POT or mixture BM method indicate that these methods provide

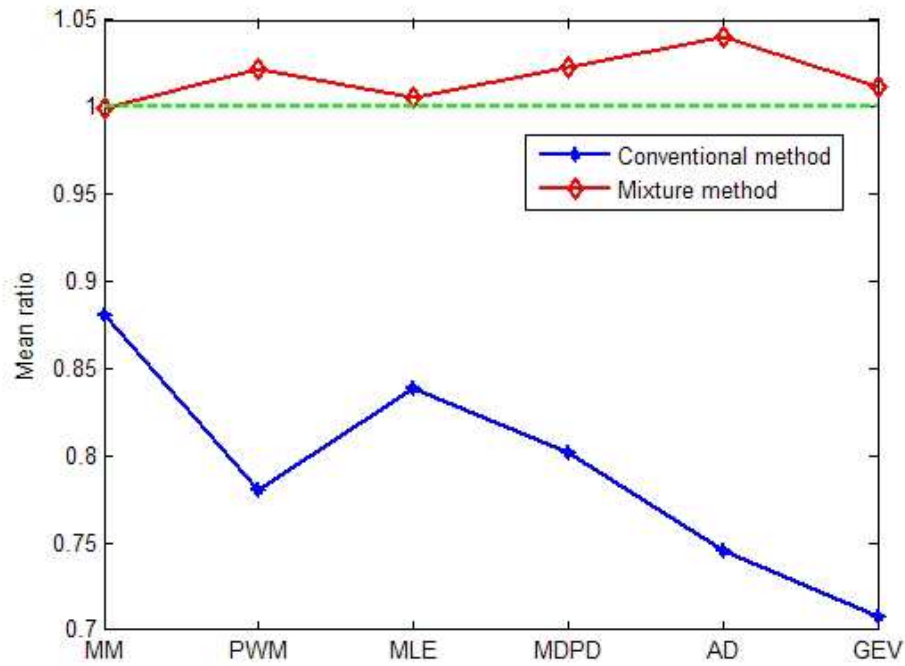


Figure 4.5: Comparison: conventional vs. mixture

more accurate prediction of return level with a maximum error of 5%. From Figure 4.5, the POT method with estimator of MM have better performance than the mixture POT method with other parameter estimators; even the mixture POT method with ML has slightly better performance than the mixture BM method.

The variation of mixture methods is illustrated with box plot given in Figure 4.6. The box plot is a standard technique for exploiting data variation. It presents the commonly used five characteristic features which consists of the minimum and maximum range values, the upper and lower quartiles and the median. On each box, the central mark is the median, the edges of the box are the 25th and 75th percentiles, the whiskers extend to the most extreme data points not considered outliers, and outliers are plotted individually with red plus sign.

Figure 4.6 shows that all the methods estimate the return level with good accuracy as the median value close to the exact value from analytical model. Among these methods, mixture GEV distribution gives a lesser range of results which, in this case, are reasonably close to the exact value. The mixture GEV distribution method seems to provide much stable prediction. It is reasonable that the rule to draw data in mixture GEV method is much clearer. The block maxima are used to fit GEV distribution, while the selected threshold is variable from sample to sample. In this case study, 1000 daily maxima are used to fit to GEV distribution; hence, the block maxima method can reasonably model the extreme value distribution. However, it has the risk to give worse modelling when the sample size is smaller, it will be studied in next

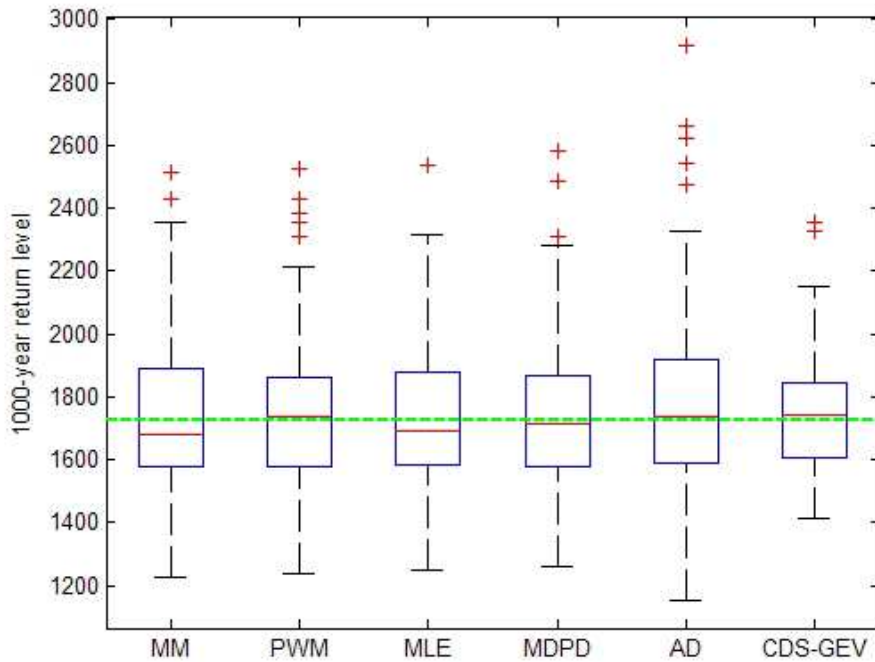


Figure 4.6: Estimated 1000-year return level

section that how the methods reflect to sample size. The MPOT method using MDPD estimator and PWM estimator provide similar narrow range of results as the mixture GEV method. Therefore, the predictions from extreme value theory based models can be considerably good, the return levels predicted by mixture GPD model are relatively close to those predicted using mixture GEV model.

The same procedure is conducted on the second example are got by the same procedure. The comparison of prediction methods is presented in Figure 4.7 and 4.8. It can be seen that the mixture model methods provide better prediction. However, the conventional methods also provide a very accuracy estimation with a maximum error of about 8%. These results indicate that the conventional methods can model the data with sufficient accuracy when the distribution composition is not very different like the shape parameters are close for the two types of loading event in this example, and also demonstrate the statement given by Reiss and Thomas [2007] that the form F^m may still serve as an approximation of the actual df of the maximum if a slight mixture in the data.

4.3.4 Study 3: Normal Distributed Sample

Normal distribution is a widely used distribution in bridge engineering, for example gross vehicle weights are usually assumed to follow multiple modal Normal distribution [Caprani,

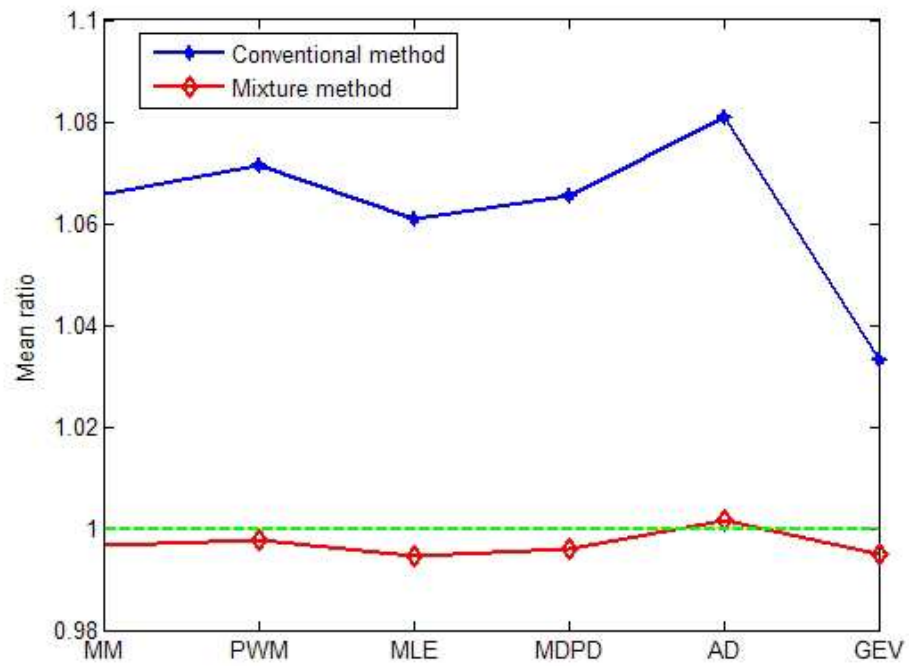


Figure 4.7: Comparison: conventional vs. mixture

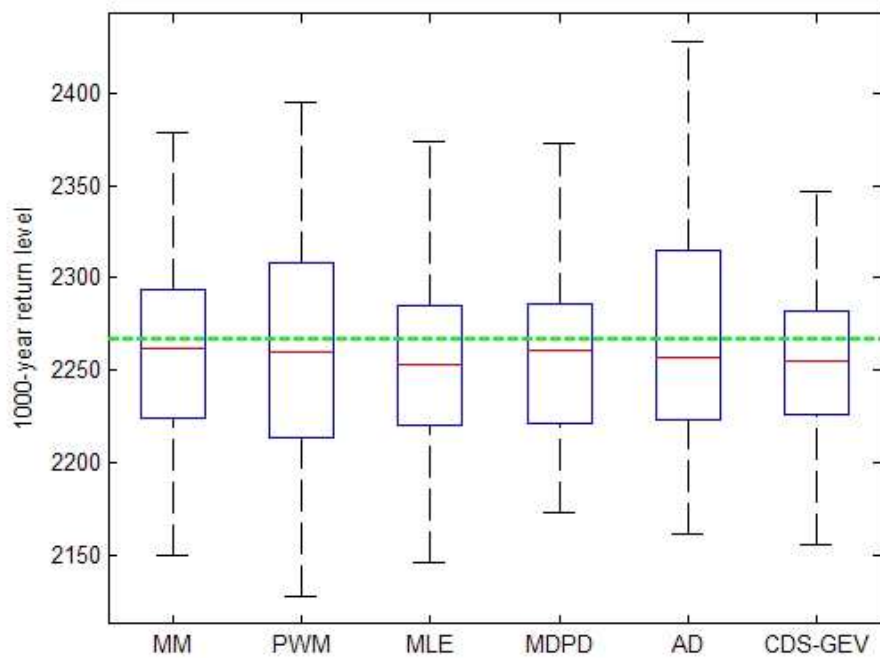


Figure 4.8: Estimated 1000-year return level

Table 4.6: Parameters of mechanisms for study 4

Example	Event type number	Scale σ	Location μ	Probability of occurrence f_j	Daily number of events n_d
First	Type 1	30	420	0.90	1000
	Type 2	45	380	0.10	

Table 4.7: Parameter estimates for CPOT method by various estimators

Estimator	Shape	Scale	Location	No. exceedances	KS, p-value
MM	-0.0767	10.21	510.52	1321	0.8823
PWM	-0.0930	10.37	510.52	1321	0.9735
ML	-0.0583	10.03	510.52	1321	0.6936
MDPD	-0.0760	10.20	510.52	1321	0.8726
ADR	-0.1059	10.46	510.52	1321	0.9420

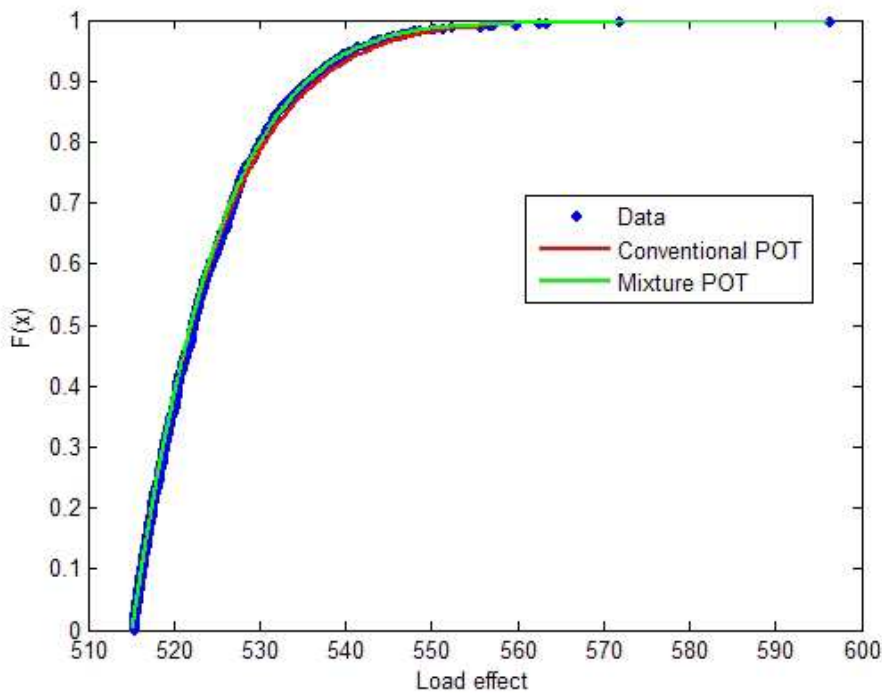
2005]. In this study, the performance of MPOT method is evaluated through its application on a sample having a parent distribution of normal distribution. The parameters of the distribution are given in Table 4.6. The core distribution is $N(420, 30)$ with the relative frequency of occurrence $\varphi_1 = 0.9$, while the "contaminating" distribution is $N(380, 45)$. It is considered that 1000 events per day occur.

Figure 4.9 displays an application of CPOT and MPOT method to the mixed normal distribution sample. Parameter estimates for CPOT method are obtained by the five previous mentioned estimators and listed in Table 4.7. The parameter estimates for mixture POT method are given in Table 4.8. Figure 4.9a provides the empirical CDF to show departures from very small values. Figure 4.9b shows the fitting in the log-scale, the goodness of the methods is apparently displayed. Both CPOT and MPOT methods capture the main part of the data very well, but the discrepancy between empirical distribution and fitted distribution becomes larger when getting close to the upper tail. The CDF obtained by MPOT captures the upper tail with significantly less bias than with the CPOT. Therefore the MPOT method has a better performance on modelling the upper tail data than the CPOT method, consistently with results of KS goodness-of-fit test as given in Table 4.8. After obtaining the upper tail distribution, it is straightforward to calculate the maximum value distribution function using equation. Daily maxima distributions are given in Figure 4.10 along with the true daily maximum value distribution obtained by equation. The result confirms the previous result that the mixture POT method estimates the daily maximum value distribution with good accuracy.

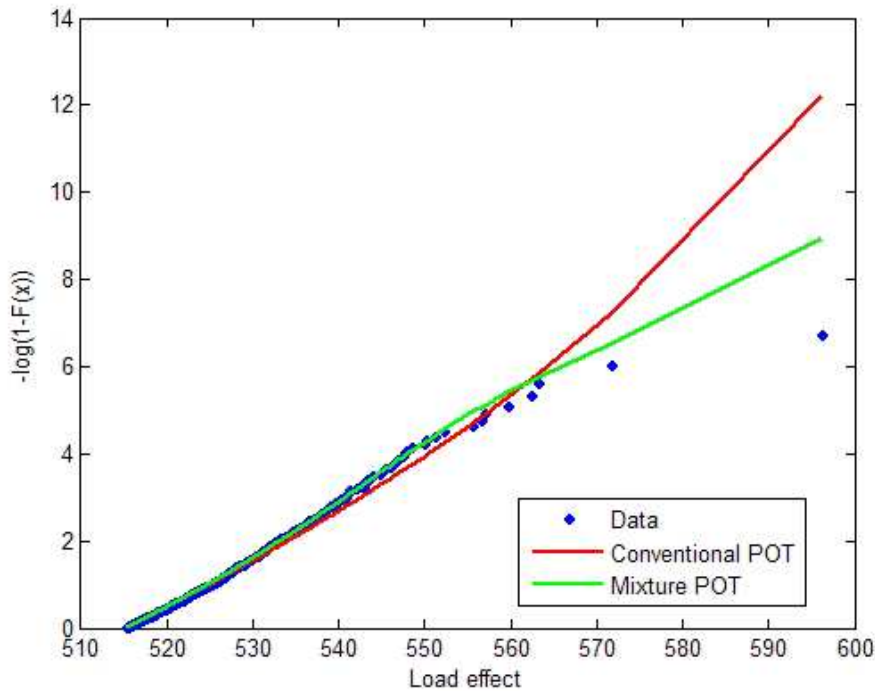
The full simulation results of quantile estimation for the sample sets obtained by applying the conventional and mixture POT methods are given in Figure 4.11. It indicates that both approaches have good performance on quantile estimation, with maximum error less than 2%, and the estimated return levels from conventional method are much closer to the true value. The results from the mixture GEV method are also obtained and approximate the true

Table 4.8: Parameter estimates for MPOT method by various estimators

Estimator	Component 1					Component 2					Mixture
	Shape	Scale	Location	No.	KS	Shape	Scale	Location	No.	KS	KS
MM	-0.173	9.9	515.2	707	0.908	-0.056	15.9	479.1	1371	0.926	0.964
PWM	-0.105	10.0	508.0	1500	0.909	-0.058	16.0	479.1	1371	0.903	0.866
ML	-0.177	10.0	515.2	707	0.922	-0.053	15.9	479.1	1371	0.945	0.979
MDPD	-0.177	10.0	515.2	707	0.922	-0.057	16.0	479.1	1371	0.918	0.974
ADR	-0.106	10.1	508.0	1500	0.937	-0.091	16.2	486.6	845	0.931	0.918



(a) Standard cumulative distribution probability plot.



(b) Gumbel scaled cumulative distribution probability plot.

Figure 4.9: These figures display the GPD fitting obtained by CPOT and MPOT approaches.

value with a small difference also, but the method does not work as well as POT methods.

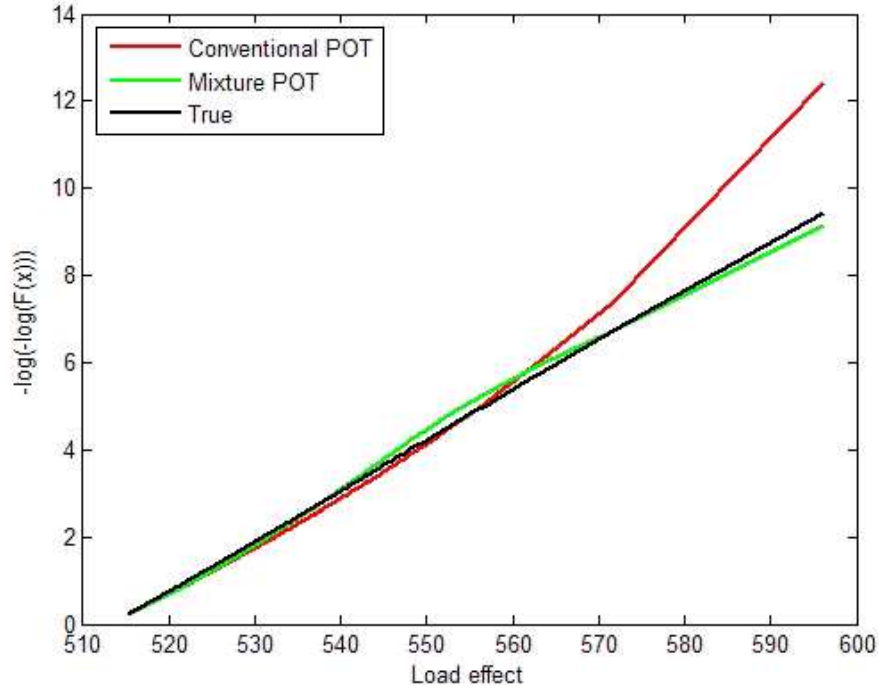


Figure 4.10: Extreme value distribution from conventional and mixture POT methods

4.4 Discussion

4.4.1 Effect of Sample Size

The study in Chapter 3 demonstrates that the sample size is important to extreme value modeling in application under standard manner. In this section, we intend to investigate the influence of sample size on MPOT method. The Example 1 of Study 2 is used to study the effect of different sizes of samples on quantile estimation as it represents the situation that threshold needs to be selected. Sample sizes of 200, 500, and 1000 are used as the basis of the procedure outlined previously. For each of these sample sizes, there are fitted GPDs for the mixture POT and conventional POT methods. As a comparison, the results of return level obtained from the mixture GEV and conventional GEV method are presented also.

Figure 4.12 presents the results using an error bar plot, displaying the mean values and the range of $[-\sigma, \sigma]$ for the return levels estimated from the different methods considered. It is clear that the mean value is consistently accurate, regardless of sample size for the mixture methods. Furthermore, the standard deviation decreases with increasing sample size. For smallest size of 200 considered in this study, the mixture POT method generally has a better performance as it provides smaller standard deviation. However, the mixture GEV method

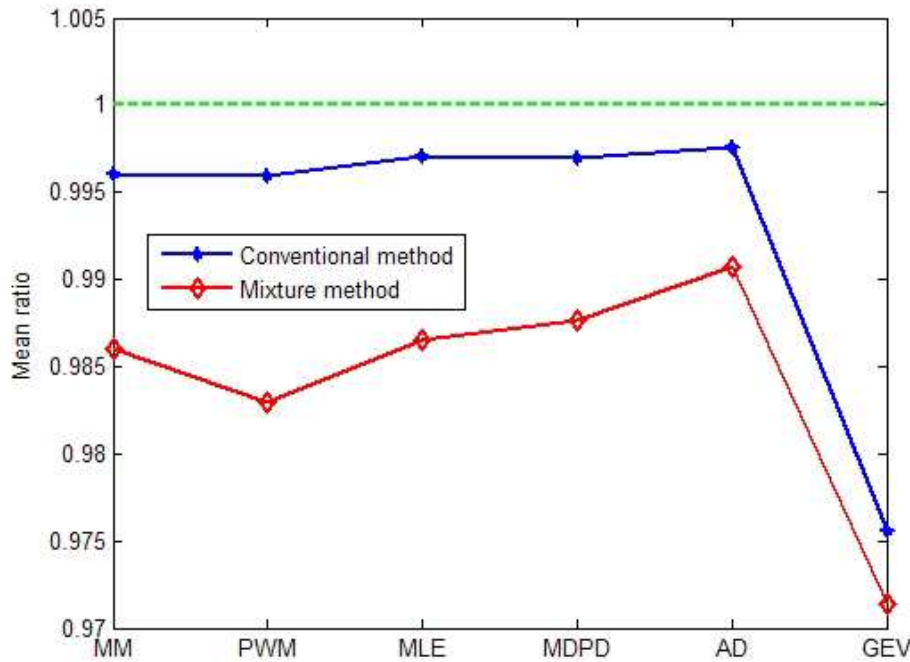


Figure 4.11: Results for Study 4

is more sensitive to the sample size; its performance remarkably improves with increasing sample size.

4.4.2 Composition

The core distribution of previous samples is assume to be slightly contaminated by other distribution, in practice the core distribution can be severely contaminated by other distribution. In order to investigate the influence of proportion of contaminated distribution on quantile estimation, two additional studies have been carried out. The combination of core distribution and contaminated distribution and corresponding parameters are listed in Table 4.9. One sample is combined with two distributions having bounded limits, and the other is combined with bounded and unbounded distribution.

Figure 4.13 and Figure 4.14 show the mean and the coefficient of variation for the ratio that is calculated by dividing the quantile estimates from the mixture and conventional methods by the true value calculated by Eq. (4.10) and Eq. (1.13), respectively. It is clear that the mean value still is consistently accurate, regardless of the proportion of contaminated distribution for the MPOT method, whereas the CPOT method converges to an inaccurate estimated value. However, it should be noted that this effect of contamination ratio has negative influence on conventional method for the Study 5, but it has a positive influence on return levels obtained

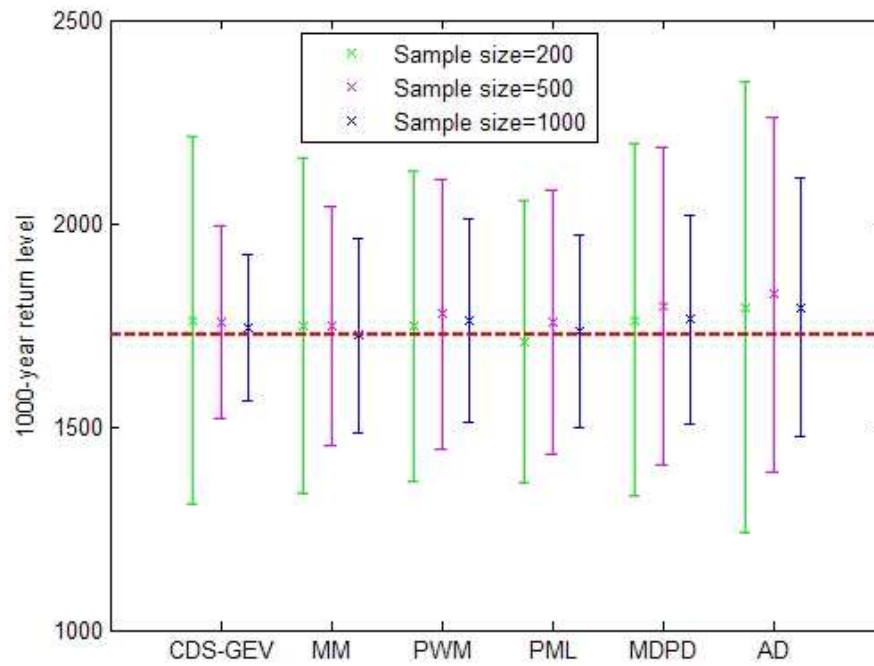
Figure 4.12: Error bar plot (mean \pm) of 1000-year return level

Table 4.9: Parameters for studies 5 and 6

Study	Example	Event type	Shape	Scale	Location	Probability weight
5	1	1	-1/3	1	0	0.9
		2	-2/3	1	0	0.1
	2	1	-1/3	1	0	0.8
		2	-2/3	1	0	0.2
	3	1	-1/3	1	0	0.7
		2	-2/3	1	0	0.3
	4	1	-1/3	1	0	0.6
		2	-2/3	1	0	0.4
6	1	1	-0.1	1	0	0.9
		2	0.1	1	0	0.1
	2	1	-0.1	1	0	0.8
		2	0.1	1	0	0.2
	3	1	-0.1	1	0	0.7
		2	0.1	1	0	0.3
	4	1	-0.1	1	0	0.6
		2	0.1	1	0	0.4

from the conventional method for the Study 6 as mean ratio approximates to true value with increasing proportion of contaminated distribution. Namely the governing event in Study 6 is Event 2, therefore the increasing of its proportion can improve the estimation. Further, the conclusion is confirmed as the coefficient of variation of the mixture method decreases with increasing proportion of contaminated distribution for Study 6, while the coefficient of variation remains in a stable level for Study 5. The results indicate that the increasing size of governing data can improve the quantile estimation.

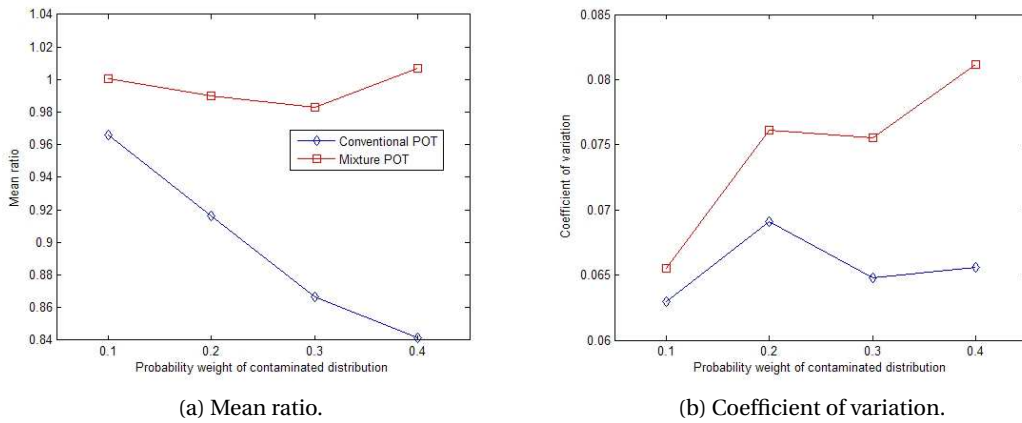


Figure 4.13: Results of proportion of contaminated distribution effect study, Study 5.

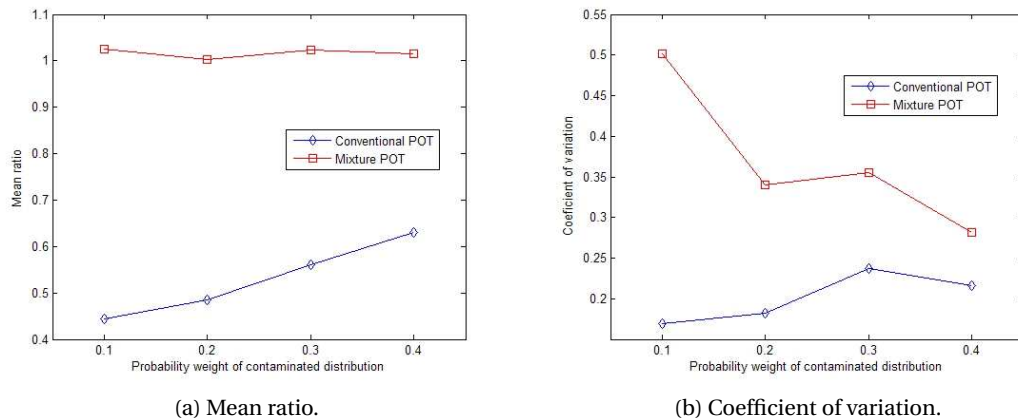


Figure 4.14: Results of proportion of contaminated distribution effect study, Study 6.

4.5 Simulated Traffic Load Effects

4.5.1 Introduction

Traffic load effects like bending moments, shear forces, deflections etc. - result from traffic passing over a bridge. The process varies in time with many periods of zero load effects

when there is no traffic on the bridge and peaks corresponding to heavy vehicle crossings or more complex vehicle meeting or overtaking scenarios (see Figure-16). The majority of the local peaks in load effect are due to cars which are relatively light and there have been many efforts to simplify the problem by excluding consideration of these data in extreme value statistic analysis as it has little contribution to extreme value. A commonly adopted way is to investigate traffic load effect induced by trucks which are usually defined as vehicles with GVW greater than 3.5 tonnes. In traffic load effect extreme value statistical analysis, the single light trucks have little contribution to extreme value. Caprani [2005] only retains load effects induced by "significant crossing events" which are defined as multiple-truck presence events and single truck events with GVW in excess of 40 tonnes. This approach is efficient for using block maximum method to model extreme value; only the maximum within a period or a block is retained. However, it may lose some information as the multiple-truck loading events may induce less load effect than single truck with GVW less than 40 tonnes. As shown in Figure 4.15, several single truck loading events induce larger load effect than those induced by 2-truck loading events. In order to use all possible relatively large load effect, the full time history of effect induced by traffic passing over the bridge is retained first, then the local extreme and its corresponding type of loading event (comprising the number of trucks) are identified. Figure 4.16 illustrates such a process, the time history of the traffic load effect is given in blue line, and the local extremes are marked with red star. The bridge experiences a complex traffic crossing sequence. At the beginning, one truck (1st truck) is on the bridge, then another truck (2nd truck) arrives on the bridge generating a 2-truck loading event, then the first arrived truck leaves the bridge and the loading event become to a single truck, then a new truck (3rd truck) enters the bridge and the loading events become to a 2-truck again, then the 2nd arrived truck exits the bridge, then a new truck (4th truck) arrives to consist a new 2-truck loading event, then the 3rd truck exits the bridge and the loading event becomes single truck loading event. In this process, four trucks have arrived on the bridge and produced 4 single truck loading events and three 2-truck loading events. The local extremes for each loading event are identified and marked in the figure. Using this procedure, local peaks for various type of loading events are identified.

As shown in Figure 4.16, the local extremes are induced by different types of loading events that consists of different numbers of trucks. These mixed load effects can thus not be treated as identically and independently distributed data, and the standard extreme value theory can not be directly applied to these data. As done by Caprani et al. [2008], load effects should be separated by type of loading event. Using the program, which is described in Appendix B, developed in this research, peaks of load effect can be identified and grouped by corresponding loading events. The proposed mixture peak-over-threshold (MPOT) method can be used to these load effects, and the applications of the method to the bridge traffic load problem are assessed in this section.

Previous studies [O'Connor et al., 2001] have demonstrated that the critical influence lines for developing load model are bending moment at mid-span of a simply supported bridge, shear force at end-support of a simply supported bridge, and hogging moment at middle support of

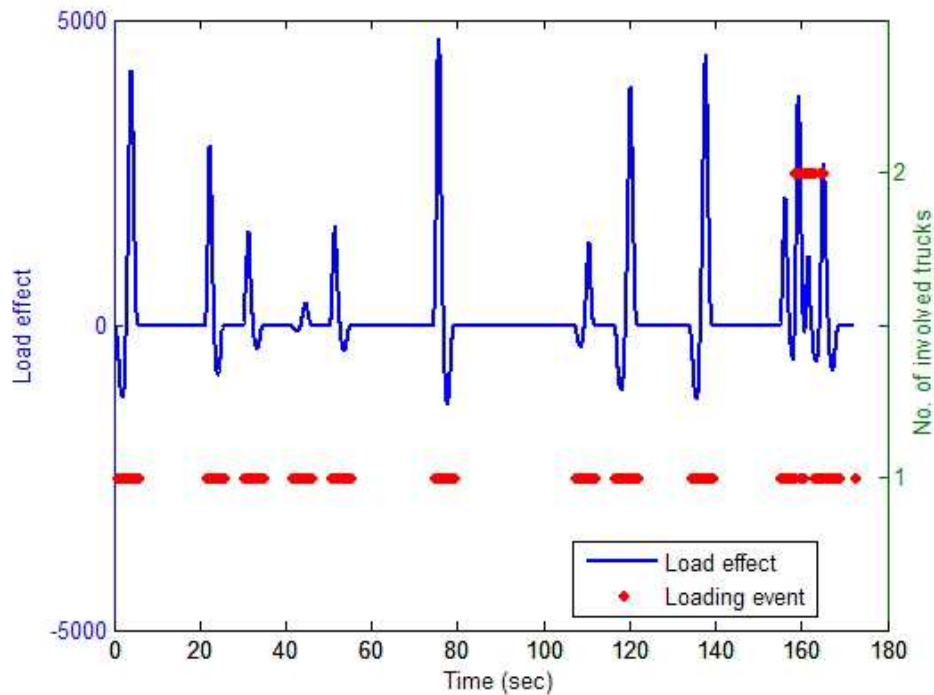


Figure 4.15: Time history of load effects

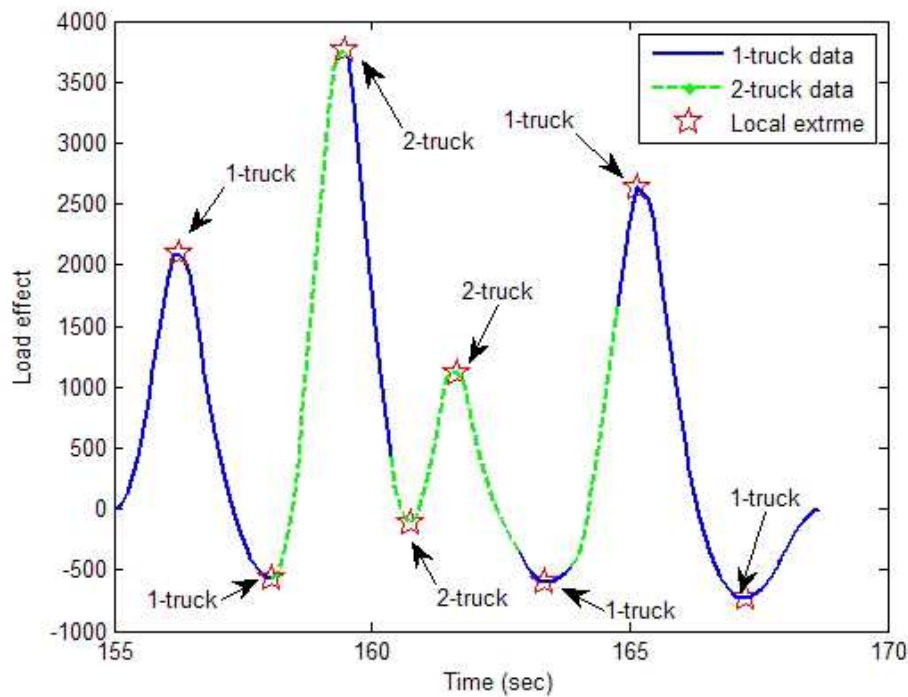


Figure 4.16: Time history and local extreme

Table 4.10: Influence lines used in calculation of load effect

Item	Description Representation
I1	Bending moment at mid-span of a simply supported bridge
I2	Right-hand support shear force in a simply-supported bridge
I9	Bending moment at middle support of a two-span continuous bridge

a two-span continuous bridge. In this study, these three types of load effect are studied and details are given in Table 4.10. Considering the time consumption and the sufficiency of data, a 1500-day simulation of Saint Jean de Vedas (SJDV) traffic on bridge lengths of 20, 30, 40 and 50 m is carried out for these load effects. The statistics of traffic data of SJDV are presented in Appendix A.

4.5.2 Composition of Loading Event

The frequency of multiple-truck presence on a fixed length of highway has been studied at several highway locations (Connecticut Route 5, I-91 at the Depot Hill Road, and I-91 at the Connecticut Route 68) by Desrosiers and Grillo [1973]. Their first objective was to determine which of the following parameters have a significant influence on the probability of multiple presence: type of highway, length of bridge, time of day, total traffic volume, truck speed, and truck volume. They conclude that the multiple presence of trucks is primarily dependent upon the length of bridge and traffic volume and it is almost independent of the other parameters, this conclusion is also made by Gindy and Nassif [2007] basing on 11 years WIM data collected from 25 WIM sites at New Jersey between 1993 and 2003. Physically, higher traffic volume leads to increasing of traffic density, therefore the probability of simultaneous presence of multiple truck increases as well. And it is also straightforward to understand the effect of length of bridge.

However, for different types of load effects, their sensitivities to multiple-truck presence are different. A series of 14 influence lines were analyzed by Harman and Davenport [1979] to investigate the sensitivity of load effects to multiple-truck presence. A sensitivity parameter, ρ , was used to indicate the feature. The parameter is the ratio of two values of effect: (1) maximum load effect caused by a unit uniformly distributed loading applied to all segments of the traffic lane where the application cause an increase of in the effect; (2) maximum load effect caused by a unit uniformly distributed loading applied to fixed length of 13.8 as it is approximately the maximum length of a truck from its first to last axle. They conclude that: (1) effects with a sensitivity parameter less than 1.8 indicates that multiple presence does not increase the mean largest effects by more than 12% relatively to the mean largest effects caused by single-truck events. Therefore, for this range of sensitivity, a live load that simulates the effects of single-truck events is most important. (2) For effects that have a sensitivity parameter greater than 3.2, multiple presence is important. Hence, truck queues caused by traffic jams should be included in the calculation of mean largest effects. (3) Within the range

of the sensitivity parameter between 1.8 and 3.2, there are some effects that are very sensitive to loading events with two trucks. For the three types of load effect, six categories of loading event have been identified from the simulation. These six categories of truck arrangements are 1-truck, 2-truck, 3-truck, 4-truck, 5-truck, and 6-truck loading events. The composition of the six types of loading events vary with bridge length, and with the values of load effects, see an example of load effect II for length of 40 in Figure 4.17. Two sets of loading event composition are listed in Table 4.11 and Table 4.12 for the three types of load effect, with four types of bridge lengths. The first group is for load effect over 90th percentile, and the second group is for load effect above 95th percentile. Figure 4.18 shows the governing type of loading event changes with increasing bridge length. For a bridge length of 20 m, and for the load effects examined, 2-truck and 3-truck loading events govern the upper tail. For a bridge length of 30 m, it can be seen from Figure 4.18a or 4.18b that the governing event is 3-truck loading event. For bridge lengths of 40 and 50 m, 3-truck events mainly govern but some 4- and 5-truck events occur at the upper end of the simulation period. In addition, it seems that the governing events are more apparent when examining the data over higher threshold.

4.5.3 Distribution

The previous sections have shown that the load effects induced by different types of loading event are not identically distributed. It thus needs to study their distribution through loading event by load event, and the full distribution of load effect is the composition of all possible components. To apply the mixture POT method, generalized Pareto distribution is fitted to the load effect with respect to the loading event. The hypothesis that the excesses of data for individual loading event are from generalized Pareto distribution is tested by goodness-of-fit test.

Specific goodness of fit test for the GPD has been established by Choulakian and Stephens [2001]; Villasenor-Alva and Gonzalez-Estrada [2009]. The one proposed by Choulakian and Stephens [2001] is based on the Cramer-von Mises statistic W^2 and the Anderson-Darling A^2 , and relies on the assumption that maximum likelihood estimates do exist. Villasenor-Alva and Gonzalez-Estrada [2009] provide a goodness of fit test for the GPD in the situation that parametric estimators do not exist, the approach is to use the nonparametric bootstrap method. Additionally, Luceno [2006] uses statistics based on the empirical distribution function such as those of Kolmogorov, Cramer-von Mises, Anderson-Darling, and their revised forms for parameter estimation, which obtains the parameter estimates through minimizing these goodness-of-fit statistics with respect to the unknown parameters. In this study, we use the method proposed by Choulakian and Stephens [2001] to evaluate the fitting. The goodness-of-fit test procedure is as follows:

- Find the estimates of unknown parameters as described previously, and make the transformation $z_{(i)} = F(x_{(i)})$, for $i = 1, \dots, n$, using the estimates where necessary.

Table 4.11: Probabilities for six categories of loading events for data above 90th percentile

Type of loading event	20 m			30 m			40 m			50 m		
	I1	I2	I9	I1	I2	I9	I1	I2	I9	I1	I2	I9
1-truck	0.047	0.079	0.068	0.050	0.067	0.056	0.047	0.051	-	0.155	0.043	-
2-truck	61.37	59.49	61.77	36.95	45.51	9.00	11.73	11.16	0.29	2.20	2.20	0.19
3-truck	37.60	38.76	36.36	59.87	49.28	81.46	79.06	70.91	50.18	75.77	63.08	37.07
4-truck	0.99	1.67	1.80	3.10	4.94	9.29	8.79	16.55	45.96	20.13	30.11	54.96
5-truck	-	-	-	0.037	0.194	0.198	0.37	1.31	3.57	1.71	4.42	7.53
6-truck	-	-	-	-	-	-	-	-	-	0.044	0.142	0.240

Table 4.12: Probabilities for six categories of loading events for data above 95th percentile

Type of loading event	20 m			30 m			40 m			50 m		
	I1	I2	I9	I1	I2	I9	I1	I2	I9	I1	I2	I9
1-truck	0.094	0.079	0.136	0.100	0.073	0.113	0.094	0.081	-	-	0.085	-
2-truck	39.87	42.38	41.97	13.72	26.73	3.87	4.25	4.07	0.57	1.38	1.59	0.29
3-truck	58.38	54.98	55.00	81.11	65.50	83.99	84.04	73.84	28.86	72.35	57.96	18.02
4-truck	1.67	2.55	2.89	5.03	7.37	11.74	11.18	20.04	65.14	23.92	34.24	69.99
5-truck	-	-	-	0.050	0.328	0.282	0.44	1.94	5.43	2.26	5.87	11.31
6-truck	-	-	-	-	-	-	-	-	-	0.089	0.255	0.384

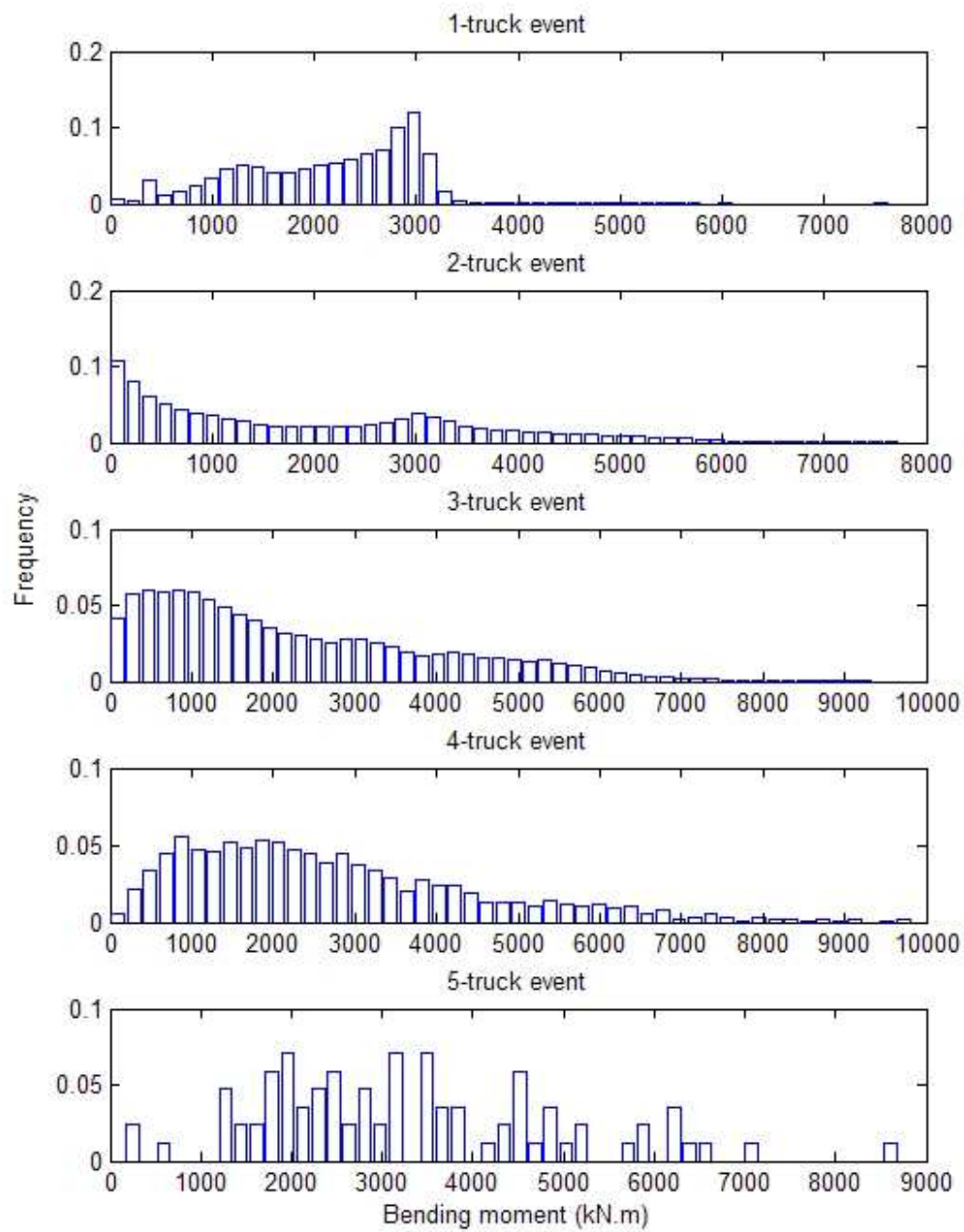


Figure 4.17: Histogram of load effects due to various type of loading event

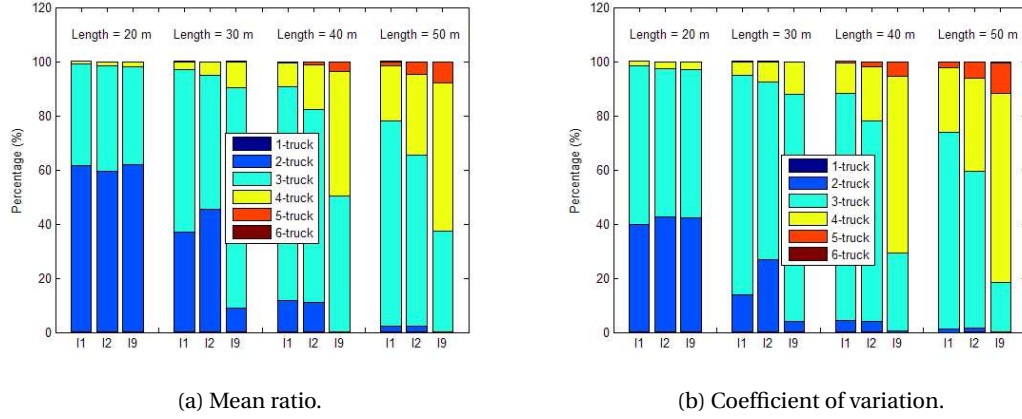


Figure 4.18: Probabilities for six types of loading events (left) over 90th and (right) 95th percentile.

Table 4.13: Both shape parameter ξ and scale parameter σ unknown: upper tail asymptotic percentage points for W^2 of Cramer-von Mises test

ξ/p	0.5	0.25	0.1	0.05	0.025	0.01	0.005	0.001
0.9	0.046	0.067	0.094	0.115	0.136	0.165	0.187	0.239
0.5	0.049	0.072	0.101	0.124	0.147	0.179	0.204	0.264
0.2	0.053	0.078	0.111	0.137	0.164	0.2	0.228	0.294
0.1	0.055	0.081	0.116	0.144	0.172	0.21	0.24	0.31
0	0.057	0.086	0.124	0.153	0.183	0.224	0.255	0.33
-0.1	0.059	0.089	0.129	0.16	0.192	0.236	0.27	0.351
-0.2	0.062	0.094	0.137	0.171	0.206	0.254	0.291	0.38
-0.3	0.065	0.1	0.147	0.184	0.223	0.276	0.317	0.415
-0.4	0.069	0.107	0.159	0.201	0.244	0.303	0.349	0.458
-0.5	0.074	0.116	0.174	0.222	0.271	0.338	0.39	0.513

- Calculate statistics W^2 and A^2 as follows:

$$W^2 = \sum_{i=1}^n \left[z_{(i)} - \frac{2i-1}{2n} \right]^2 + \frac{1}{12n}$$

and

$$A^2 = -n - (1/n) \sum_{i=1}^n (2i-1) [\log z_{(i)} + \log 1 - z_{(n+1-i)}]$$

Additionally, the root mean squared errors (RMSE) of cumulative distribution function are calculated also to act as a measure to evaluate the performance of fitting.

To show what is the difference between convention POT and mixture POT method for modelling excesses over a threshold, in Figure 4.19 we present the probability diagnostic graphic,

Table 4.14: Both shape parameter ξ and scale parameter σ unknown: upper tail asymptotic percentage points for A^2 of Anderson-Darling test

ξ/p	0.5	0.25	0.1	0.05	0.025	0.01	0.005	0.001
0.9	0.339	0.471	0.641	0.771	0.905	1.086	1.226	1.559
0.5	0.356	0.499	0.685	0.83	0.978	1.18	1.336	1.707
0.2	0.376	0.534	0.741	0.903	1.069	1.296	1.471	1.893
0.1	0.386	0.55	0.766	0.935	1.11	1.348	1.532	1.966
0	0.397	0.569	0.796	0.974	1.158	1.409	1.603	2.064
-0.1	0.41	0.591	0.831	1.02	1.215	1.481	1.687	2.176
-0.2	0.426	0.617	0.873	1.074	1.283	1.567	1.788	2.314
-0.3	0.445	0.649	0.924	1.14	1.365	1.672	1.909	2.475
-0.4	0.468	0.688	0.985	1.221	1.465	1.799	2.058	2.674

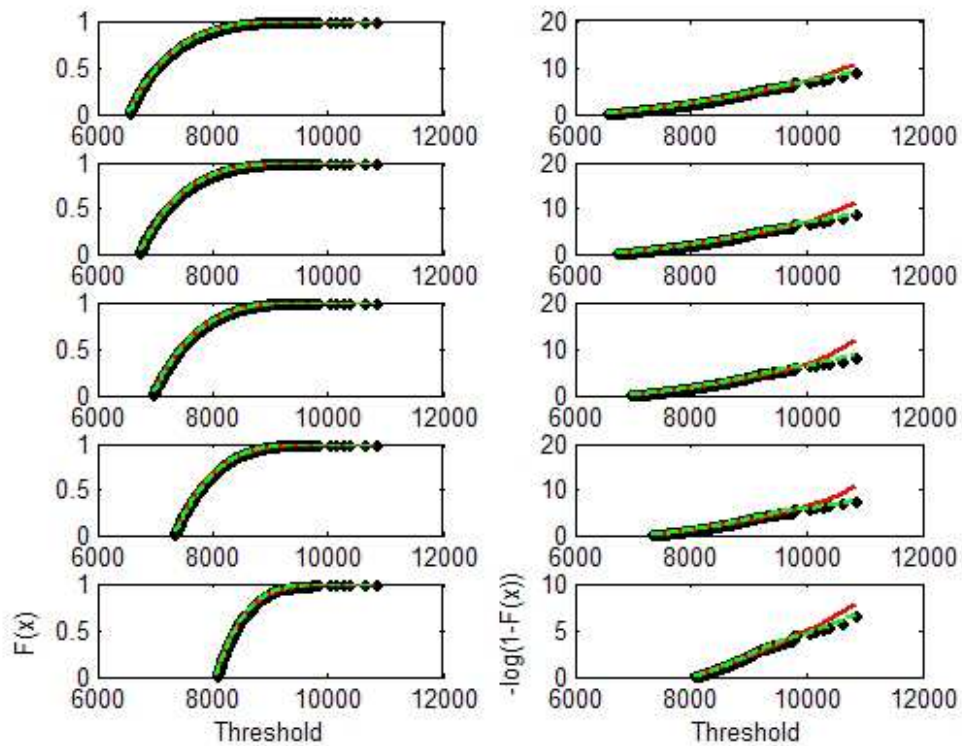


Figure 4.19: Diagnostic plot for threshold excess model fitted to load effect

the distribution parameters are estimated by maximum likelihood method. The left plots show the empirical survival function (black dots), fitted function with conventional POT estimates (red solid lines), and Equation parameterized with mixture POT estimates (green dash lines) for various thresholds. The right plots show the previous mentioned survival function in logarithm scale. In this study, several fixed thresholds of, 90th, 92nd, 94th, 96th, and 98th percentiles, are tested. The results corresponding to the threshold show in ascending order. Figures presented and discussed till now give us a qualitative but quite clear idea of mixture POT supremacy on the conventional fit. Nevertheless, in order to provide an objective evaluation of the mixture POT method performances, we evaluated goodness-of-fit test statistic, bias and RMSE of the two fitting approaches for each group of dataset. In Table 4.13, we display the Anderson-Darling statistic A^2 , Cramer-von Mises statistic M^2 , and RMSE for fitting generalized Pareto distribution to bending moment at mid-span of a simply-supported beam with length of 40 m using various parameter estimators. The values in the parentheses are for mixture POT method, while those outside are for conventional POT method. The full results are given in the appendix C.

From Figure 4.19 it shows that mixture POT method models the exceedances over threshold with good accuracy. The results reported in Table-16 confirm this conclusion that the mixture POT method improves the modelling as it provides lower goodness-of-fit statistics. The goodness-of-fit statistics for fitting from either conventional POT method or mixture POT method, there are some features on parameter estimators. The ADR almost gives smallest statistic of A^2 and W^2 , while the MM or PWM provide larger values. It can be reasonable that the ADR estimator is to obtain the optimal estimates through minimizing the distance between empirical distribution function and fitted distribution function. Although it gives smallest goodness-of-fit statistic, it provides larger RMSE. It is widely stated de Zea Bermudez and Kotz [2010]; Hosking and Wallis [1987] that MM and PWM are efficient estimators for sample with small size such as less than 100, while there are many data exceeding the high threshold such 1281 exceedances over 98th percentile. Therefore, in this considered study, the MM and PWM give less accurate estimates. ML and MDPD estimators have similar performance, and the goodness-of-fit statistics are close to those acquired by ADR. Further, these two estimators give smaller RMSE than others, and the ML almost gives the smallest RMSE. Again, the ML is recommended to estimate parameter for large sample by de Zea Bermudez and Kotz [2010]; Hosking and Wallis [1987]. Hence, it can be concluded that ML and MDPD are better than others.

In statistical analysis, the confidence coefficient is a widely used factor to assess the fitting quality, such as 95% confidence. Using the critical value in Table 4.13 and Table 4.14 corresponding to various confidence percentage provided by Choulakian and Stephens [2001], the asymptotic 5% critical values z_5 for A^2 and W^2 corresponding to the estimate of the shape parameter ξ from conventional POT method are given in Table 4.16. By comparing the critical values with the calculated EDF test statistics, the fitting quality can be revealed. For estimators, neither MM nor PWM estimated GPD do not fit the dataset well at the considered threshold, in contrast, the ADR estimated GPD fits the dataset well as the test statistics are lower than the

Table 4.15: Empirical distribution function statistics for load effect of length 40m, Load effect I1

Statistic	Threshold	No.	MM	PWM	ML	MDPD	ADR
AD	90th PCT	6403	3 (1.01)	2.68 (1.44)	0.56 (0.38)	0.72 (0.56)	0.47 (0.27)
	92nd PCT	5122	3.28 (1.27)	2.68 (1.4)	0.52 (0.43)	0.67 (0.62)	0.37 (0.26)
	94th PCT	3842	3.12 (0.83)	2.69 (1.95)	1.45 (0.33)	1.34 (0.69)	0.55 (0.33)
	96th PCT	2561	3.07 (0.84)	2.7 (1.7)	0.97 (0.34)	1.02 (0.67)	0.48 (0.3)
	98th PCT	1281	2.41 (0.81)	2.66 (1.27)	0.74 (0.34)	0.65 (0.64)	0.37 (0.26)
CM	90th PCT	6403	0.54 (0.24)	0.46 (0.29)	0.16 (0.14)	0.19 (0.16)	0.14 (0.12)
	92nd PCT	5122	0.6 (0.29)	0.48 (0.3)	0.15 (0.15)	0.17 (0.18)	0.12 (0.12)
	94th PCT	3842	0.56 (0.2)	0.47 (0.35)	0.34 (0.12)	0.32 (0.17)	0.16 (0.14)
	96th PCT	2561	0.55 (0.2)	0.46 (0.31)	0.24 (0.12)	0.25 (0.17)	0.14 (0.13)
	98th PCT	1281	0.43 (0.2)	0.44 (0.25)	0.2 (0.13)	0.16 (0.17)	0.12 (0.12)

z_5 . While some of the ML or MDPD estimated GPDs fit the dataset well, they fail to fit in some cases. For level of threshold value, it is hard to conclude which threshold has better performance, but it is notable that the threshold value of 94th percentile has worse performance as it fails to pass the test for almost all cases except ADR.

The goodness-of-fit test for GPD provided by Choulakian and Stephens [2001] is specified for single GPD, and the critical value is found through its corresponding shape parameter estimate and test statistic. In the case of mixture POT, there are two or more shape parameter estimates, therefore it is impossible to find the critical value and to assess whether the mixture GPD fitting the dataset well or not. A nonparametric test is needed to evaluate the fitting quality; at here we use the Kolmogorov-Smirnov (KS) test. In statistics, the KS test is a nonparametric test, and qualifies a distance between the empirical distribution function of the sample and the cumulative distribution function of the reference distribution (Stephens, 1974). The p-values for confidence level of 0.05 are given in Table 4.18 for the examined samples. Again, the results confirm the previous remark that the mixture POT fits the sample better than the conventional POT as the KS test statistics from mixture POT are greater than those from convention POT. Further, the results indicate that the null hypothesis of modelling datasets with GDP or mixture GPD from conventional POT and mixture POT method are accepted as the p-values are greater than 0.05. However, the conclusion is inconsistent with previous, for instance, the AD or CM test reveals that GPD from MM or PWM estimates does not fit the samples well. The possible reason is that AD test and CM test are kinds of probability weighted methods that give more weight on the tail, while the KS test gives the same weight to all data. Therefore, the AD or CM test is recommended to quality the goodness-of-fit for single GPD, then use nonparametric test to evaluate the mixture POT method modelled GPD.

The previous studies test the performance of mixture POT approach for modelling tail data with linear models of GPD. To choose the threshold, a number of methods exist. The classical approaches use graphical diagnostics to select optimal threshold. Some of the commonly used diagnostics are mean residual life plot, threshold stability plots. A benefit of these

Table 4.16: Root mean square error

Threshold	No.	MM	PWM	ML	MDPD	ADR
90th PCT	6403	0.0091 (0.004)	0.0083 (0.0059)	0.0035 (0.0032)	0.0066 (0.0062)	0.0095 (0.0084)
92nd PCT	5122	0.0079 (0.0033)	0.0079 (0.0054)	0.0034 (0.0032)	0.0063 (0.0065)	0.0078 (0.0079)
94th PCT	3842	0.0099 (0.0061)	0.0083 (0.0079)	0.0064 (0.0042)	0.0099 (0.0071)	0.0107 (0.0096)
96th PCT	2561	0.0095 (0.0051)	0.0084 (0.0071)	0.0048 (0.0039)	0.0083 (0.0069)	0.0096 (0.0091)
98th PCT	1281	0.0086 (0.0035)	0.0086 (0.0059)	0.0041 (0.0033)	0.0061 (0.0068)	0.0079 (0.0081)

Table 4.17: Critical value

Statistic	Threshold	MM	PWM	ML	MDPD	ADR
AD	90th PCT	1.03	1.04	1.07	1.06	1.01
	92nd PCT	1.02	1.03	1.07	1.07	1.03
	94th PCT	1.04	1.04	1.05	1.05	1.01
	96th PCT	1.03	1.05	1.06	1.05	1.01
	98th PCT	1.02	1.05	1.07	1.07	1.03
CM	90th PCT	0.16	0.16	0.17	0.17	0.16
	92nd PCT	0.16	0.16	0.17	0.17	0.16
	94th PCT	0.16	0.16	0.17	0.17	0.16
	96th PCT	0.16	0.17	0.17	0.17	0.16
	98th PCT	0.16	0.17	0.17	0.17	0.16

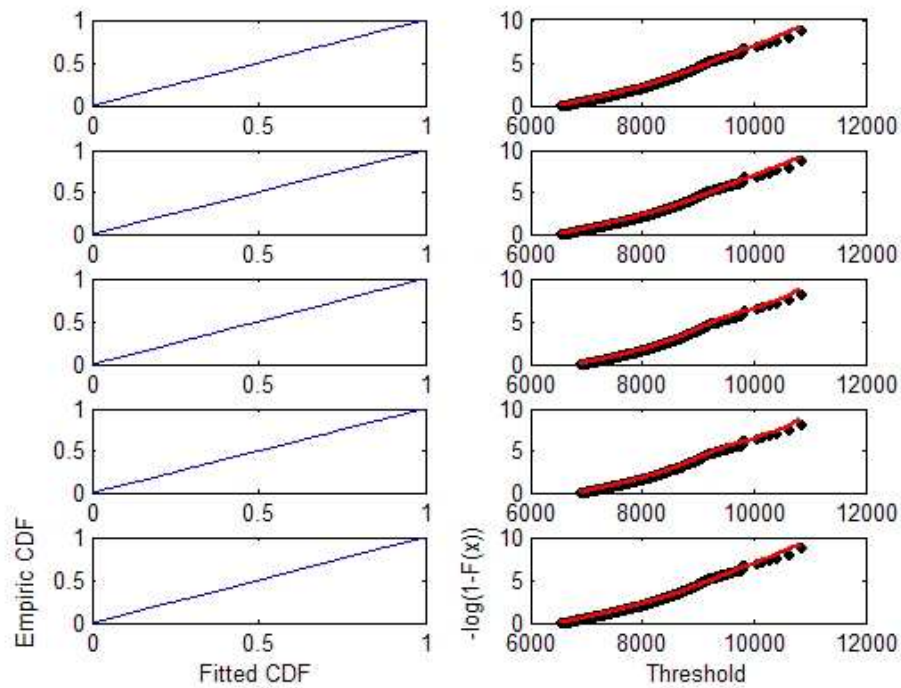
Table 4.18: KS test

Threshold	No.	MM	PWM	ML	MDPD	ADR
90th PCT	6403	0.072 (0.408)	0.014 (0.296)	0.12 (0.542)	0.1 (0.529)	0.164 (0.57)
92nd PCT	5122	0.172 (0.453)	0.098 (0.208)	0.157 (0.146)	0.148 (0.239)	0.107 (0.42)
94th PCT	3842	0.65 (0.759)	0.644 (0.754)	0.339 (0.839)	0.567 (0.796)	0.737 (0.843)
96th PCT	2561	0.641 (0.718)	0.702 (0.673)	0.307 (0.867)	0.453 (0.829)	0.633 (0.778)
98th PCT	1281	0.422 (0.676)	0.697 (0.677)	0.087 (0.601)	0.173 (0.611)	0.537 (0.596)

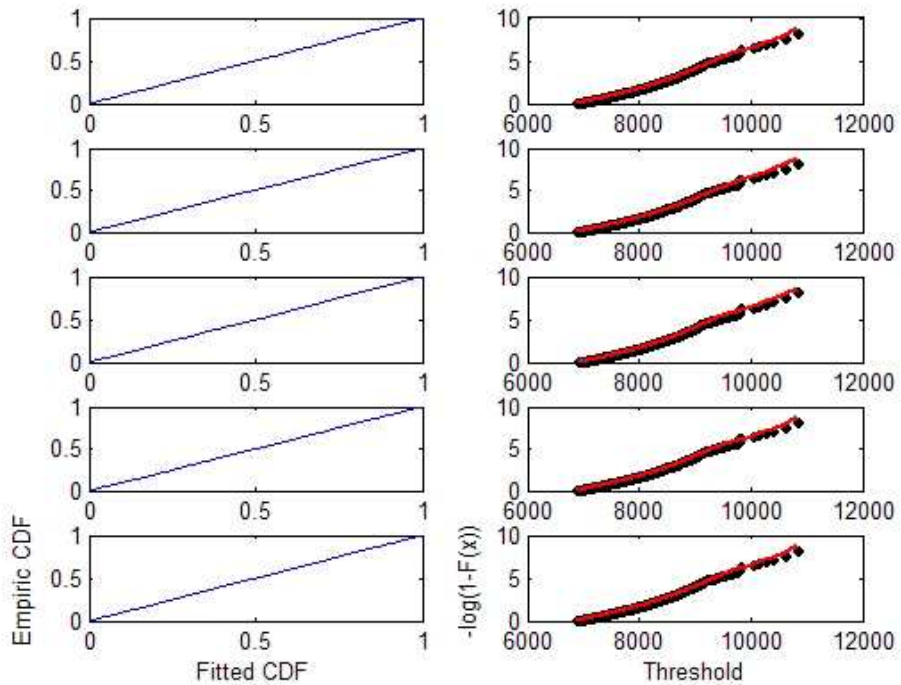
approaches is that they require practitioners to graphically inspect the data, understand their features and assess the model fit, when choosing the threshold. A key drawback with these approaches is they can require substantial expertise and can be rather subjective. In contrast, some automated approaches have been proposed to determine optimal and avoid subjective judgement. For instance, Ferreira et al. [2003] determine the optimal threshold by minimising the mean square error of the quantiles. However, the commonly used statistics like mean square error is not the optimal rule for determine threshold as it gives same weight to every point. Choulakian and Stephens [2001] proposed that the AD and CM tests can help in choosing a threshold value in the standard GPD model, and Dupuis [1999] provides a threshold selection guide based on these goodness-of-fit test. Although it is impossible to evaluate mixture GPDs directly by using the AD or CM test, it can help to select optimal threshold for each component. Hence, it is straightforward to determine the optimal threshold for the mixture threshold. Using this approach, the optimal thresholds for load effect type 1 for bridge with length of 40 m have been determined, and the parameters estimates for corresponding optimal threshold are listed in Table 4.19. The KS test statistics reveal that the mixture GPD models fit the dataset well. The diagnostic graphics of Probability-probability plots are given in Figure 4.20.

Table 4.19: Optimal threshold selection

Statistic	Estimator	2-truck			3-truck			4-truck			KS p-value
		Shape	Scale	Threshold	Shape	Scale	Threshold	Shape	Scale	Threshold	
AD	MM	0.0628	262.5	6540	-0.2185	830.4	6540	-0.1874	1114.0	6540	0.09
	PWM	0.0952	253.5	6540	-0.2056	821.6	6540	-0.1918	1118.2	6540	0.10
	ML	0.0725	259.9	6540	-0.2771	812.7	6864	-0.1887	1115.5	6540	0.74
	MDPD	0.0884	256.4	6540	-0.2728	808.9	6864	-0.1873	1113.9	6540	0.55
	ADR	0.1162	252.4	6540	-0.2116	829.0	6540	-0.1910	1116.0	6540	0.79
CM	MM	0.0536	269.8	6571	-0.2567	798.0	6864	-0.1874	1114.0	6540	0.66
	PWM	0.0952	253.5	6540	-0.2483	792.7	6864	-0.1918	1118.2	6540	0.48
	ML	0.0725	259.9	6540	-0.2813	803.3	6921	-0.1887	1115.5	6540	0.86
	MDPD	0.0884	256.4	6540	-0.2728	808.9	6864	-0.1873	1113.9	6540	0.55
	ADR	0.1162	252.4	6540	-0.2561	799.7	6864	-0.1910	1116.0	6540	0.70



(a) Anderson Darling test.



(b) Cramer-von Mises test.

Figure 4.20: Diagnostic graphics

Table 4.20: Difference for 100-year return level between conventional and mixture model

Load effect	Length	BM/GEV	POT/GPD				
			MM	PWM	ML	MDPD	ADR
I1	20	-8.49	0.11	0.43	0.19	0.17	-0.63
	30	-9.56	-6.31	-10.40	-8.18	-9.66	-13.25
	40	-14.63	-8.27	-7.90	-1.82	-7.19	-9.54
	50	-16.98	15.78	-2.71	20.32	21.18	24.61
I2	20	5.12	-0.47	1.54	0.20	0.36	-0.96
	30	-20.60	-3.02	-0.32	-6.33	-3.66	0.17
	40	-9.51	-3.02	-16.38	-16.02	-21.40	-25.99
	50	-11.22	0.08	-2.73	1.20	1.04	2.04
I9	20	-29.92	-4.55	-7.11	-1.63	-4.30	-16.47
	30	-15.22	-5.89	-9.69	-4.11	-5.92	-9.26
	40	-8.28	5.76	20.09	16.59	23.89	28.61
	50	-17.85	8.44	24.03	9.14	14.40	30.28

4.5.4 Results of Simulation

The previous study has demonstrated that the MPOT method can improve the modelling of tail distribution of traffic load effects. For the load effects and bridge lengths described, 100-year and 1000-year return period characteristic values, calculated from the conventional block maxima method, the composite distribution statistic (CDS) approach proposed by Caprani et al. [2008], the CPOT approach and the MPOT approach, are presented in Table 4.20 and Table 4.21. The differences between return level estimates from conventional and mixture methods are listed in Table 4.20 and Table 4.21 for 100-year return period and 1000-year return period, respectively.

The first conclusion can be made on performances of the methods for estimating 100-year and 1000-year return levels. The differences between conventional and mixture estimates are smaller for 100-year return level than for 1000-year return level. For example, the difference between convention method and mixture for 100-year return level of load effect I1 with span of 30 m shown in 4.20 is around 10%, while the difference for 1000-year return level in 4.21 is around 10% more. It confirms the common impression that the extrapolation to remote future is not stable.

It seems that the difference between conventional method and mixture method is smaller for load effects for shorter spans, either the BM or the POT. For instance, the difference is -8.49% for BM for 100-year return level of load effect I1 at length of 20 m in 4.20, but it increases to about 17% at span length of 50 m. It is due to the composition of loading events becoming more complex when span length increases.

Among the three types of load effects, the performances of the methods are different. The differences are larger for load effects of I9 than for the other two. As been stated by Harman and Davenport [1979], the load effect of I9 is more sensitive to the multiple presence of trucks.

Table 4.21: Difference for 1000-year return level between conventional and mixture model

Load effect	Length	BM/GEV	POT/GPD				
			MM	PWM	ML	MDPD	ADR
I1	20	-10.62	0.24	0.64	0.30	0.28	-0.62
	30	-16.20	-13.50	-22.30	-22.38	-24.88	-25.21
	40	-29.67	-9.78	-11.11	-1.00	-9.44	-18.01
	50	-36.45	34.53	-1.39	44.65	46.16	53.06
I2	20	8.65	-0.80	1.93	0.05	0.28	-1.37
	30	-25.62	-8.36	-8.90	-11.17	-8.81	-4.43
	40	-11.39	-4.48	-36.71	-36.18	-42.90	-48.55
	50	-13.91	1.26	-2.68	2.69	2.58	3.80
I9	20	-41.27	-8.28	-12.52	-3.83	-7.92	-25.76
	30	-17.82	-7.10	-13.42	-6.72	-10.99	-19.27
	40	-10.21	9.40	34.22	28.00	40.81	47.71
	50	-17.65	15.34	40.60	16.50	24.94	51.36

This shows that the differences for return level of type I9 load effect between convention method and mixture method becomes larger with increasing span length.

Moreover, comparisons of the 100-year return levels and the 1000-year return levels from mixture GEV distribution and mixture GP distribution are given in Table 4.22. The two methods seem to provide consistent results. In general, the differences are less than 10%, it can be concluded that the two methods have similar performance. However, it is also clear that some of the differences are significant, especially for longer span lengths.

4.6 Conclusion

A detailed analysis of load effect is presented in this chapter. This analysis assesses the two primary assumptions of extreme value theory with respect to bridge loading events. It is shown that the events may be considered as independent but they are not identically distributed. A modification has been proposed in order to make it applicability of the extreme value modeling for bridge traffic load effects, and it helps to derive a new method - mixture peaks over threshold.

The MPOT method is shown to give results which differ from a conventional POT approach. From the analysis of load effect distributions presented, theoretical examples are developed through which the performance of the proposed method is assessed and compared with that of the conventional approach. It is shown that the violation of the assumption of identically distributed data by the conventional method, results in different predictions as compared to the MPOT method, especially when the components come from significantly different distributions. In addition, the proposed generalized Pareto distribution based MPOT is compared with the generalized extreme value distribution based method, which also acknowledges the

Table 4.22: Difference (mixture POT vs. mixture GEV)

Load effect	Length	100-year					1000-year				
		MM	PWM	ML	MDPD	ADR	MM	PWM	ML	MDPD	ADR
I1	20	0.43	-0.65	-0.57	0.89	-4.16	0.48	-0.74	-0.65	1.02	-5.44
	30	2.14	0.13	1.22	9.21	-5.44	8.13	8.84	11.73	17.17	-14.59
	40	-0.14	-0.05	0.25	0.46	1.75	1.80	0.14	1.32	8.82	-1.71
	50	-1.78	0.50	-0.10	-1.38	17.33	-2.44	0.70	-0.14	-1.85	10.28
I2	20	0.13	-1.91	-1.38	1.74	7.33	0.08	-2.45	-1.79	2.14	3.26
	30	-3.81	3.98	0.60	-3.03	22.85	-0.92	3.74	0.41	-3.95	11.82
	40	16.27	15.95	23.47	32.22	4.78	51.41	50.41	67.44	87.83	-0.18
	50	2.79	-0.85	-0.99	-1.23	21.55	3.93	-1.07	-1.35	-1.53	17.72
I9	20	5.27	-4.12	-0.21	15.40	-1.25	8.39	-6.18	-0.32	25.15	-10.28
	30	3.34	-1.77	-0.06	2.40	-0.39	6.06	-0.29	4.23	13.06	-6.51
	40	-0.07	-0.72	0.00	5.57	4.22	-0.12	-1.28	-0.03	10.09	-11.32
	50	-5.15	1.49	0.36	-2.09	15.64	-7.19	2.18	0.51	-2.80	8.10

Table 4.23: Comparison of 100-year return levels (or characteristic values)

Load effect effect	Length (m) (m)	Conventional/Mixed						Composite distribution statistics					
		GEV	GPD					GEV	GPD				
			MM	PWM	ML	MDPD	ADR		MM	PWM	ML	MDPD	ADR
I1	20	4361	3717	3744	3696	3698	3722	4765	3713	3728	3688	3691	3746
	30	7353	7221	7054	7086	7048	7302	8130	7708	7873	7717	7802	8418
	40	10864	10489	10515	11220	10639	10390	12725	11434	11418	11428	11463	11486
	50	15058	19394	16006	20254	20277	20585	18138	16750	16452	16834	16733	16520
I2	20	939	807	825	797	803	817	893	811	812	796	800	825
	30	1008	969	958	973	968	971	1269	999	961	1039	1005	969
	40	1055	1052	1055	1056	1053	1061	1166	1085	1261	1258	1339	1434
	50	1142	1169	1168	1172	1168	1177	1286	1168	1201	1158	1156	1154
I9	20	-1696	-1105	-1132	-1092	-1106	-1116	-2420	-1158	-1219	-1110	-1155	-1336
	30	-1645	-1678	-1664	-1679	-1676	-1656	-1940	-1783	-1842	-1751	-1782	-1826
	40	-2463	-3114	-3534	-3408	-3648	-3998	-2685	-2945	-2943	-2923	-2945	-3109
	50	-3817	-4076	-4422	-4163	-4315	-4794	-4646	-3759	-3565	-3815	-3772	-3680

Table 4.24: Comparison of 1000-year return levels (or characteristic values)

Load effect	Length (m) (m)	Conventional/Mixed						Composite distribution statistics					
		GEV	GPD					GEV	GPD				
			MM	PWM	ML	MDPD	ADR		MM	PWM	ML	MDPD	ADR
I1	20	4658	3772	3805	3746	3749	3777	5211	3763	3781	3735	3738	3801
	30	7558	7381	7169	7209	7162	7477	9020	8533	9227	9288	9535	9998
	40	11142	10679	10711	11733	10860	10560	15841	11836	12050	11852	11992	12880
	50	15601	23973	17143	25957	26010	26771	24549	17820	17385	17945	17796	17490
I2	20	1033	837	860	823	830	850	951	843	844	823	828	861
	30	1059	1006	991	1012	1005	1008	1423	1098	1088	1139	1102	1054
	40	1089	1087	1091	1093	1088	1100	1230	1138	1724	1712	1906	2138
	50	1181	1221	1220	1225	1220	1233	1372	1206	1253	1193	1190	1188
I9	20	-2253	-1169	-1208	-1150	-1169	-1184	-3836	-1274	-1381	-1195	-1270	-1595
	30	-1684	-1765	-1744	-1767	-1762	-1734	-2049	-1900	-2015	-1894	-1980	-2148
	40	-2621	-3786	-4640	-4373	-4872	-5628	-2919	-3461	-3457	-3416	-3460	-3810
	50	-4190	-4638	-5247	-4787	-5050	-5916	-5088	-4021	-3732	-4109	-4042	-3908

differences in distribution of data, and the results show that the GPD based method has better performance than the GEV based method in terms of bias and standard deviation.

The MPOT method is applied to full traffic simulations on a range of bridge lengths and load effects. It is shown that some forms of loading events tend to govern certain lengths and load effects, and that this behavior is dependent on the physical nature of the bridge loading problem. The differences between the conventional and the mixture approach are great especially for longer span, it seems that the applications have greatest difference on the load effects for 40 m.

5 Effects of Transverse Location Distribution of Vehicles on Bridge Local Effects from WIM Measurements

5.1 Introduction

The aim of this chapter is to investigate the influence of transverse location distribution of vehicles on bridge load effects. The transverse location of a vehicle (referring to the distance from centreline of the vehicle to the longitudinal centreline or outer edge of a bridge) on bridge is critical to bridge design as the effect of live load on the main longitudinal members is a function of the magnitude and location of wheel loads on the deck surface and of the response of the bridge to these loads [Huo et al., 2005]. In bridge engineering, the three-dimensional behaviour of the structural system is usually reduced to an equivalent live load lateral distribution factor which assigns a proportion of the load effect to the structural elements depending on their position relative to the applied load. These factors are generally available for the longitudinal effects governed by gross vehicle weights (GVWs) [Bakht and Jaeger, 1983]. However, the attention regarding fatigue safety should focus on the transverse behavior, rather than that in longitudinal performance for bridges with box cross-sections. As in [Huo et al., 2005], load effects like stresses on decks [American Institute of Steel Construction, 1963; Troitsky and Foundation, 1987] are more sensitive to the transverse loading position in lane. The use of a relatively coarse vehicle transverse location for calculating longitudinal effects will lead to under- or over-estimation of the effects induced by an individual wheel load. Modern Weigh-in-Motion (WIM) systems permit the measurement of vehicle transverse position as well as vehicle track (the distance from the centreline of the tyre pressure area on one side of an axle to the centreline on the other side). Using the newly collected WIM data, this chapter tries to assess the influence of the distribution of transverse location of vehicle centreline in lane on the bridge traffic load effects. Two types of bridge were utilized to evaluate the influence of transverse location of vehicle on traffic load effects. One is orthotropic steel deck bridge [Gomes, 2012], and another is reinforced concrete box-girder prestressed bridge [Treacy and Bruhwiler, 2012]. In the following, the term "transverse location of vehicle" refers to the transverse eccentricity of the centreline of a vehicle with respect to the longitudinal centreline of a lane where the vehicle is located.

Chapter 5. Effects of Transverse Location Distribution of Vehicles on Bridge Local Effects from WIM Measurements

Measurements of transverse location of vehicles on four French highways were collected by WIM systems in 2010 and 2011. The measurements showed a completely different distribution model of transverse location of vehicle to that recommended in EC1. In order to evaluate the influence of the distribution of transverse location of vehicle on load effects on bridge decks, finite element analyses were carried out in Section to model a typical orthotropic steel deck bridge like the Millau Viaduct in France and a prestressed concrete box-girder bridge in Switzerland. The Millau case is extended further to assess the influence of transverse location on fatigue lifetime. The sensitivity of stress to the loading location was evaluated, and the influence surface of stresses for critical joints, which are susceptible of fatigue cracking, were obtained. Stress spectrum analysis and fatigue damage calculation were performed using the calculated stresses induced by traffic. By comparing the stresses and damages induced by different traffic patterns (through distributions of transverse location of vehicle), it was found that the histogram of stress spectrum and cumulative fatigue damage were significantly affected by the distribution. Actually, knowing the precise distribution of transverse location of vehicles can not only avoid under- or over-estimation of the fatigue damage for details under consideration, but also helps to constitute the inspection program. Due to the large number of welded connection details in OSDs, it is impossible to inspect every connection. Sample connections prone to fatigue cracking need to be predetermined to represent the health of the deck [Connor et al., 2012]. Numerical analysis that integrates finite element modelling and traffic data with distributions of transverse location of vehicles can help to make an accurate predetermination of which welded connections should be sampled to represent the health of the deck.

5.2 Related Research

Orthotropic steel decks have become standard components of major steel bridges because of their favourable characteristics such as high load-carrying capacity, light weight, and short installation time [Huo et al., 2005]. However, as the orthotropic steel deck undergoes many cycles of live load stress of high magnitude, fatigue cracks may develop at the welded connections between deck plate and the rib and other points of stress concentration. Fatigue cracks in several types of welded joints and geometrical details have been reported to occur in a large number of slender orthotropic decks of existing steel bridges in many parts of the world [de Jong, 2004]. Among the various fatigue cracks observed in orthotropic decks with closed ribs, cracks in rib-to-deck (one sided) partial-joint-penetration welds are of particular concern [Pfeil et al., 2005; Sim and Uang, 2012; Xiao et al., 2006, 2008; Ya et al., 2010]. This type of welded joint is prone to fatigue cracking because it is subjected to a very localized out-of-plane bending moment, particularly in the transverse direction, from the directly applied wheel loads. The stress behaviour of orthotropic steel decks especially for rib-to-deck joints has been studied widely through lab testing [Ben and WanChun, 2005; Gomes, 2012; Tsakopoulos and Fisher, 2003], field measurements [Pfeil et al., 2005], and analytical modelling or finite element modelling [Cullimore and Smith, 1981; Gomes, 2012; Sim and Uang, 2012; Xiao et al., 2008].

Many factors affecting the stress on the critical joints like deck plate and rib web thicknesses, surfacing layer properties, loading location, etc. have been studied [Ji et al., 2011; Sim and Uang, 2012; Xiao et al., 2008], but loading location in the transverse direction is perhaps the prominent one among them [Xiao et al., 2008]. In order to consider the influence of the loading location on effect calculation, some special clauses are given in design codes. There exists difference among them, such some recommend positioning the wheel to induce maximum stress at the detail under consideration like AASHTO, while some propose to use a random distribution of wheel path like EC3. Due to the randomness of driver behaviour, setting the wheel path to a stochastic variable should be more reasonable. Although this assumption is acceptable for design of new structures, this simplified assumption will lead to excessively conservative results for examination of the current safety of existing structures.

5.3 Measurements, Finite Element Models

5.3.1 Vehicle Lateral Position Collection Device

To get a better understanding of the load effect on bridges, WIM devices were used to record and identify gross vehicle weights and axle weights as vehicles pass over the devices. In each lane, there were two transversal piezo-sensors (*A* and *B* in Figure 5.1). The voltage in the piezo-sensor changes due to the pressure on the sensor caused by a crossing vehicle axle, and the axle weights can thus be calculated based on such a change. This passing vehicle axle also interrupts the magnetic signal produced by the loop sensors, and therefore, the configuration information like the number of axles, the axle spacing and the number of vehicles can be determined [Jacob et al., 2000].

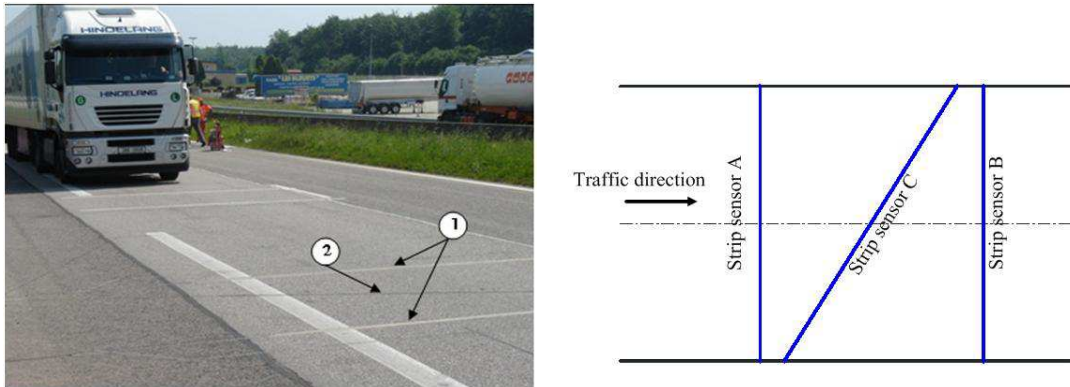


Figure 5.1: WIM device for collection of transverse vehicle position.

To measure vehicle lateral position (relative position with respect to the lane centre), an additional declining position sensor (*C*) was installed with an angle, θ , as shown in Figure 5.1. Assuming the vehicle runs over the device from left to right and in a straight line. The vehicle arrives at sensor *A* at time, t_a , and leaves the device at time, t_b , the speed of the vehicle can be determined from $v = d/(t_b - t_a)$ as the distance, d , between sensor *A* and *B* is known. When

Chapter 5. Effects of Transverse Location Distribution of Vehicles on Bridge Local Effects from WIM Measurements

the left and right tires cross strip C , the associated times, $t_{c,left}$, and $t_{c,right}$, are registered respectively and the vehicle width, w , can be found from the formula:

$$w = v(t_{c,left} - t_{c,right}) / \tan \theta \quad (5.1)$$

The lateral location of the vehicle centreline in lane is found based on the known position of lane centreline, l_0 ,

$$e = l_0 - 1/2[v(t_{c,left} - t_a) / \tan \theta + v(t_{c,right} - t_a) / \tan \theta] = l_0 - v(t_{c,left} - t_{c,right}) / 2 \tan \theta \quad (5.2)$$

Thus, a negative value means the vehicle is shifted to left side, and positive corresponds to right side. A field test of this system was carried out on Maulan open experimental site, on RN4 highway, in France, and the test results are very homogeneous and consistent [Jacob et al., 2008].

5.3.2 Measurements of Transverse Location of Vehicles

This type of WIM system has been installed on several highways to collect traffic information and data, and four of them were used in present study. The four WIM stations (see Figure 5.2) were located at Vienne, Saint Jean de Vedas, Loisy, and Maulan on the French A7, A9, A31, and RN4 highways respectively. The data was collected between 2010 and 2011. These WIM systems provide high quality measurements as they were classified in the class of B (10) or C (15) according to the Cost 323 standard [Jacob et al., 2000]. However due to the dynamic nature of moving loads, low percentages of erroneous results can arise during everyday use, filtration is required to remove unreliable data before conducting the analysis [Sivakumar et al., 2011]. In the first step, some commonly used filtration criteria were used to eliminate unreasonable records with error in axle weights, axle spacing, etc [Sivakumar et al., 2011]. In addition, the quality of WIM measurements can be further improved by using lateral position records [Klein et al., 2012], vehicles driving outside the lane and unreasonable vehicle widths were thus eliminated according to the lateral position records, see in Figure-3.

Heavy trucks are critical when modelling traffic load effects for bridge design or assessment and the majority of them drive in the right lane (also said slow lane) as most of European Union countries restrict them to the right lane, which is also required by traffic laws (<http://cga.ct.gov/2005/rpt/2005-R-0814.htm>). The trucks in the slow lane were used in the following. Transverse locations of vehicle for the four sets were given in Figure 5.3a, and the EC1 recommended model was given in the figure also as a reference. In order to illustrate the deviations, the error bar (with mean value and with an interval with length of 2 standard deviations) was utilized to describe statistics of the data. In the figure, the vertical red line was used to represent the lane centre; therefore the negative value at left side means the vehicle shift to the left side of lane and the contrary for the vehicle shifting to right side. The EC1 model is symmetric with a mean value of 0. For the four sites measurements, three of them



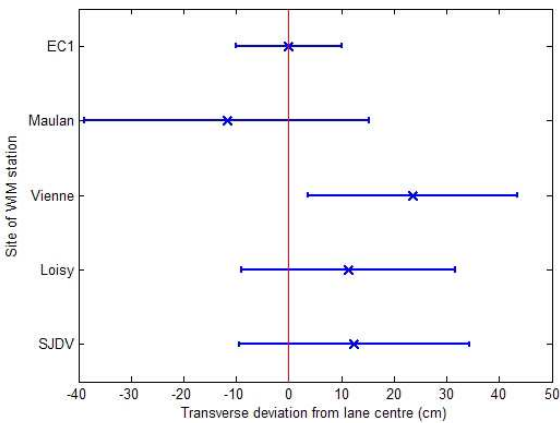
Figure 5.2: WIM station locations and measured period.

have positive mean value except measurements from Maulan. This means that most of the trucks driving on highway at Maulan were prone to drive at left side of the lane, and the trucks running in the other sites preferred to drive near right side or outer edge of roadway. In other words the majority of heavy trucks on all sites except Maulan tended to keep away from the faster traffic on the inner lane. Additionally, the differences of the mean values indicated that the distribution of transverse location of trucks in lane was site-specific.

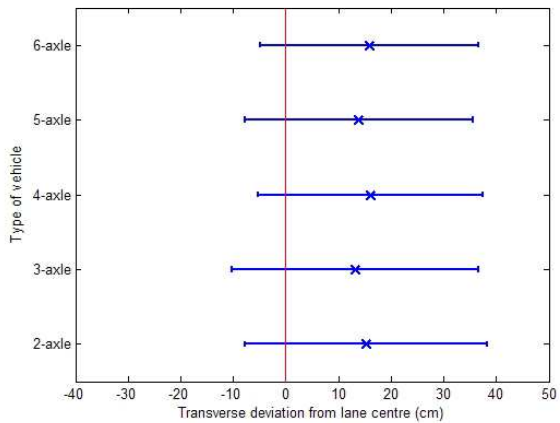
The aggressivity of truck load on bridges is strongly related to the type of trucks [Wang et al., 2005], thus it is important to know whether the distribution of transverse locations of truck is type-specific or not. In EC1, the common trucks in European routes are represented by five types of standard trucks that are extracted from traffic measurements collected from Auxerre [Sedlacek et al., 2006]. To investigate this feature, the measurements from SJVD were used as it contains more measurements than others. The recorded trucks were classified by number of axles, and the mean value and standard deviation of transverse location of vehicle are obtained for each type of truck. All types of truck showed similar behaviour: the mean value was positive, and the main part of truck in each class was prone to drive toward the right side. The error bar plot indicates that the distribution of transverse location of trucks did not show significant vehicle-type feature (see Figure 5.3b), the mean value and standard deviation have slight difference (see Figure 5.4).

Figure 5.3c shows the relationship of the lateral shift with different speeds. The measured trucks were grouped by their speeds, and the trucks were classified into seven groups with

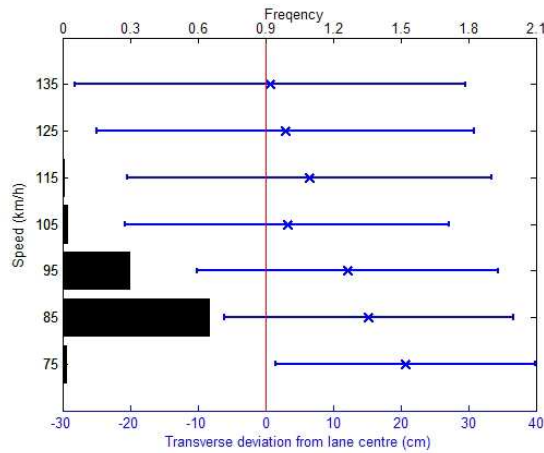
Chapter 5. Effects of Transverse Location Distribution of Vehicles on Bridge Local Effects from WIM Measurements



(a) Various site.



(b) Type of vehicle.



(c) Speed.

Figure 5.3: Sensitivity analysis.

mean speed from 75 km/h to 135 km/h. The transverse locations of trucks in each group were presented with their mean value and standard deviation in error bar plot, in bottom axis of Figure 5.3c. The result indicates that higher speed leads to a concentration of the wheel paths in a lane or left shifts.

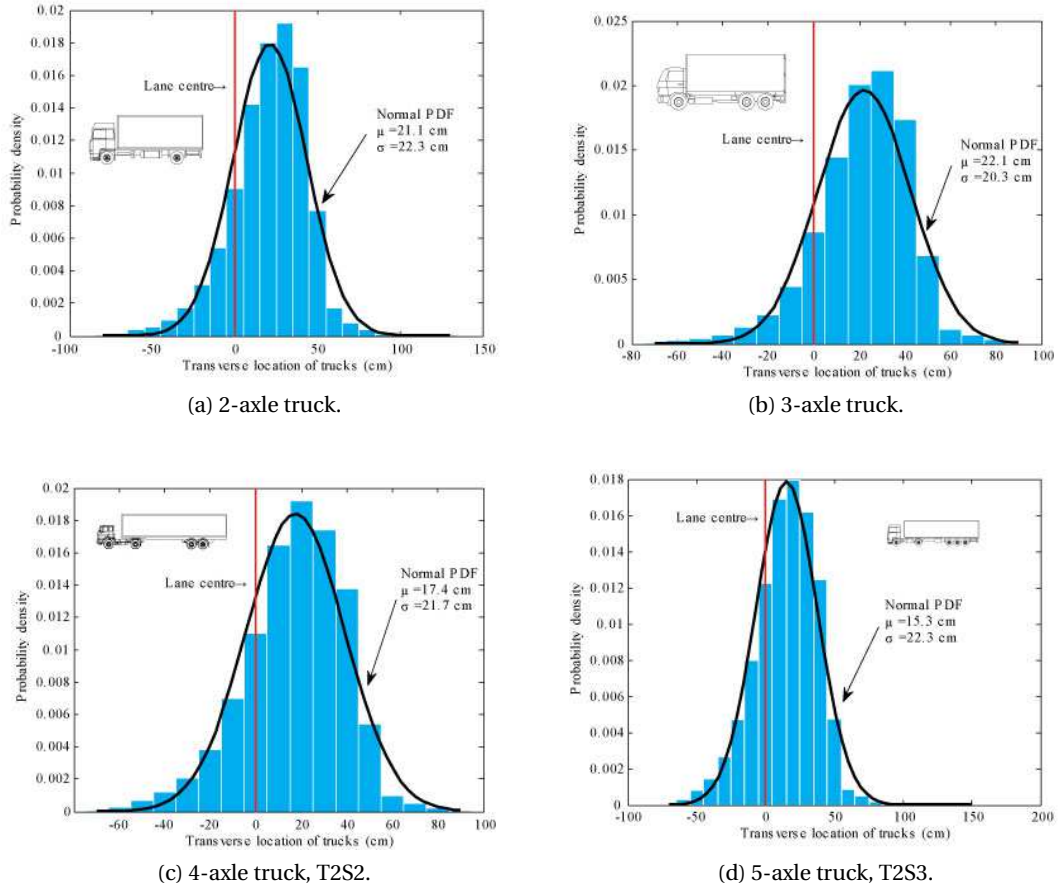


Figure 5.4: Distribution of transverse location of centre line of trucks for various types of truck.

Although the speeds of the recorded trucks range from 65 km/h to 140 km/h, the measurements showed that the majority of the trucks have a speed around 85 km/h. In the measurements, about 90% of trucks were classified in the range of 80 km/h to 100 km/h as the histogram of speed shown in Figure 5.3c for the upper axis, and the trucks with higher speeds tended to have lower GVWs. In fact, most European Union countries have a maximum speed limit of about 80 km/h for heavy good vehicles (generally greater than 3.5 t). Trucks with speeds between 80 and 100 km/h were used to analyze the statistical behaviour of the measurements. The frequency distributions in bar chart form (Figure 5.5) were prepared to show the pattern of transverse location of vehicle. In the figure, the ordinate shows the probability density and the abscissa is the distance from the centre of either wheel to the lane centre. The vertical line in the figure indicates the lane centre, and the positive value means the wheel centre deviates to the right side of the lane. The Gumbel or normal distribution fits the measurements very well,

Chapter 5. Effects of Transverse Location Distribution of Vehicles on Bridge Local Effects from WIM Measurements

and it has a right skew shape that is different from the commonly used symmetric distribution in literature such as [Xiao et al., 2008]. The fitted parameters are given in Table 5.1 for the four sites.

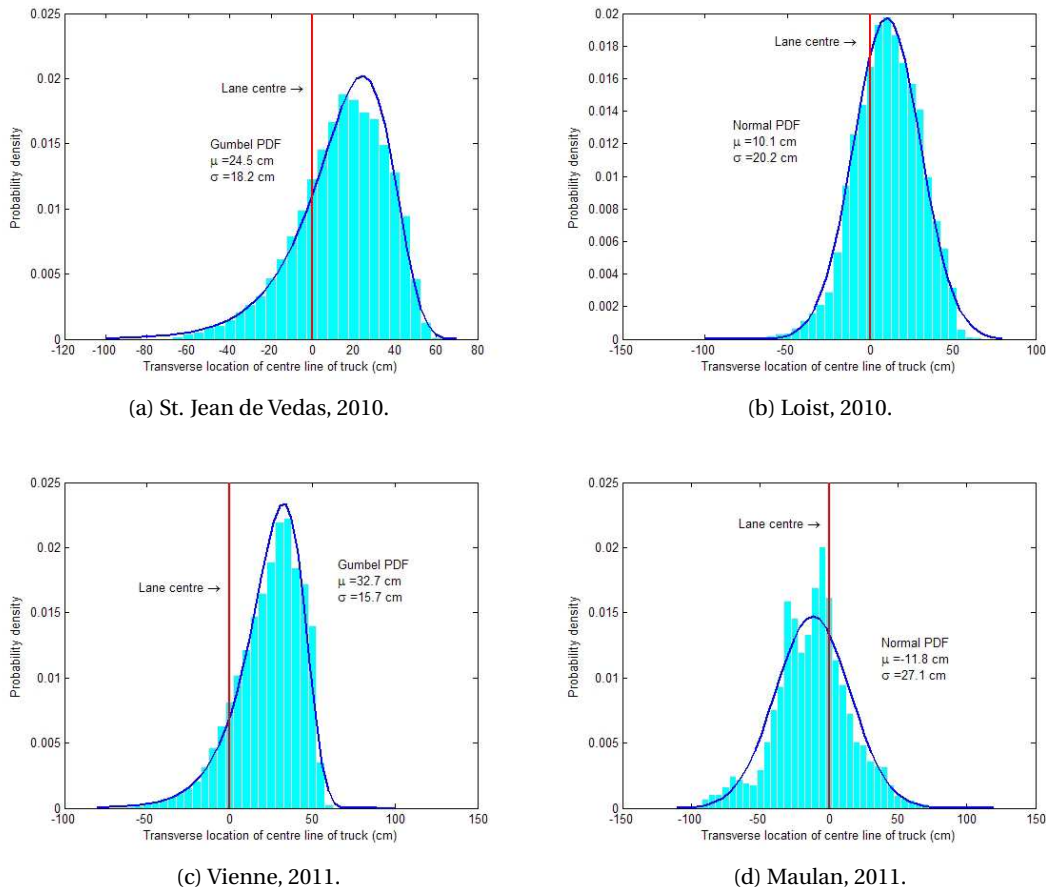


Figure 5.5: Distribution of transverse location of centre line of trucks on slow lane for various location

In the above investigation, the distribution of transverse locations of a vehicle in-lane position based on several sites measurements is considered. Three aspects influencing the distribution of transverse location of vehicles were investigated including site location, vehicle type, and vehicle speed. The distribution is insensitive to the type of vehicles, but it is strongly related to site location and vehicle speed. For the aspect of site location, three of the four sites are located on expressway, and the Maulan is located on a national highway, RN4. The three sets of data from the expressway have a similar feature in which the majority of the trucks are shifted to the right side relatively to the lane centre, while the distribution for the national way is shifted to the left side. After a further investigation of the lane profile, the slow lane on the three expressways have a emergency lane at their right side, while the RN4 only has two driving lane without an emergency lane. From a safety point of view, drivers are more comfortable with wider lanes [Ma et al., 2008; Prem et al., 1999]. Therefore, differences in the transverse

Table 5.1: Fitted distribution parameters

Parameter	SJDV, 2010	Loisy, 2010	Vienne, 2011	Maulan, 2011
Distribution type	Gumbel	Normal	Gumbel	Normal
Location, μ (cm)	24.5	10.1	32.7	-11.8
Scale, σ (cm)	18.2	20.2	15.7	27.1

location distribution of vehicles among different sites may be considered to mainly arise from the profile of lane cross section. For the aspect of vehicle speed, as illustrated in Figure 5.3c, it is seen that higher speed vehicles prefer to drive along the lane centre. Similar phenomena have been reported by Blab and Litzka [1995]. However, the measurements indicate that most of trucks travel at speeds ranging from 80 to 100 km/h, thus the distribution of transverse location of vehicle can be represented by these trucks. The Gumbel distribution is shown to fit the measurements of transverse location of vehicles well, which present different feature with the commonly used symmetric model such as the normal distribution. Even though measurements from

5.4 Finite Element Model

5.4.1 Reinforced Concrete Bridge Deck Slab

Deck slabs are among the most vulnerable elements of reinforced concrete road bridges with respect to fatigue as they experience each axle load resulting in very high numbers of stress cycles. Figure 5.6 illustrates an example of the passage of a 60 tonne truck over the deck slab of a Swiss box girder highway bridge. The bridge is a 110.5 m long, three-span, twin box-girder structure. A monitoring system, described in detail in [Treacy and Bruhwiler, 2012], was installed in 2011. The bridge was equipped with a series of strain gauges on steel reinforcement bars in the deck slab. Two 10 mm diameter bars in the transversal direction and two 12 mm diameter bars in the longitudinal direction in the bottom layer of the deck slab reinforcement were instrumented. The three strain gauge arrangement on the transverse bars (S1a to S2c) shown in Figure 5.6 capture the movement in the positive transverse bending moment in the deck slab which is dependent on the vehicle lane position. The sensors S1c and S2c closest to the vehicle wheels experience very sharp peaks due to each axle.

A finite element study was carried out to examine the sensitivity of the measured rebars to vehicle positioning. The 8-noded shell element is used. In order to analyze the local effects, the model is carefully meshed into element with size of 50 mm by 50 mm at the locations under investigation with a coarser mesh throughout the global model (see Figure 5.7).

To determine the transverse stress behaviour of the rebar in the deck slab, a unit load of 10 kN (approximately 1 tonne) is applied on the deck, and the load is acted as a pressure that is spread to a square area of 400mm x 400 mm as a typical tire contact area. The load runs over the bridge from left to right with a step of 0.1 m in the area close to sensor position, and a

Chapter 5. Effects of Transverse Location Distribution of Vehicles on Bridge Local Effects from WIM Measurements

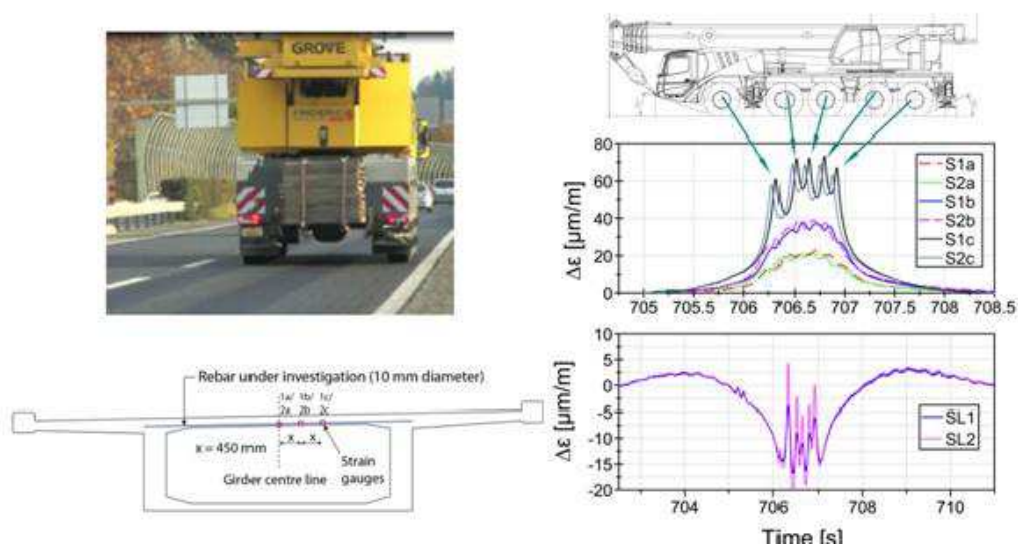


Figure 5.6: Signature of extreme vehicle seen as: (a) Influence on transverse reinforcing bar tensile strains and; (b) Influence on longitudinal bar strains from start of bridge to end

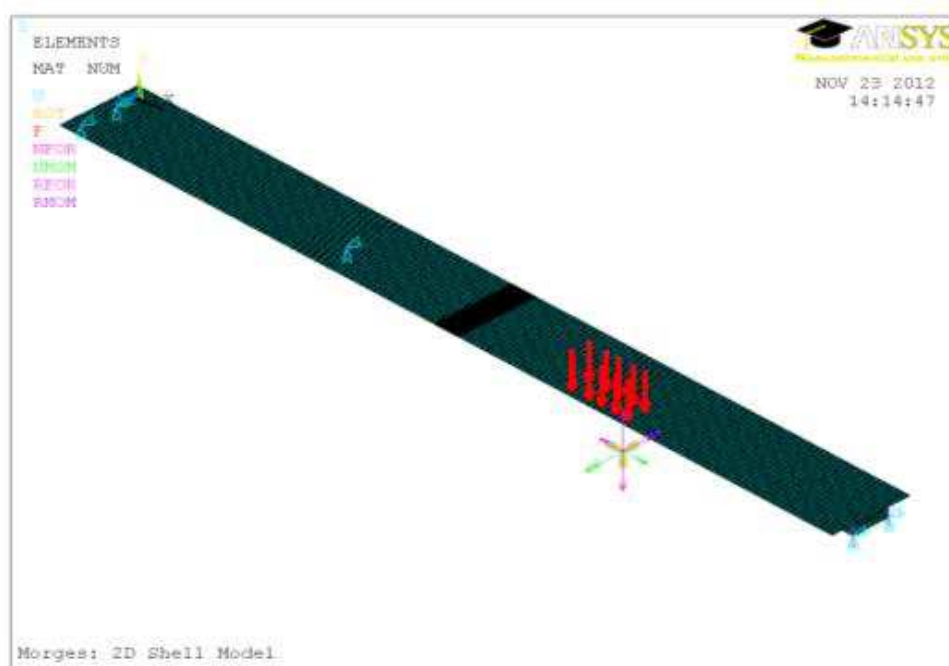


Figure 5.7: Finite element model for Morge bridge

larger step is used for area far from the sensor to reduce computation time. In Figure 5.8, the transverse stress on the top face of deck is plotted at location of sensor S1A for 13 loading tracks in transverse direction. Safety verification on the same structure have shown that the structure is considerable over-designed [Ludescher and Brühwiler, 2008], and the maximum monitored strain caused by traffic over a 300 day period is quite low at $130\mu\epsilon$ (corresponding to stress of about 27MPa). However, the local feature of the transverse stress is clearly shown, the track riding exactly over the sensor generates a larger transverse stress than other tracks. Although the stress does not disappear as quickly as in the orthotropic deck that will be presented in Section 5.5, a load positioned further than 2 m away has a negligible contribution to the effect. Zanuy et al. [2011] report the transverse fatigue behaviour of lightly reinforced concrete bridge decks; Fu et al. [2010] state repeated truck wheel load may cause cracks to become wider, longer, and more visible in concrete bridge deck, although the magnitude of transverse stress is low. Therefore, the transverse location of vehicle in lane or on deck is also critical for concrete bridge deck as it will increase transverse fatigue crack growth ratio.

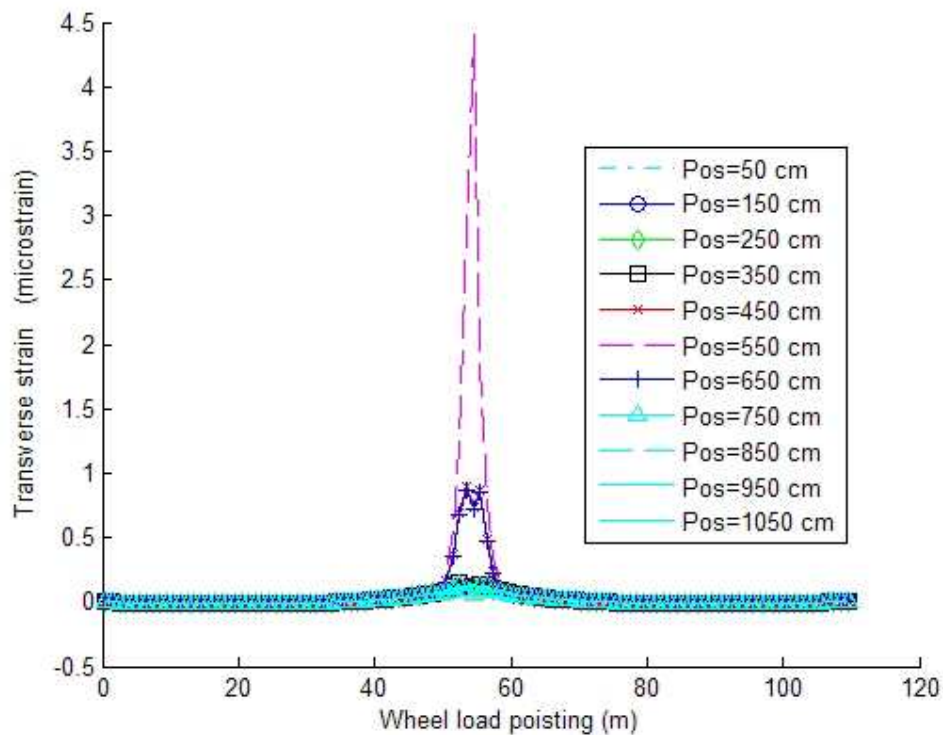


Figure 5.8: Change of transverse strain on the rebar at sensor position S1A

5.4.2 Orthotropic Bridge Deck

The Millau Viaduct (Figure 5.9) was chosen as an example of an orthotropic steel deck (OSD). It is a multi-tower cable-stayed bridge located in Southern France. The main girder was designed

Chapter 5. Effects of Transverse Location Distribution of Vehicles on Bridge Local Effects from WIM Measurements

as a closed box with trapezoidal cross section with an all-welded orthotropic roadway deck, with a structural depth of 4.2 m and width of 32 m, which carries 2 lanes and an emergency lane in each direction (see Figure 5.10 for a cross-sectional view). The surfacing is composed of a 3 mm thick sealing sheet (ParaforPont) and a 70 mm thick bituminous surfacing layer. The deck of the bridge consists of a deck plate of thickness, $t = 12 - 14$ mm (14 mm for deck under slow lane and $t=12$ mm for other lanes), and trough stiffeners with a wall thickness of 6 mm spacing at a distance of 600 mm. The troughs are 300 mm wide at the top and 200 mm at the bottom, and they are 300 mm deep. Thus, the deck is uniformly supported every 300 mm by a trough wall. The orthotropic deck is supported on transverse cross-bracing element at every 4 m.



Figure 5.9: General arrangement of Millau viaduct

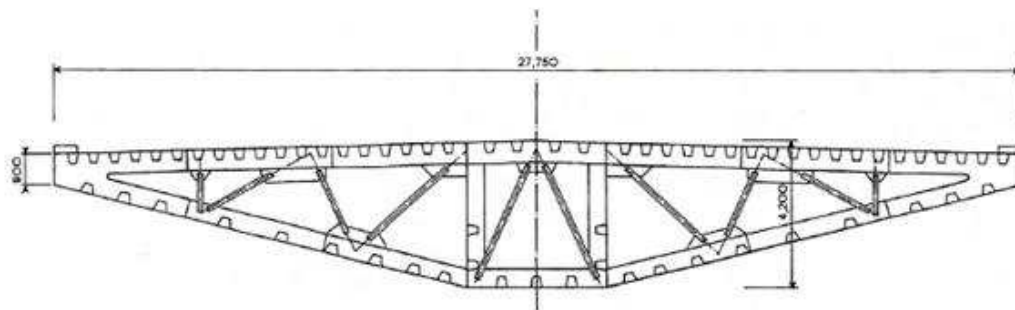


Figure 5.10: Cross-sectional view of the steel girder of the Millau Viaduct

The transverse stress in the deck is of interest in this study, which can be dealt with the third

system described in American Institute of Steel Construction [1963], where a partial structure is modelled instead of the whole bridge structure. 3D shell elements are frequently used to carry out such stress behaviour analysis [Cullimore and Smith, 1981; Xiao et al., 2008]. FE model was developed for the deck under slow lane that consists of the seven trapezoidal ribs supported by four transverse floor beams. Figure 5.11 shows the model using the finite-element analysis software ANSYS. Troughs and decks were modelled by using linear elastic three-dimensional shell elements where four nodes placed in the same plane define a plate. The element is capable of accounting for in-plane tension/compression, in-plane/out-of-plane shear and out-of-plane bending behaviours. In balancing between computation time and result accuracy certain elements of the structure feature a finer mesh. The three inner troughs and the deck between them are the focus of modelling and meshed with 25 mm by 25 mm elements, see in Figure 5.12. The other parts were meshed with 50 mm by 50 mm elements. The steel was considered as isotropic linear elastic with classical parameters values (Young's modulus of 210 GPa and a Poisson's rate of 0.3). The deck plates were restrained for vertical translation (z-direction) of the two longitudinal boundaries and were allowed to rotate, and they were constrained against vertical and transverse translations (z- and y-directions) and were allowed to rotate about the y-axis to model continuous or overhanging floor beams extending beyond girder webs. The finite element analysis results will be presented in next section.

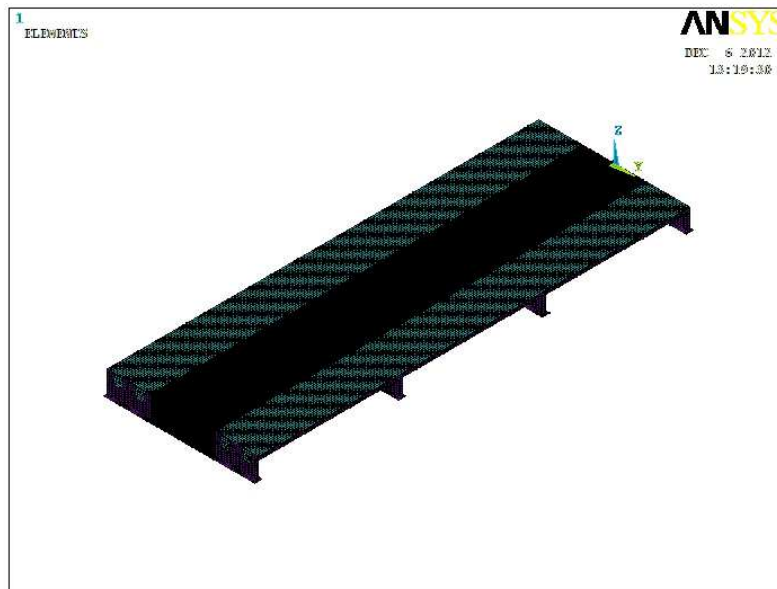


Figure 5.11: Finite element model of simplified orthotropic steel deck of Millau Viaduct

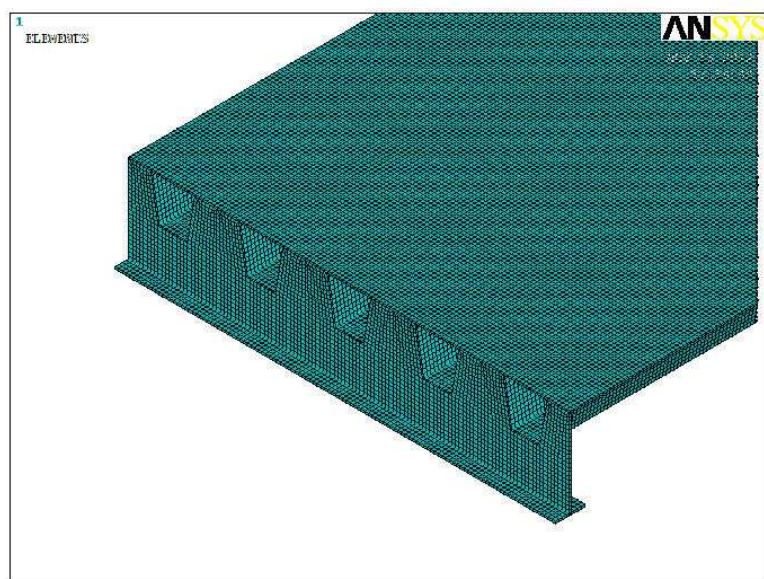


Figure 5.12: Highlight of the meshing

5.5 Results from Orthotropic Deck Study

This study extends in more detail into the Millau bridge deck presented in the previous section and shows how the lateral eccentricity can benefit the examination of such structures. Three types of tire of single wheel for steer axle, dual wheel, and single wheel are very common for trucks on European roads, they distribute wheel to different size of area. Assuming a load distributes to the vertical in an angle of 45° and the 74 mm bituminous surfacing layer is rigid, the distribution area on the OSD for the three tires are 368 mm by 450 mm, 688 mm by 450 mm, and 428 mm by 450 mm, respectively, see in Figure 5.13. To investigate the stress behaviour for the locations of concern, two models of wheel load paths were considered. One moves the wheel load along longitudinal direction, and another runs along transverse direction. The wheel load is simulated crossing along 37 paths in the transverse direction and 99 tracks in longitudinal direction on the deck, thus 3663 cases of wheel loads were considered for each type of wheel. Most of the load cases were distributed to the inner three ribs for the second span. In this particular area, the load advances with step of 0.1 m in longitudinal direction and 0.075m in transverse direction.

5.5.1 Results for Transverse Bending Moment

The longitudinal influence lines for several stresses at mid-span in between the second and third cross beam are presented in Figure 5.14. In the figure, the ordinate shows stress and the abscissa is the load position along longitudinal direction. Previous studies have shown that the longitudinal influence lines have a similar shape for wheel load along different longitudinal paths [Xiao et al., 2008], therefore, the influence lines under wheel loads riding over the joint

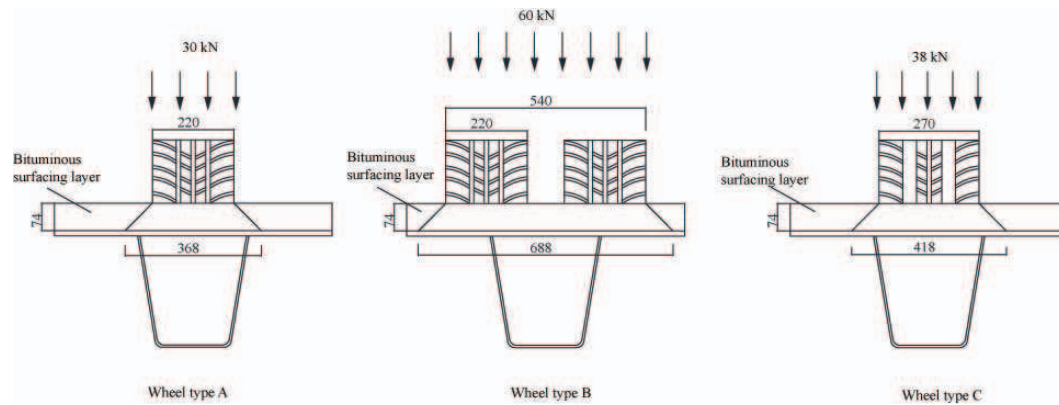


Figure 5.13: Load distribution of wearing surface (unit: mm) and proposed load

were shown as the representatives. For the stress on the deck bottom surface, two locations were of interest as they may be susceptible to fatigue crack. "Deck Outer" in Figures 5.14 and 5.15 refers to the deck plate outside of the trough wall, while "Deck Inner" refers to the deck plate inside the trough wall. Stresses at the location "Deck Outer" may be associated with fatigue crack that initiates at the weld toe on the bottom surface of the deck plate and propagates upward into the deck plate. Stress at "Deck Inner" may be associated with fatigue crack that initiates at the weld root and also propagates upward into the deck plate Kolstein [2007]. Three stresses on trough web were considered in this study. "Trough upper" in Figures 5.14 and 5.15 refers to trough wall at the trough-to-deck joint. Stresses at this location may be associated with fatigue crack that initiates at the weld toe on the web. "Trough side" and "Trough bottom" refer to stiffener splice joint. Longitudinal stresses at these locations may be associated with fatigue crack Kolstein [2007]. Usually cracks are initiated at the toe of the weld, but sometimes they can initiate at the root. The type of modelling approach is interested in the global behaviour and does not include the weld geometry in this work. The stresses presented later represent the stresses near rib-to-deck intersection rather than exact rib-to-deck joint.

As shown in Figure 5.14 all the stresses longitudinal influence lines are very short, and the stresses outside the range of middle span are small and can be neglected. The further the wheel load away from the object joint was, the smaller the stresses were generated. The maximum stress range always occurred when the wheel load was close to the section. Stresses at "Deck Outer" and "Deck Inner" had similar stress behaviour, the stresses experienced very complicate process. The stress completely changed from tension to compression when the load gets close to the section. A stress range of 53.7 MPa was obtained for "Deck Outer" under the over-rib wheel loads. The wave of the transverse stress at "Trough upper" was given in the figure with green line for the over-rib loads. The stress range of 20.6 MPa was much smaller than those of the deck plate under the same load. The influence lines for stresses with respect to trough splice joint on "Trough side" and "Trough bottom" were given also in the figure.

Beside the longitudinal influence lines, transverse influence lines for these points at mid-span are presented in Figure 5.15 also. In the figure, ordinate shows stress and abscissa is the

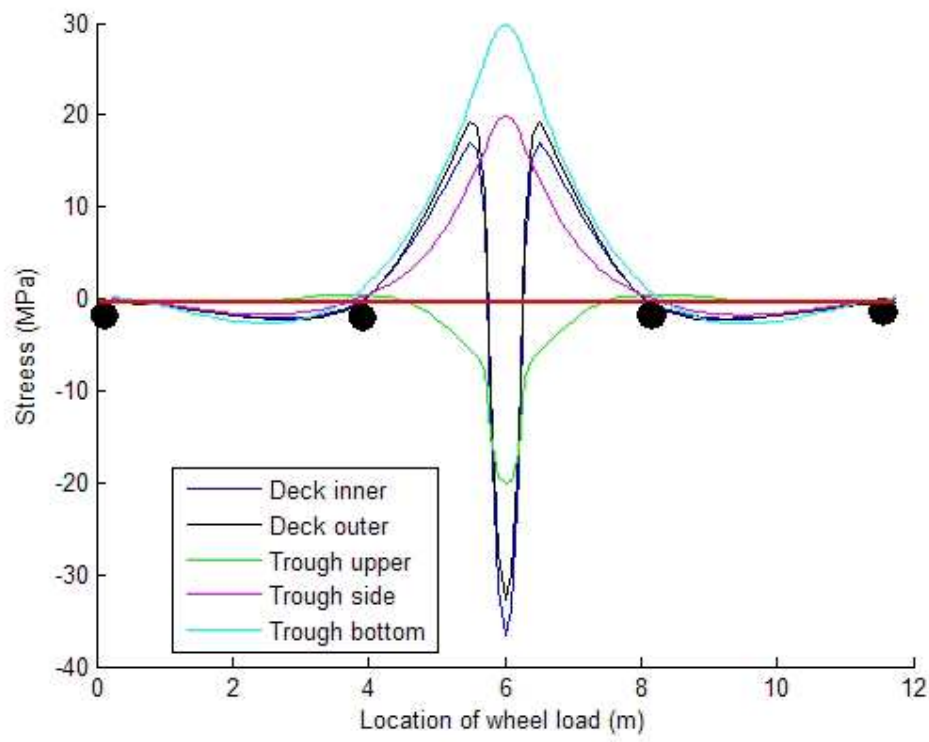


Figure 5.14: Longitudinal influence line

distance from the centre of wheel to the concerned load effect. It is clearly indicated that the stresses in the trough web and the deck plate are significantly reduced as the loading location moves away from the object joint, and all the stresses become zero when the loading location is around 600 mm away. For the two stresses ("Deck Outer" and "Deck Inner") on deck plates' bottom surface, both stress ranges disappear rapidly as the loading location moves away from the joint. The over-rib wall loads ($e=0$) generate the largest stress or stress range. The stress wave on the trough wall at "Trough upper" due to wheel load's transversal move fluctuates significantly. The trough wall experiences compression when the loading is located at the left side of the trough wall, while the tension stress is generated when the loading is at the left side. The maximum tension or compression stress occurs when the loading location is about 200 mm away from the rib-to-deck joint rather than the over-rib load. The stress at "Trough side" and "Trough bottom" had similar feature as the stress on the deck plate near the joint that reach peak values as the wheel load moves over the section of stress investigation, and significant stresses appear only when the wheel is rather close.

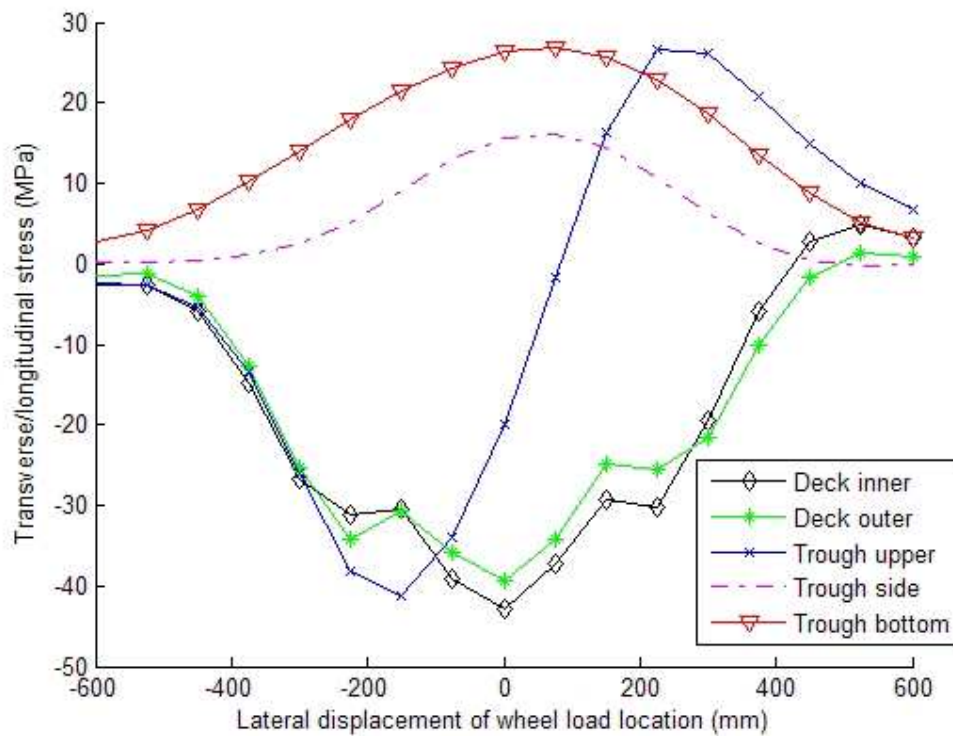


Figure 5.15: Transverse influence line

These previous results show that the loading location has a very significant influence on the investigated stresses. In order to establish the relationship of fluctuation of stress wave with loading location, the stress generated for various loading locations were compared with those generated when the load was exact over the investigated object. Because the load over the deck above the object generates peak values for the stresses at "Deck Outer", "Deck Inner",

Chapter 5. Effects of Transverse Location Distribution of Vehicles on Bridge Local Effects from WIM Measurements

Table 5.2: Stress (relative percentage difference, %)

Deviation (mm)	Deck Outer	Deck Inner	Trough upper	Trough side	Trough bottom
-600	-80.3	-84.6	-66.1	-98.6	-81.4
-450	-68.9	-75.2	-42.9	-91.4	-59.0
-300	-18.3	-16.4	59.9	-66.3	-30.2
-150	-22.1	-15.1	125.8	-20.4	-7.2
0	0	0	0	0	0
150	-38.5	-43.0	-202.7	-25.2	-15.8
300	-59.4	-44.0	-265.3	-70.9	-48.5
450	-114.8	-98.5	-206.1	-92.4	-77.3
600	-113.9	-104.5	-154.1	-96.5	-88.4

"Trough side", and "Trough bottom", the stresses were reduced when the loads moved away. When the loading location was 300 mm away, the stress reduced by more or less half, and most of them reduced by 100% when the loading location is 450 mm away. In addition, the stresses reduce much faster when the load moves away in right (or inside trough) than in left (outside trough). The stress at "trough upper" is the most sensitive to the loading location among the five investigated.

5.5.2 Discussion

The longitudinal influence lines for the several frequently fatigue susceptible joints shown in Figure 5.14 indicate that the load effects in OSD are governed by wheel loads. Particularly, when a load crosses over the OSD, its transverse location has a significant influence on the amplitude of the induced stress range. Because of the localized feature of stress on OSD, it was used to weigh the vehicles passing over as a bridge weigh-in-motion (BWIM) system [Dempsey et al., 1998; Jacob et al., 2010]. In Figure 5.15, the stress on bottom surface of deck plate "Deck Inner" and "Deck Outer" that near rib-to-deck is subjected to large compression. The compression stress reduces as the loading moves away from the joint in transverse direction. The stress on trough wall near the rib-to-deck joint ("Trough upper") changes from tension to compression as the loading location varies from the joint. The trough wall is subjected to axial compression when the loading acts on the joint, thus the transverse stress is much smaller. The trough wall is subjected to positive or negative bending when the loading location is away from the joint position, thus the trough wall is subjected to tension or compression. The relative differences listing in Table 5.2 indicate that the loading location should be very precise, for instance, a 150 mm shift of the loading location leads the stress on deck plate reducing by about 40%. Therefore, the location of the loading should be known as accurately as possible for OSD, otherwise the stress is possibly either over- or under-estimated.

Influence on Bridge Traffic Effect

Fatigue resistance of rib-to-deck welded joints can be affected by several parameters, including loading location, deck and rib plate thicknesses, weld penetration ratio, fabrication procedure, and surfacing layer [Sim and Uang, 2012; Xiao et al., 2008]. Among them the influence from loading location has been parametrically studied through finite element model in the previous. To evaluate further its influence, load effects induced by the combination of traffic data and corresponding influence surface are statistically analyzed. In the following study, we use the traffic data collected from SJDV, it has a typical feature of traffic on highway in France. For instance, the most standard 5-axle container truck on European roads, the distribution of loads for each type of axle is presented in the form of a histogram (see Figure 5.16). It can be seen that the drive axle load is the most severe with 60.7% of the GVW on average taken by this axle. To study the effects of the distribution of transverse location of vehicle on the fatigue resistance of rib-to-deck joints, parametric study based on the previous obtained influence lines were performed, and the results are summarized in the following.

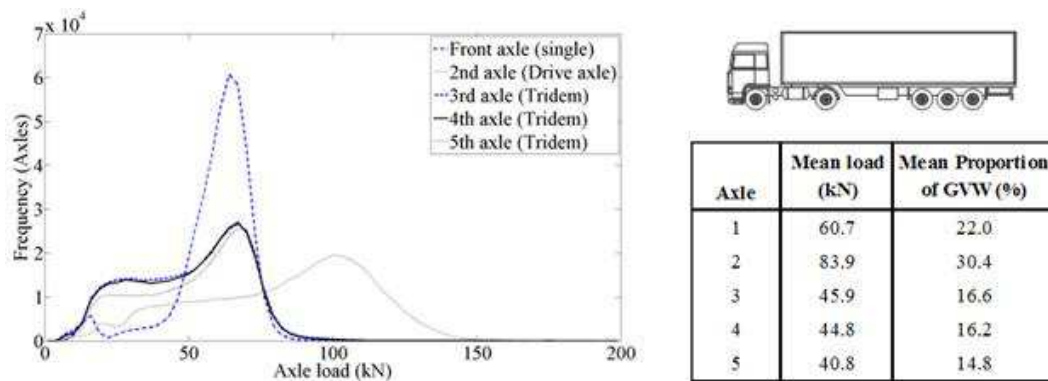


Figure 5.16: Histogram of individual axle loads for standard 5-axle container truck

Effects of Distribution of Transverse Location of Vehicle

To identify the position of local damage on the steel deck caused by vehicle load for different distributions of transverse location, the peak points and valley points of the stress time-history for the fatigue susceptible points were first determined by simulation of vehicles crossing over the influence surface. By executing the rainflow cycle counting technique to the stress time history data, a stress spectrum was obtained. Figure 5.17 shows the histogram of the two stress spectra for "Deck Outer" (see Figure-15) attained under these two patterns of traffic. It can be seen that when the vehicle transverse location distribution model of EC1 is used, stress amplitudes mainly range from 5 to 60 MPa. In contrast, when the distribution of transverse vehicle location is measured, stress amplitudes mainly range from 5 to 45 MPa. The comparison provides evidence that the distribution model of transverse location of truck has noticeable influence on the resulting stress spectra. Using the EC1 model generates higher number of stress cycles than traffic with measured transverse distribution model for almost all

the stress ranges.

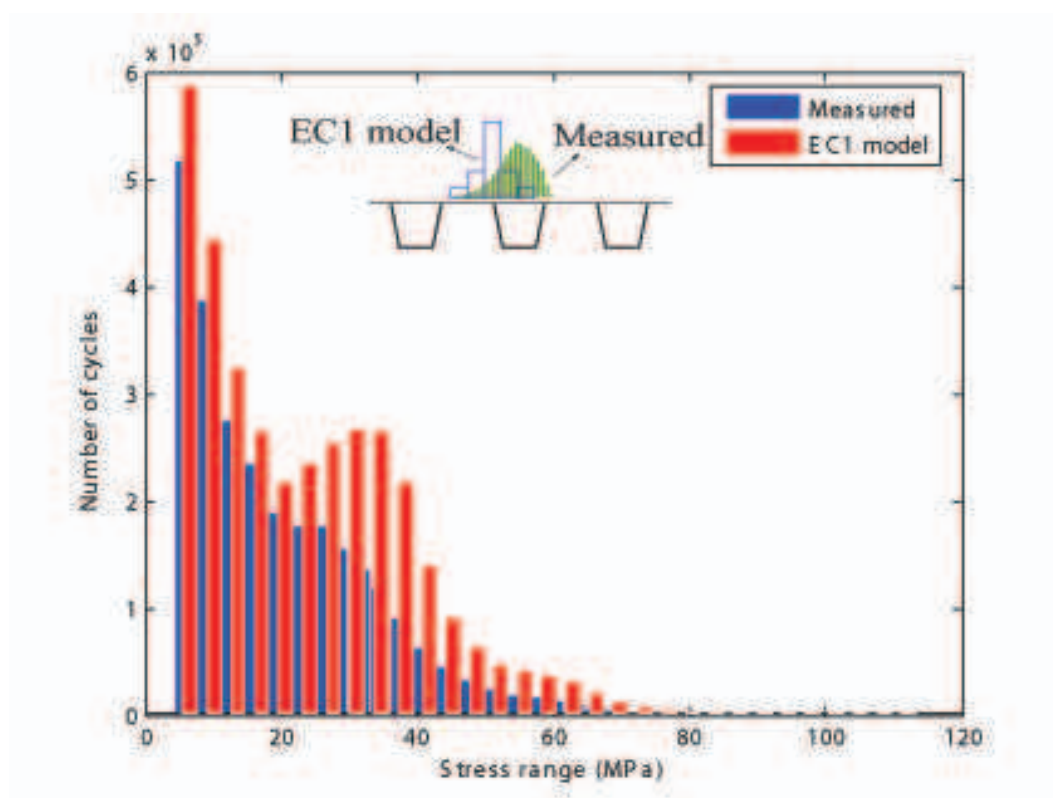


Figure 5.17: Stress spectrum of "Trough out" - distribution model of transverse location of vehicle

Effects of Vehicle Widths

To identify the position of local damage on the steel deck caused by vehicle loads for different models of vehicle width, the stress spectrum histogram has been established by performing rainflow counting for the calculated time history of stress as shown in Figure 5.18. It can be seen that stress amplitudes mainly range from 5 to 60 MPa in both cases. The figure shows that the stress range near the rib-to-deck joint is insensitive to the vehicle width.

5.5.3 Fatigue Damage

To examine the fatigue state of the joint when the distributions of transverse location of vehicle are different, the fatigue damage degree for the joint has been calculated by applying Miner's rule. In order to calculate the cumulative fatigue damage on a structural component by the Miner's rule, the number of repetitions to failure of the specified stress range is needed. This information is obtained from the S-N curves or S-N relationships, which are established from the experimental results for different materials and different categories of welded details. Each

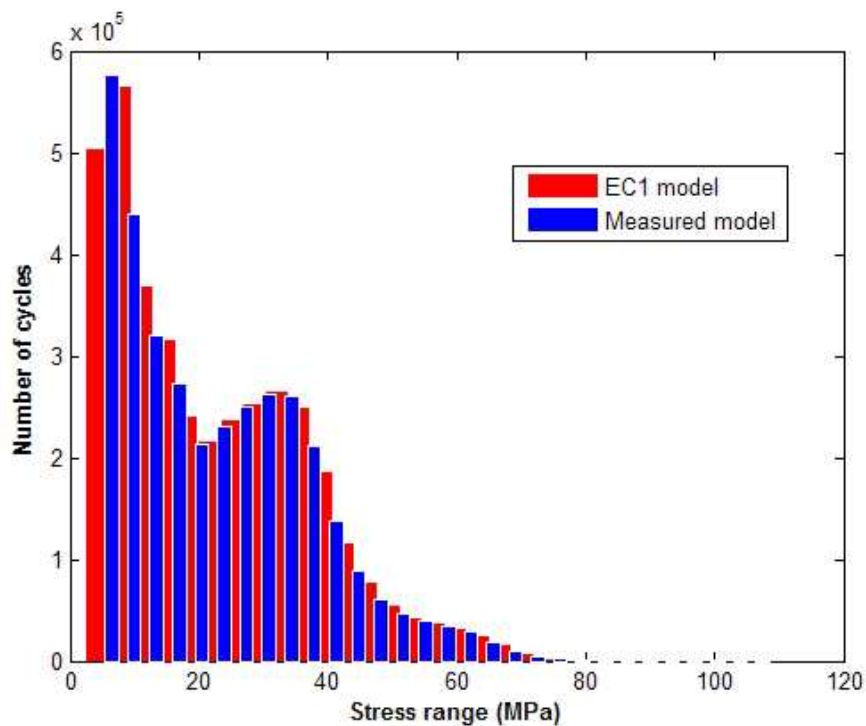


Figure 5.18: Stress spectrum of "Trough out" - distribution model of vehicle width

connection detail subject to fluctuation of stress should, where possible, have a particular class designated in EC3. The detail of the welded joint of rib-to-deck intersection is categorized as class 50 or 71 in EC3 depending on the type of welding.

Five loading cases have been established by combining the distribution models of transverse location of vehicle and vehicle widths (Figure 5.19). The cases are given in Table 5.3. The wheel load measurements at SJDV were used to simulate the traffic load effects induced by these five cases. The array of peaks valleys were obtained by the rain flow counting method, and the cycles of stress range were counted for stress amplitude and the resulting histogram is given in Figure 5.20.

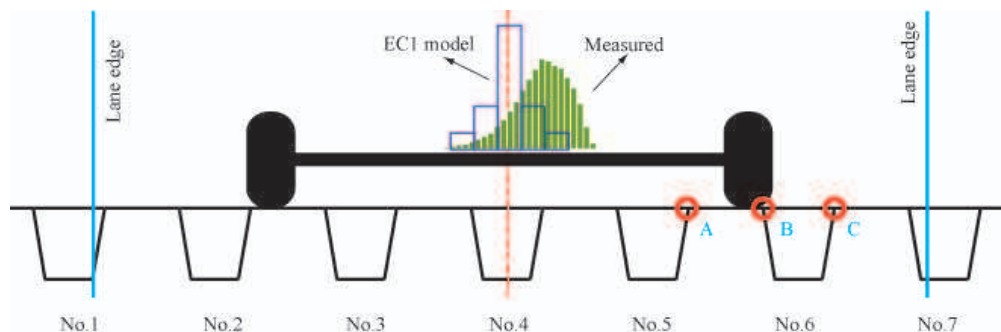


Figure 5.19: Transverse distribution of wheel path

Chapter 5. Effects of Transverse Location Distribution of Vehicles on Bridge Local Effects from WIM Measurements

Table 5.3: Cumulative damage in rib-to-deck joint under SJDV traffic

Case	Cumulative Damage with different distribution models of transverse location of vehicle			
	Cat 50		Cat 71	
Constant vehicle width and no deviation	1.32E-02	(40.6)	5.23E-03	(52.44)
Constant vehicle width and EC1 deviation	9.36E-03	(0)	3.43E-03	(0)
Measured vehicle width and EC1 deviation	9.10E-03	(-2.8)	3.33E-03	(-2.87)
Constant vehicle width and measured deviation	4.46E-03	(-52.4)	1.49E-03	(-56.57)
Measured vehicle width and measured deviation	4.26E-03	(-54.5)	1.42E-03	(-58.69)

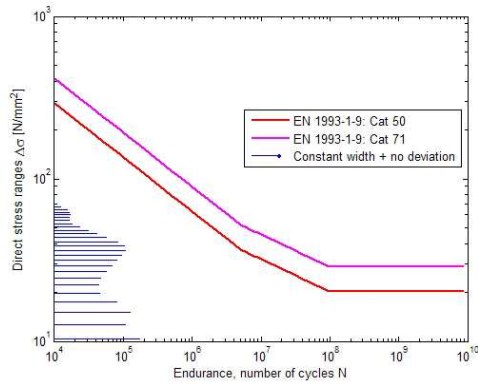
Table 5.3 shows the damage degree for rib-to-deck joint ("Trough outer") under the SJDV traffic with five different patterns. In general, the case of constant vehicle width and without deviation generates the largest damage in the joint, while the case of measured vehicle width and deviation generates the lowest damage in the joint. By comparison, for same distribution model of transverse location of vehicle, the damage caused with constant width is almost the same as that caused by measured vehicle widths, although the latter case generates somewhat smaller damage. It confirms the previous conclusion that the vehicle width has an insignificant influence. For the same vehicle width model, the damage under EC1 model of transverse location of vehicle can be one time that when the distribution model is measured. In addition, the damage caused without consideration of transverse deviation is about 40% more than that under EC1 model. Therefore, it can be concluded that distribution of transverse location of vehicle has an obvious influence on the fatigue life of the rib-to-deck joint.

5.5.4 Inspection Strategy

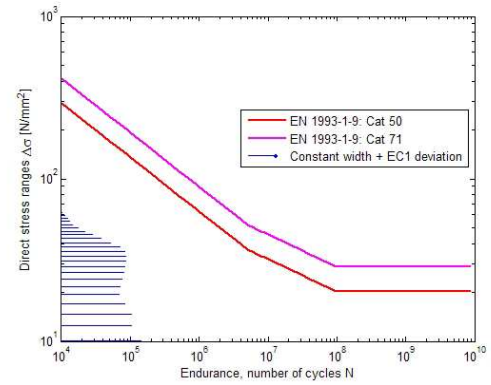
Due to the large number of welded connection details, inspecting orthotropic bridges presents unique challenges as compared to other more common bridge types. It is prudent that a sampling of welds of representative orthotropic details receive periodic inspections. These predetermined details are then monitored over time to ascertain whether the detail is exhibiting any fatigue cracking [Connor et al., 2012; Ma et al., 2008]. The predetermined details mainly are those under the wheel path. In general, when there are no measurements of wheel path, the model of transverse distribution in the specification is used. However, it will over- or under-estimated damage as the stresses on OSDs are very sensitive to the transverse loading location as shown in the previous sections.

Three adjacent rib-to-deck joints, which are A, B, and C in Figure 5.19, near the wheel location were selected to evaluate the influence of transverse distribution on the damage induced. The wheel load measurements at SJDV combined with the two transverse distribution models were used to simulate the traffic load effects. The array of peak points and valley points were obtained by the rain flow counting method, and the cycles of stress range were counted to calculate fatigue damage accumulation. The calculated cumulative damage levels by using Miner's rule for each joint are listed in Table 5.3. As expected, the fatigue damage levels are

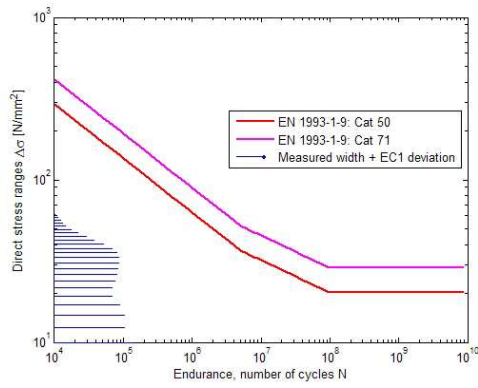
5.5. Results from Orthotropic Deck Study



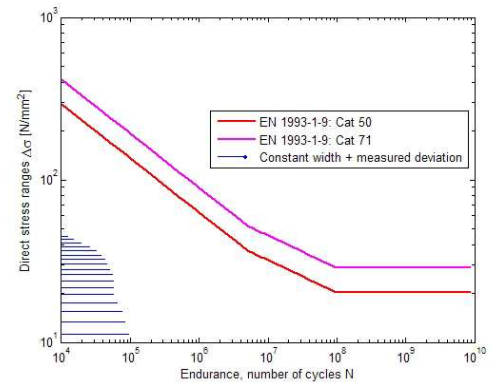
(a) Case 1.



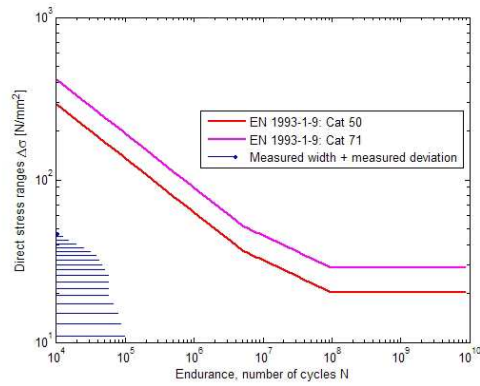
(b) Case 2.



(c) Case 3.



(d) Case 4.



(e) Case 5.

Figure 5.20: Stress histograms plotted on Eurocode S-N curves

Chapter 5. Effects of Transverse Location Distribution of Vehicles on Bridge Local Effects from WIM Measurements

Table 5.4: Inspection strategy

Category	Cumulative Damage with different distribution models of transverse location of vehicle					
	EC1			Measured		
	A	B	C	A	B	C
Cat 50	2.11E-03	9.36E-03	1.32E-03	1.15E-03	4.26E-03	5.59E-03
Cat 71	5.17E-04	3.43E-03	3.51E-04	2.99E-04	1.42E-03	1.93E-03
Damage order	2	1	3	3	2	1

quite different between the two models for each joint. The EC1 model generates about two times larger damage on joint A and B, while the measured model induces around 4 times more damage on joint C. In addition, the largest damage for EC1 case is joint B, but this study would indicate joint C may be the first to experience fatigue cracking. For EC1 model, the damage is concentrated on the joint B, while the joints B and C have equivalent damage for measured model. It gives a significant different picture for these two transverse distribution models, thus it will generate quite different inspection program, should such calculations be used as part of an inspection approach.

5.6 Conclusion

Measured datasets of transverse location of vehicle centre lines were collected from four highway sites in France using weigh-in-motion system. The measurements showed that the distribution of transverse location of vehicle centre lines is different from the model recommended in EC1, and also different from the commonly used normal distribution in references. Three sets of data were from expressways, and the other was from a national highway. The three motorway datasets showed similar statistical feature such that the trucks tend to maintain a driving position towards to the right side with a shift from lane centre line, while the data from national highway exhibits a contrary trend that trucks transverse locations shift to the left side of lane centre line. The analysis indicates that the difference arises from the profile of lane cross section. Sensitivity analysis also showed that the transverse distribution is related to the vehicle speed but is insensitive to the type of vehicle. The number of sites available is inconclusive to provide generalised distributions of the lateral 'in lane' positioning of trucks but highlights the importance of obtaining local data and assessing local features of the road geometry in such analyses.

To investigate the influence of transverse distribution of vehicle on bridge traffic load effects, two types of bridge decks were selected. One is an orthotropic steel deck (OSD) as the local effects in orthotropic steel decks are governed by wheel loads [Cullimore and Smith, 1981], the other is a reinforced concrete deck as fatigue studies of such structures are now required [Fu et al., 2010]. Finite element analyses of the bridges show the localized stress/strain at loading location. However the amplitude of strain in the concrete deck reinforcement is very small

because of conservatism in the original design and design requirements for global behaviour. A refined stress analysis was conducted on an OSD. Transverse distribution of loading was shown to generate significant out-of-plane bending moments at the rib-to-deck joint. Bending stresses were dominant on deck plate and rib. For the several frequently reported fatigue crack susceptible joints on OSD, the influence of transverse location of loading on their stresses were evaluated. The transverse stress on rib wall near rib-to-deck is most sensitive to loading location.

By integrating measured traffic load and transverse location of centre line of vehicles on lane, the stresses induced by traffic considering vehicle lateral position were obtained. The statistical analysis performed on the stress spectra revealed that transverse distribution of wheel loads has a significant influence on fatigue damage induced by traffic. For instance, the damage on a rib-to-deck joint generated by using the transverse distribution of EC1 is twice as large as that with a measured transverse distribution model. Due to the large number of welded connection details, it is impossible to inspect every connection. Sample connections prone to fatigue cracking need to be predetermined to represent the health of the deck. This can be achieved using realistic vehicle in-lane position simulations as presented within. From fatigue calculations of critical details, potential fatigue cracking connections can be identified by using precise transverse location of the wheel centre. Knowing the distribution of transverse wheel location within lanes is important not only for assessing fatigue life of orthotropic decks but also for developing maintenance strategies.

Conclusions

This thesis presents a statistical analysis of traffic load effects for the evaluation of the structural safety of existing road bridges with the final goal of improving existing techniques for the management of bridges. The following tasks were carried out as steps to achieve this objective:

- Review current existing methods for modeling maximum traffic load effects and propose ways to improve some prediction methods to obtain more accurate estimates.
- Investigate the parameter estimation methods for generalized Pareto distribution, and give guidance for selecting estimations in applying POT methods to bridge traffic load effects.
- Develop a method to improve the statistical analyses for lifetime load effect when the loading events can be identified.
- Investigate the influence of distribution of transverse location of vehicles on bridge traffic load effects that governs the loading capacity and local safety.

Conclusion of Thesis

Interesting results have been obtained during the work which was carried out in order to achieve the previous presented aims. The main results are given in this section with respect to these aims.

- Many different methods have been used in the literature to model bridge traffic load effects. These methods include fitting distribution (Normal, Gumbel, Weibull) to tail, extreme value modeling methods and level crossing method, and all of them concern the tail behavior. The early stage used method of fitting distribution to tail needs to pre-determine type of distribution, subjective judgements are thus involved in the estimation. The same problem exists in applying level crossing method to model bridge traffic load effect as it assume the traffic load effect process to be stationary and Gaussian. In recent years, extreme value theory based block maximum method has gained a lot of attention and has been applied to model bridge traffic load effects. However, many applications of BM method have been found to fit extreme value distribution to upper

tail of block maxima rather than the whole observed block maxima. It apparently lacks theoretical ground and needs subjective judgement to determine the fraction of tail to be fitted. Actually, another extreme value theory based method named peaks over threshold (POT) can achieve this goal with concrete theoretical support. The POT method has been widely used in other disciplines, in place of BM method for modeling extreme values but has less application in modeling bridge traffic load effect.

- To quantitatively evaluate performance of these existing methods on modeling extreme value distribution, numerical simulation sample from a Normal distribution and traffic load effect data generated by Monte Carlo simulation have been used. The evaluation is based on 75-year characteristic value and annual probability of failure, and results are presented in Chapter 3. Although the results indicate that no one of the investigated methods provides accurate estimates for characteristic value or annual probability of failure, the approaches fitting distribution to tail have better performance than other methods for numerical sample and the POT method shows better performance for Monte Carlo simulated traffic load effects. Additionally, the methods generally have better performance on characteristic value estimation than annual probability of failure.
- As concluded in Chapter 2, POT method has the best performance for modeling extreme bridge traffic load effects. To further introduce the POT method and to improve its performance, a comparative study has been carried out in Chapter 3 on the performance of parameter estimation methods. Although maximum likelihood estimation is the most widely used method, other methods like method of moments actually have better performance in situations like samples with small size. A number of parameter estimation methods have been investigated, and numerical sample and traffic load effect data are used to evaluate their performance. Results presented in Chapter 4 show that no method has always better performance than others, but methods like MM, PWM, ML, PML and ADR have well performance. In addition, the MDPD method has better performance for bridge traffic load effect data than numerical samples.
- Literature has shown that load effects due to different compositions of loading event are not identically distributed, thus standard extreme value theory can not be used in its strict validity domain for modeling the maximum traffic load effects. A composite distribution statistics method has already been proposed in the literature based on block maxima method. In chapter 4, a new method termed mixture peaks over threshold has been developed which accounts for the different parent distribution of load effect, and combines them to determine the characteristic load effect.

Theoretical studies were firstly used to verify the mixture peaks over threshold (MPOT) approach against the conventional peaks over threshold (CPOT) approach. It was shown for several examples that the MPOT corresponds to the exact distribution far more closely than the CPOT approach. In addition, the MPOT approach was also compared with the composite statistics distribution method proposed by Caprani et al. [2008], the results indicate that these two methods have similar performance and provide more

accurate results as compared to the traditional methods.

The MPOT method is applied to full traffic simulations on a range of bridge lengths and load effects. It is shown that some types of loading events tend to govern certain lengths and load effects, and that this result is dependent on the physical nature of the bridge loading problem. The differences between the conventional and the mixture approach are great especially for longer span, it seems that the applications have greatest difference on the load effects for 40 m span.

- Measurements of transverse location of vehicles on four French highways were collected by WIM systems in 2010 and 2011. The measurements showed a completely different distribution model of transverse location of vehicle to that recommended in EC1. In order to evaluate the influence of the distribution of the transverse location of the vehicles on load effects of the bridge deck, finite element analyses were carried out to model a typical orthotropic steel deck bridge like the Millau Viaduct in France and a prestressed concrete box-girder bridge in Switzerland. The Millau case is extended further to assess the influence of transverse location on fatigue life. The sensitivity of stress to the loading location was evaluated, and the influence surface of stresses for critical joints, which are susceptible of fatigue cracking, is obtained. Stress spectrum analysis and fatigue damage calculation are performed using the calculated stresses induced by traffic. By comparing the stresses and damages induced by different traffic patterns (through distributions of transverse location of vehicles), it is found that the histogram of stress spectrum and cumulative fatigue damage are significantly affected by the distribution.

Discussion of Future Research

The modeling of extreme bridge traffic load effects is a necessary part of the evaluation of existing highway bridges. There is thus space for further work which would complement this thesis:

- As it has been emphasized, POT method has been successfully used in disciplines like hydrology, insurance and etc., but limited study can be found on its application to bridge traffic load effects. The possible reasons are (i) the traffic load effects are not critical to bridge structures as such river level to reservoir design and assessment, (ii) the BM method is very easy to use. However, it deserves to introduce POT method to bridge traffic load effect. In this thesis, we deal with one of the critical issue, which is parameter estimation, in applying POT method to bridge traffic load effect. Alternative issues of threshold selection have not been deeply discussed, there is thus a need to study the choice of threshold.
- All the existing methods for modeling bridge traffic load effects ignore the time dependency and assume stationary of the process. However, it is widely reported that traffic

is increasing year by year in forms of traffic volume and loaded weight of single truck. Meanwhile, the load carrying capacity of structures decrease with the environment aggressions, degradations and natural aging. Therefore, it is necessary to study the traffic load effects with consideration of time dependency. How are the methods affected by evolution of loadings with time, when non-stationary processes are assumed?

- Although a mixture peaks over threshold method was introduced for modeling traffic load effects due to mixed loading events, it should be noticed that it is always impossible or difficult to classify load effects by their originating loading events. Therefore the mixture peaks over threshold as well as composite statistic distribution methods are not available for monitoring data in practice when loading events can not be identified. There is thus a need to introduce more efficient and robust parameter estimation methods similar to MDPD to estimate the distribution parameters for generalized extreme value distribution or generalized Pareto distribution.

Bibliography

- American Institute of Steel Construction (1963). *Design manual for orthotropic steel plate deck bridges*. American Institute of Steel Construction Inc, New York.
- Ashkar, F. and Nwentsa Tatsambon, C. (2007). Revisiting some estimation methods for the generalized Pareto distribution. *Journal of Hydrology*, 346(3-4):136–143.
- Ashkar, F. and Ouarda, T. B. M. J. (1996). On some methods of fitting the generalized Pareto distribution. *Journal of Hydrology*, 177(1):117–141.
- Bailey, S. F. (1996). *Basic principles and load models for the structural safety evaluation of existing road bridges*. PhD thesis, Department of Civil Engineering, École Polytechnique Fédéral de Lausanne, Lausanne, Switzerland.
- Bailey, S. F. and Bez, R. (1999). Site specific probability distribution of extreme traffic action effects. *Probabilistic Engineering Mechanics*, 14(1-2):19–26.
- Bakht, B. and Jaeger, L. G. (1983). Effect of vehicle eccentricity on longitudinal moments in bridges. *Canadian Journal of Civil Engineering*, 10(4):582–599.
- Bakht, B. and Jaeger, L. G. (1987). Multi-presence reduction factors for bridges. In *Bridge and transmission line structures*, pages 17–20, Orlando, Florida. ASCE Structures Congress.
- Basu, A., Harris, I. R., Hjort, N. L., and Jones, M. C. (1998). Robust and efficient estimation by minimising a density power divergence. *Biometrika*, 85(3):549–559.
- Ben, T. Y. and WanChun, J. (2005). Stress in orthotropic steel deck components due to vehicular loads. In *Structures Congress 2005*, pages 1–4. American Society of Civil Engineers.
- Blab, R. and Litzka, J. (1995). Measurements of the lateral distribution of heavy vehicles and its effects on the design of road pavements. In *4th International Symposium on Heavy Vehicle Weights and Dimensions*, pages 389–396.
- Bulinskaya, E. (1961). On the mean number of crossings of a level by a stationary gaussian process. *Theory of Probability & Its Applications*, 6(4):435–438.
- Butler, R. (1986). Predictive likelihood inference with applications. *Journal of the Royal Statistical Society. Series B (Methodological)*, 48(1):1–38.

Bibliography

- Caprani, C. C. (2005). *Probability analysis of highway bridge traffic loading*. PhD thesis, School of Architecture, Landscape and Civil Engineering, University College Dublin.
- Caprani, C. C., Grave, S. A., O'Brien, E. J., and O'Connor, A. J. (2002). Critical loading events for the assessment of medium span bridges. In Topping, B. H. V. and Bittnar, Z., editors, *Sixth International Conference on Computational Structures Technology*, pages 1–11, Stirling, Scotland. Civil-Comp Ltd.
- Caprani, C. C. and O'Brien, E. J. (2010). The use of predictive likelihood to estimate the distribution of extreme bridge traffic load effect. *Structural Safety*, 32(2):138–144.
- Caprani, C. C., Obrien, E. J., and McLachlan, G. J. (2008). Characteristic traffic load effects from a mixture of loading events on short to medium span bridges. *Structural Safety*, 30(5):394–404.
- Castillo, E. and Hadi, A. S. (1997). Fitting the generalized Pareto distribution to data. *Journal of American Statistical Association*, 92(440):1609–1620.
- Castillo, E., Hadi, A. S., Balakrishnan, N., and Sarabia, J. M. (2004). *Extreme Value and Related Models with Applications in Engineering and Science*. Wiley Series in Probability and Statistics. Wiley.
- Cebrian, A. C., Denuit, M., and Lambert, P. (2003). Generalized Pareto fit to the society of actuaries large claims database. *North American Actuarial Journal*, 7(3):18–36.
- Chaouche, A. and Bacro, J.-N. (2006). Statistical inference for the generalized Pareto distribution: Maximum likelihood revisited. *Communications in Statistics - Theory and Methods*, 35(5):785–802.
- Choulakian, V. and Stephens, M. A. (2001). Goodness-of-fit tests for the generalized Pareto distribution. *Technometrics*, 43(4):478–484.
- Coles, S. G. and Dixon, M. J. (1999). Likelihood-based inference for extreme value models. *EXTREMES*, 2(1):5–23.
- Connor, R., Fisher, J., Gatti, W., Gopalaratnam, V., Kozy, B., Leshko, B., McQuaid, D. L., Mdelock, R., Mertz, D., Murphy, T., Paterson, D., Sorensen, O., and Yadlosky, J. (2012). Manual for design construction and maintenance of orthotropic steel deck bridges. Technical Report FHWA-IF-12-027, HDR Engineering Inc.
- Cooper, D. I. (1997). Development of short span bridge-specific assessment live loading. In Das, P. C., editor, *The safety of bridges*, pages 64–89. Thomas Telford.
- COST 345 (2002a). Procedures required for assessing highway structures: Final report. Technical report, European Commission Directorate General Transport and Energy.

- COST 345 (2002b). Procedures required for assessing highway structures: Working group 1 report on the current stock of highway structures in european countries, the cost of their replacement and the annual costs of maintaining, replacing and renewing them. Technical report, European Commission Directorate General Transport and Energy.
- Cowan, R. J. (1975). Useful headway models. *Transportation Research*, 9(6):371–375.
- Cremona, C. (1995). Evaluation des effets extremes du trafic sur les haubans d'un pont. *Bulletin des LPC*, 199:71–80.
- Cremona, C. (2001). Optimal extrapolation of traffic load effects. *Structural Safety*, 23(1):31–46.
- Cremona, C. (2011). The surveillance of bridges in france. In *6th International Conference on Acoustical and Vibratory Surveillance Methods and Diagnostic Techniques*, pages 1–17, Paris, France.
- Cremona, C. and Carracilli, J. (1998). Evaluation of extreme traffic load effects in cable stayed and suspension bridges using wim records. In O'Brien, E. and Jacob, B., editors, *2nd European Conference on Weigh-in-motion of Road Vehicles*, pages 243–251.
- Crespo-Minguillon, C. and Casas, J. R. (1997). A comprehensive traffic load model for bridge safety checking. *Structural Safety*, 19(4):339–359.
- Cullimore, M. S. G. and Smith, J. W. (1981). Local stresses in orthotropic steel bridge decks caused by wheel loads. *Journal of Constructional Steel Research*, 1(2):17–26.
- Davison, A. C. and Smith, R. L. (1990). Models for exceedances over high thresholds. *Journal of the Royal Statistical Society. Series B (Methodological)*, 52(3):393–442.
- de Jong, F. B. P. (2004). Overview fatigue phenomenon in orthotropic bridge decks in the netherlands. In *2004 Orthotropic Bridge Conference*, pages 489–512, Sacramento, California.
- de Zea Bermudez, P. and Kotz, S. (2010). Parameter estimation of the generalized Pareto distribution-part I & II. *Journal of Statistical Planning and Inference*, 140(6):1353–1388.
- de Zea Bermudez, P. and Turkman, M. (2003). Bayesian approach to parameter estimation of the generalized Pareto distribution. *TEST*, 12(1):259–277.
- Deidda, R. (2010). A multiple threshold method for fitting the generalized Pareto distribution and a simple representation of the rainfall process. *Hydrol. Earth Syst. Sci. Discuss.*, 7(4):4957–4994. HESSD.
- Deidda, R. and Puliga, M. (2009). Performances of some parameter estimators of the generalized Pareto distribution over rounded-off samples. *Physics and Chemistry of the Earth, Parts A/B/C*, 34(10-12):626–634.
- Dempsey, A., Jacob, B., and Carracilli, J. (1998). Orthotropic bridge weigh-in-motion for determining axle and gross vehicle weights. In *2nd European conference on Weigh-in-Motion*, pages 435–444.

Bibliography

- Desrosiers, R. and Grillo, R. (1973). Estimating the frequency of multiple truck loadings on bridges: Final report. Technical report, University of Connecticut.
- Ditlevsen, O. (1994). Traffic loads on large bridges modeled as white noise fields. *Journal of Engineering Mechanics*, 120(4):681–694.
- Dupuis, D. J. (1996). Estimating the probability of obtaining nonfeasible parameter estimates of the generalized Pareto distribution. *Journal of Statistical Computation and Simulation*, 54(1-3):197–209.
- Dupuis, D. J. (1999). Exceedances over high thresholds: A guide to threshold selection. *EXTREMES*, 1(3):251–261.
- Dupuis, D. J. and Field, C. A. (1998). Robust estimation of extremes. *The Canadian Journal of Statistics / La Revue Canadienne de Statistique*, 26(2):199–215.
- Dupuis, D. J. and Tsao, M. (1998). A hybrid estimator for generalized Pareto and extreme-value distributions. *Communications in Statistics - Theory and Methods*, 27(4):925–941.
- Enright, B. (2010). *Simulation of traffic loading on highway bridges*. Doctoral thesis, School of Architecture, Landscape and Civil Engineering, University College Dublin.
- Enright, B. and O'Brien, E. J. (2011). Cleaning weigh-in-motion data: techniques and recommendations.
- Enright, B. and O'Brien, E. J. (2012). Monte carlo simulation of extreme traffic loading on short and medium span bridges. *Structure and Infrastructure Engineering*, 1:1–16.
- Eugenia Castellanos, M. and Cabras, S. (2007). A default Bayesian procedure for the generalized Pareto distribution. *Journal of Statistical Planning and Inference*, 137(2):473–483.
- European Commission (2008). *European energy and transport: trends to 2030 - updated 2007*. Luxembourg: Office for Official Publications of the European Communities, Belgium.
- European Commission (2012). *EU Transport in Figures: Statistical Pocketbook*. Luxembourg Publications Office of the European Union.
- Eymard, R. and Jacob, B. (1989). Un nouveau logiciel: le programme castor pour le calcul des actions et sollicitations du trafic dans les ouvrages routiers. *Bulletin des LPC*, pages 64–77.
- Fekpe, E. (1997). Vehicle size and weight regulations and highway infrastructure management. *Journal of Infrastructure Systems*, 3(1):10–14.
- Ferreira, A., Haan, L. d., and Peng, L. (2003). On optimising the estimation of high quantiles of a probability distribution. *Journal of Theoretical and Applied Statistics*, 37(5):401–434.
- Fisher, R. (1973). *Statistical methods and scientific inference*. Hafner Press.

- Fu, G. and van de Lindt, J. W. (2006). LRFD load calibration for state of Michigan trunkline bridges. Technical Report Report RC-1466, Wayne State University Colorado State University.
- Fu, G. and You, J. (2009). Truck loads and bridge capacity evaluation in China. *Journal of Bridge Engineering*, 14(5):327–335.
- Fu, G. and You, J. (2010). Extrapolation for future maximum load statistics. *Journal of Bridge Engineering*, 16(4):527–535.
- Fu, G., Zhuang, Y., and Feng, J. (2010). Behavior of reinforced concrete bridge decks on skewed steel superstructure under truck wheel loads. *Journal of Bridge Engineering*, 16(2):219–225.
- Getachew, A. (2003). *Traffic load effects on bridges - statistical analysis of collected and Monte Carlo simulated vehicle data*. Doctoral thesis, Department of structural engineering.
- Getachew, A. and O'Brien, E. J. (2007). Simplified site-specific traffic load models for bridge assessment. *Structure and Infrastructure Engineering*, 3(4):303–311.
- Ghosn, M. and Moses, F. (1985). Markov renewal model for maximum bridge loading. *Journal of Engineering Mechanics*, 111(9):1093–1104.
- Ghosn, M. and Moses, F. (2000). Effect of changing truck weight regulations on U.S. bridge network. *Journal of Bridge Engineering*, 5(4):304–310.
- Ghosn, M., Sivakumar, B., and Miao, F. (2012). Development of state-specific load and resistance factor rating method. *Journal of Bridge Engineering*, in print.
- Gindy, M. (2004). *Development of a reliability-based deflection limit state for steel girder bridges*. Doctoral thesis, Graduate School-New Brunswick.
- Gindy, M. and Nassif, H. H. (2006). Comparison of traffic load models based on simulation and measured data. In *Joint International Conference on Computing and Decision Making in Civil and Building Engineering*.
- Gindy, M. and Nassif, H. H. (2007). Multiple presence statistics for bridge live load based on weigh-in-motion data. *Transportation Research Record: Journal of the Transportation Research Board*, pages 125–135.
- Gomes, F. (2012). *Influence du revêtement sur le comportement en fatigue des dalles orthotropes: étude d'une solution en BFUP*. Phd thesis, École doctorale sciences ingénierie et environnement, Université Paris-Est.
- Grave, S., O'Brien, E. J., and O'Connor, A. J. (2000). The determination of site-specific imposed traffic loadings on existing bridges. In Ryall, M. J., Parke, G., and Harding, J. E., editors, *Bridge management 4 - inspection, maintenance, assessment and repair*, pages 442–449. Thomas Telford Limited.

Bibliography

- Greenwood, J. A., Landwehr, J. M., Matalas, N. C., and Wallis, J. R. (1979). Probability weighted moments: Definition and relation to parameters of several distributions expressible in inverse form. *Water Resour. Res.*, 15(5):1049–1054.
- Grimshaw, S. D. (1993). Computing maximum likelihood estimates for the generalized Pareto distribution. *Technometrics*, 35(2):185–191.
- Guo, T., Frangopol, D., Han, D., and Chen, Y. (2011). Probabilistic assessment of deteriorating prestressed concrete box-girder bridges under increased vehicle loads and aggressive environment. *Journal of Performance of Constructed Facilities*, 25(6):564–576.
- Harman, D. J. and Davenport, A. G. (1979). A statistical approach to traffic loading on highway bridges. *Canadian Journal of Civil Engineering*, 6(4):494–513.
- He, X. and Fung, W. K. (1999). Method of medians for lifetime data with weibull models. *Statistics in Medicine*, 18(15):1993–2009.
- Hewitt, J., Stephens, J., Smith, K., and Menuet, N. (1999). Infrastructure and economic impacts of changes in truck weight regulations in Montana. *Transportation Research Record: Journal of the Transportation Research Board*, 1653(1):42–51.
- Holmes, J. D. and Moriarty, W. W. (1999). Application of the generalized Pareto distribution to extreme value analysis in wind engineering. *Journal of Wind Engineering and Industrial Aerodynamics*, 83(13):1–10.
- Hosking, J. R. M. (1990). L-Moments: Analysis and estimation of distributions using linear combinations of order statistics. *Journal of the Royal Statistical Society. Series B (Methodological)*, 52(1):105–124.
- Hosking, J. R. M. and Wallis, J. R. (1987). Parameter and quantile estimation for the generalized Pareto distribution. *Technometrics*, 29(3).
- Huang, C., Lin, J.-G., and Ren, Y.-Y. (2012). Statistical inferences for generalized Pareto distribution based on interior penalty function algorithm and Bootstrap methods and applications in analyzing stock data. *Computational Economics*, 39(2):173–193.
- Huo, X., Wasserman, E., and Iqbal, R. (2005). Simplified method for calculating lateral distribution factors for live load shear. *Journal of Bridge Engineering*, 10(5):544–554.
- Husler, J., Li, D., and Raschke, M. (2011). Estimation for the generalized Pareto distribution using maximum likelihood and goodness of fit. *Communications in Statistics - Theory and Methods*, 40(14):2500–2510.
- Hyndman, R. J. and Koehler, A. B. (2006). Another look at measures of forecast accuracy. *International Journal of Forecasting*, 22(4):679–688.

- Iman, R. L. and Conover, W. J. (1982). A distribution-free approach to inducing rank correlation among input variables. *Communications in Statistics - Simulation and Computation*, 11(3):311–334.
- Ito, K. (1963). The expected number of zeros of continuous stationary gaussian processes. *Journal of Mathematics of Kyoto University*, 3(2):207–216.
- Ivanov, V. (1960). On the average number of crossings of a level by the sample functions of a stochastic process. *Theory of Probability & Its Applications*, 5(3):319–323.
- Jacob, B. (1991). Methods for the prediction of extreme vehicular loads and load effects. Technical report, LCPC.
- Jacob, B. (2000). Assessment of the accuracy and classification of weigh-in-motion systems part 1: Statistical background. *International Journal of Heavy Vehicle Systems*, 7(2):136–152.
- Jacob, B., Bouteldja, M., and Stanczyk, D. (2008). Installation and experimentation of MS-WIM systems with three strip sensor technologies - early results. In Jacob, B., editor, *5th International Conference on Weigh-In-Motion*, pages 149–158.
- Jacob, B., Hannachi, H., and Ieng, S. (2010). *Bridge weigh-in-motion on steel orthotropic decks - Millau viaduct and Autreville bridge*, pages 209–209. Bridge Maintenance, Safety and Management. CRC Press.
- Jacob, B., O’Brien, E. J., and Newton, W. (2000). Assessment of the accuracy and classification of weigh-in-motion systems: Part 2. european specification. *Heavy Vehicle Systems*, 7(2-3):153–168.
- James, G. (2003). *Analysis of Traffic Load Effects on Railway Bridge*. PhD thesis, Structural Engineering Division.
- Jenkinson, A. F. (1955). The frequency distribution of the annual maximum (or minimum) values of meteorological elements. *Quarterly Journal of the Royal Meteorological Society*, 81(348):158–171.
- Ji, B., Chen, D., Ma, L., Jiang, Z., Shi, G., Lv, L., Xu, H., and Zhang, X. (2011). Research on stress spectrum of steel decks in suspension bridge considering measured traffic flow. *Journal of Performance of Constructed Facilities*, 26(1):65–75.
- Juárez, S. F. and Schucany, W. R. (2004). Robust and efficient estimation for the generalized Pareto distribution. *EXTREMES*, 7:237–251.
- Klein, E., Stanczyk, D., and Ieng, S.-S. (2012). Improvement of weigh-in-motion accuracy by taking into account vehicle lateral position. In Jacob, B., editor, *Interation Conference on Weigh-in-Motion, ICWIM6*, pages 206–213.

Bibliography

- Kolstein, M. H. (2007). *Fatigue classification of welded Jjoints in orthotropic steel bridge decks*. Doctoral thesis, Faculty of Civil Engineering and Geosciences, Delft University of Technology.
- Koubi, B. and Schmidt, F. (2009). LCPC-Pollux.
- Kozikowski, M. (2009). *WIM based live load model for bridge reliability*. Doctoral, Graduate College.
- Kwon, O., Kim, E., and Orton, S. (2011a). Calibration of live-load factor in LRFD bridge design specifications based on state-specific traffic environments. *Journal of Bridge Engineering*, 16(6):812–819.
- Kwon, O.-S., Kim, E., Orton, S., Salim, H., and Hazlet, T. (2011b). Calibration of the live load factors in LRFR design guidelines. Technical report, Missouri Transportation Institute and Missouri Department of Transportation.
- Leadbetter, R. M., Lindgren, G., and Rootzen, H. (1983). *Extremes and related properties of random sequences and processes*. Springer-Verlag, New York Heidelberg Berlin.
- L'Ecuyer, P., Simard, R., Chen, E. J., and Kelton, W. D. (2002). An object-oriented random-number package with many long streams and substreams. *Operations Research*, 50(6):1073–1075.
- Leutzbach, W. (1972). *Introduction to the theory of traffic flow*. Springer-Verlag, New York.
- Luceno, A. (2006). Fitting the generalized Pareto distribution to data using maximum goodness-of-fit estimators. *Computational Statistics & Data Analysis*, 51(2):904–917.
- Ludescher, H. and Brühwiler, E. (2008). Dynamic amplification of traffic loads on road bridges. *Structural Engineering International*, 19(2):190–197.
- Ma, R., Zeng, Y., and Chen, A.-r. (2008). *Maintenance strategies for large span suspension bridges against fatigue and corrosion*, pages 513–518. CRC Press.
- Mackay, E. B. L., Challenor, P. G., and Bahaj, A. S. (2011). A comparison of estimators for the generalized Pareto distribution. *Ocean Engineering*, 38(11-12):1338–1346.
- Maes, M. A. (1995). Tail heaviness in structural reliability. In *International Conference on Applications of Statistics and Probability*, pages 997–1002.
- Mathiasen, P. E. (1979). Prediction functions. *Scandinavian Journal of Statistics*, 6(1):1–21.
- Meshgi, A. and Khalili, D. (2009). Comprehensive evaluation of regional flood frequency analysis by L- and LH-moments. II. development of lh-moments parameters for the generalized Pareto and generalized logistic distributions. *Stochastic Environmental Research and Risk Assessment*, 23(1):137–152.

- Messervey, T. B., Frangopol, D. M., and Casciati, S. (2010). Application of the statistics of extremes to the reliability assessment and performance prediction of monitored highway bridges. *Structure and Infrastructure Engineering*, 7(1-2):87–99.
- Miao, T. J. and Chan, T. H. T. (2002). Bridge live load models from WIM data. *Engineering Structures*, 24(8):1071–1084.
- Moharram, S. H., Gosain, A. K., and Kapoor, P. N. (1993). A comparative study for the estimators of the generalized Pareto distribution. *Journal of Hydrology*, 150(1):169–185.
- Nowak, A. S. (1993). Live load model for highway bridges. *Structural Safety*, 13:53–66.
- Nowak, A. S. and Hong, Y.-K. (1991). Bridge live-load models. *Journal of Structural Engineering*, 117(9):2757–2767.
- Nowak, A. S., Nassif, H., and DeFrain, L. (1993). Effect of truck loads on bridges. *Journal of Transportation Engineering*, 119(6):853–867.
- O'Brien, E. and Caprani, C. C. (2005). Headway modelling for traffic load assessment of short to medium span bridges. *The Structural Engineer*, 86(16):33–36.
- O'Brien, E., Enright, B., and Caprani, C. (2008). Implications of future heavier trucks for Europe bridges. In Znidaric, A., editor, *Transport Research Arena Europe*. Slovenia National Building and Civil Engineering Institute.
- O'Brien, E., Enright, B., and Getachew, A. (2010). Importance of the tail in truck weight modeling for bridge assessment. *Journal of Bridge Engineering*, 15(2):210–213.
- O'Brien, E. J., Caprani, C. C., and O'Connell, G. J. (2006). Bridge assessment loading: a comparison of west and central/east europe. *Bridge Structures*, 2(1):25–33.
- O'Brien, E. J., Caprani, C. C., Znidaric, C. C., and Quilligan, M. (2003). Site-specific probabilistic bridge load assessment. In *Third International Conference on Current and Future Trends in Bridge Design, Construction and Maintenance*, pages 341–348. Thomas Telford Limited.
- O'Brien, E. J. and Enright, B. (2013). Using weigh-in-motion data to determine aggressiveness of traffic for bridge loading. *Journal of Bridge Engineering*, 18(3):232–239.
- O'Brien, E. J., Sloan, D. T., Bulter, K. M., and Kirkpatrick, J. (1995). Traffic load 'fingerprinting' of bridges for assessment purposes. *The Structural Engineer*, 73(19):320–324.
- O'Brien, E. J., Znidaric, A., Brady, K., González, A., and O'Connor, A. (2005). Procedures for the assessment of highway structures. *Proceedings of the ICE - Transport*, 158:17–25.
- O'Connor, A. and Eichinger, E. M. (2007). Site-specific traffic load modelling for bridge assessment.
- O'Connor, A. and Enevoldsen, I. (2008). Probability based modelling and assessment of an existing post-tensioned concrete slab bridge. *Engineering Structures*, 30(5):1408–1416.

Bibliography

- O'Connor, A., Jacob, B., O'Brien, E., and Prat, M. (1998). Report of studies on performed on the normal load model, LM1, ENV 1991-3 Traffic Loads on Bridges. Technical report, LCPC.
- O'Connor, A., Jacob, B., O'Brien, E., and Prat, M. (2001). Report of current studies performed on normal load model of EC1. *Revue Francaise de Génie Civil*, 5(4):411–433.
- O'Connor, A. and O'Brien, E. J. (2005). Traffic load modelling and factors influencing the accuracy of predicted extremes. *Canadian Journal of Civil Engineering*, 32(1):270–278.
- O'Connor, A. J. (2001). *Probabilistic traffic load modelling for highway bridges*. Doctoral, Department of Civil Engineering.
- Pelphrey, J. and Higgins, C. (2006). Calibration of LRFR live load factors for Oregon stated-owned bridges using weigh-in-motion data. Technical report, Department of Civil Engineering, Oregon State University.
- Pelphrey, J., Higgins, C., Sivakumar, B., Groff, R., Hartman, B., Charbonneau, J., Rooper, J., and Johnson, B. (2008). State-specific LRFR live load factors using weigh-in-motion data. *Journal of Bridge Engineering*, 13(4):339–350.
- Peng, L. and Welsh, A. H. (2001). Robust estimation of the generalized Pareto distribution. *EXTREMES*, 4(1):53–65.
- Pfeil, M. S., Battista, R. C., and Mergulhao, A. J. R. (2005). Stress concentration in steel bridge orthotropic decks. *Journal of Constructional Steel Research*, 61(8):1172–1184.
- Pickands III, J. (1975). Statistical inference using extreme order statistics. *The Annals of Statistics*, 3(1):119–131.
- Pisarenko, V. F. and Sornette, D. (2003). Characterization of the frequency of extreme earthquake events by the generalized Pareto distribution. *Pure and Applied Geophysics*, 160(12):2343–2364.
- Prem, H., Austroads, Gleeson, B., ARRB Transport Research, George, R., Fletcher, C., and Ramsay, E. (1999). *Estimation of lane width requirements for heavy vehicles on straight paths*. ARRB Transport Research.
- Rasmussen, P. F. (2001). Generalized probability weighted moments: Application to the generalized Pareto distribution. *Water Resour. Res.*, 37(6):1745–1751.
- Reiss, R. D. and Thomas, M. (2007). *Statistical analysis of extreme values - with Applications to Insurance, Finance, Hydrology and Others Fields*. Birkhauser, Boston.
- Rice, S. O. (1944). Mathematical analysis of random noise. *Bell Systems technical Journal*, 23:282–332.
- Rice, S. O. (1945). Mathematical analysis of random noise. *Bell Systems technical Journal*, 24:46–156.

- Scarrott, C. and MacDonald, A. (2012). A review of extreme value threshold estimation and uncertainty quantification. *REVSTAT - Statistical Journal*, 10(1):33–60.
- Sedlacek, G., Merzenich, G., Paschen, M., Bruls, A., Sanpaolesi, L., Croce, P., Calgaro, J. A., Pratt, M., Jacob, B., Leendertz, M., Boer, V. d., Vrouwenfelder, A., and Hanswille, G. (2006). Background document to EN 1991 - Part 2 - Traffic loads for road bridges - and consequences for the design. Technical report.
- Siebert, D., Estivin, M., Billo, J., Barin, E., and Toutlemonde, F. (2008). Extreme effects of the traffic loads on a prestressed concrete bridge. In Jacob, B., editor, *10th International Conference on Heavy Vehicle*, pages 379–387, Paris, France.
- Sim, H. and Uang, C. (2012). Stress analyses and parametric study on full-scale fatigue tests of rib-to-deck welded joints in steel orthotropic decks. *Journal of Bridge Engineering*, 17(5):765–773.
- Singh, V. P. and Ahmad, M. (2004). A comparative evaluation of the estimators of the three-parameter generalized Pareto distribution. *Journal of Statistical Computation and Simulation*, 74(2):91–106.
- Sivakumar, B. and Ghosn, M. (2009). Collecting and using weigh-in-motion data in LRFD bridge design. *Bridge Structures*, 5(4):151–158.
- Sivakumar, B., Ghosn, M., Moses, E., and TranSystems Corporation (2011). Protocols for collecting and using traffic data in bridge design. National Cooperative Highway Research Program (NCHRP) Report 683, Lichtenstein Consulting Engineers, Inc., Washington, D. C.
- Smith, R. (1984). *Threshold methods for sample extremes*, volume 131, chapter NATO Adv. Sci. Inst. Ser. C Math. Phys. Sci., pages 621–638. Reidel.
- Todorovic, P. and Zelenhasic, E. (1970). A stochastic model for flood analysis. *Water Resour. Res.*, 6(6):1641–1648.
- Treacy, M. A. and Bruhwiler, E. (2012). A monitoring system for determination of real deck slab behaviour in prestressed box girder bridges.
- Troitsky, S. and Foundation, J. F. L. A. W. (1987). *Orthotropic bridges theory and design*. James F. Lincoln Arc Welding Foundation.
- Tsakopoulos, P. and Fisher, J. (2003). Full-scale fatigue tests of steel orthotropic decks for the Williamsburg bridge. *Journal of Bridge Engineering*, 8(5):323–333.
- van de Lindt, J., Fu, G., Zhou, Y., and Pablo, R. (2005). Locality of truck loads and adequacy of bridge design load. *Journal of Bridge Engineering*, 10(5):622–629.
- van de Lindt, J. W., Fu, G., Pablo, R. M., and Zhou, Y. (2002). Investigation of the adequacy of current design loads in the state of Michigan. Technical Report Report RC-1143, Michigan Technological University Wayne State University.

Bibliography

- Victoria-Feser, M.-P. and Ronchetti, E. (1994). Robust methods for personal-income distribution models. *The Canadian Journal of Statistics / La Revue Canadienne de Statistique*, 22(2):247–258.
- Villasenor-Alva, J. A. and Gonzalez-Estrada, E. (2009). A bootstrap goodness of fit test for the generalized Pareto distribution. *Computational Statistics & Data Analysis*, 53(11):3835–3841.
- von Mises, R. (1936). La distribution de la plus grande de n valeurs. *Revue de l'Union Interbalkanique*, 1:1–20.
- Wang, Q. J. (1997). LH moments for statistical analysis of extreme events. *Water Resour. Res.*, 33(12):2841–2848.
- Wang, T., Liu, C., Huang, D., and Shahawy, M. (2005). Truck loading and fatigue damage analysis for girder bridges based on weigh-in-motion data. *Journal of Bridge Engineering*, 10(1):12–20.
- Xiao, Z.-G., Yamada, K., Inoue, J., and Yamaguchi, K. (2006). Fatigue cracks in longitudinal ribs of steel orthotropic deck. *International Journal of Fatigue*, 28(4):409–416.
- Xiao, Z.-G., Yamada, K., Ya, S., and Zhao, X.-L. (2008). Stress analyses and fatigue evaluation of rib-to-deck joints in steel orthotropic decks. *International Journal of Fatigue*, 30(8):1387–1397.
- Ya, S., Yamada, K., and Ishikawa, T. (2010). Fatigue evaluation of rib-to-deck welded joints of orthotropic steel bridge deck. *Journal of Bridge Engineering*, 16(4):492–499.
- Ylvisaker, N. D. (1965). The expected number of zeros of a stationary gaussian processes. *Annals of Mathematical Statistics*, 36(3):1043–1046.
- Zanuy, C., Maya, L. F., Albajar, L., and de la Fuente, P. (2011). Transverse fatigue behaviour of lightly reinforced concrete bridge decks. *Engineering Structures*, 33(10):2839–2849.
- Zhang, J. (2007). Likelihood moment estimation for the generalized Pareto distribution. *Australian & New Zealand Journal of Statistics*, 49(1):69–77.
- Zhou, X. Y., Schmidt, F., and Jacob, B. (2012). Assessing confidence intervals of extreme traffic loads. In Jacob, B., McDonnell, A.-M., Schmidt, F., and Cunagin, W., editors, *6th International Conference on Weigh-in-Motion, ICWIM6*, pages 400–410. IFSTTAR.

A Weigh-in-Motion Data and its Statistical Analysis

A.1 WIM data

This work includes five sets of Weigh-in-Motion (WIM) data collected very recent years between 2009 and 2011 at four sites - Saint Jean de Vedas (SJDV), Loisy, Vienne and Maulan, on three motorways and one highway - A9, A31, A9 and RN4, respectively, in France. The locations and measured periods are shown in Figure A.1. An overview of the data is given in Table A.1. The WIM data are used to develop a model for simulating truck loading on highway bridges.

In SJDV, there are WIM sensors in the three lanes of the 6-lane highway, and data were col-

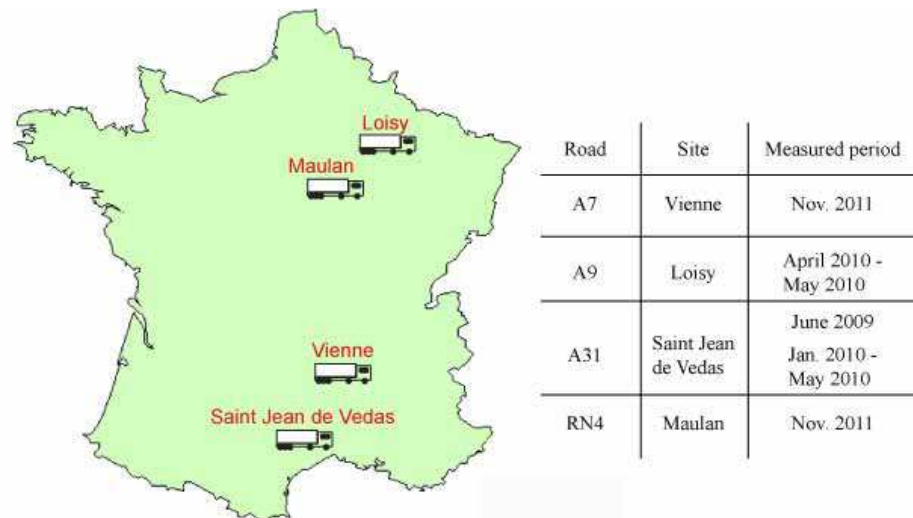


Figure A.1: The measurement locations and periods

lected during two periods. A total number of 841 609 trucks weighing 3.5 t or more with time stamps recorded with a precision of 0.01 second were recorded from 1st January to 31st May,

Appendix A. Weigh-in-Motion Data and its Statistical Analysis

Table A.1: Overview of WIM data

	St Jean de Vedas		Loisy	Vienne	Maulan
Road No.	A9		A31	A7	RN4
No. of lanes	2 × 3		2 × 2	2 × 3	2 × 2
Type of sensor	Piezoceramics		Piezoceramics	Piezoceramics	Piezoquartz
Measurement period	2010 Jan. - 2010 May	2009 Jun.	2010 Apr. - 2010 May	2011 Nov.	2011 Nov.
No. of days	138	28	61	30	30
No. of equipped lanes with WIM systems	3	2	2	3	1
No. of vehicles	841 609	841 786	273 190	180 252	73 010
The statistics below are based on cleaned data.					
No. of vehicles	757 969	144 579	263 328	149 930	64 546
No. of vehicles (Slow lane)	676 630	131 484	257 254	147 222	64 546
Average daily flow (Slow lane)	4903	4696	4217	4907	2152
Max. GVW (t)	74	73.9	90.3	86.9	99.9
Average GVW (t)	27.5	26.9	25.1	27.0	27.4
Average Speed (km/h)	89	89	86	82	86
Max. No. of axles	8	8	8	8	8
No. vehicles over 40t	46 638	8 391	21 987	9 140	4 709
No. vehicles over 44t	3 308	743	2 298	1 055	358
No. vehicles over 60t	96	29	26	44	10

2010. And another set of data was provided for truck traffic in the two outer lanes, and a total of 841 786 vehicles weighing from 0.6 t were recorded in June, 2009, no measurements were provided for the fast lane.

In Loisy, there are WIM sensors in the two lanes of the 4-lane motorway. Data were recorded for truck traffic in these two lanes for the 61 days period from 1st April to 31st May, 2010. A total of 273 190 trucks weighing 3.5 t or more with time stamps recorded with a precision of 0.01 seconds.

In Vienne, there are WIM sensors in the three lanes of the 6-lane motorway. Data were recorded for truck traffic in these three lanes in Novembre 2011. A total of 180 252 trucks weighing 3.5 t or more were recorded with a precision of 0.01 seconds.

In Maulan, there are WIM sensors in the slow lane of the 4-lane highway. Data were provide for truck traffic in the lane for Novembre 2011. A total of 73 010 trucks weighing 3.5 t or more with time stamps recorded to a precision of 0.01 seconds.

A.2 Cleaning Unreliable WIM Data

Although weigh-in-motion techniques have significantly advanced in this decade, the recorded data still include some unreliable observations due to the roughness of pavement where the

WIM system is located, the environment, the unstability of WIM system and etc. Therefore it is important to examine the WIM data to remove unreliable data containing unlikely trucks to ensure that only quality data is used to model traffic load Enright and O'Brien [2011]; Sivakumar et al. [2011]. WIM data cleaning rules have been recommended by Enright and O'Brien [2011]; Sivakumar et al. [2011]. However, the feature of traffic data, the type of WIM system are different from country to country. In this thesis, some modifications are made on these two recommended rules with respect to the French WIM data. The cleaning techniques used in this thesis are listed in Table A.2 and compared with others [Enright and O'Brien, 2011; Getachew, 2003; Sivakumar et al., 2011].

A.3 Statistical Description of WIM Data

A.3.1 Traffic composition

A common rule to define the class of truck is the number of axles [Caprani, 2005; Enright and O'Brien, 2012]. Although this classification is very efficient in use, it may not be reasonable. For truck with same number of axles, the loading capacity is different between rigid connection truck and articulate connection ones, and also the load distribution is different. Therefore they lead to various aggressions to bridge structure or components especially those are sensitive to axle load. A more refined classification was applied in some studies [Bailey, 1996; O'Connor and O'Brien, 2005]. Coupling with French WIM data, a further subclassification of trucks has been used in this thesis as given in Figure A.2. The trucks were firstly classified by their number of axles in a traditional way, the composition is shown in Figure A.3. Then the data were further classified by axle configurations, and the classification is given in Table A.3.

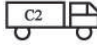
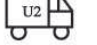
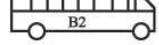

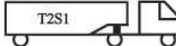


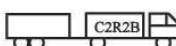
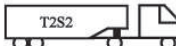






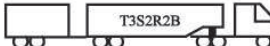
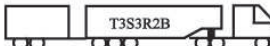
2-axle	 	
3-axle		  
4-axle		 
5-axle		  
6-axle		
7-axle		
8-axle		

Figure A.2: Truck classification

Table A.2: Comparison of data cleaning rules

Getachew [2003]	Enright and O'Brien [2011]	Sivakumar et al. [2011]	This thesis
Accept one axle vehicles with length less than 12 m	At least 2 axles; and no upper limitation	Total number of axles less than 3 or greater than 12	Exclude vehicles with less than 2 axles; and the observed maximum number of axle is 8.
–	Exclude if speed below 20 to 60 km/h varies with site.	Speed below 16 km/h	Clean if speed below 40 km/h
–	Exclude if speed above 120 km/h.	Speed above 160 km/h	Clean if speed above 120 km/h
–	-	Truck length greater than 36 m	Truck length greater than 30 m and GVW greater than 20 t
–	Exclude if sum of axle spacing greater than length of truck	Sum of axle spacing greater than length of truck	Sum of axle spacing greater than length of truck or less than 65% of truck length
–	Exclude if sum of the axle weights differs from the GVW by more than 0.05t	Sum of the axle weights differs from the GVW by more than 10%	Exclude if the sum of axle weights differs from the GVW by more than 10%
–	GVW less than 3.5 t are excluded	GVW less than 5.4 t	–
–	Vehicles with individual axle greater than 40 t are excluded.	Individual axle weight greater than 32 t	Exclude vehicles if the proportion of axle weight is greater than 85% of GVW
–	–	Steer axle greater than 11.3 t	–
–	–	Steer axle less than 2.7 t	–
Exclude if distance between the first axle and last axle is less than 3 meters for four axle vehicles	–	First axle spacing less than 1.5 m	–
Any axle spacing less than 1 m for five or more axle vehicles	Any axle spacing less than 0.4 m	Any axle spacing less than 1 m	–
–	–	Any individual axle less than 1 t	Keep only vehicles with axle weight greater than 0.6 t
–	–	–	Exclude if lateral position outside the notional lane

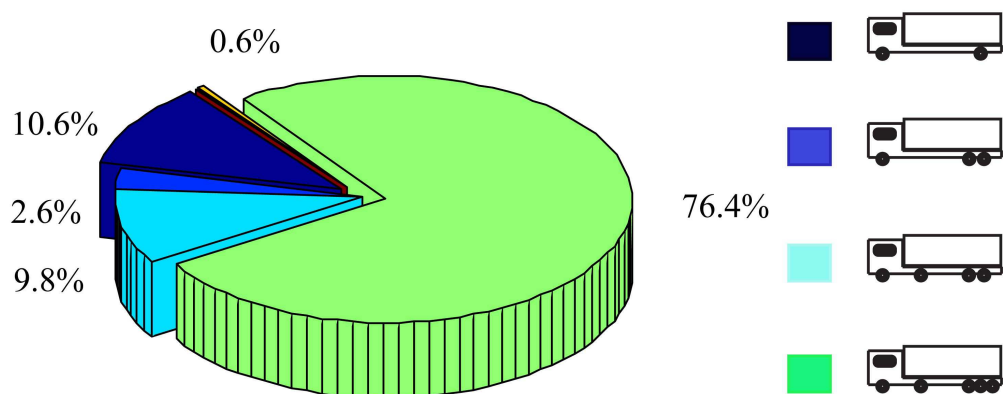


Figure A.3: Traffic composition

Table A.3: Classification of truck and traffic composition

Class		Subclass			
2-axle	Category	C2	B2	U2	
	Percentage	60	22	18	
3-axle	Category	C3B	T2S1	B3	U2R1
	Percentage	41	16	24	19
4-axle	Category	T2S2	C2R2B	U2R2	
	Percentage	65	31	4	
5-axle	Category	T2S3	C2R3B	C3BR2A, C3BR2B	
	Percentage	95	2	3	
6-axle	Category	T2S2R2B			
	Percentage	100			
7-axle	Category	T3S2R2B			
	Percentage	100			
8-axle	Category	T3S3R2B	T3S3R2A		
	Percentage	93	7		

A.3.2 Flow Rate

Truck traffic has evident variation, the hourly average truck flow for traffic at Saint Jean de Vedas is calculated and shown in Figure A.4. It can be found that the fast lane and the slow one have similar variation during the day, it indicates that the hourly average truck flow reaches its highest level between 10 am and 15 pm.

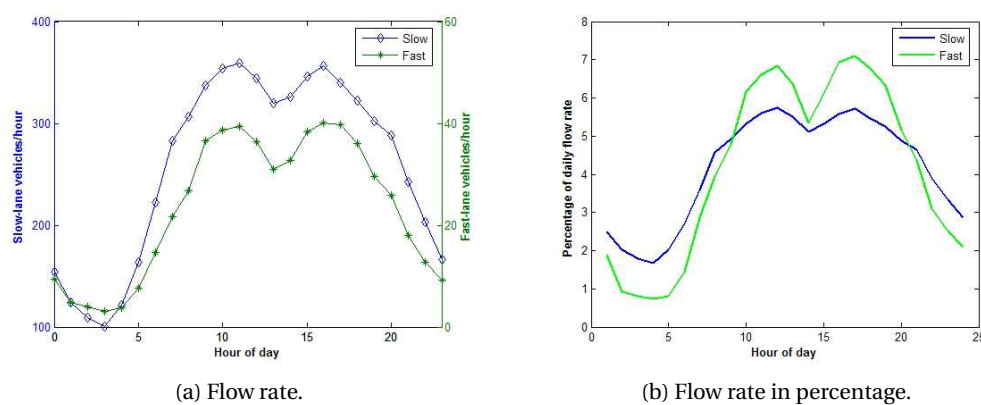


Figure A.4: Flow rate and percentage

A.3.3 Gross vehicle weight

Many models for GVW have been used by authors. Bailey [1996] has used a Beta distribution to model the weights of axle groups (tandems and tridem) and has built up the GVW from this. Crespo-Minguillon and Casas [1997] use the measured empirical distribution as the basis for performing simulation. Enright and O'Brien [2012] has used a semi-parametric approach to model GVW. For GVWs up to a certain value, an empirical bivariate distribution, which is a function of GVW and number of axles, is used to fit the data. Above the threshold, GVW is modeled by a bivariate normal distribution. Caprani [2005] has used bimodal or trimodal normal distribution to model the GVW of each truck class.

In this thesis, we have adopted uni-, bi- and tri-modal normal distributions to model GVW of each subclass. It is found that the range of GVW is quite different for various subclass of vehicle, even if they have the same number of axles. Figures A.5 to A.8 illustrate the GVW distribution fitting for traffic data collected at Saint Jean de Vedas.

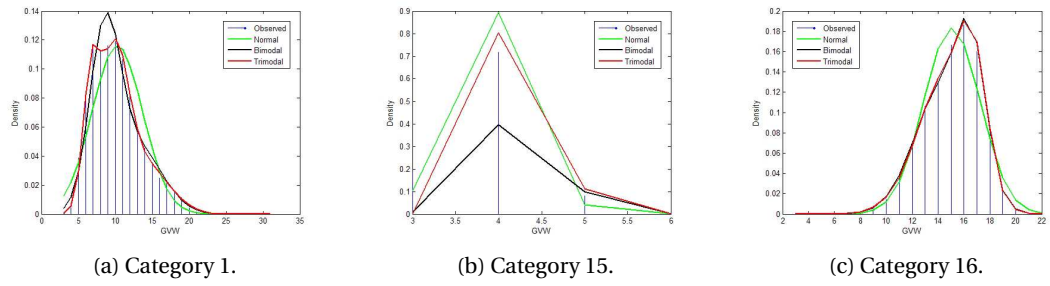


Figure A.5: GVW histogram and fitting for 2-axle trucks

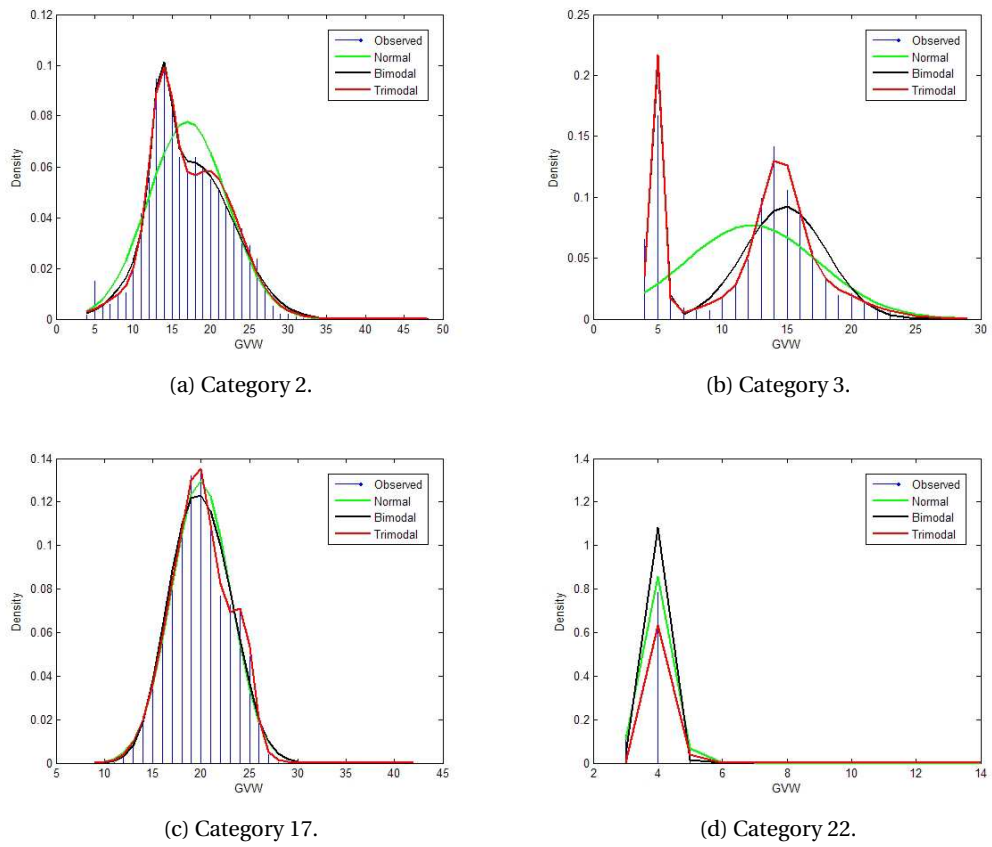


Figure A.6: GVW histogram and fitting for 3-axle trucks

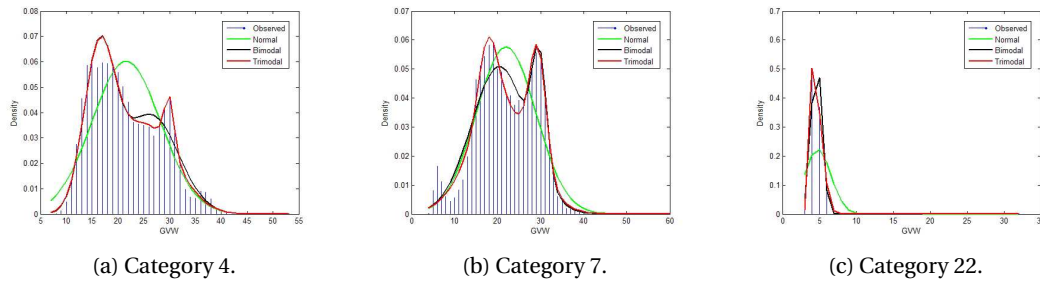


Figure A.7: GVW histogram and fitting for 4-axle truck

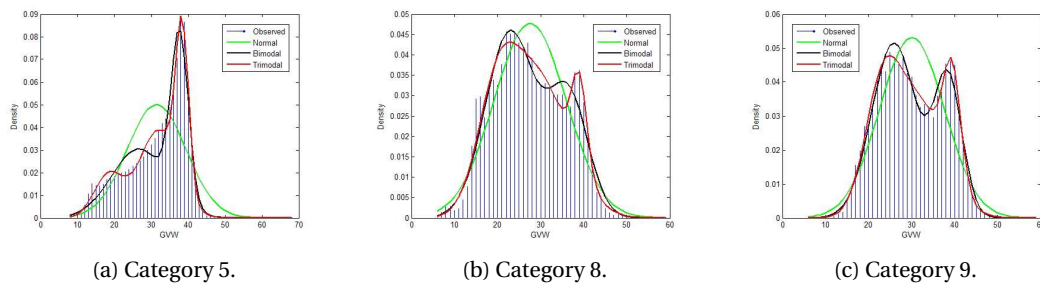


Figure A.8: GVW histogram and fitting for 5-axle trucks

A.3.4 Axle Loads

For short- to medium span bridges, the axle loads are particularly important. Various methods have been proposed in the literature to model the axle loads. Caprani [2005]; O'Brien et al. [2006] have used a mixture of Normal, bimodal Normal and trimodal Normal distributions to each class of truck. Enright and O'Brien [2012] have used a bimodal Normal distribution. Bailey [1996] has used a bimodal Beta distribution for axle groups, and normal distribution for single axles. As the multi-modal Normal distribution is extensively used to model axle wght. In this study, the percentage of the GVW carried by each axle is modelled using uni-, bi- and tri-modal normal distributions. Sample distributions are shown in Figure A.9 for category 5 of 5-axle trucks.

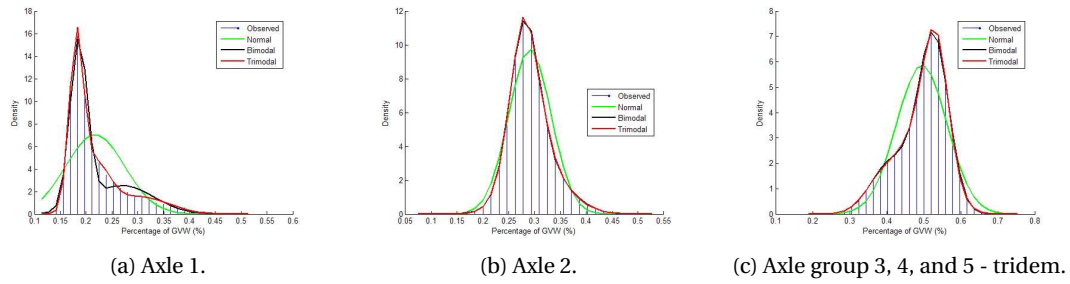


Figure A.9: Percentage of GVW carried by each axle for 5-axle trucks, category 5

A.3.5 Axle Spacing

As the axle loads, the axle spacing is vital important to short- to medium span bridge. Particular attention have been paid on modeling axle spacing in the literature. For axle spacing, each vehicle class is modeled seperatedly. Caprani [2005] have used bi- or tri-modal Normal distributions to model the measurements. Bailey [1996] have used Beta distributions to model the distance between axle groups and the front and rear vehicle overhangs. Enright and O'Brien [2012] have proposed to focus on the maximum axle spacing for each vehicle. For each vehilce measured, all axle spacings are ranked in descending order, starting with the maximum. Then an empirical distribution is used to model the maximum axle spacing for each vehicle class, and trimodal Normal distributions are used to model other spacings. Simultaneously, the authors have modeled the position of each of the ranked spacings on the vehicle by using empirical distributions for all spacings in each axle class. In this study, it is not necessary to rank the axle spacings to find the maximum axle spacing for each vehicle as the vehicles are classified by their silhouutte as given in Figure A.2. For each vehicle class, the axle spacings are almost constant value corresponding to their positions on the vehcile as the histograms of axle spacing always has very sharp shape, which indicates a small standard deviation, see for example in Figure A.10. Uni- bi- or trimodal Normal distributions are used to model the measured axle spacing for eahc vehicle class.

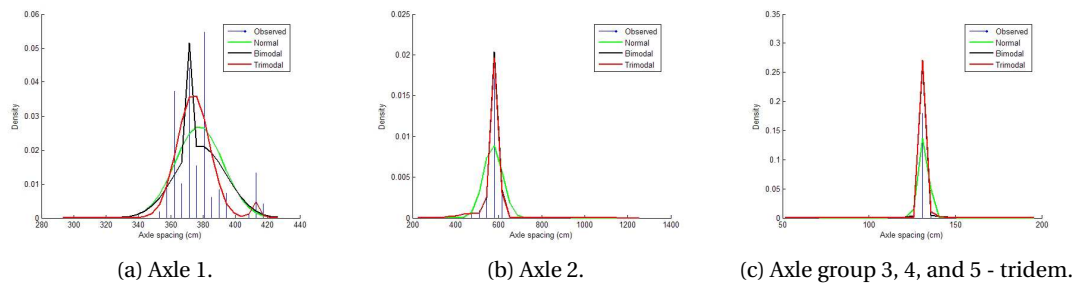


Figure A.10: Percentage of GVW carried by each axle for 5-axle trucks, category 5

A.3.6 Headway Distribution

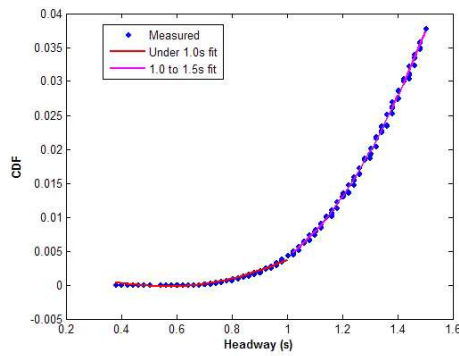
Headway is a measurement of the distance or time between successive vehicles, it is an important factor to describe traffic flow. A lot of investigations and studies have been carried out about the headway distribution. Most of distribution formulae are derived from probability statistics. These formulae can be categorized into two classes. One is under the assumption of free traffic flow, the other is developed for congest traffic flow. For short- to medium span bridge, the free flowing is deemed to be the governing traffic condition [Bakht and Jaeger, 1987]. Especial focus have been given on two trucks following or side-by-side situations in many studies [Nowak and Hong, 1991; Nowak et al., 1993] during the development of AASHTO. According to the scope of this thesis, the free flowing traffic is concerned. The most used model is that assuming the arrival of vehicles is Poisson process, and the corresponding time interval between two successive arrivals are exponential distribution Leutzbach [1972]. The Poisson and exponential distribution are valid only when traffic flows are light. Moreover, the headway can be zero if the exponential distribution is used, which in practice is impossible. Therefore, a shifted exponential distribution has been proposed by Cowan [1975] with a minimum time interval between successive vehicles. Bailey [1996] has used the shifted exponential distribution to describe the free flowing traffic with a minimum headway of 0.25 s.

Although the shifted exponential distribution model considers the traffic more reasonable, it still can not fit the heavy traffic flow well. Vehicles need frequently adjust their speeds to that of a vehicle in front in heavy traffic situation, Leutzbach [1972] has found that the Erlang distribution can describe the headway in heavy traffic. Other models like using Pearson type III distribution, log-normal distribution are also used to model heavy traffic.

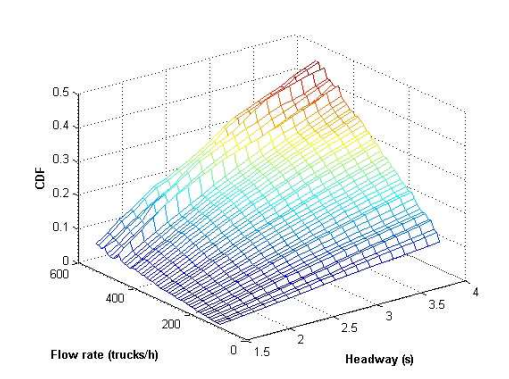
For a given traffic, the density of traffic is mixture as shown in Figure A.4. The traffic is heavy between 10 h to 20 h, and the traffic is light in other time. A mixture model can therefore describe the traffic more accurately. Basing their measurements of five days WIM data from Auxerre in France, O'Brien and Caprani [2005] have proposed a mixture model, which consists of a flow dependent sub-model and a flow independent sub-model, to describe headway distribution. For headways of less than 1.5 seconds, a flow independent model has been used. For headways greater than 1.5 seconds, a flow dependent model has been proposed, but two sub-models have been considered. For headways between 1.5 and 4 seconds, the first is used to describe headways greater than 1.5 seconds and the other is used to describe headways greater than 4 seconds. Enright and O'Brien [2012] has used the model proposed by O'Brien and Caprani [2005] in similar manner but with two modifications. One is to use gap instead of headway to eliminate the influence of vehicle length on headway. The gap is the time between the rear axle of the front truck and the front axle of the following truck. The other is to allow for different gap distributions for different flow rates at very small gaps like less than 1.0 second.

In this thesis, we also adopt the model described by O'Brien and Caprani [2005] to model headways used for single-lane traffic in each direction, and the headway is same as the gap used by Enright and O'Brien [2012]. Measurements from Saint Jean de Vedas is used to

illustrate the modeling processing. The cumulative distribution probability of headways less than 1.5 seconds are plotted in Figure A.11a. The measured distribution is fitted with two quadratic equations, one for less than 1 second, and another between 1 and 1.5 seconds. For measured headways between 1.5 and 4 seconds, they are categorized by hourly flow in intervals of 10 trucks/h. The resulting cumulative distribution functions are illustrated in Figure A.11b. A quadratic equation is fitted to each grouped data with respect to average hourly flow. For headways greater than 4 seconds, an average hourly flow based shifted exponential distribution is used.



(a) Less than 1.5 s.



(b) Between 1.5 s and 4 s.

Figure A.11: Cumulative distribution function for headway

B Bridge Traffic Load Effect Calculation and Simulation Program

B.1 Introduction

This appendix presents the function and use of the bridge traffic load effect calculation and simulation (BTLECS) program developed as part of this research. The model for traffic load effect is based on a program named CASTOR developed by Eymard and Jacob [1989] and updated by Koubi and Schmidt [2009] under the name LCPC-Pollux. The CASTOR software was written in FORTRAN, and it is a procedural oriented programming, which is not easy to be extended to carry out traffic load effect extreme value analysis by using block maxima method or peaks over threshold approach. Furthermore, the CASTOR or LCPC-POLLUX software can only be used to calculate traffic load effects by using collected traffic data like from WIM, but it is impossible to conduct a Monte Carlo Simulation to extend the available traffic files. Therefore, the new program, BTLECS, was developed, the program is object-orientated and was written in C++ language.

B.2 Program Description

B.2.1 Algorithm for Traffic Load Effect Calculation

Using influence surfaces, $S(x, y)$, or lines $L(x, y)$ to calculate the load effect at a certain point (x, y) is an extensively way in the purpose of bridge design and assessment. The influence surface can be decomposed into longitudinal influence line $L(x)$ and transversal influence line $T(y)$ as:

$$S(x, y) = L(x) \cdot T(y) \quad (\text{B.1})$$

$$T(x, y) = \frac{1}{2} (S(x, y - e) + S(x, y + e)) \quad (\text{B.2})$$

Appendix B. Bridge Traffic Load Effect Calculation and Simulation Program

For calculating load effect induced by the passage of vehicles, the leading vehicle is assumed to move in a time step Δt . At each step, the program counts the number of vehicles, N , which is the total number of vehicles currently on the bridge. Then the load effect induced by these N vehicles can be obtained by using:

$$X_n = \sum_{j=1}^N C(y_j) \sum_{k=1}^{s(j)} P_{(j,k)} L_{i(j)} [V_j(t_n - t_j) - d_{(j,k)}] \quad (\text{B.3})$$

N : number of vehicle,
 j : index of j th vehicle,
 y_j : transversal location of j th vehicle,
 V_j : speed of j th vehicle,
 t_j : time that the first axle of j th vehicle passes over the position $x = 0$,
 $i(j)$: number of lane of j th vehicle,
 $s(j)$: number of axles of j th vehicle,
 $P_{(j,k)}$: axle load of k th of j th vehicle,
 $d_{(j,k)}$: distance between steering axle to k th axle of j th vehicle.

In each step of the calculation, we assume that the involved vehicles keep constant speed and lateral position during the time interval Δt . The process of the calculation is to carry out a N times loop for the vehicles currently on the bridge. The loop starts from the leading vehicle to the N^{th} vehicle. The information of number of axles $s(j)$, axle loads $P_{(j,k)}$, axle spacings $d_{(j,k)}$, and speed V_j associated to the j^{th} vehicle are used to obtain: (i) the longitudinal position of each axle $x(j, k)$ that is used to determine the value on influence line, (ii) the contribution to total load effect. The influence line can be obtained by theoretical analysis (see Figure B.1a) or measurement (see Figure B.1b). At the end of each step, the program needs to judge whether the leading vehicle is still on the bridge or not. If it exits the bridge then it will be eliminated and another vehicle will be appointed to be the leading vehicle. This process is carried out until all the input vehicles from WIM data or generated by Monte Carlo simulation crossing over the bridge be considered.

B.2.2 Flowchart

The flowchart in Figure B.2 shows the various modules of the simulation program, which are described below.

Module of generation The program provides two options to input traffic data. One is read from a file, and another is generated by Monte Carlo simulation.

If the traffic data input mode is read from an existing file, the file should be prepared in a certain format as shown in the Table B.1. An example of the input of traffic data is given in Figure B.3.

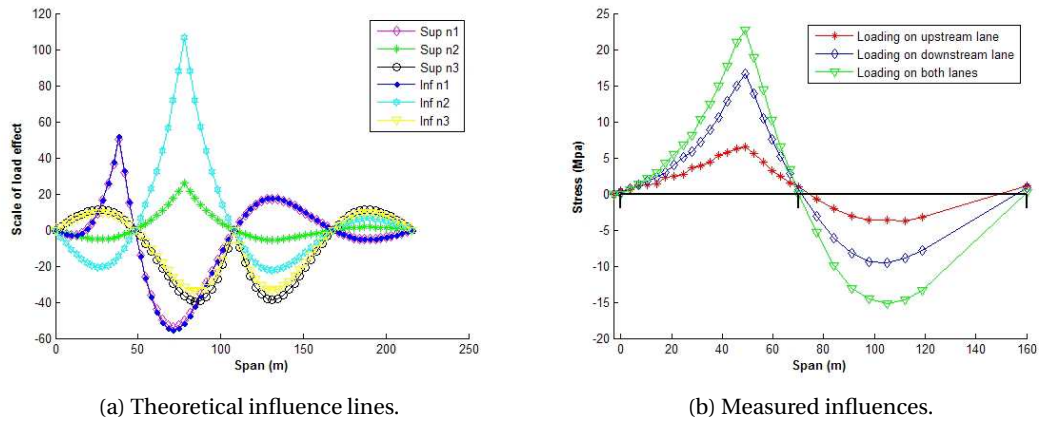


Figure B.1: Influence lines.

Table B.1: Traffic data file format

Description	Unit	Format
Order		I7
Head		I4
Lane		I1
Day		I2
Month		I2
Year		I4
Week		I1
Hour		I2
Minute		I2
Second		I2
Second/100		I2
Speed	km/h	I3
Gross Vehicle Weight - GVW	dt	I4
Length	dm	I3
Number of axles		I2
Category of vehicle		I2
Transverse deviation in lane	cm	I3
Width of vehicle	cm	I3
Bumper	cm	I3
Type of axle		I10
Load - axle 1	dt	I3
Spacing - axle 1 - axle 2	cm	I4
Load - axle 2	dt	I3
⋮	⋮	⋮
Load - axle $n - 1$	dt	I3
Spacing - axle $n - 1$ - axle n	cm	I4
Load - axle n	dt	I3

Appendix B. Bridge Traffic Load Effect Calculation and Simulation Program

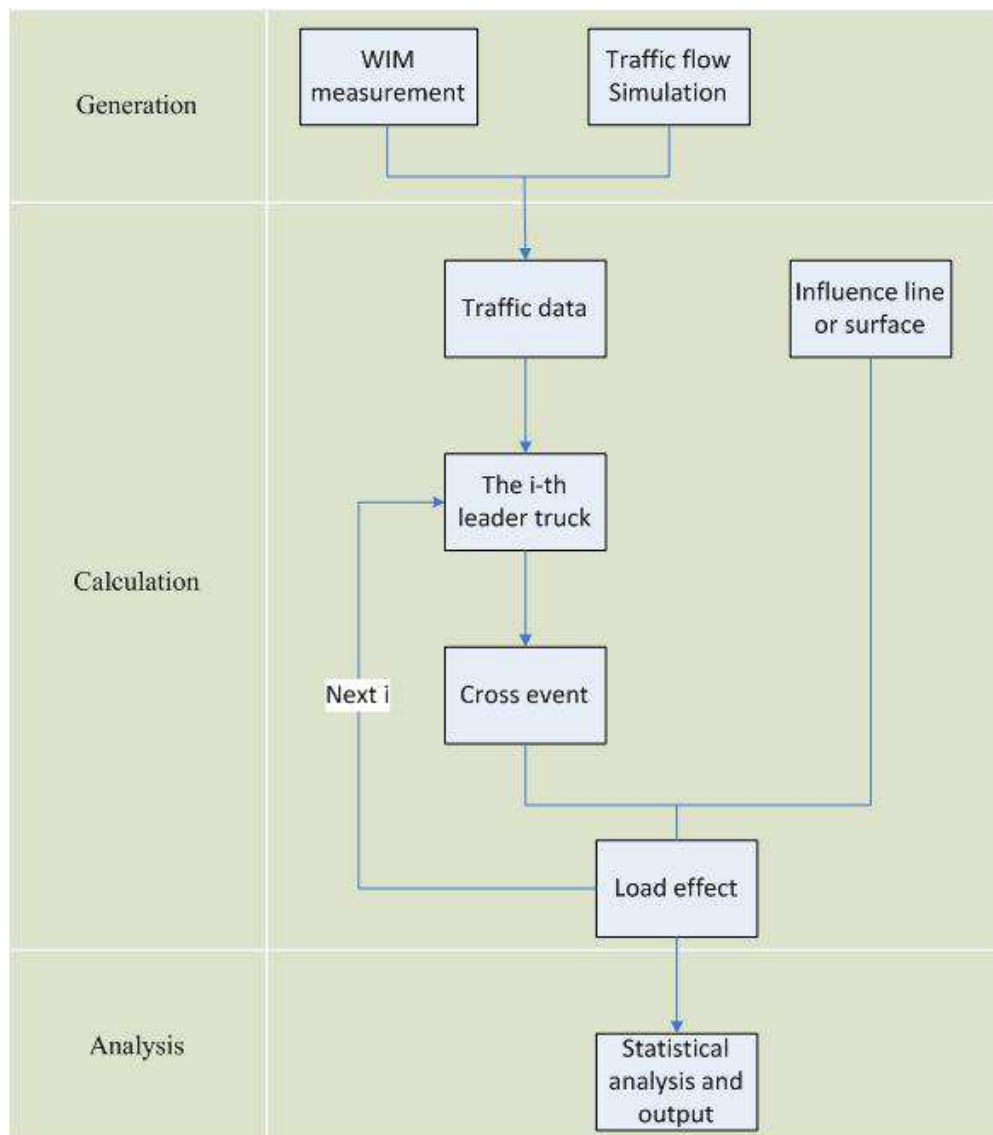


Figure B.2: Flowchart of BTLECS Program

```

0000001200020501201030000071209003131690505001220408500000153330690361092060305101320520132051
0000002200020501201030000286008902581720505000720609200000153330600362074060304001310420131045
0000003200020501201030000295408902821710505101821108900000153330600362077061304901320510132046
0000004200020501201030000335408902141670505102120206700000153330550372058058703301310350131034
0000005200010501201030000373608903611700505000519908600000153330660372099058406401310650133068
000000620001050120103000050340900149146040410212090770000001522054038104405730250132026
0000007200020501201030001075808902841640505105420009400000153330710371093058404101340390131042
0000008200020501201030001135808901721350505101321505500000153330550414047042902301310240134024
000000920002050120103000137440930299207040700062000850000001122065054110808330590137068
  
```

Figure B.3: Sample of input traffic data file

If the traffic data is assigned to be generated by MC simulation, and the program activates the module of MC simulation. To carry out the simulation, basic information on the traffic is required. It includes the information on traffic namely traffic composition, flow rate and headway, and the information of vehicles of axle load, axle spacing, gross vehicle weight and speed. These traffic information files should be prepared according to the specific format. Details on the input files for performing Monte Carlo simulation of traffic flow are given in Section B.3. The programs generate traffic day by day until the required number of days is achieved. The random number is produced by the random number generator provided by L'Ecuyer et al. [2002]. The simulation procedure is as follows:

- For each day, the program firstly generates a number for daily traffic volume according to the input statistical distribution of traffic volume, then the hourly traffic volume can automatically be obtained with the input flow rate information.
- Secondly, the program combines the assigned hourly traffic volume with the input headway model to generate the traffic flow that gives arrival time to each vehicle.
- Thirdly, the feature of each vehicle is assigned by using the information of traffic composition, axle load, axle spacing, gross vehicle weight and speed.

Module of calculation Each randomly generated daily traffic is superimposed on structures of interest. Effects are thus calculated combining the loads and positions of vehicle stored in the traffic flow with the given influence function (line or surface). Traffic is stepped over a bridge by incrementing the vehicle positions, the traffic flow is stepped as a function of the speed of vehicles. When an vehicle is stepped off the influence line or surface being considered, it is deleted from the traffic flow, and a new vehicle is assigned to be leading vehicle.

Module of statistical analysis At the end of each crossing event, the load effect time history during this crossing event is passed to the statistical analysis module to obtain statistics of interest. The statistics includes histogram of value, histogram of level crossing counting, histogram of rainflow cycle counting, block maxima and peaks over threshold. Details on these statistics are presented in Section B.4.

Module of output results At the end of the simulation of the defined number of days the statistics of calculated traffic load effects are written to files. These statistics are output in tables. Samples of the results are given in Section B.4.

B.3 Traffic Files

B.3.1 Traffic Composition and Flow

The files of traffic composition hold the data of percentage of trucks in each class that is named by number of axles, and for percentage of trucks in each subclass that is grouped by their silhouette mainly the types of connection that is rigid or articular. An example is given and explained in Table B.2.

Table B.2: Traffic composition input file

Class	Percentage	Subclass			
		1	2	3	4
2-axle	10.57	0.6288	0.2127	0.1586	0
3-axle	2.64	0.4284	0.1618	0.2258	0.1839
4-axle	9.82	0.6544	0.3064	0.0392	0
5-axle	76.35	0.9547	0.0189	0.0264	0
6-axle	0.55	0.4935	0.5065	0	0
7-axle	0.05	1	0	0	0
8-axle	0.01	0.0889	0.9111	0	0

The file for flow rate holds the average number of trucks, for the hour under consideration, for each lane. An example is given in Table B.3.

Table B.3: Flow rate input file

Time	0	1	2	3	4	5
Slow lane	148.7	121	105.1	96.5	116.4	154.6
Fast lane	9.1	4.6	3.6	2.9	3.5	7.1
Time	6	7	8	9	10	11
Slow lane	209	264.9	288.8	317.3	335.5	339.9
Fast lane	13.4	20.2	24.9	34.5	36.1	37
Time	12	13	14	15	16	17
Slow lane	328.3	304.5	312.4	328.2	338	325.3
Fast lane	34.3	29.5	31.1	36.1	37.6	37.8
Time	18	19	20	21	22	23
Slow lane	309.8	288.3	272.7	228.8	191.6	161.9
Fast lane	34.6	27.9	24.4	16.8	12	9.1

B.3.2 Axle Spacing

This file stores the axle spacing data for all classes of trucks measured on the site. As described, the axle spacings are modeled by uni- or multi-modal normal distribution, therefore there are three parameters required for each of the modes: the weight, the mean, and the standard

deviation. An example for 2-axle is given in Table B.4.

Table B.4: Axle spacing input file for 2-axle truck

Mode	Category 1			Category 2			Category 3		
	Mean	Std	Weight	Mean	Std	Weight	Mean	Std	Weight
Mode 1	386	39	0.1965	382	42	0.8027	591	10	0.1601
Mode 2	508	59	0.5246	407	4	0.1973	614	10	0.5925
Mode 3	624	37	0.2790	-	-	-	683	11	0.2473

B.3.3 Axle Weight

In order to avoid the summation of generated axle weights greater than the gross vehicle weight, here the axle weight is presented as a ratio of the gross vehicle weight. Axle weight data may be fitted by a mix of a number of Normal distributions; that is, the data may be multi-modally normally distributed. There are three parameters required for each of the modes: the weight, the mean and the standard deviation. The maximum number of modes allowed in the program is three; hence the 3×3 tabular format of the data. An example is given in Table B.5.

Table B.5: Axle weight input file for 2-axle truck

Axle	Mode	Category 1			Category 2			Category 3		
		Mean	Std	Weight	Mean	Std	Weight	Mean	Std	Weight
1 st	Mode 1	0.6987	0.0267	0.029	0.4363	0.054	1	0.3639	0.0254	1
	Mode 2	0.4321	0.0649	0.971	-	-	-	-	-	-
	Mode 3	-	-	-	-	-	-	-	-	-
2 nd	Mode 1	0.3045	0.0266	0.0289	0.5695	0.0541	1	0.6378	0.0254	1
	Mode 2	0.5706	0.0649	0.9711	-	-	-	-	-	-
	Mode 3	-	-	-	-	-	-	-	-	-

B.3.4 Gross Vehicle Weight

The file contains the parameters of the distributions that characterize the GVW for each class of trucks. Again the distribution of GVW is assumed to be a multimodal normal distribution, and an example is given in Table B.6.

Table B.6: GVW input file for 2-axle truck

Mode	Category 1			Category 2			Category 3		
	Mean	Std	Weight	Mean	Std	Weight	Mean	Std	Weight
Mode 1	6.73	1.11	0.2363	3.91	0.44	1	14.31	2.17	0.6708
Mode 2	9.89	1.85	0.4749	-	-	-	16.61	1.11	0.3292
Mode 3	13.83	3.34	0.2888	-	-	-	-	-	-

Appendix B. Bridge Traffic Load Effect Calculation and Simulation Program

B.3.5 Headway

The headway model proposed by O'Brien and Caprani [2005] is adopted here. This model includes three parts, the first two are represented by 2nd ordered polynomes that are independent on flowrate or traffic volume, and the third part is assumed to be a flow rate dependent 2nd order polynomial function. An example is given in Table B.7, in which Line 1 indicates the number of flow dependent headway models. Line 2 and 3 give the parameters of the quadratic-fit headway CDF for under 1.0 s and between 1.0 s and 1.5 s respectively. The following lines return the parameters of the quadratic fit to the headway CDF for that flow of the first column.

Table B.7: Headway

49	0	0	0				
0	0.020977	-0.023663	0.0064589				
0	0.074462	-0.11972	0.049445				
76.494	-0.005048	0.03664	-0.03753	326.49	-0.0088234	0.14493	-0.15758
86.494	-0.003435	0.03725	-0.04142	336.49	-0.0098058	0.15188	-0.16346
96.494	-0.001821	0.037858	-0.045312	346.49	-0.012647	0.17339	-0.18853
106.49	-0.00020793	0.038469	-0.049201	356.49	-0.011238	0.16607	-0.17909
116.49	0.00014333	0.038854	-0.050425	366.49	-0.012221	0.17531	-0.18756
126.49	0.00071673	0.043011	-0.054727	376.49	-0.012819	0.18111	-0.19447
136.49	0.0019588	0.035748	-0.045866	386.49	-0.013319	0.18528	-0.1951
146.49	-0.0024351	0.064459	-0.077179	396.49	-0.013467	0.18543	-0.19307
156.49	-0.0037983	0.072362	-0.08712	406.49	-0.011538	0.17933	-0.18754
166.49	-0.002969	0.068716	-0.081166	416.49	-0.015111	0.20076	-0.21707
176.49	-0.0035484	0.075985	-0.091239	426.49	-0.012236	0.18559	-0.19269
186.49	-0.0024476	0.074726	-0.088546	436.49	-0.013004	0.19368	-0.20524
196.49	-0.0031514	0.084054	-0.098513	446.49	-0.013614	0.19991	-0.20832
206.49	-0.0026836	0.081375	-0.095341	456.49	-0.027381	0.27029	-0.25708
216.49	-0.001686	0.077476	-0.088758	466.49	-0.018902	0.23881	-0.26091
226.49	-0.00087772	0.07778	-0.090408	476.49	-0.017222	0.22718	-0.24762
236.49	-0.0061718	0.10843	-0.1256	486.49	-0.022359	0.2607	-0.28449
246.49	-0.0032954	0.096443	-0.11098	496.49	-0.039003	0.34888	-0.37748
256.49	-0.0063687	0.11365	-0.12688	506.49	-0.02307	0.28119	-0.30551
266.49	-0.0077585	0.1234	-0.1387	516.49	-0.018633	0.23902	-0.24853
276.49	-0.0074835	0.12469	-0.13685	526.49	-0.016264	0.23547	-0.23677
286.49	-0.009353	0.13932	-0.15657	536.49	-0.016264	0.23547	-0.23677
296.49	-0.0068702	0.12611	-0.14018	546.49	-0.016264	0.23547	-0.23677
306.49	-0.0091684	0.14265	-0.16066	556.49	-0.016264	0.23547	-0.23677
316.49	-0.0095783	0.14991	-0.16679				

B.4 Output

B.4.1 Time History File

Full time history files present all information of the calculated load effects, they include the information of the leading trucks like position on the bridge, number of involved trucks for inducing the load effect, and the value of load effect. Due to the numerous information which are included, it is an extremely large file for a long run simulation. Although the full time history is not used very often in bridge traffic load effect analysis, it is necessary to be generated to check the program.

In the program, the full time history file can be generated when the specific option is selected, and the program creates a single file named: *01_TotEff.txt*. A sample is given:

Line	No. trucks	No. invovled trucks	Time (second)	Effect (kN.m)
1	0	1	89.21	801.408
2	0	1	89.31	565.968
3	0	1	89.41	401.396
4	0	1	89.51	268.961
5	0	1	89.61	136.526
6	0	1	89.71	62.2444
7	0	1	89.81	4.4145
8	0	1	89.91	0
9	1	1	232.14	0
10	1	1	232.24	79.4201
11	1	1	232.34	218.24
12	1	1	232.44	422.124
13	1	1	232.54	630.669
14	1	1	232.64	937.44
15	1	1	232.74	1342.44
16	1	1	232.84	1749.02

The format is:

- Column 1: The order of leading truck;
- Column 2: The number of trucks currently on the bridge;
- Column 3: The current time counted from the arrival of the first truck;
- Column 4: The value of the load effect induced by the truck configuration on the bridge.

An example output is given showing the number of trucks on the bridge and the corresponding value of load effects. As can be seen, the main loading event is a single truck whilst 2-truck event occurs.

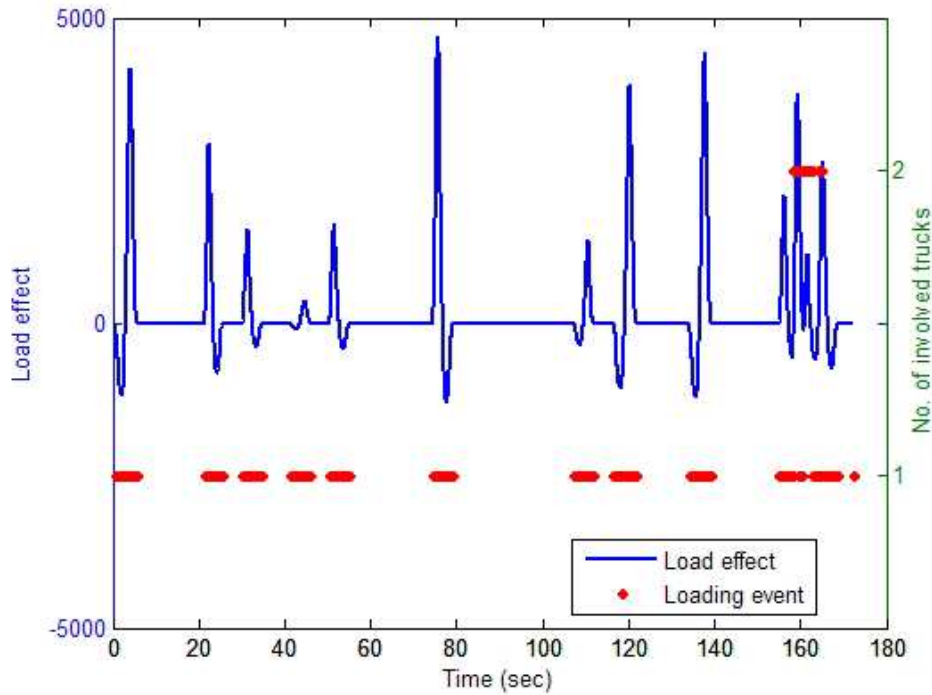


Figure B.4: Full time history

B.4.2 Histograms of Value, Level Crossing, Rainflow Cycle Counting

During the calculation process, several useful statistics, including histogram of values, histogram of level crossing and histogram of rainflow cycle counting of the load effects can be produced simultaneously if the corresponding options are activated.

These three types of histograms have a common requirement that the bin value or number of bins should be determined before conducting calculation. In the CASTOR and LCPC-Pollux, the minimum and maximum are needed to input for all in table two. However, it is impossible to know the exact minimum and maximum before the calculation, therefore the inputs of minimum and maximum are problematic. In BTLECS, the minimum V_{min} and maximum V_{max} are given by an automatic procedure. Before implementing the calculation, a two days of traffic is used to get the 2-days minimum and maximum, and the possible minimum and maximum for the simulation period are estimated on the basis of pre-calculated 2-days values such as multiplying by a factor like 2.

After knowing the minimum V_{min} and maximum V_{max} , another important issue to construct histograms is to determine the number of bins N_b or the bin width h . There is no optimal number of bins, and different bin sizes can reveal different features of the data. Some suggestions have been proposed to determine an optimal number of bins, but almost all of them are based on known the total data, which is impossible during the calculation process, such as Sturge's

formula suggests that the optimal number of bins for a sample of n data is $N_b = \log_2 n + 1$. In this program, we propose to set the bin size as large as possible such as 200, because it is possible to merge like two bins to one when the amount of data is large, but it will be problematic if we want to decompose one bin to two bins if the pre-set bin size has been taken too small. The bin width is thus:

$$\Delta h = \frac{V_{max} - V_{min}}{N_b} \quad (B.4)$$

Histogram of value

For arbitrary E_n , it can be classified to the i^{th} according to

$$i = \text{int} \left(\frac{X_n - V_{min}}{\Delta h} \right) \quad (B.5)$$

as $X_n \in [V_{min} + i \cdot \Delta h, V_{min} + (i + 1) \cdot \Delta h]$. An example of histogram of values is given in Figure B.7.

Histogram of Rainflow cycle counting

In fatigue applications it is generally agreed that the shape of the curve connecting two intermediate local extremes in the load is of no importance, and that only the values of the local maximum and minima of the load sequence influence the life time. A load process can thus, for fatigue applications, be characterized by its sequence of local extremes, also called turning points. For the load effect process X_t with a finite number of local extremes occurring at the time time points t_1, t_2, \dots . For simplicity, we assume that the first local extreme is a minimum, then we can denoted the sequence of turning points by

$$TP(\{X_t\}) = \{X_{t_1}, X_{t_2}, X_{t_3}, X_{t_4}, X_{t_5}, \dots\} = \{m_0, M_0, m_1, M_1, m_2, M_2, \dots\}$$

where m_k denotes a minimum and M_k a maximum, see Figure B.5.

A rainflow cycle is defined as (see also Figure B.6): Let $X(t)$, $0 \leq t \leq T$, be a function with finitely many local maxima of height M_k occuring at times t_k . For the k^{th} maxima at time t_k define the following left and right minima

$$\begin{aligned} m_k^- &= \inf\{X(t) : t_k^- < t < t_k\} \\ m_k^+ &= \inf\{X(t) : t_k < t < t_k^+\} \end{aligned}$$

where

$$t_k^- = \begin{cases} \sup\{t \in [0, t_k] : X(t) > X(t_k)\}, & \text{if } X(t) > X(t_k) \text{ for some } t \in [0, t_k], \\ 0 & \text{otherwise,} \end{cases}$$

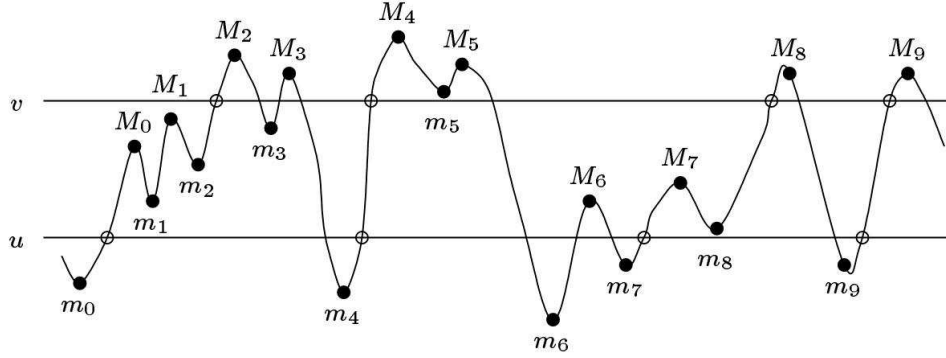


Figure B.5: The local minima and maxima (marked by dots) for a stochastic process.

$$t_k^+ = \begin{cases} \inf\{t \in [t_k, T] : X(t) \geq X(t_k)\}, & \text{if } X(t) > X(t_k) \text{ for some } t \in [t_k, T], \\ T & \text{otherwise.} \end{cases}$$

Then, the k^{th} rainflow cycle is defined as (m_k^{rfc}, M_k) , where

$$m_k^{rfc} = \begin{cases} \max(m_k^-, m_k^+), & \text{if } t_k^+ < T, \\ m_k^- & \text{if } t_k^+ = T. \end{cases}$$

The three typical statistics in fatigue applications are therefore defined as:

$$\begin{aligned} \text{amplitude} &= (M_k - m_k^{rfc})/2 \\ \text{range} &= M_k - m_k^{rfc} \\ \text{mean} &= (M_k + m_k^{rfc})/2 \end{aligned}$$

see also Figure B.6. From these definitions and the rainflow counting algorithm, a histogram

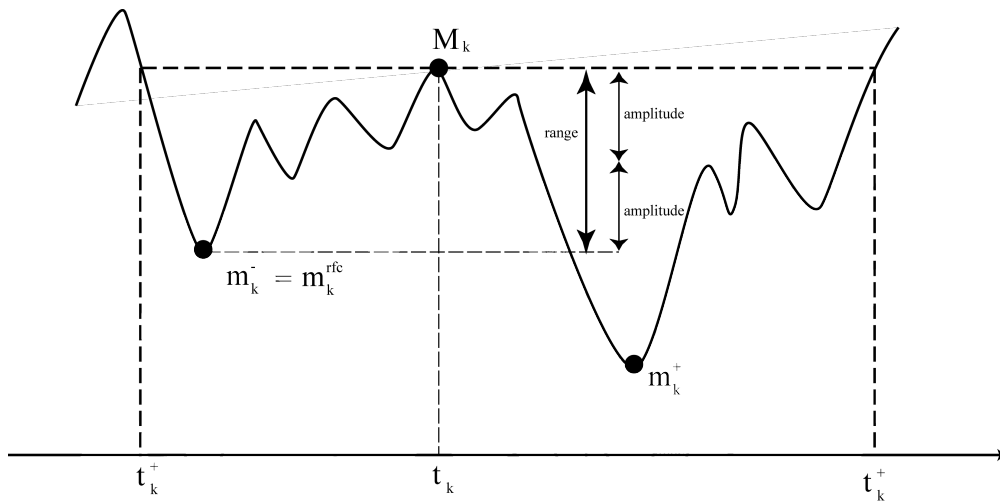


Figure B.6: The definition of rainflow cycle

of rainflow cycles generated is shown in Figure B.9.

Histogram of level crossing counting

The definition and details of level crossing is given in Section 1.2.3. An example of histogram for level crossing counting is given in Figure B.8.

Example

An example of output file for these histogram is given:

Line	Bin value	Level crossing	No.	Rainflow
1	0	50866	152582	155
2	49.0705	51423	62132	77
3	98.141	51866	43396	114
4	147.212	52172	36957	103.5
5	196.282	52402	39518	128
6	245.353	52621	37109	203.5
7	294.423	52741	33216	948
8	343.494	51972	29193	621.5
9	392.564	51503	29037	270.5
10	441.635	51490	28286	219
11	490.705	51473	26288	271.5
12	539.776	51391	24683	292.5
13	588.846	51300	23528	351
14	637.917	51182	22605	361
15	686.987	51001	21700	342.5
16	736.058	50818	20618	407
17	785.128	50593	19788	419
18	834.199	50329	19496	499
19	883.269	49995	19265	532
20	932.34	49595	18537	570
21	981.41	49166	18360	631.5
22	1030.48	48675	18207	689
23	1079.55	48081	18044	780.5
24	1128.62	47396	17644	856
25	1177.69	46609	17050	893.5

B.4.3 Block Maximum Vehicle Files

Two types of block maximum can be obtained from this program. One is the traditional daily maximum that is taken out of the full data regardless of the type of loading events, and another type of daily maximum is drawn with respect to the type of loading event that is classified by

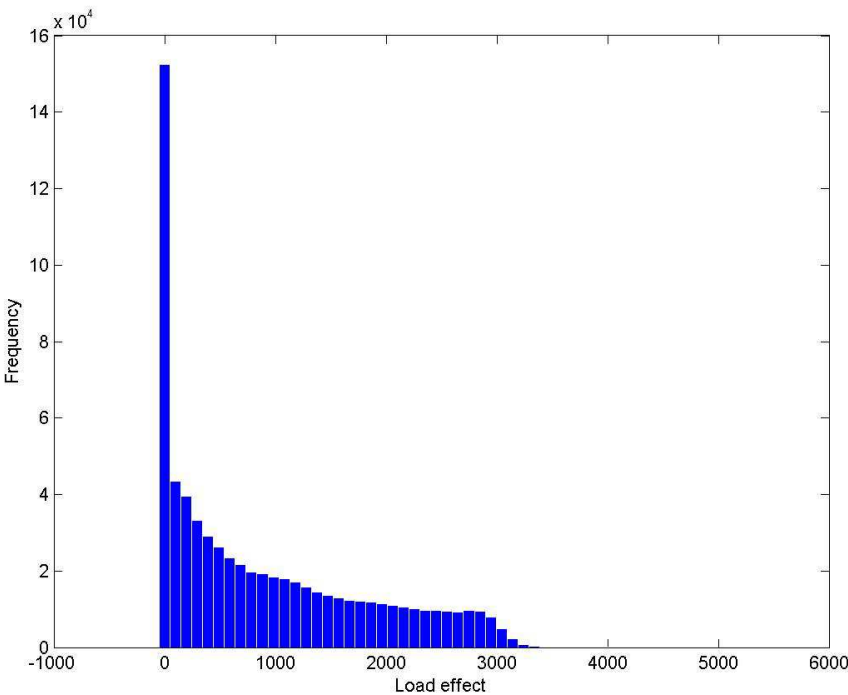


Figure B.7: Standard histogram

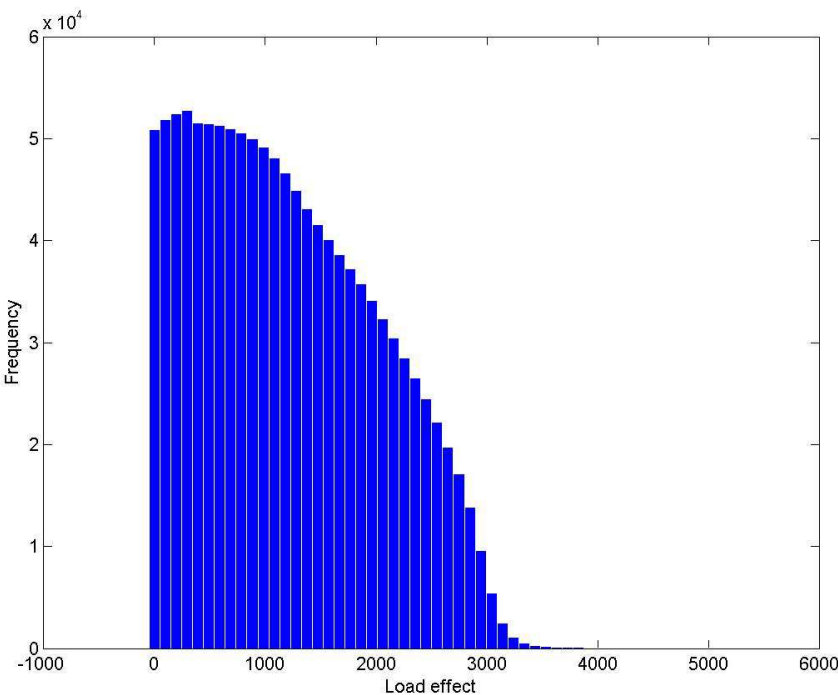


Figure B.8: Level up-crossing histogram

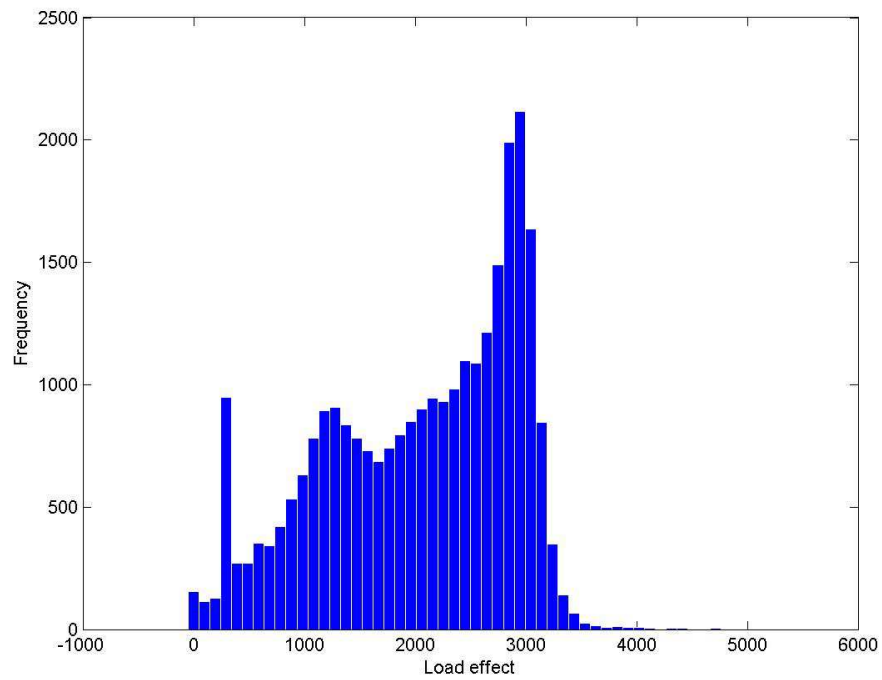


Figure B.9: Rainflow cycle counting histogram

the number of involved trucks. Sample output files are given, and a sample of the Gumbel probability paper for the block maxima is presented in Figure B.10.

	No. involved trucks	Time	Position	Effect (kN.m)
Day 1	1	72607.9	10.6678	4728.27
Day 2	2	24475	18.9944	5802.9
Day 3	2	66844.9	19.96	5789.66
Day 4	2	54157.8	20.4478	4716.15
Day 5	2	70650.5	19.68	4897.4
Day 6	2	25604	23.04	4390.7
Day 7	1	72119.7	9.75111	4819.12
Day 8	1	60144.7	12.8189	4756.69
Day 9	2	49056.3	22.2667	4732.47
Day 10	2	71432.9	20.4856	4936.96

	1-truck	2-truck	3-truck
Day 1	4728.27	4716.16	3239.17
Day 2	4332.16	5802.9	4852.12
Day 3	5215.37	5789.66	1117.7
Day 4	4587.94	4716.15	3526.49
Day 5	4276.61	4897.4	
Day 6	4260.94	4390.7	2956.42
Day 7	4819.12	4643.44	1998.82
Day 8	4756.69	4433.81	2564.87
Day 9	4050.06	4732.47	
Day 10	4432.9	4936.96	2902.31

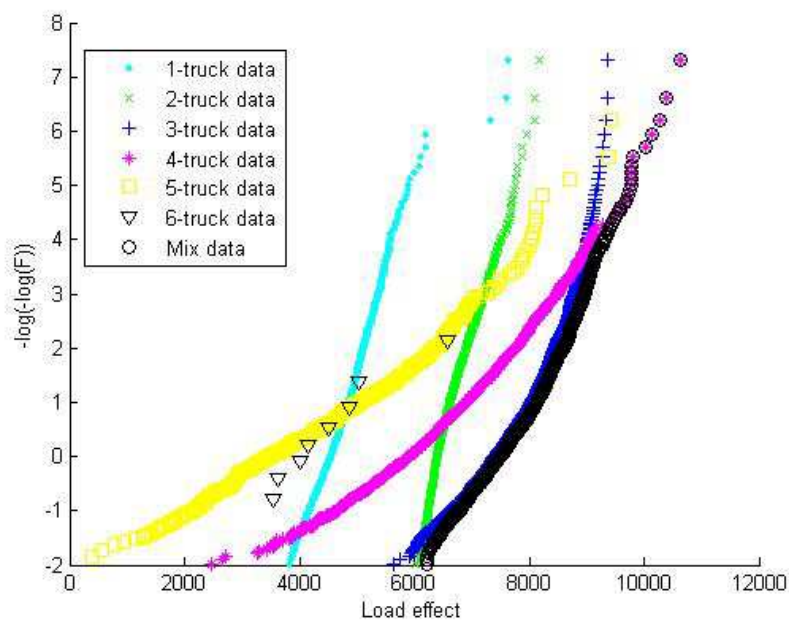


Figure B.10: Mixed daily maxima and maxima for individual loading event

B.4.4 Peaks over Threshold

If peaks over threshold files are required to be output, BTLECS creates two files. One is for negative load effects like hogging moment at middle support of a two-span continuous bridge, and another is for positive load effects like bending moment at mid-span of a simply supported bridge. A sample output is given:

Line	No. involved trucks	Effect (kN.m)
1	2	3482.46
2	1	3478.91
3	2	4716.16
4	2	3459.95
5	1	3687.64
6	2	3492.83
7	1	3534.15
8	1	3536.53
9	1	3446.75
10	1	3585.69
11	2	4438.47
12	1	3462.49
13	2	4137.03
14	2	3822.01
15	2	3824.27

A sample of mean excess plot for the recorded peaks over threshold is shown in Figure B.11.

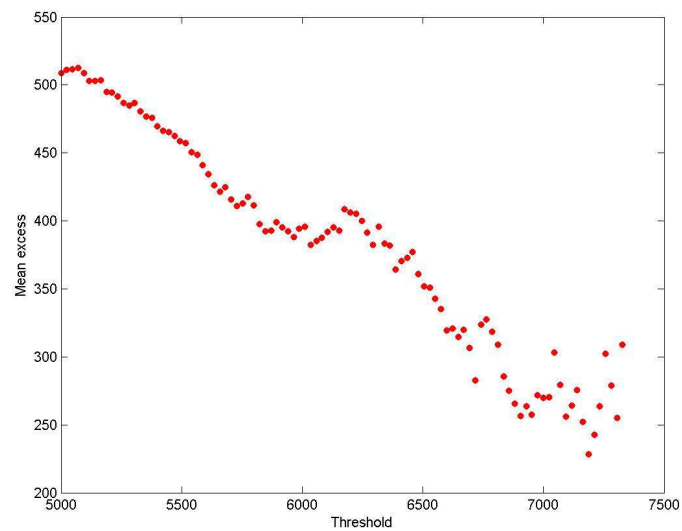


Figure B.11: Mean excess plot

C Mixture Peaks over Threshold Method

The following plots display the diagnosis of GPD obtained by MPOT and conventional POT. The left plots show the comparison in standard probability paper, and the right plots show the comparison in log-scale CDE. In the plots, the black dots represent the observations, the red line represents the GPD fitting from conventional POT method, and the green line represents the GPD fitting from MPOT method. From the top to bottom, the threshold is increased from 90th quantile to 98th quantile. Five parameter estimators (MM, PWM, ML, ADR and MDPD) were used to estimate the GPD parameter.

The legend used in the graphic diagnosis plots is given by Figure C.1.



Figure C.1: Legend for the graphic diagnosis plots of the following figures

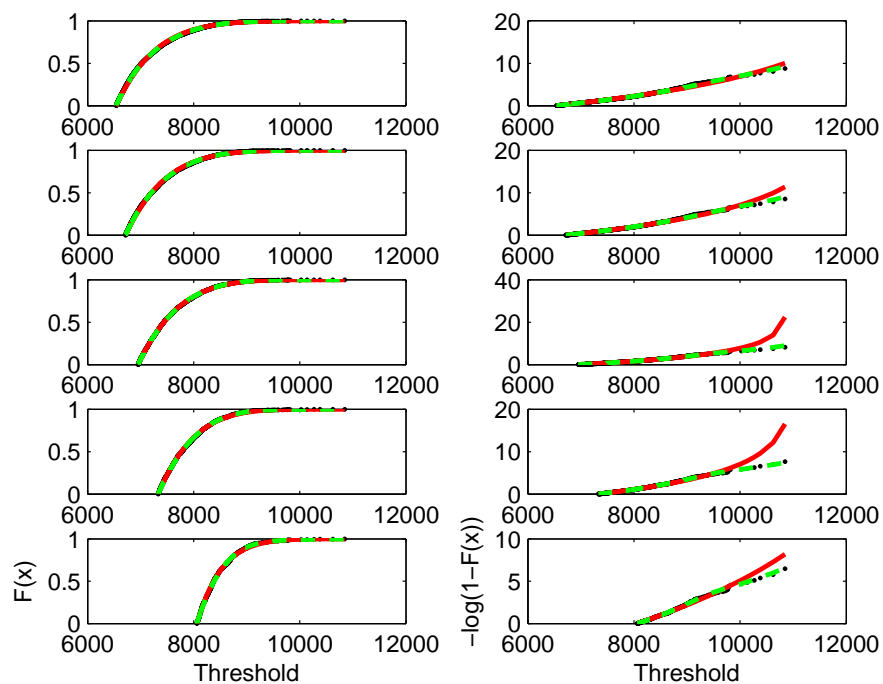


Figure C.2: Diagnosis plot, LE I1, 40 m, MM estimator

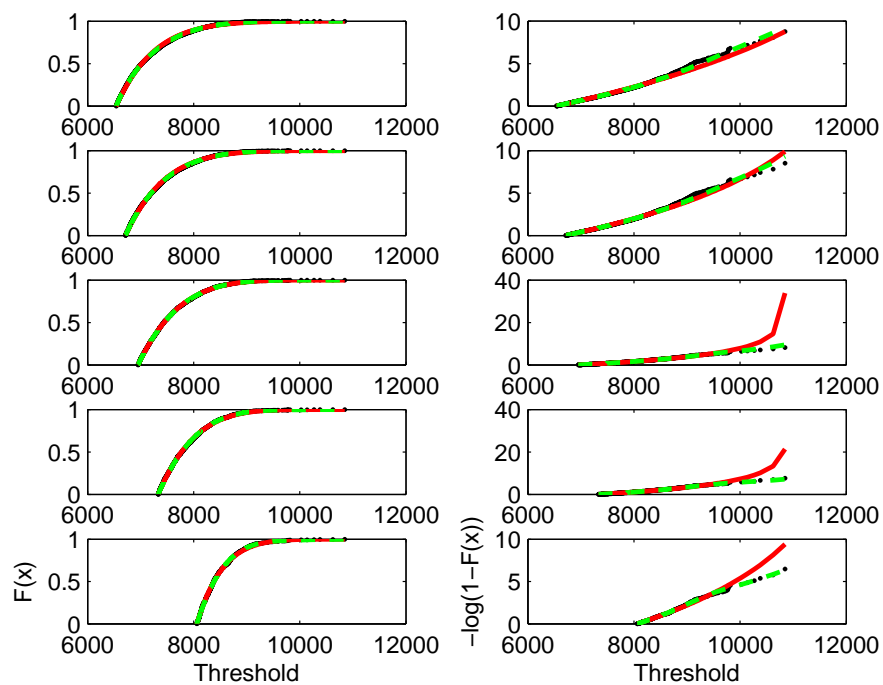


Figure C.3: Diagnosis plot, LE I1, 40 m, PWM estimator

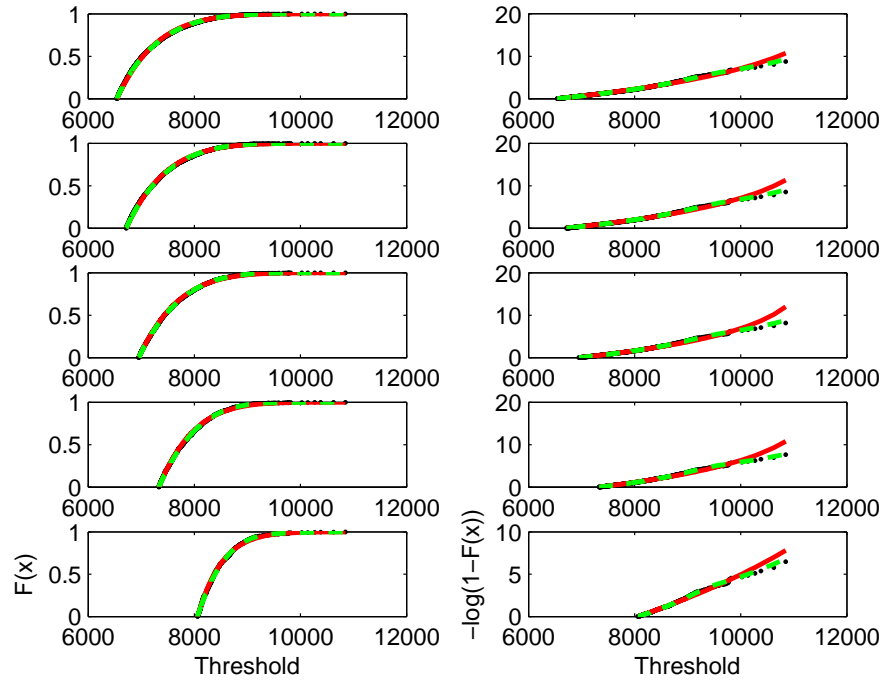


Figure C.4: Diagnosis plot, LE II, 40 m, ML estimator

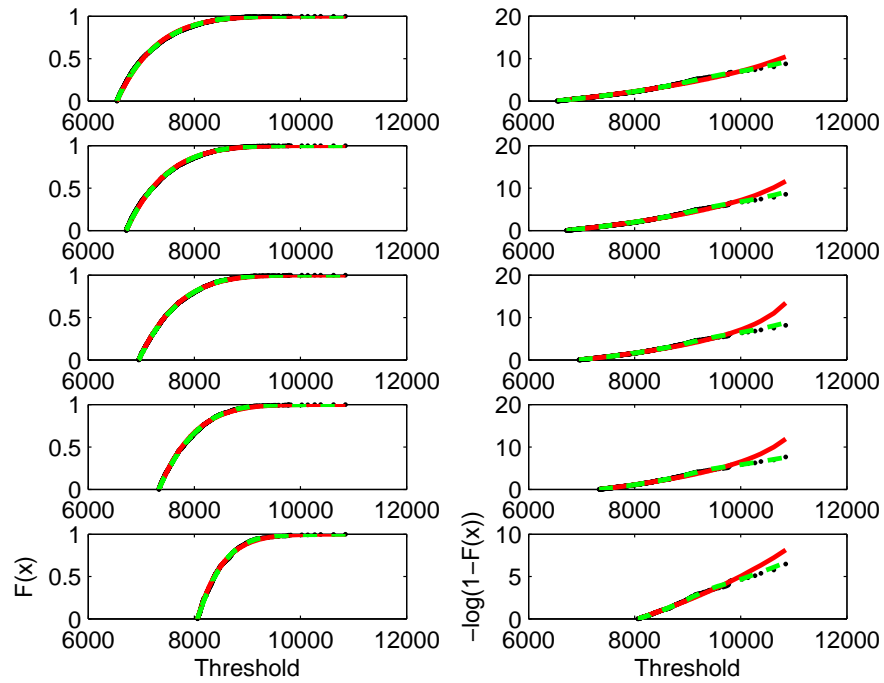


Figure C.5: Diagnosis plot, LE II, 40 m, MDPD estimator

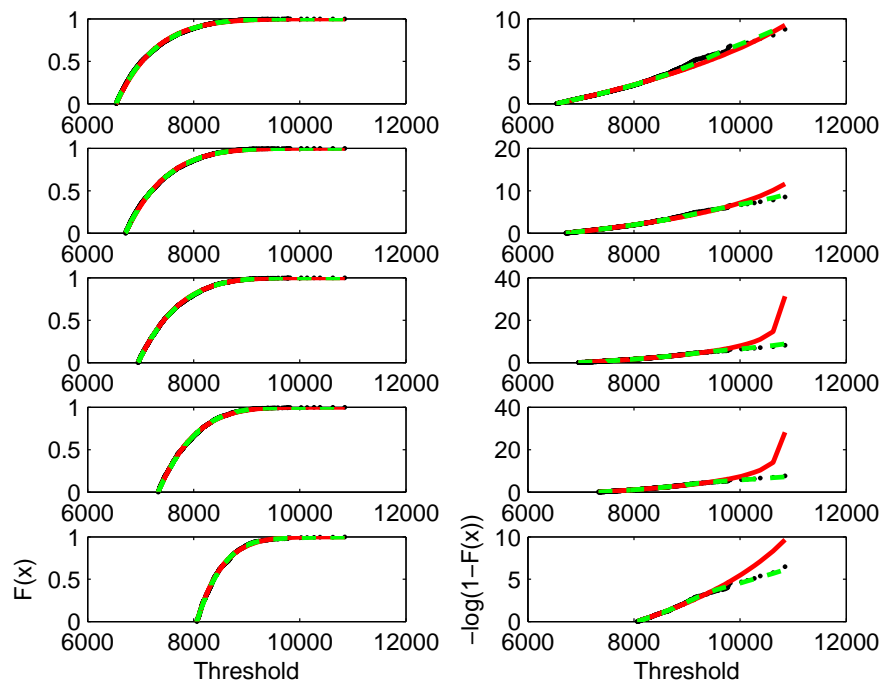


Figure C.6: Diagnosis plot, LE I1, 40 m, ADR estimator